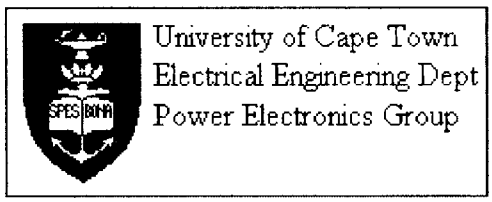

Using Passive Elements and Control to Implement Single- to Three-Phase Conversion

Prepared by: Stuart Marinus
University of Cape Town
South Africa

Prepared for: Mr. M. Malengret
Department of Electrical Engineering
University of Cape Town

Due Date: 30 September 1999

Acknowledgments

I wish to thank the following people for their invaluable contribution towards this project:

Mr M. Malengret, my thesis supervisor, for helping me a great deal with the initial formulation of ideas and making it possible for me to complete my Master of Science Degree at the University of Cape Town.

My parents, Shirley and Andy, for sacrificing so much for me. Their unconditional love and belief in me has made it possible for me to get this far.

Caroline, for her support, understanding and thoughtfulness.

Dan Archer, who gave up much of his time, knowledge and experience on a daily basis, especially in the design of the saturable-core reactors and switch-mode power supplies.

Clive Granville for his advice and excellent technical assistance.

The research group: Huey, Dave, Elvis, Dan, Sven and Kurt, and staff and students of the Power Machines Laboratory- Chris, Clive, Brian, Colin and Phineas who were always ready and willing to help when needed and who made my time spent at UCT very enjoyable.

Terms of Reference

This thesis was commissioned and supervised by Mr Malengret of the Electrical Engineering Department at the University of Cape Town in partial fulfilment of the requirements for a MSc Degree in Electrical Engineering.

Mr Malengret's requirements were:

1. To do a literature review of methods of single- to three-phase conversion already devised.
2. To purchase and then determine through testing the equivalent circuit parameters of a 15kW, 3ϕ, 380 $V_{L\text{-}L}$, delta connected, four-pole, 50Hz, squirrel-cage induction motor.
3. To do a literature review into saturable-core reactors and to obtain a better understanding of their working.
4. To design a robust single- to three-phase converter, based on the theory researched, that utilises only passive components. The possibility of using the saturable-core reactor is suggested. The aim of this would be to demonstrate the viability of running the 15 kW, three-phase, induction motor from a single-phase supply. The motor is to run a centrifugal water pump.
5. To devise a stand alone controller that is capable of maintaining a steady, well balanced, three-phase supply to the motor, without requiring any external speed monitoring devices, such as tacho-generators, to be attached to the motor-pump system.
6. To test the converter through analysing its performance.

I have attempted to address all of these issues, with the design of a converter that utilises the saturable-core reactor and passive components.

Declaration

This thesis could not have been carried out without the help of many people, all of whom have been mentioned in the Acknowledgements. A breakdown of the work done, on various aspects of the thesis, is given below for clarity:

- **Single- to Three-Phase Converter Review.**

  Much of this comes from preliminary work done by M. Malengret towards his Ph.D. with contributions by the author.

- **Load Balancing Review.**

  Largely from literature review with additions by M. Malengret.

- **Calculating Motor Characteristics.**

  Entirely authors own work, guided by literature example.

- **Calculating Compensating Elements.**

  Entirely authors own work, using derived formulas.

- **Saturable-Core Reactor Review.**

  Largely from literature review.

- **Design and Construction of Saturable Reactors.**

  Actual construction was done by MLT Drives, specifications by author, initial calculations resulted from a joint venture between author and Dan Archer, testing and experimental determination of air-gap by author.

- **Converter Design.**

  Initial ideals formulated in discussion between author and M. Malengret. All other work contributed by author.

- **Control Theory.**

  Entirely authors own work.

- **Controller Simulation and Design and Construction of Controller Circuitry.**

  Entirely authors own work.

- **Design and Construction of Switch-Mode Power Supplies.**

  Controller circuit design and printed circuit board (PCB) provided by Dan Archer. PCB population and power supply construction done by author.

- **Experimental Construction, Testing and Results, Conclusions and Recommendations.**

  Entirely authors own work.

- **Final working state of the project.**

  The final state of the project was as follows:

  - The converter functions, producing balanced phase currents over nearly the full slip range of the motor (from start up to near no load speed.)
  - Recommendations were made, however, they could not be implemented owing to lack of time.

Signature: _____ Date: _____

Synopsis

The most costly element of countrywide electrification is that of distribution. If only one phase is transmitted instead of three, then the overall cost of distribution is considerably lessened. However, the problem is that the majority of large machines used in industrial and farming equipment, rely on three-phase power. This is typical of the situation as found in rural and developing areas where the cost of distributing three-phase power is prohibitively high but three-phase machines are in demand. As a result of this, there is a growing need to perform single- to three-phase conversion.

For any balanced three-phase load, such as an induction motor, it is shown that a two-element reactive phase converter can offer exact phase balance.
The principal is illustrated below in Fig 0.1.

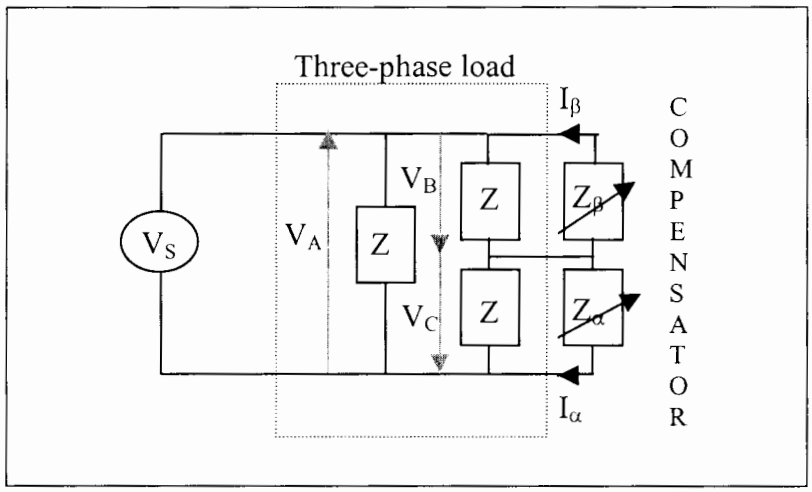

Figure 0.1 Reactive phase-shift, two-element, converter.

The two compensating elements, Z_α and Z_β, are found to be inductive and capacitive, and therefore act only as energy storage units, wasting no power.

With the use of the saturable reactor, it is found that this proposed converter topology is realisable, however two main problems are encountered.
Firstly, producing a continuously variable source of power capacitance proves to be difficult, especially when working with high voltages.

Secondly, many control strategies for the compensating elements involve instability. These problems are addressed and suggested solutions made.

As a single- to three-phase conversion technique, this is attractive, not only because of its simplicity, but also from a harmonic perspective. If truly passive components are utilised, the total harmonic distortion of this converter is near zero.

Table of Contents

List of illustrations

1 Introduction

This thesis aims to demonstrate the viability of running a 15 kW, three-phase, induction motor from a single phase supply by producing a balanced, three-phase supply for the motor using passive components only. The motor will drive a centrifugal pump and it is envisaged that this system will be used for remote rural water pumping stations.

1.1 The Need for Single to Three-phase Conversion

Three-phase motors are well established in industrial machinery. They are generally more efficient, less expensive, more readily available, and more reliable than equivalent single-phase motors. It is for this reason that manufacturers design three-phase motors into their equipment, often without considering three-phase service availability. Electric utilities do distribute three-phase power to large industrial and commercial customers, as well as areas of high load density, yet they have seldom found it economical to run three-phase service to residential areas or to certain small businesses. Commonly affected are small businesses that depend on equipment with three-phase motors, such as bakeries, woodworking shops, laundries, printers, service stations and small machine shops. Also affected, particularly in South Africa, are home business owners, farmers and rural communities.

The need for running three-phase equipment from a single-phase supply is driven by economic factors including utility charges for extending three-phase lines, construction delays in obtaining new service, and limited availability of single phase equipment. If the cost of extending a customers line cannot be paid back quickly enough through energy revenues, the utility will charge the customer for the new service. Charges vary according to the terrain and the complexity of the change, but commonly range from R100 000 to R300 000 per kilometre. In addition to this there is the expense of installing phase distribution panels in the building. Even if the utility does agree to provide the new service, the time lapse before a line is installed can cost the business substantial revenue. Many owners of three-phase machinery, lacking three-phase service, try to substitute a single-phase for a three-phase motor.

Unfortunately, the availability of integral-hp single-phase motors is limited, especially above 8kW. Special motor designs such as multispeed types or custom flange arrangements make finding a single-phase replacement impractical or impossible.

In this context, a converter can adapt any three-phase machine to a single-phase power service with potential savings in comparison with alternative utility costs.

1.2 The Objectives of this Thesis

This thesis begins with a review of single- to three-phase conversion techniques. The next chapter describes the operation of the passive element converter. Following this the motor characteristics are determined and the necessary calculations are performed to find the balancing elements required. The saturable-core reactor is then covered, followed by a detailed explanation of the evolution of the converter design.
The converter design is followed by the control method used. Simulations are carried out followed by construction. The final converter design is then tested and based on these results conclusions and recommendations are made.

2 Review of Single-phase to Three-phase Converters

2.1 Introduction

In this chapter several single-phase to three-phase converters (SP3PC) are reviewed. Existing methods that have been proposed by others are briefly described. Their various merits are discussed and compared. The converters have been classified into three categories:

- Reactance compensators.
- Rotary converters.
- Semiconductor converters.

2.2 Reactance Compensator Converters

2.2.1 Capacitor Phase-Shift Method

The most simple and least costly version of a SP3PC is the capacitor phase-shift [2] or simply capacitor type. The capacitor provides the third terminal as seen in Fig. 2.1 and the single-phase supply the other two.

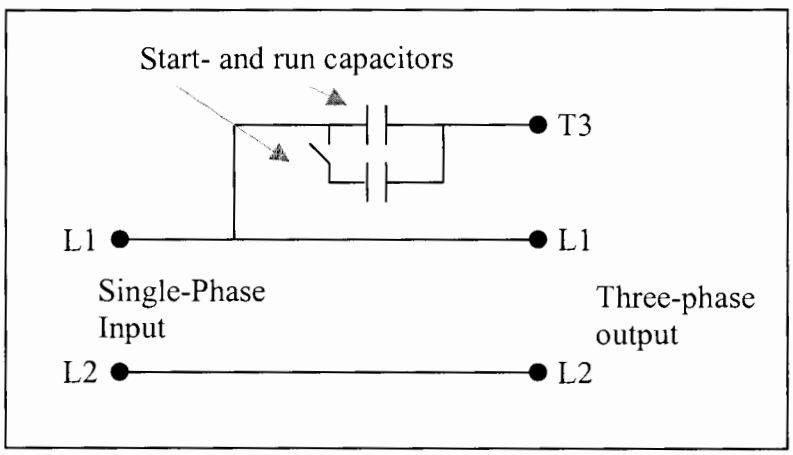

Figure 2.1 Capacitor phase-shift static converter

This is a crude method and cannot provide a balanced three-phase supply. For a balanced supply, in addition to a variable capacitor, a variable inductance is necessary, as it will be shown later in section 2.3. The capacitor only method often uses a combination of start and run capacitors to somewhat attempt to balance the currents. This method is sometimes useful in the case of a light, non-varying, load. The motor is likely to suffer from poor performance, draw excessive currents and therefore overheat. This method is known to work better with low power factor loads [6].

2.2.2 Autotransformer type Converter

A somewhat better method is to use an autotransformer in conjunction with capacitors as seen in Fig. 2.2.

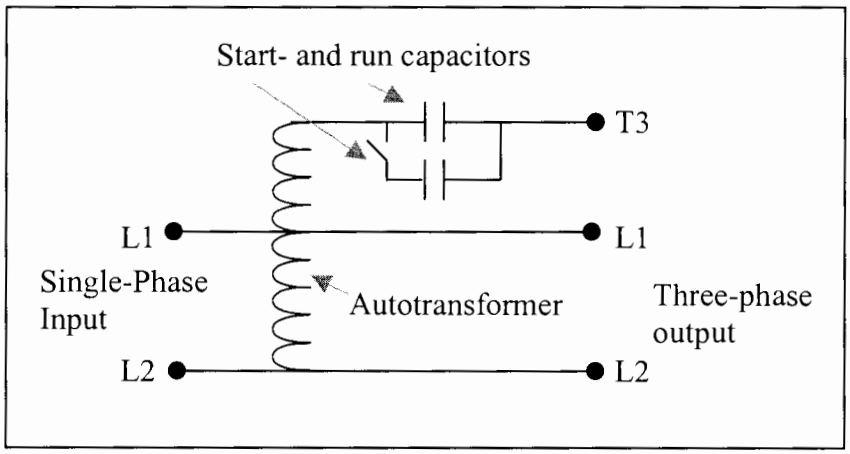

Figure 2.2 Autotransformer phase-shift capacitor converter

Taps on the autotransformer can be switched onto as the load varies, so as to obtain better phase angle and amplitude of the manufactured phase. These converters have been applied successfully on equipment such as fans, pumps, and elevators [6]. The switching sequence is experimentally done so as to get best performance. This method is also very limited in its application. The autotransformer could also have additional taps so as to augment the voltage. For example to raise 230V to 400V.

2.2.3 Two-Element Converter

Holmes [5] shows that exact phase balance of a three-phase induction motor can never be achieved with a single impedance phase converter. However a two-element phase converter can offer balanced operation. For example, in order to maintain a three-phase induction motor balanced under varying slip, a converter, consisting of two compensating reactance that can be dynamically controlled to vary as functions of the motor slip, is required. The principal is illustrated in Fig 2.3.

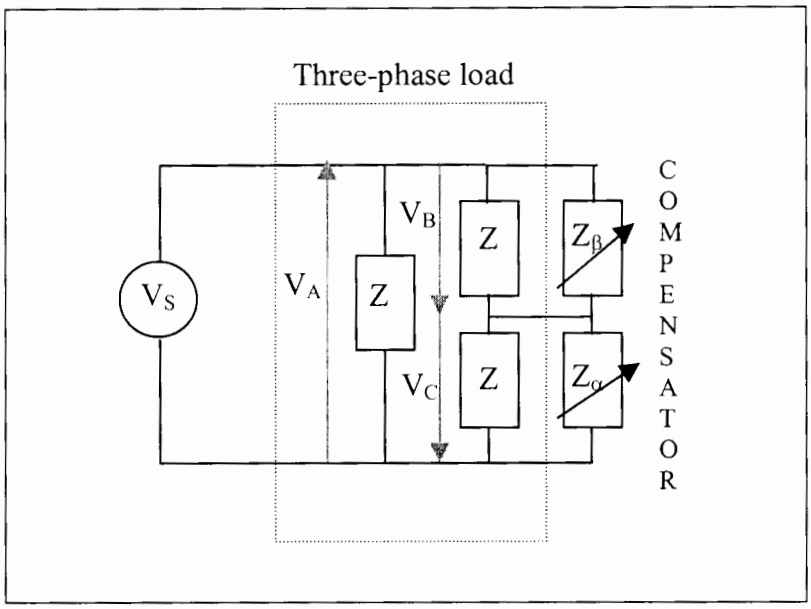

Figure 2.3 Reactive phase-converter drive

ac phase control and ac current regulation are used to maintain the converter parameters at the required values. Balanced phase conversion can be achieved from standstill to full speed in a direct-on-line starting, cage induction motor drive. The system is capable of accelerating a loaded motor and of maintaining supply balance to the motor as the load changes. However accurate phase balance will depend on an accurate assessment of the motor parameters during operation. In order to achieve this Holmes uses a cumbersome direct slip measurement and negative sequence voltage minimisation. A new simpler method will be demonstrated in chapter 9.

A three-phase induction motor has slip-dependent impedance. If the phase converter does not produce an exactly balanced three-phase supply, positive and negative sequence voltages producing forward and counter rotating fields which will be applied to the motor. Fig 2.4 shows the equivalent circuit of an induction motor.

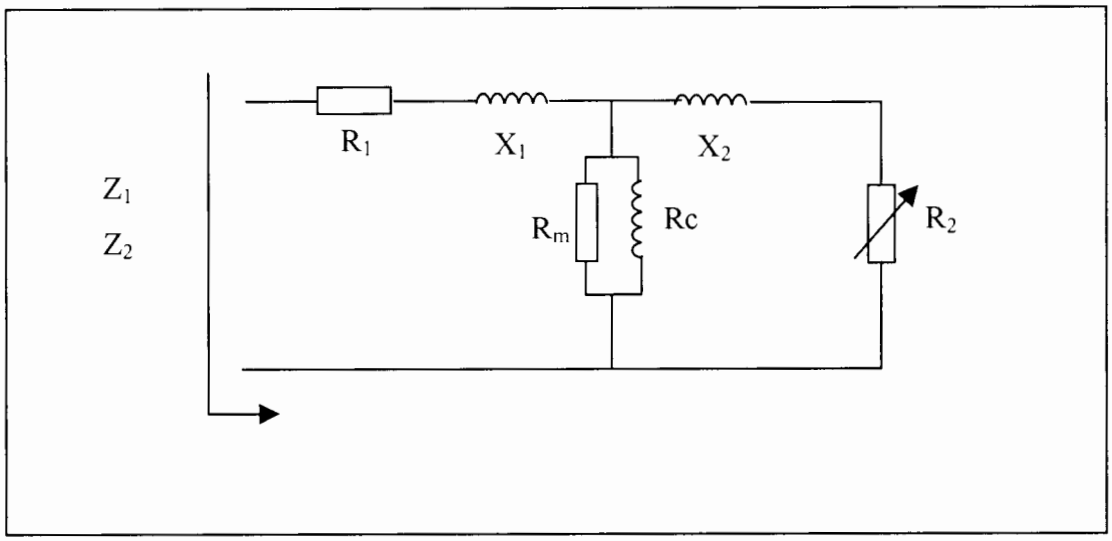

Figure 2.4 *Positive- and negative sequence motor equivalent circuit*

The positive sequence impedance is obtained when the variable resistance is r2/s and the negative-sequence impedance when the resistance is r2/(2-s).

Rx = R2/s for Z1

Rx = R2/(2-s) for Z2

Accurate phase balance will depend on an accurate assessment of the motor parameters on acceleration or load change. Fig. 2.5 shows the real and imaginary components of the motor positive- and negative sequence impedances; R1 +jX1 and R2 +j X2, as functions of slip.

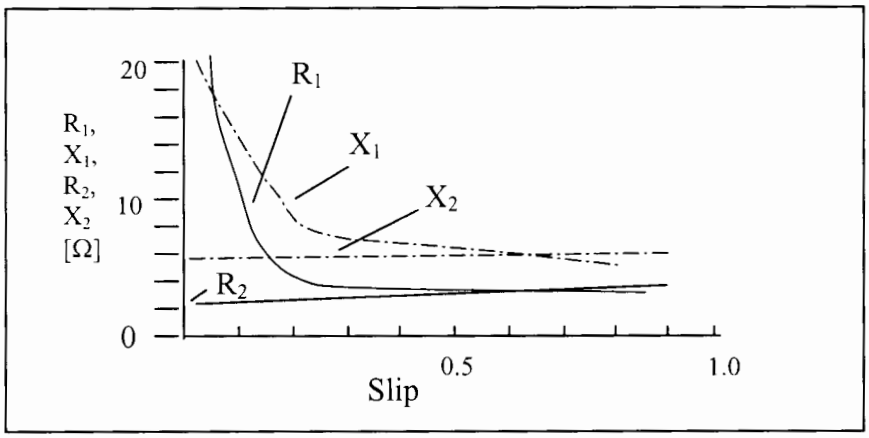

Figure 2.5 Resistive- and reactive sequence components against slip

These parameters were obtained by Holmes by standard tests on a 3 kW experimental cage-induction motor. Holmes in his paper [5] uses a complicated derivation to calculate Z_α and Z_β. A much more simple analysis by Malengret [9], using admittances rather than impedances, is shown in chapter 3, section 3.8.

Z_α and Z_β are essentially non-dissipating energy storage elements of variable reactance , X_α and X_β. Changes in reactance give corresponding changes in I_α and I_β. The required current changes can be achieved with variable electronic impedances as shown in Fig. 2.6.

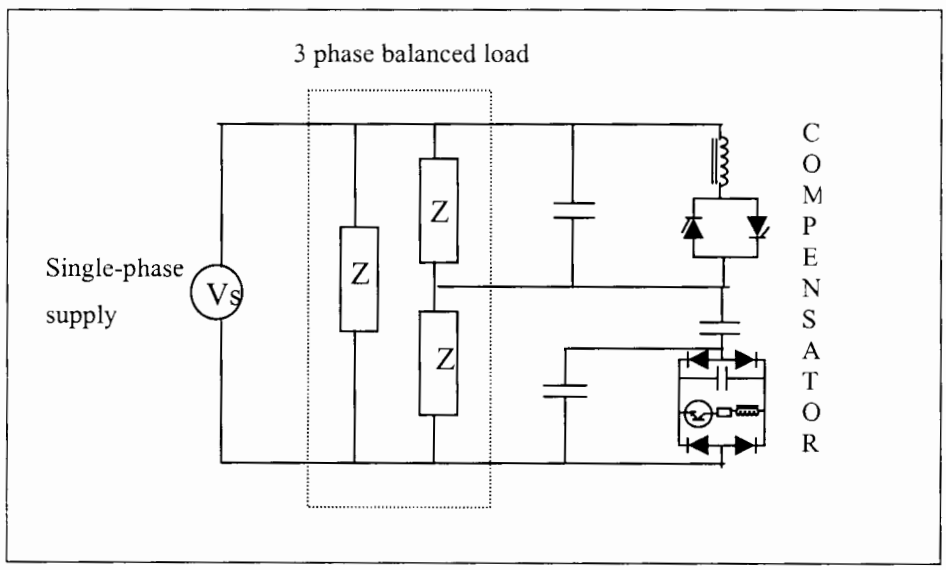

Figure 2.6 Transient phase balancing network

2.3 *The Rotary Converter*

2.3.1 Introduction

Of the various means of obtaining a three-phase supply from a single-phase source, the rotary phase converter, or Ferraris-Arno system [8] is most frequently employed. A rotary converter is a three-phase induction motor that operates on a single-phase supply and produces a true three-phase output. The rotary converter is really a combined single-phase motor-generator set, the manufactured phase of which is a true sinusoid. In Fig. 2.7 below a typical phase converter system is shown.

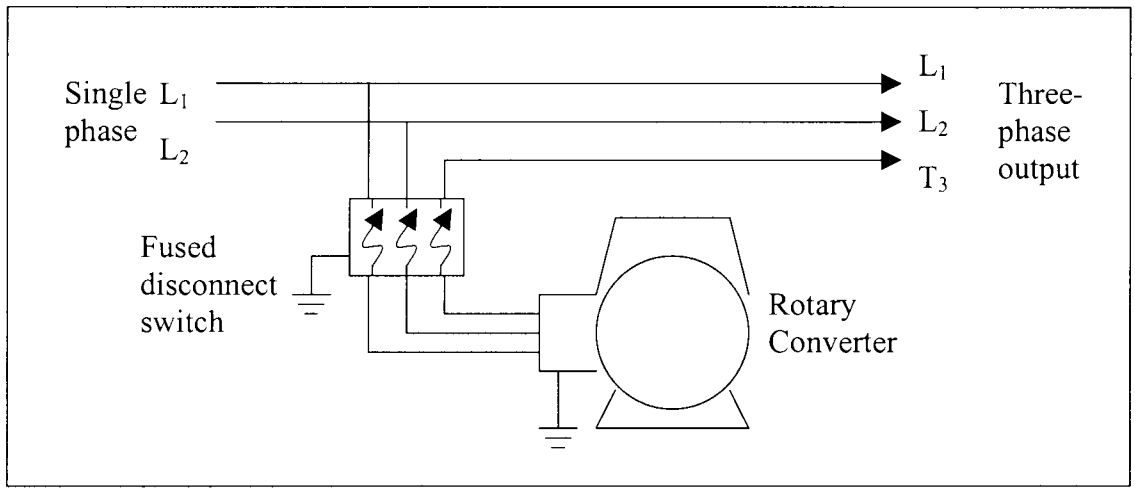

Figure 2.7 A typical phase converter system

Tests show that the combined efficiency of an induction phase converter and a three-phase motor load is higher than a single-phase motor of the same size at the same load [6].

2.3.2 Construction

The converter has a single-armature similar to a three-phase induction motor. It usually has a symmetrically wound stator and a specially modified squirrel-cage rotor. A large capacitor bank is placed across a coil group between one input line and the manufactured phase as shown in Fig. 2.8 below.

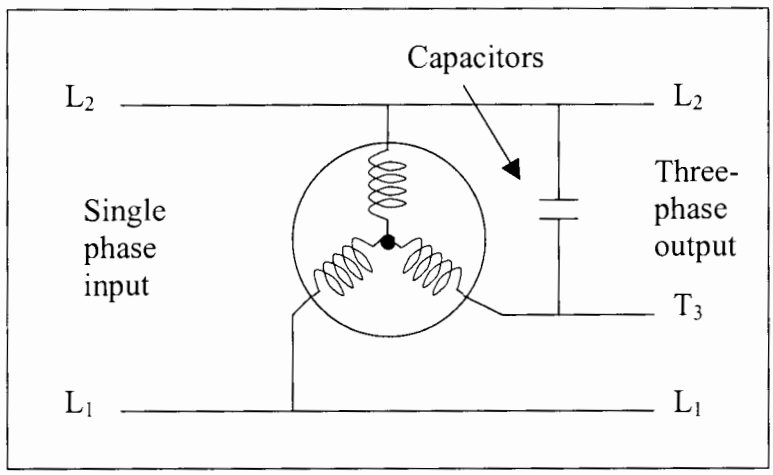

Figure 2.8 Simplified equivalent circuit for a rotary converter

2.3.3 Operation

When first energised, a single-phase voltage is applied to one coil group producing an internal magnetic field. The capacitor bank provides a 90° phase-shifted voltage to an adjacent coil group, which produces another internal field and hence rotor torque. The rotor spins and through induction picks up a replica of the utility supply and internally generates the manufactured phase voltage. The normal action of an induction motor induces voltages into the squirrel-cage rotor. These voltages produce current in the short-circuited turns of the rotor. The currents in turn produce magnetic poles on the rotor surface. These magnetic poles generate back e.m.f.'s in each of the stator coil groups, separated by 120 mechanical degrees. The back e.m.f. is also generated in the manufactured phase of the three-phase winding. This produces a three-phase sinusoidal output with each phase shifted by 120°; however, the manufactured phase is *unbalanced*, since the back e.m.f. does not quite match the line voltage in the other two phases.

While running the capacitor bank helps to improve the power factor and raises the voltage of the manufactured phase. This not only increases the carrying capacity of the converter, but also improves its voltage regulation. The output voltage of the converter is always a three-phase, three-wire, closed delta version of the input voltage. If a different output voltage or four-wire wye output is required, a transformer must be used.

2.3.4 Output Characteristics

The most important output characteristic is the behaviour of the manufactured phase voltage relative to the utility supply. The output is load dependant as is shown in Fig. 2.9.

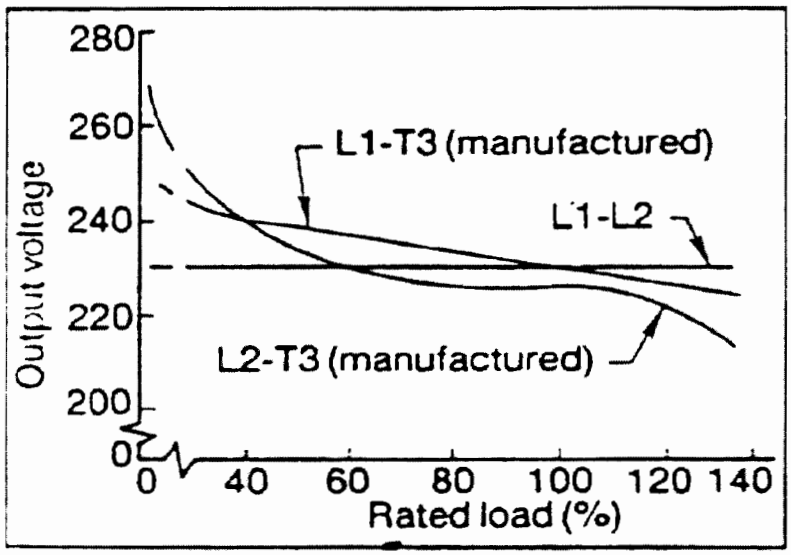

Figure 2.9 Output voltage vs. load for a rotary converter with 230V supply

At no load the manufactured phase voltages, L1-T3 and L2-T3, are much higher than the supply voltage. As the load increases, the voltage drops until, at full load, the three voltages are nearly balanced. If the load exceeds the converter capacity, the manufactured phase voltage drops off sharply.

2.3.5 Ratings

Fortunately, two of the three-phase lines are supplied directly, and the converter is only loaded by the current in its manufactured phase. A rotary converter can start one three-phase motor equal to its rated nameplate power at any one time. However, when the motor it is operating reaches full speed, it has a supporting effect on the system. For this reason, a rotary converter can operate approximately four times its rated nameplate power, while still maintaining good voltage balance, as long as all the motors are not started simultaneously.

It is possible, however, to increase the number of motors that may be started and run from a single rotary converter indefinitely, but if this is done, the motors must be de-rated by at least one third of their three-phase rating. This is because the manufactured line current from the rotary converter is divided among so many motors that the benefit to each is negligible. Then the manufactured line serves only the purpose of starting another motor or of assisting an overloaded motor. If the motors are run at full capacity, the inherently low manufactured line voltage causes very unbalanced currents and overheating which eventually results in motor failure.

In a large system where fully rated three-phase motors are required, either a larger converter, or more than one converter can be used to maintain the necessary voltage balance. The latter arrangement renders the system less dependent on one converter and also enables some converters to be switched off during periods of light-load, so reducing light-load losses.

Converter capacity is only truly restricted by the maximum single-phase load that the utility allows. Rotary converters can be paralleled indefinitely for any load. This feature is convenient for systems where load is often added or for situations where the utility supply lines cannot withstand the inrush currents of a single large rotary converter. Typically available converter ratings range from 0.75kW to 75kW.

2.3.6 Cost, Size and Weight

The following table gives a comparison of two sizes of rotary converters.

Actual Rotary Rating [kW]	Largest Starting Load* [kW]	Average Multi-Motor Load** [kW]	Shipping Weight [kg]	Size [mm^3]
7.5	3.7	12.7	90	450*450*500
22	11	37	210	560*560*710

* For light loads over-rate by 25%, for heavy loads de-rate by 25%.

** Presumes that not all motors are heavily loaded at the same time.

The table below gives prices for the above two rotary converters. Included are the hidden costs of converter accessories.

Accessory	Cost for 7.5 kW Rotary Converter [$]	Cost for 22 kW Rotary Converter [$]
Rotary Converter	1474	3265
Magnetic Starter	419	925
Soft Start	575	925
Capacitor Module	351	706
Hard-Start Panel	373	704
Total Cost	**$3192**	**$6525**

Although these costs are high, they are in many cases substantially lower than the cost of utility installed three-phase.

2.3.7 Advantages and Disadvantages

The advantages and disadvantages of rotary converters are listed below.

Advantages:

- Low capital cost.
- Proved reliability with low maintenance.
- High conversion efficiency.
- Compact and easy to install.
- Reasonable voltage control, improved by accessories.
- Support broad load range (rectifiers, resistive loads, welders, and lasers).

Disadvantages:

- Manufactured voltage fluctuation with load.
- Poor starting torque.
- Produce noise pollution.
- High no-load losses.
- 2-3 seconds, initial converter run-up time, before a load can be connected.

2.4 Semiconductor Converters

2.4.1 Diode Rectifier and Three-Phase Full Bridge Inverter

With the recent progress in price and performance of semiconductors, high switching frequency inverters have become very popular and common. Most of the three-phase output inverters have a dc link. In the case of the SP3PC, the dc is obtained by rectifying the single-phase supply as seen in Fig. 2.10.

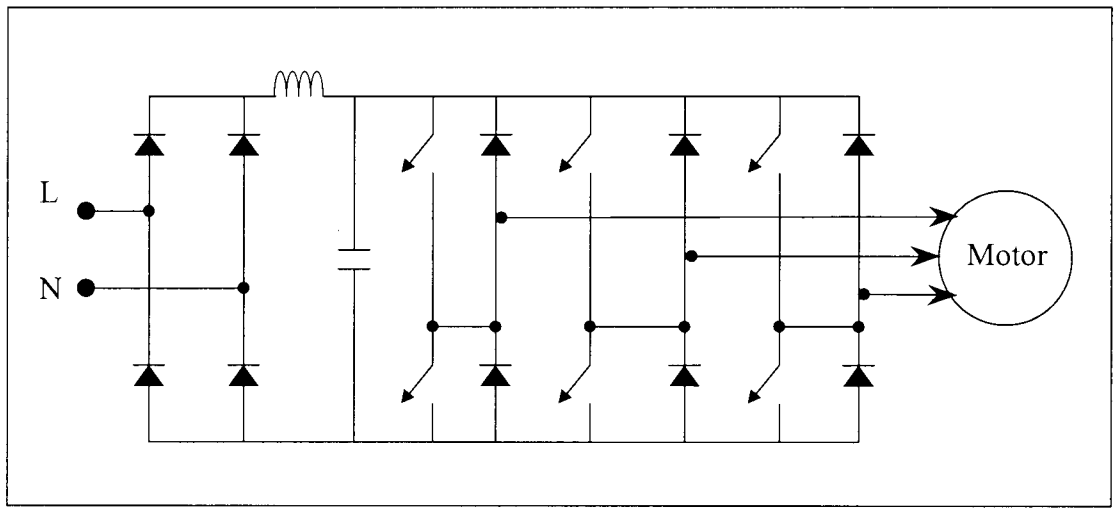

Figure 2.10 Three-phase PWM inverter with a dc link from a single-phase supply rectified by diodes

The diode bridge approach is found in many, commercially available, variable speed drives. The ones that have a single-phase input do not usually exceed 1 or 2kVA. The diode bridge approach suffers from poor input current quality and lack of bi-directional power flow capability [2,17].

The dc bus voltage is limited and hence the motor must have an appropriate voltage rating. For instance in the case of South Africa, a 230V input single-phase supply, the motor is rated at 230V line to line when connected in delta. One should bear in mind that 3 phase motors ratings are usually 400V line to line in the case of a 50 Hz 230V live to neutral reticulation system. Larger motors are connected in star whilst starting, which limits the current and effectively applies a voltage which is divided by $\sqrt{3}$.

Motors meant to run on 230 V are not common and usually only limited to 1 or 2 kW. It is possible to boost the voltage with an autotransformer if required to operate a 400V three-phase motor from a 230 single-phase supply.

2.4.2 Converter with Active Rectifier

A diode bridge single-phase converter as shown in Fig. 2.10 is notorious for the distorted current drawn from the supply [11]. The current deviates substantially from a sinusoidal waveform. A very poor power factor results and hence a large effective current is drawn from the supply. This current can lead to high demand from the supply and cause distortion in the line voltage for other consumers connected to the line.

Stricter harmonic current standard are now being enforced, therefore the rectifier must be improved by using active current shaping schemes or adequate filters. Fig. 2.11 shows an active current shaping rectifier which uses an additional boost switch and blocking diode to the previous scheme.

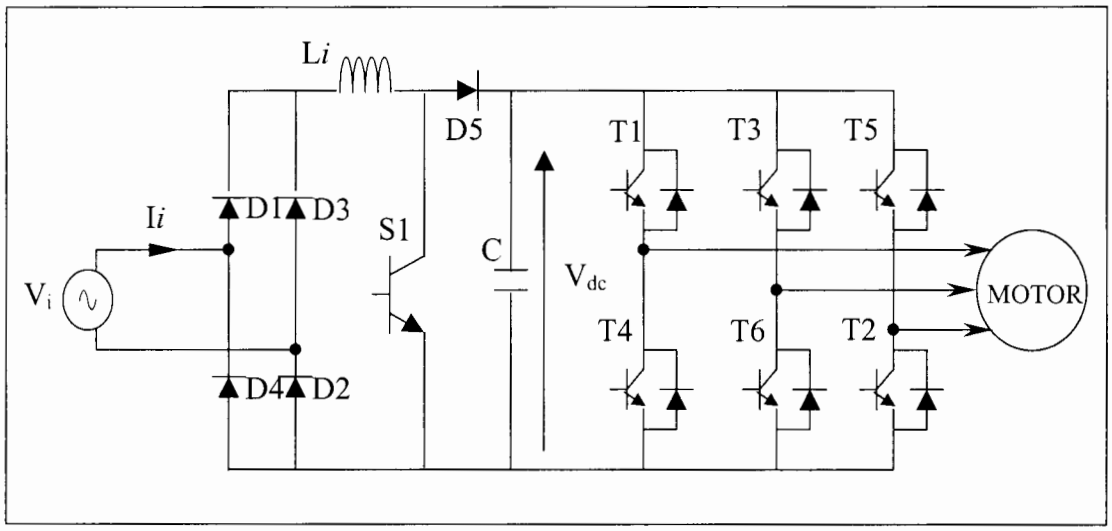

Figure 2.11 SP3PC with current shaping rectifier provided by the addition of a boost switch and a blocking diode

The need for additional power devices to maintain input current quality adds to the cost and powers losses.

Several resonant circuit topologies are suggested in [2,7,12,13] and are illustrated in Fig. 2.11 through 2.14. The increase in component count to reap the additional benefit of low switching losses is apparent from these topologies.

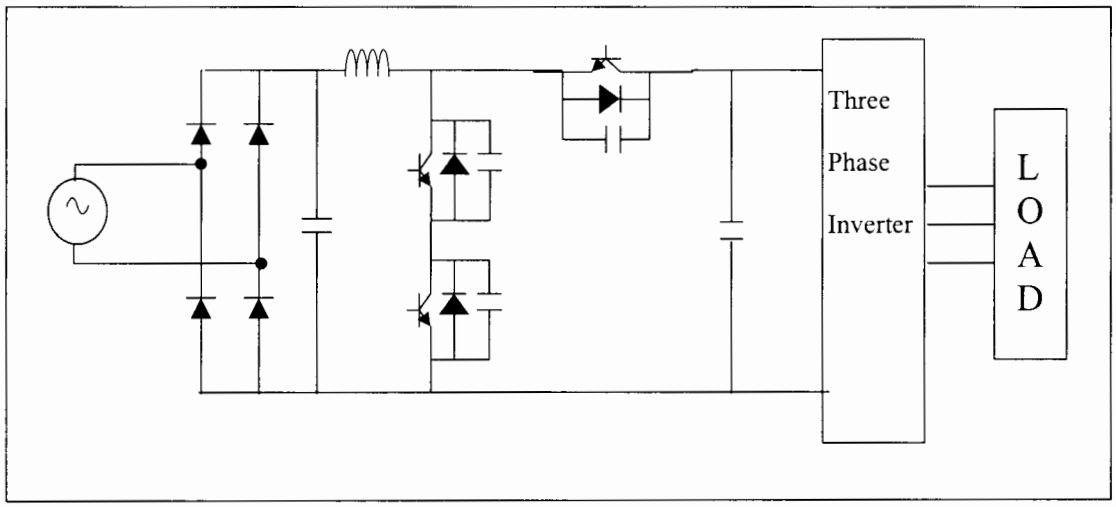

Figure 2.12 SP3PC with resonant circuit for input current shaping, zero voltage switching type

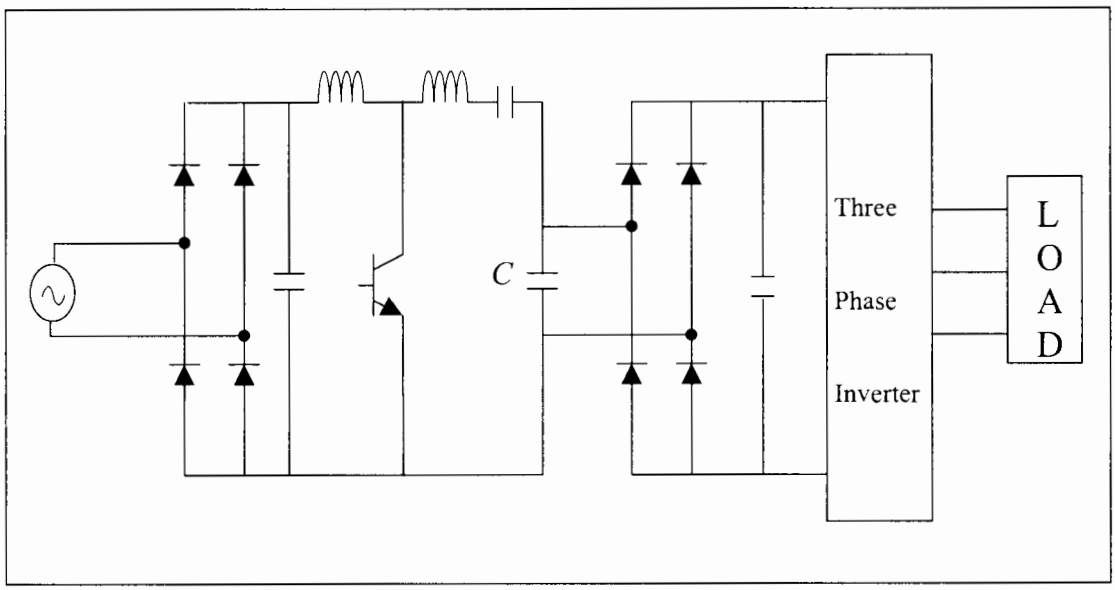

Figure 2.13 SP3PC with reasonant circuit for input current shaping, class E

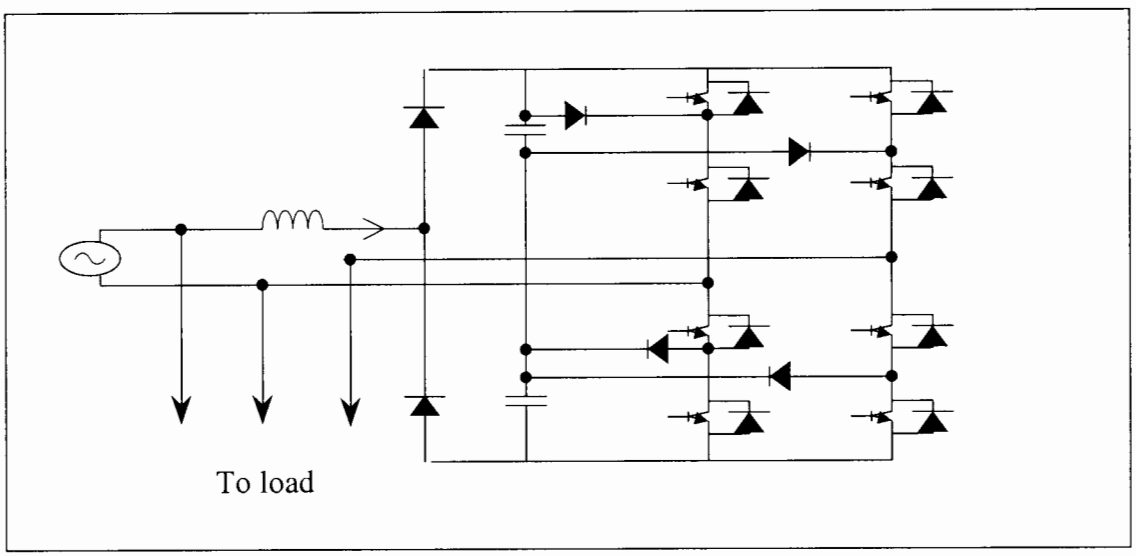

Figure 2.14 Neutral point-clamped: converter for single-phase to three-phase conversion, the power configuration

Another front end active rectifier [17] is a standard single phase full bridge rectifier as shown in Fig. 2.14. The front-end converter feeding the PWM inverter regulates the dc link voltage, draws sinusoidal current from the ac mains, without drawing reactive power, and power flow can be bi-directional The PWM type front-end converter with an ac inductor meets all the requirements and has been used as a voltage source for PWM inverters driving ac motors [7]. Control techniques for three-phase PWM front-end converters have been reported [16,19]. These applications, including single-phase ac traction, where operation from a single phase supply is of interest and techniques of control in this context have been reviewed [17].

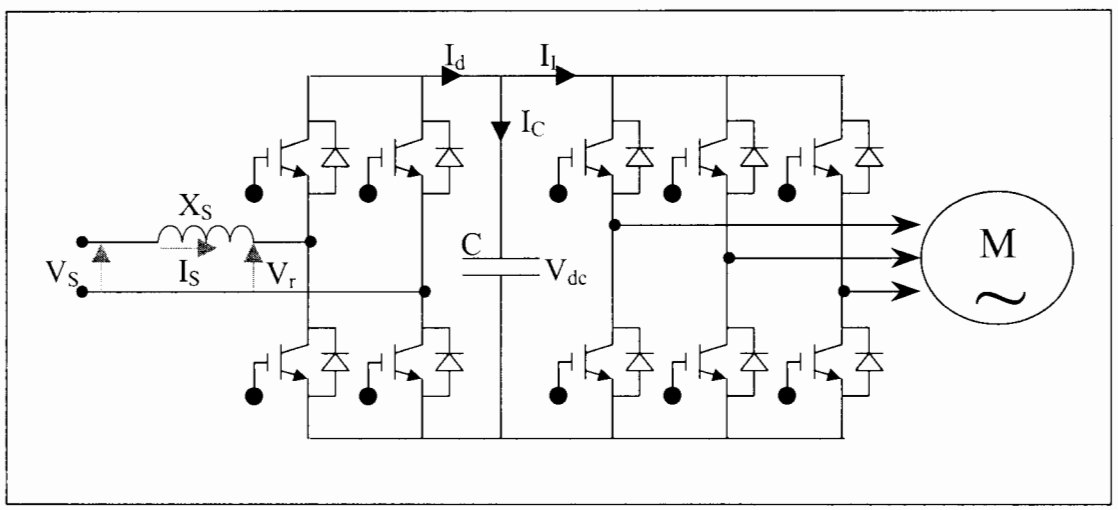

Figure 2.15 IGBT PWM rectifier/inverter system

2.4.3 Reduced Count Semiconductor Converters

2.4.3.1 Front-end Half-bridge Rectifier with B4 Bridge

The proposed configuration by Enjeti incorporates a front-end half-bridge rectifier structure that provides the dc link with an active input current shaping feature shown in Fig. 2.16.

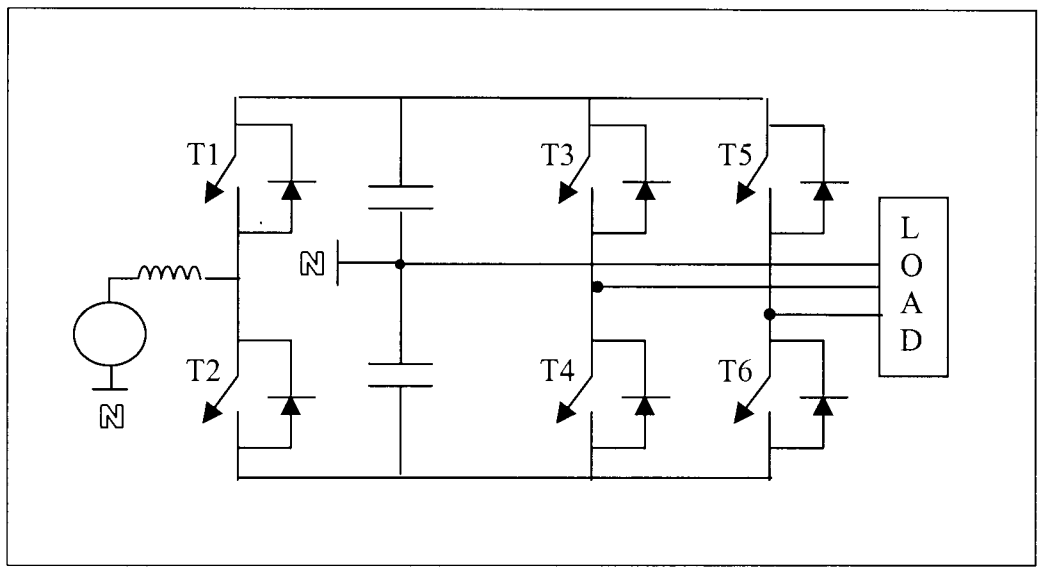

Figure 2.16 Front-end half-bridge rectifier with B4 bridge

Further, the front-end rectifier allows bi-directional power flow between the dc link and the single-phase ac mains. A four-switch inverter configuration with split capacitors in the dc link provides a balanced three-phase output to the ac load at adjustable voltage and frequency. The configuration is essentially the B4 inverter configuration with the addition of a single arm split capacitor active rectifier.

Using PWM techniques the converter can be controlled to draw sinusoidal input currents at close to unity power factor and to deliver three-phase balanced fundamental frequency voltage output.

However the line-to-line voltage V_{ac},V_{bc}, V_{ab} are not identical as shown in Fig. 2.17.

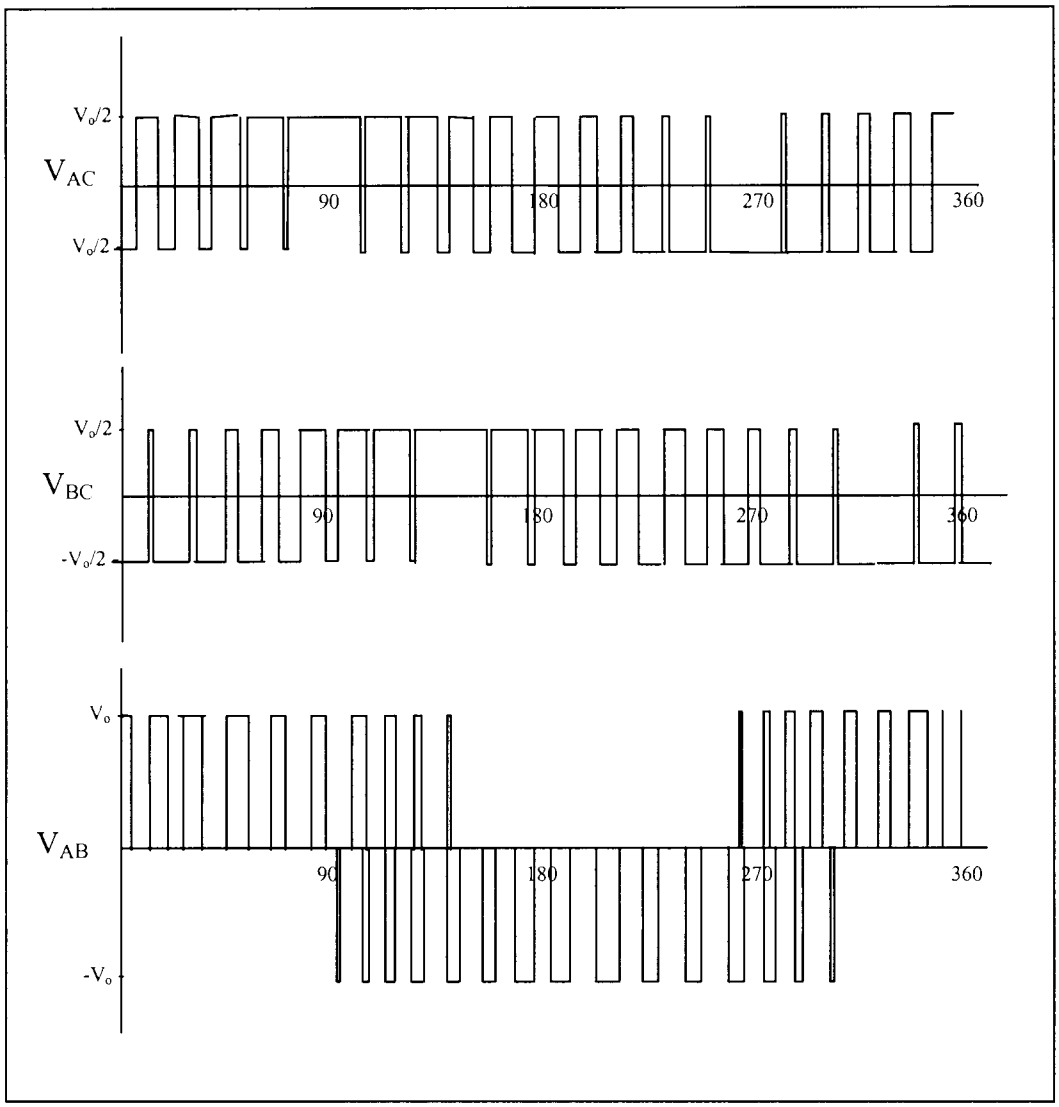

Figure 2.17 ***Inverter output voltage with programmable PWM pattern. (a) Two level line to line voltage V_{ab}. (b) Two level line to line voltage V_{bc}. (c) Three level line to line voltage V_{ab}***

It is noted that that voltage V_{ab} a three-level PWM swinging between $V_0/2$, 0, and $-V_0/2$. On the other hand, the voltages V_{ac} and V_{bc} are the two-level types swinging between $V_0/2$ and $-V_0/2$. This voltage asymmetry is a disadvantage as it brings harmonic unbalance.

Positive sequence as well as negative sequence harmonics will cause additional losses. However judicial choice of the switching frequency to fundamental ratio will reduce to this. For example non-triplen harmonics if not eliminated from the PWM switching function will appear in the output voltages.

The advantages of the converter are:

- It employs only six switches for single-phase to three-phase variable-voltage and variable-frequency conversion, hence, low cost.
- It draws near sinusoidal current for the ac mains at close to unity power factor and therefore satisfies strict harmonic current standards.
- Bi-directional power flow is possible between the ac mains and the dc link. Voltage regulation can be achieved.

The disadvantages are:

- The voltage utilisation is poor, as the maximum line-to-line fundamental voltage is approximately the single-phase line to neutral output. A step up transformer or unconventional load would be required.
- The Voltage asymmetry may cause extra power losses or vibration in some three-phase loads such as motors.
- The input inductance has to be chosen so as to obtain only near unity power factor.

2.4.3.2 The Modified Front-end Half-bridge Rectifier with B4 Bridge

The topology has been proposed by Malengret, and is a variation on the above topology. The advantage here lies in that symmetrical PWM on each arm of the three-phase inverter bridge can be obtained. Moreover full line to line voltage can be obtained. If for example the single phase supply is 230V then a symmetrical 400 V line to line is obtained. This is an important advantage.

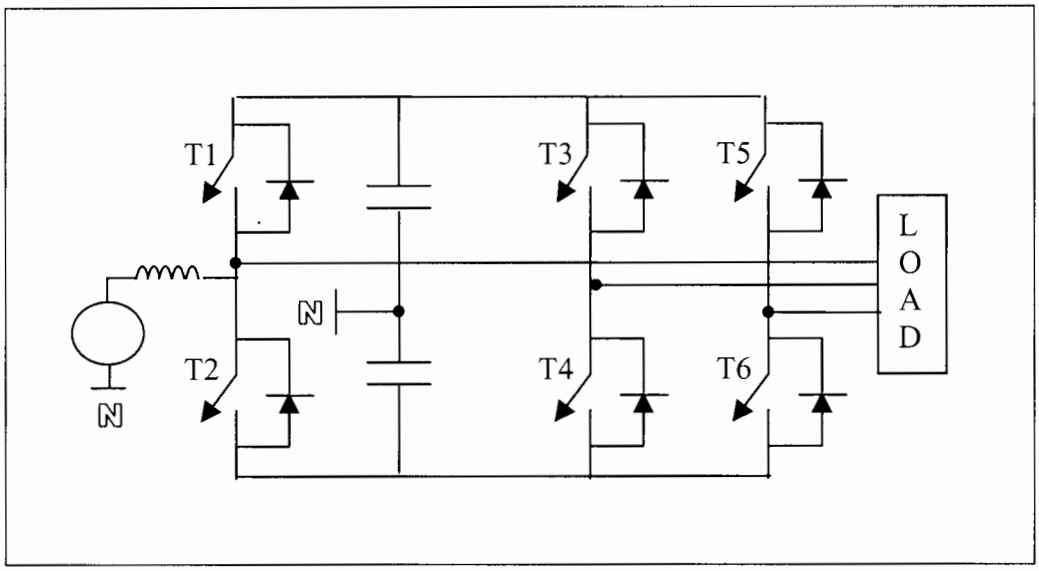

Figure 2.18 Modified front-end half-bridge rectifier with B4 bridge

The first arm also forms the active rectifier. A disadvantage is that this arm has to carry twice the current compared to the others. This scheme lends itself to a fixed frequency converter and is much more complex and limited if applied to variable speed drives. This is presently under investigation as a variable speed drives.

2.4.4 Single-Phase Cycloconverter

This approach utilises direct cyclo-conversion principles.

Proposed converter by Khan et al [11]

The proposed converter only employs semiconductor components in the transformation from single phase to three-phase as shown in Fig. 2.19. The switches must be able to switch and conduct in both direction and therefore are bi-directional.

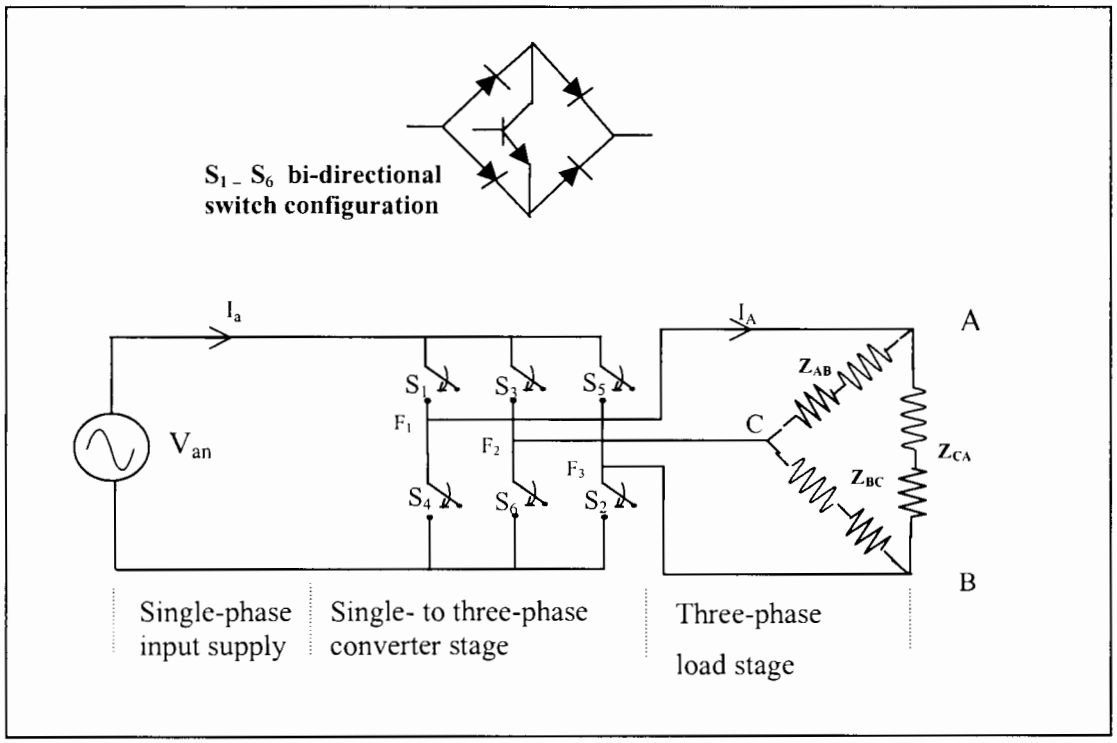

Figure 2.19 Proposed single- to three-phase cycloconverter based converter

The waveforms describing the basic operation of the converter are shown in Fig 2.20 through 2.22.

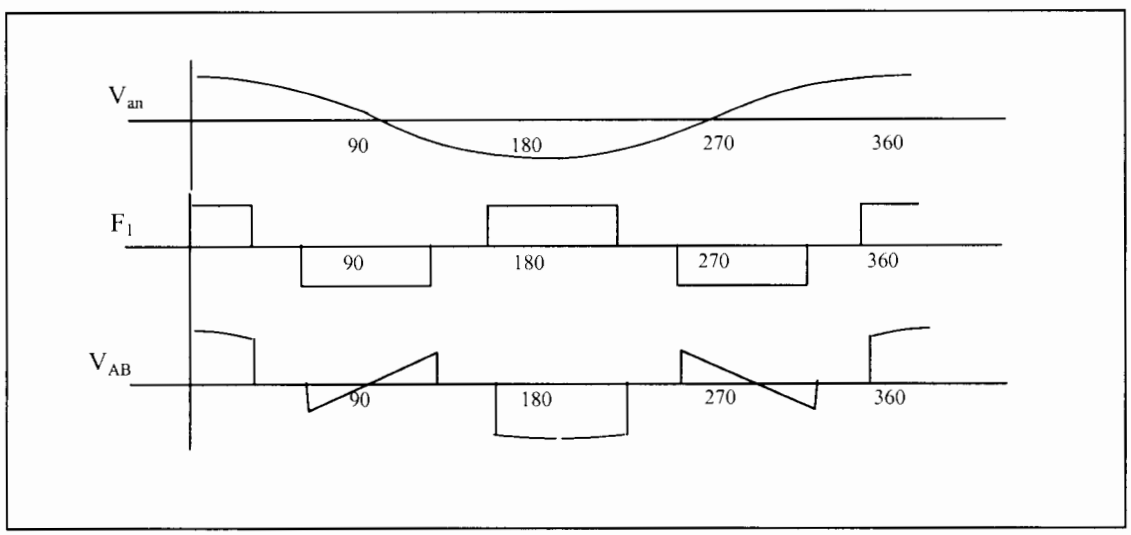

Figure 2.20 Waveforms describing basic operation of the single- to three-phase converter. (a) single-phase input voltage. (b) Converter switching function F_1. (c) Converter output voltage V_{AB}

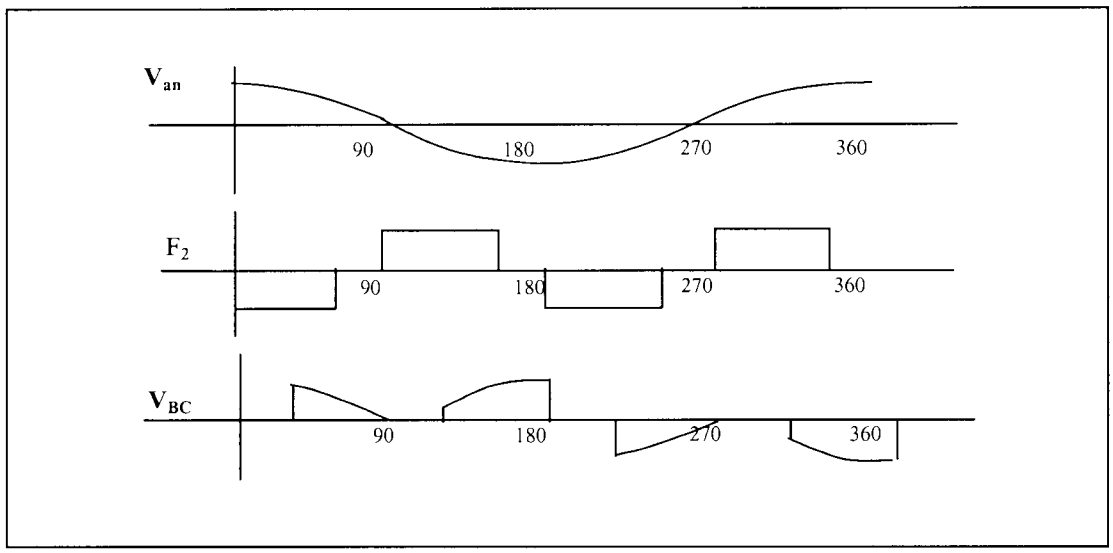

Figure 2.21 ***Waveforms describing basic operation of the single- to three-phase converter. (a) single-phase input voltage. (b) Converter switching function F_1. (c) Converter output voltage V_{BC}***

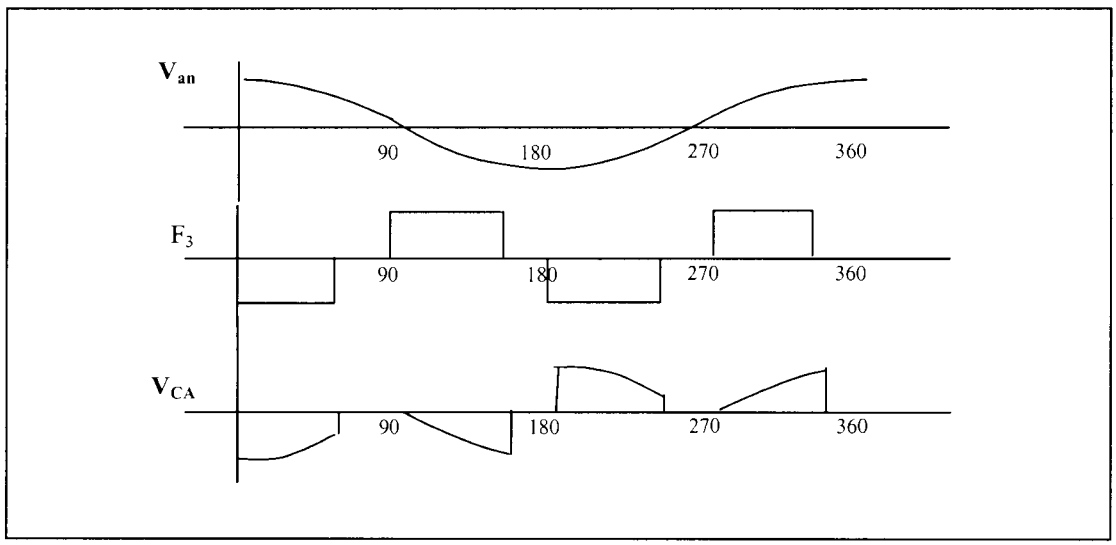

Figure 2.22 ***Waveforms describing basic operation of the single- to three-phase converter. (a) single-phase input voltage. (b) Converter switching function F_1. (c) Converter output voltage V_{CA}***

3 Load Balancing

3.1 Introduction

Loads in factories and rural distribution are seldom balanced, resulting in a deterioration of the power factor and voltage symmetry in the power system. This can cause overloading of one phase, the need to over-design transformers, cables and even circuit breakers. Normally, an attempt is made to distribute the load as equally as possible. However, this is not always possible for reasons such as:

- Unpredictable load patterns.
- Large single-phase load in comparison to total system load.
  (eg. Alternating-direct current railways and electric furnaces.)
- Uneconomical rewiring.
- Lack of time and capital to redistribute loads in existing factories.

Even with the best of efforts, loads are seldom better than 80% balanced.

The effect of voltage unbalance is severe on induction motors and three-phase power electronic converters and drives. In induction motors the effect of voltage unbalance is to circulate large currents in the rotor and to reduce the available output torque. Often the result of unbalanced operation is burn-out of the machine windings due to overheating. Measured rotor currents in induction motors operating with unbalanced voltages show that 5% unbalance can decreases motor life by up to 30% [1]. Moreover, some harmonics not present at symmetrical conditions occur in systems with non-linear loads. Thus, voltage asymmetry is considered a factor that deteriorates supply quality and, therefore, should be kept to an acceptable level. The unbalance caused by single-phase loads is mainly responsible for the voltage asymmetry, thus a balanced distribution of such loads is the prime method for voltage symmetrisation.

3.2 Phase Balancing of Single-Phase Loads

The flow of power in a single-phase circuit pulsates at a frequency equal to twice that of the alternate-current supply. Consequently, it is readily apparent that some means of energy storage is necessary in order to convert a single-phase load with pulsating power to a balanced load of constant power. In order to reduce the periodic variation in power, it is necessary, in general, to utilise load from some other phase on the system. Failure to recognise the significance of the pulsating character of single-phase loads has led to frequent proposal to draw equal current from the different phases. Typical of these schemes is the one shown below in Fig. 3.1 which has one winding reversed and which draws equal currents in the three phases.

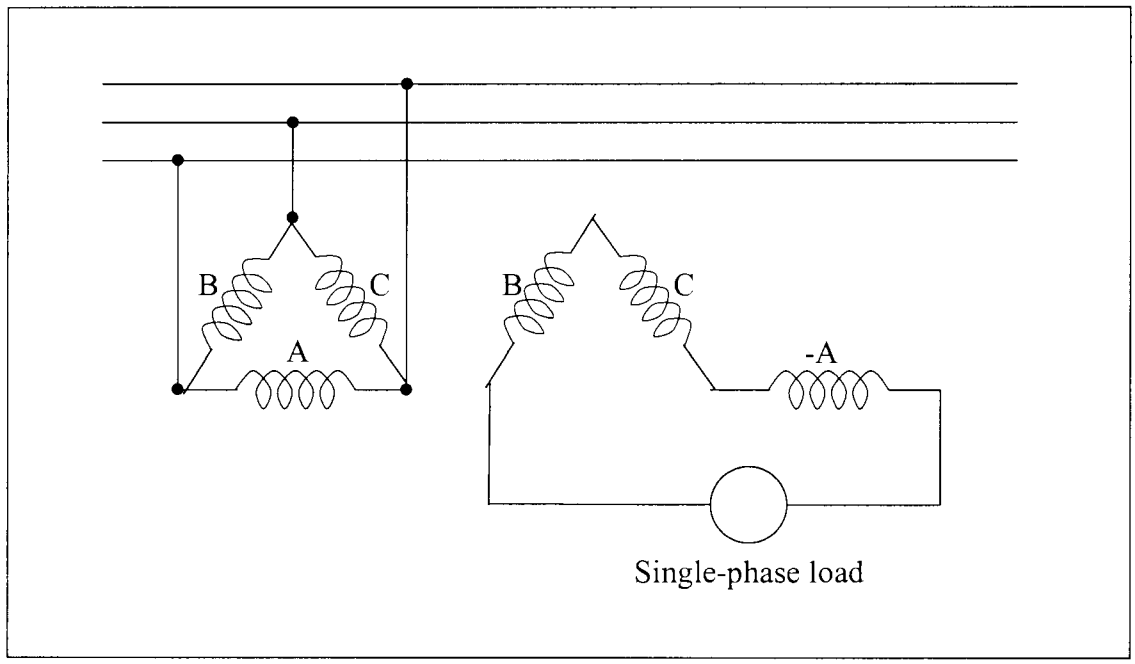

Figure 3.1 Unsound attempt to balance a single-phase load

A little consideration will show that additional apparatus capacity is required for handling a single-phase load but in spite of this the power remains single-phase in character. Consequently, nothing is gained by the use of the three-phase transformers and a single transformer is preferable. In case the load can be subdivided and distributed among the different phase, the balance of the system is of course greatly improved.

It is not necessary, however, to balance the loads by using identical impedance in the different phases. All that is necessary is that the total pulsating power be balanced. The fact that loads of different power factor on different phases can produce balanced power is illustrated in the connections of Fig. 3.2 which illustrates a two-phase generator supplying a transformer whose secondary is connected to form a two-phase three-wire system.

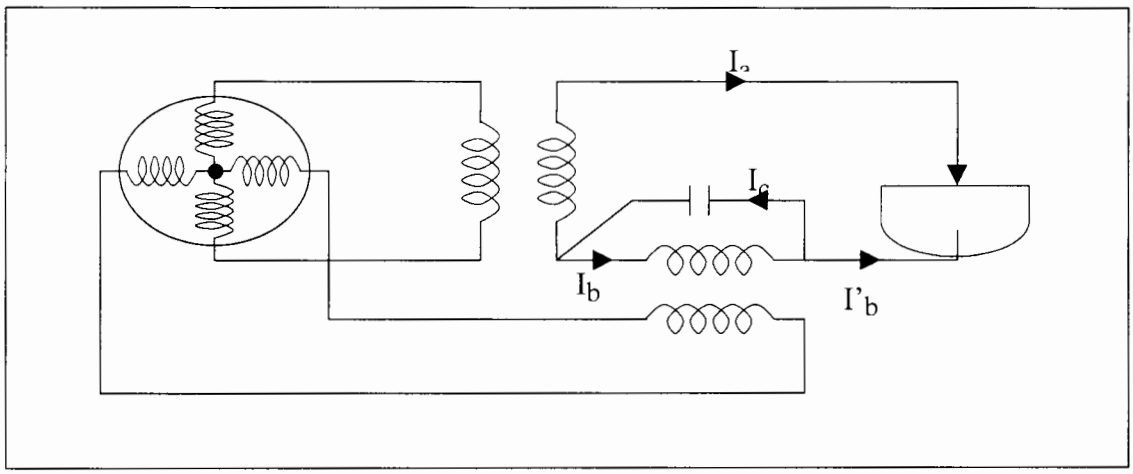

Figure 3.2 ***Diagram illustrating method of balancing single-phase resistance (furnace) load by adding a capacitor load to one phase***

With the *a* and *b* phases connected to the single-phase furnace load, as illustrated, the vector diagrams shown in Fig. 3.3 will result.

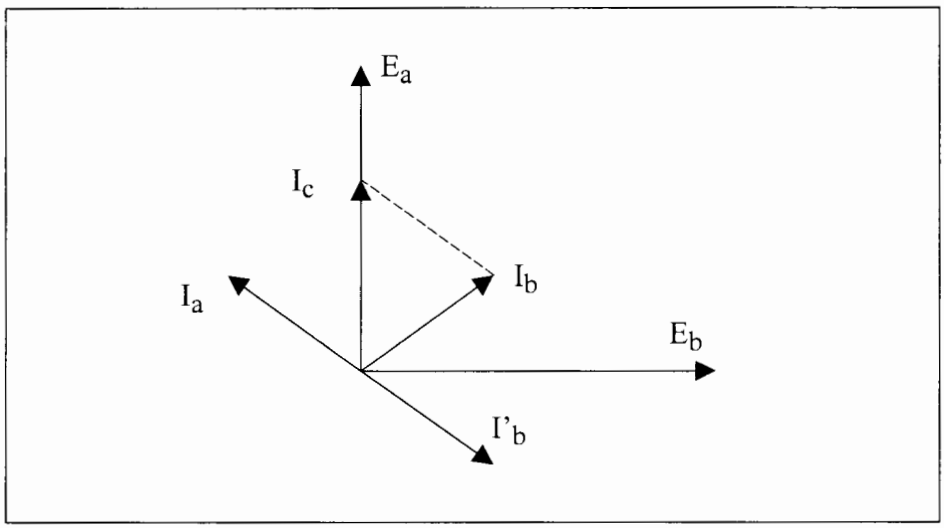

Figure 3.3 ***Vector diagram of single-phase furnace load with capacitive phase balancing***

By adding a capacitor connected across phase *b*, the total current on the supply lines will be indicated by the terms I_a and I_b which form a balanced system.

Another method of improving the balance of systems by static means is to alter the transformer ratios from their nominal values. For example, consider a three-phase generator supplying the principal load between phases *b* and *c* as illustrated in Fig. 3.4.

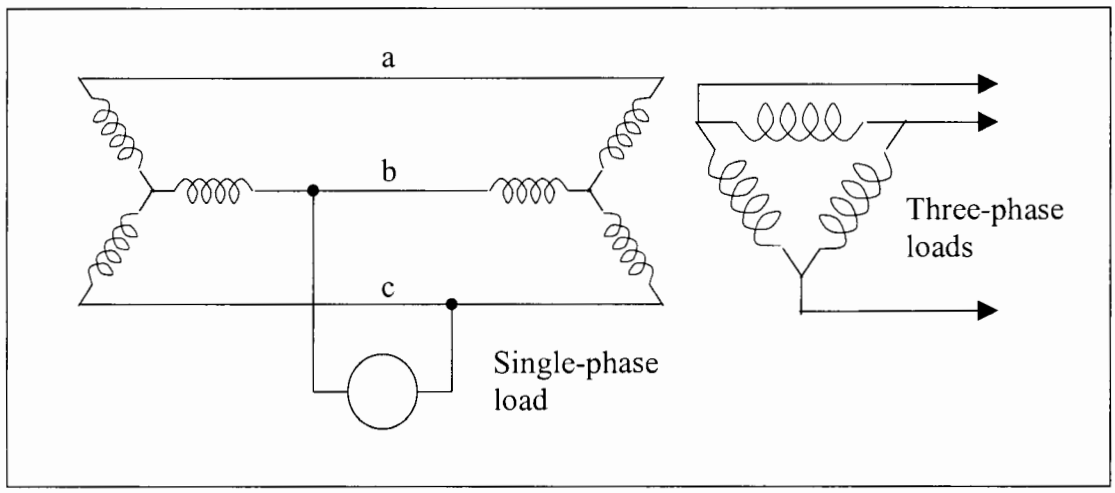

Figure 3.4 Method of using unsymmetrical transformer taps to improve balance on a three-phase circuit

Assume that the voltage is maintained constant across phases *b* and *c* under all load conditions. Then under light load conditions the voltage triangle *abc* will be substantially balanced, as shown in Fig. 3.5.

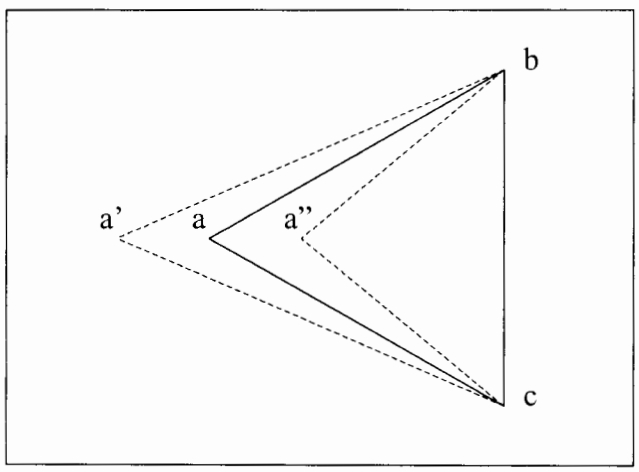

Figure 3.5 Voltage triangle of circuit in Fig 2.4

However, under heavy load conditions the unloaded phases will be of higher value and the voltage triangle is *a'bc*. Consequently, it is possible to choose the transformer ratios so that the system is approximately balanced under an average load conditions, being unbalanced in one direction under no load and unbalanced in the other direction at full load. This may be accomplished by adjusting the taps on the transformer windings to give *a"bc* under light load.

In connection with static methods for phase balancing, it is to be realised that if one load is variable, the other loads must be correspondingly adjusted if balance is to be maintained.

3.3 Rotating Balancers

Rotating balancers tend to balance the voltages and currents on a power system by periodically absorbing and restoring energy to the system using in the process the energy stored by the inertia of rotating parts. Thus rotating machines tend to provide balancing by inherent action and do not require the adjustable feature characteristic of static balancing systems. Rotating balancers are of two general types:

1. Negative-sequence e.m.f. generator.
2. Impedance-type balancer.

Balancers may also be classified as to their connection to the system which may involve either series or shunt connections or their combinations. The principal types of balancers will be taken up and discussed separately.

3.4 Negative-Sequence E.M.F.-Type Phase-Balancer

Probably the earliest proposal for obtaining accurate phase-balancing is that due to E.F.W. Alexanderson [18] and illustrated in Fig. 3.6.

The method is based on the idea of generating a negative-sequence e.m.f. of the proper magnitude and phase position to cancel the negative-sequence currents due to the single-phase loads, which flow through the generator and other symmetrical portions of the system.

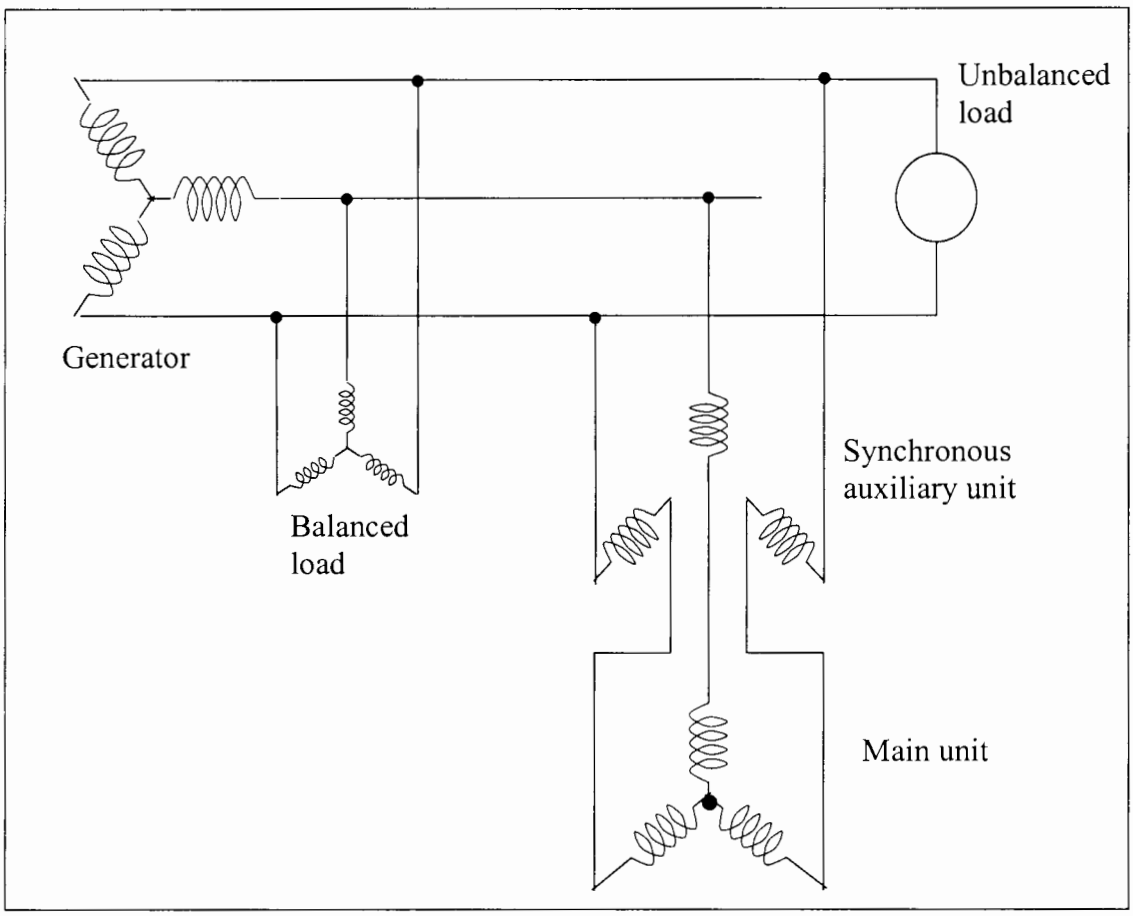

Figure 3.6 Negative-sequence e.m.f. type of phase balancer (Alexanderson)

This negative-sequence e.m.f. is generated in the auxiliary machine shown in the diagram which machine is mounted on the same shaft as the main unit and is provided with excitation in two axes so that the desired magnitude and phase relation can be controlled. The auxiliary machine is in series with the main unit that is of the ordinary synchronous condenser construction except for the heavy damper winding provided to take care of the negative-sequence current. The main machine draws balanced positive-sequence power from the system which the auxiliary generator converts to negative-sequence power and supplies to the system, thus cancelling the pulsating component of load in the generator and other symmetrical parts of the system.

3.5 *Impedance-Type Phase-Balancers*

The first proposal to use impedance-type balancers was due to C.L. Fortescue [18] who suggested the series impedance balancer illustrated in Fig. 3.7.

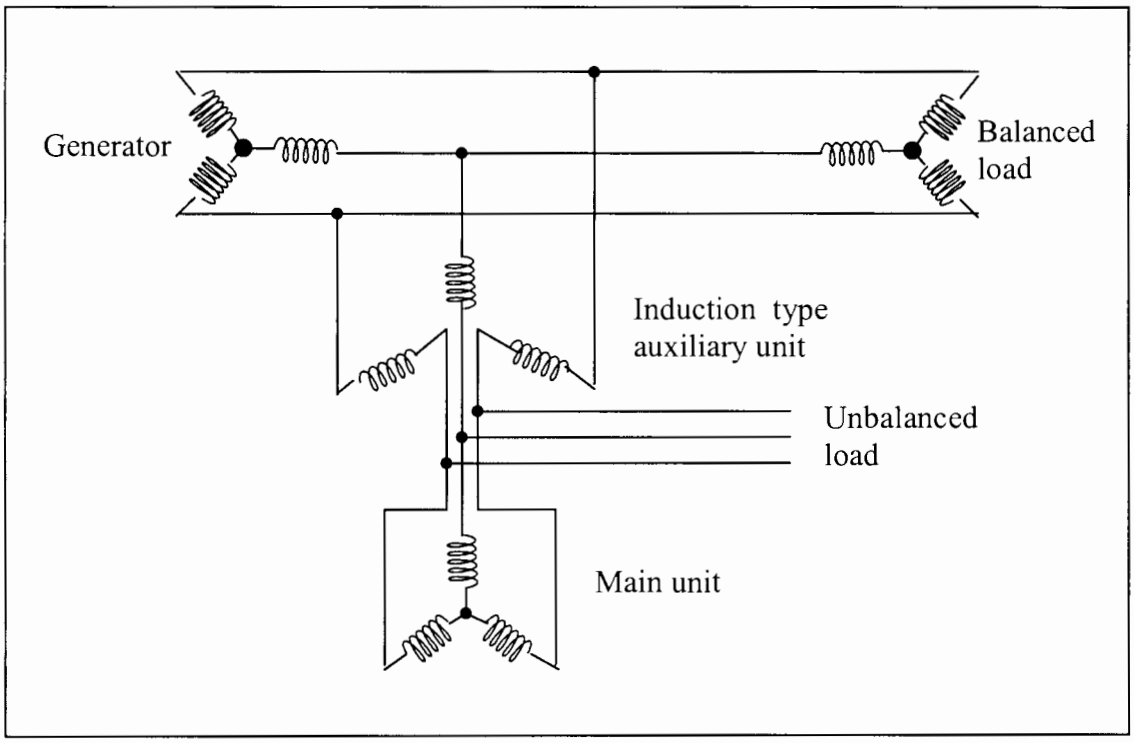

Figure 3.7 Series impedance type of phase balancer (Fortescue)

The auxiliary machine in this case is of the induction-motor type and is connected so that its phase rotating is opposite to that in which it would normally run as an induction motor. Consequently, the auxiliary machine offers very low impedance to positive-sequence currents and very high impedance to negative-sequence currents, and advantage is taken of this fact. The negative-sequence current required by the unbalanced load must, therefore, be supplied by the main unit, which may be of either the induction or synchronous types. The ratings of the auxiliary machine is determined by the impedance drop due to the negative-sequence current flowing through the main unit and the positive-sequence current flowing into the load.

Power-factor correction may be secured by the main units of either the Fortescue or Alexanderson-type of phase-balancer. Due to the fact that single-phase loads are frequently of low power-factor, the phase-balancing unit would normally be designed to give power-factor correction as well.

It might be pointed out that the shunt-type balancer requires automatic adjustments in the voltage regulator to correct for the change in the unbalanced conditions. Consequently, it will not be so rapid in its action generally as the inherent type of phase-balancer making use of the impedance principal, such as illustrated in Fig. 3.6. If the single-phase load can be segregated from the remainder, then the series machine will have its current rating determined by the positive-sequence component of the load. If the single-phase load cannot be segregated from a considerable amount of balanced load, the shunt-type balancer may be more attractive.

The shunt impedance balancer of Fig. 3.8 is the simplest scheme that has been proposed for phase-balancing.

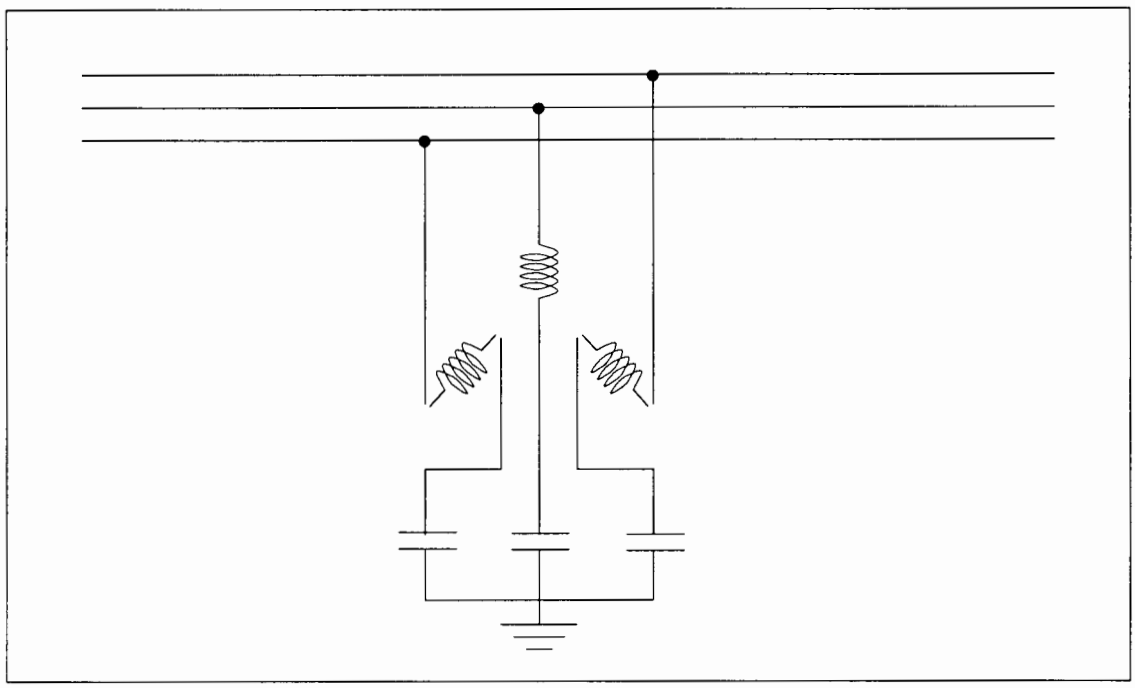

Figure 3.8 Shunt impedance balancer with series capacitor (Slepian)

This scheme, proposed by J.Slepian [18], uses a synchronous machine similar to the main unit of either of the previously described balancer and in the addition, in series with each phase, a set of capacitor of such value that the impedance to negative-sequence is made negligible. The arrangement will, therefore, prevent negative-sequence current from flowing past this shunt machine to the generator other balanced machines on the system. The scheme has not been used commercially but looks promising. The principal problem involves is in the protection of the series capacitor units at times of short-circuit. It has proposed to take care of this by connecting the capacitors in the circuit through transformers which would saturate for loads in excess of the normal rating of the balancer and thus prevent full balancing action, which greatly relieves the stresses due to short-circuit currents that would otherwise flow.

3.6 Adaptive Compensator for Unbalanced and Reactive Three-Phase Loads

The idea of simultaneously adaptive balancing and reactive compensation was formulated for the first time in 1975 by Gyuggi, Otto and Putman [3]. More recently in 1995 a new approach by Czarnecki [3] is based on the measurement and calculation of the specially defined equivalent susceptance, $\underline{Y}_e$, and unbalanced admittance $\underline{A}$ of the three-phase load. These parameters are given by Czarnecki [3] and conforms to the derived orthogonality between defined current components . His idea of unbalanced current was applied to a balancing compensator. This approach is not widespread. Admittances $\underline{A}$ and $\underline{Y}_e$ are related to the line to line admittances of the loads Y_{RS}, Y_{ST}, and Y_{TR} as shown in Eq. 3.1.

$$\underline{Y}_e = G_e + jB_e = \underline{Y}_{RS} + \underline{Y}_{ST} + \underline{Y}_{TR}$$

$$\underline{A} = -\left(\underline{Y}_{ST} + \underline{\alpha} \cdot \underline{Y}_{TR} + \underline{\alpha}^* \cdot \underline{Y}_{RS}\right)$$

Equation 3.1

where $\underline{\alpha} = e^{j2\pi/3}$ and asterisk denotes a conjugate number.

A passive compensator connected as shown in Fig. 3.9 can compensate entirely the unbalanced and reactive currents. It is built of three branches that provide controlled susceptances T_{RS} , T_{ST}, T_{ST}.

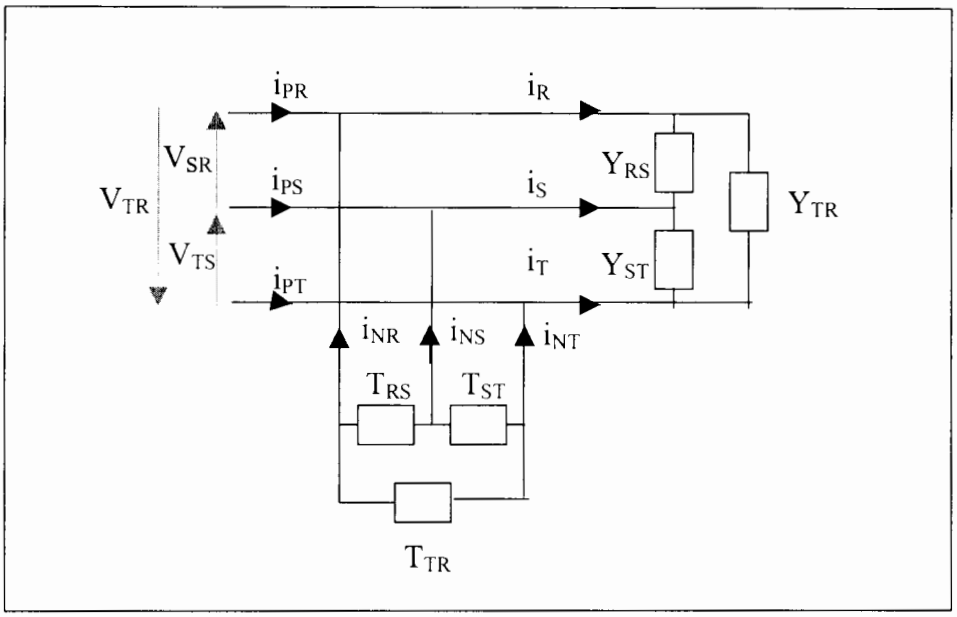

Figure 3.9 Three-phase load with balancing compensator

Czarnecki derives the necessary susceptances in term of his defined space phasor parameters B_e and $\underline{A}$. These are shown in Eq. 3.2.

$$T_{RS}=\frac{\left[\sqrt{3}\Re\underline{A}-\Im\underline{A}-B_e\right]}{3}$$

$$T_{ST}=\frac{\left[2\Im\underline{A}-B_e\right]}{3}$$

$$T_{TR}=-\frac{\left[\sqrt{3}\Re\underline{A}+\Im\underline{A}+B_e\right]}{3}$$

Equation 3.2

Thus only two complex parameters specify the susceptances necessary to compensate unbalance and reactive loads components. T_{RS}, T_{ST}, T_{TR} are pure **reactive** components and hence draw no active power.

3.7 Three- to Single-Phase Conversion as a Special Case of Load Balancing

The above theory is now applied to an unbalanced three-phase load consisting of only one load admittance with the other two equal to zero as shown in Fig. 3.10.

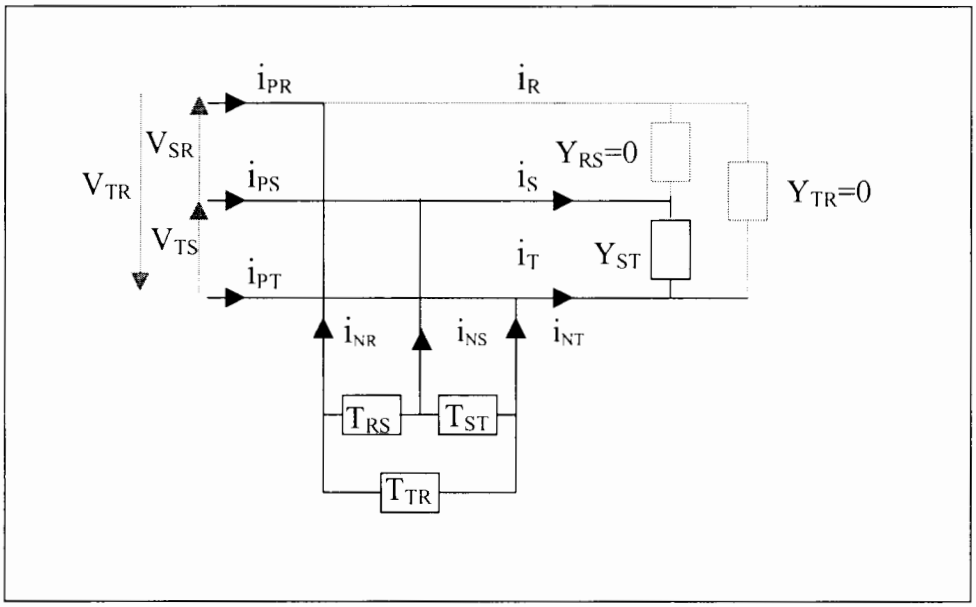

Figure 3.10 Load balancing of a single-phase load

The load is single-phase in nature. Admittances Y_{RS} and Y_{TR} are considered as open circuit, hence, $Y_{RS}=0$ and $Y_{TR}=0$. Substituting these values into Eq. 3.1 yields:

$$\underline{Y}_e=\underline{Y}_{ST}=G_l+jB_l$$

$$\underline{A}=-\underline{Y}_{ST}=-G_l-jB_l$$

Equation 3.3

Where G_l is the conductance and B_l is the susceptance of the single-phase load.

Substituting $\underline{Y}_e$ and $\underline{A}$ into Eq. 3.2 results in:

$$T_{RS}=\frac{\left[\sqrt{3}\cdot\Re(-G_1-jB_1)-\Im(-G_1-jB_1)-B_1\right]}{3}$$

$$T_{ST}=\frac{\left[2\cdot\Im(-G_1-jB_1)-B_1\right]}{3}$$

$$T_{TR}=-\frac{\left[\sqrt{3}\cdot\Re(-G_1-jB_1)+\Im(-G_1-jB_1)+B_1\right]}{3}$$

Which is simplified to:

$$T_{RS}=\frac{-1}{\sqrt{3}}G_1$$

$$T_{ST}=-B_1$$

$$T_{TR}=\frac{1}{\sqrt{3}}G_1$$

Equation 3.4

Therefore the three susceptances above would correct unbalance and reactive power seen by the three-phase supply.

If a balanced susceptance B_1 is added to T_{RS}, T_{ST}, and T_{TR} respectively. The following results are obtained:

$$T_{RS}=\frac{-1}{\sqrt{3}}G_1+B_1$$

$$T_{ST}=-B_1+B_1=0$$

$$T_{TR}=\frac{1}{\sqrt{3}}G_1+B_1$$

Equation 3.5

Thus the compensator reduces to two elements as shown in Fig. 3.11.

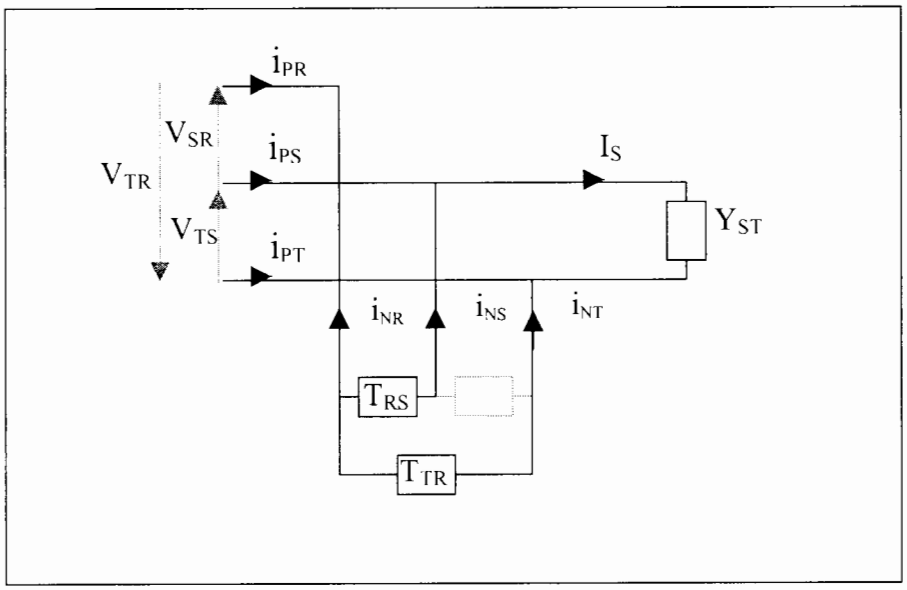

Figure 3.11 Two element compensator

It is noted that only two susceptances are necessary to balance the load. However the supply will now have to supply the **balanced reactive power** required by the three impedance B_1 that have been added. The three phase supply would have to deliver the active power $P=V^2G_1$ Watts of the single-phase load and the reactive power $Q= 3V^2B_1$VARS. The power factor would be Cos $(\arctan(3B_1/G_1))$.

The compensating susceptances ,T_{RS} and T_{TR} ,"inject" the negative sequence currents necessary to balance the unbalanced load single-phase load. The vector diagram of the positive- and negative sequence currents for the two element compensator supplying a **purely resistive load** can be seen in Fig. 3.12.

A derivation of the compensator currents, by Malengret [9], is given in Appendix A.

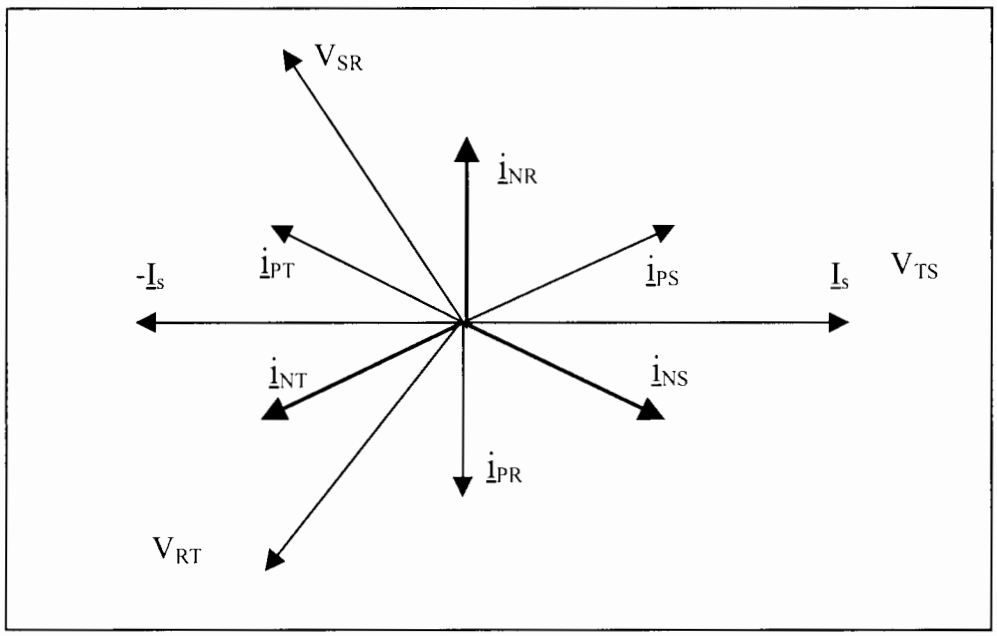

Figure 3.12 Balanced supply positive sequence current: $\underline{i}_{PS}$, $\underline{i}_{PT}$, $\underline{i}_{PR}$, compensator negative sequence current: $\underline{i}_{NS}$, $\underline{i}_{NT}$, $\underline{i}_{NR}$ and single phase load current $\underline{I}_s$

A relevant point to highlight is that for a purely resistive single-phase load, $\underline{i}_{NT} = \underline{i}_{PS}$ and $\underline{i}_{PT} = \underline{i}_{NS}$. The negative sequence components are the conjugates of the positive sequence.

The susceptances in Fig. 3.11 need to vary with the load in order to achieve a three-phase balanced supply. In this case the susceptances are of equal value but of opposite sign. The one is capacitive and the other inductive.

3.8 Single- to Three-Phase Conversion as a Special Case of Load Balancing

The circuit of the two-element compensator in Fig 3.11 is capable of bi-directional power flow. Thus it is possible to replace the single-phase load with a single-phase source and the balanced three-phase source with a **balanced** three-phase load, as is shown in Fig. 3.13.

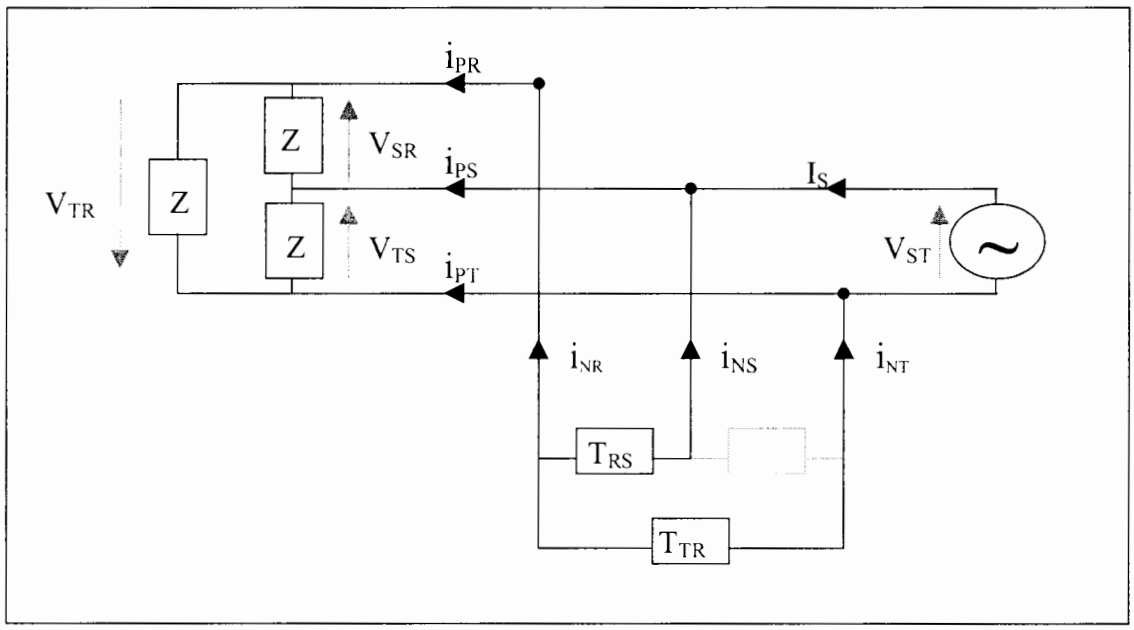

Figure 3.13 Two-element converter with reversed power flow

In this way it is possible to generate balanced three-phase power from a single-phase supply. The values of the susceptances, T_{RS} and T_{TR}, required to balance the load are determined by Malengret [9] as follows:

In order for the total load to draw balanced currents, the unbalanced impedances must be zero. Thus:

$$\underline{A}=Y_1+\alpha\cdot Y_2+\alpha^2\cdot Y_3=0$$

Therefore, rearranging we get:

$$\alpha\cdot Y_2+\alpha^2\cdot Y_3=-Y_1$$

Equation 3.6

Subsituting $\underline{\alpha} = e^{j2\pi/3}$ into Eq. 6 yields:

$$\left(\frac{1}{2}+j\frac{\sqrt{3}}{2}\right)(G_2+jB_2)+\left(\frac{1}{2}-j\frac{\sqrt{3}}{2}\right)(G_3+jB_3)=-G_1-jB_1$$

$$j\frac{\sqrt{3}}{2}(G_2+jB_2)+\frac{1}{2}(G_2+jB_2)-j\frac{\sqrt{3}}{2}(G_3+jB_3)+\frac{1}{2}(G_3+jB_3)=-G_1-jB_1$$

$$\frac{1}{2}j\sqrt{3}(G_2-G_3)+\frac{1}{2}\sqrt{3}(-B_2+B_3)+\frac{1}{2}(G_2+G_3)+\frac{1}{2}j(B_3+B_2)=-G_1-jB_1$$

Hence:

$$\frac{1}{2}(G_2+G_3)-\frac{1}{2}\sqrt{3}(B_2-B_3)=-G_1 \qquad \frac{1}{2}j(B_3+B_2)+\frac{1}{2}j\sqrt{3}(G_2-G_3)=-jB_1$$

or

$$2G_1=\sqrt{3}(B_2-B_3)-G_2-G_3 \qquad 2B_1=-\sqrt{3}(G_2-G_3)-B_2-B_3$$

If $G_2=G_3=0$, then:

$$B_2-B_3=2\frac{G_1}{\sqrt{3}} \qquad B_2+B_3=-2B_1$$

Hence:

$$B_2=\frac{G_1}{\sqrt{3}}-B_1 \qquad B_3=-\frac{G_1}{\sqrt{3}}-B_1$$

Now converting B_2 and B_3 to impedances gives.

$$Z_a=-\frac{j(X_1^2+R_1^2)}{X_1-\sqrt{3}R_1} \qquad Z_b=-\frac{j(X_1^2+R_1^2)}{X_1+\sqrt{3}R_1}$$

These are the same equations that are obtained by Holmes and Malengret in chapter 2.

4 Calculating the Motor Characteristics

4.1 Introduction

In this section the steady-state per-phase equivalent circuit parameters for the General Electric Company, 15kW, 3ϕ, 380 $V_{L\text{-}L}$, delta connected, four-pole, 50Hz, squirrel-cage induction motor are determined from the results of a no-load test, a locked-rotor test and from measurement of the d-c resistance of the stator winding. This is based on an example used by Sen [15]. These equivalent circuit parameters will then later be used to predict the performance of the machine mathematically with reasonable accuracy.

All measurements are taken using the Fuke 43 Power Quality Analyser. For both motor tests the following setup, as shown below in Fig. 4.1, is used.

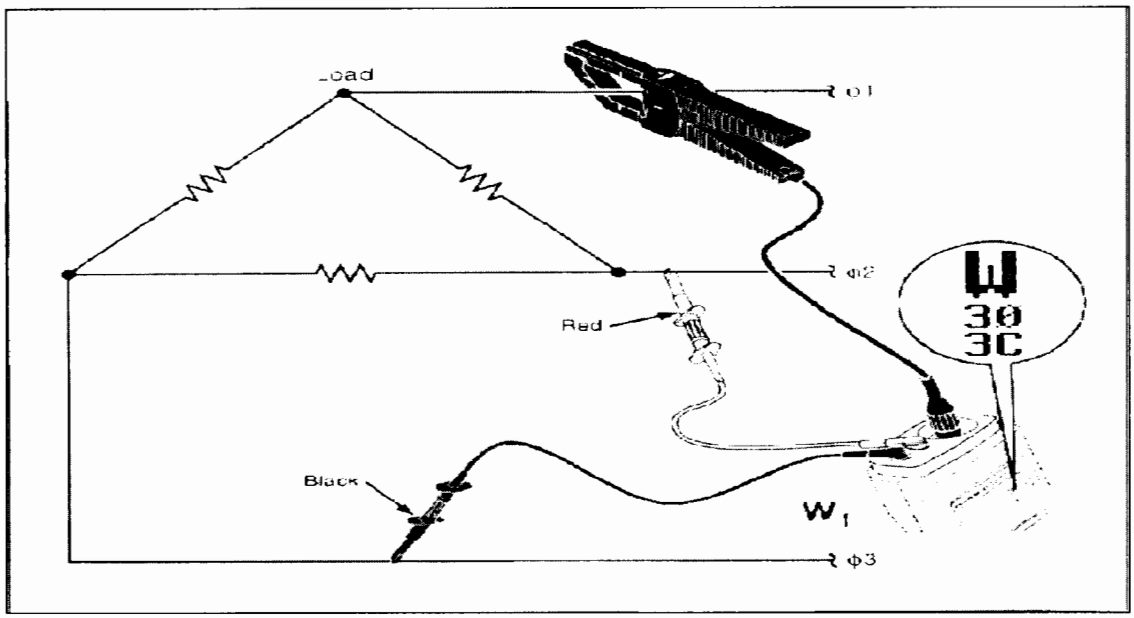

Figure 4.1 Diagram of Fluke 43 Power Quality Analyser in motor test circuit configuration

Measurement of the d-c resistance of the stator winding is accomplished with the use of a Wheatstone bridge. The d-c resistance of the stator was found to be 700mΩ.

4.2 The Complete Equivalent Circuit

The complete equivalent circuit for one phase of an induction motor is shown in Fig. 4.2 below.

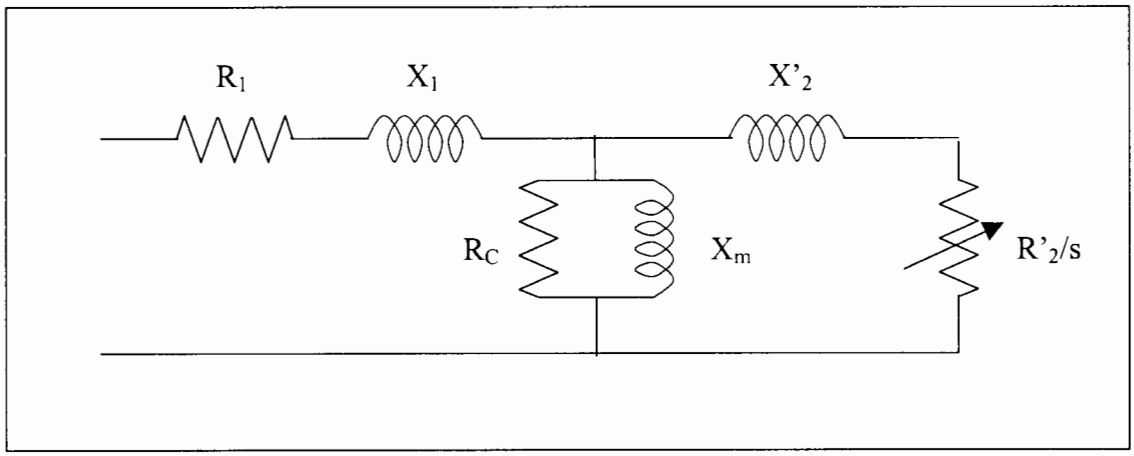

Figure 4.2 Per phase equivalent circuit of a three-phase induction motor

In the equivalent circuit above, the significance of the different parameters are as follows:

R_1 - represents the resistance of one phase of the stator.

X_1 - represents the leakage reactance of one phase of the stator circuit.

R_C - is the equivalent resistance for representing the core losses in the magnetic core due to hysteresis and eddy currents.

X_m - represents the mutual flux linkage common to both stator and rotor due to the magnetic flux linking with both the stator and the rotor windings.

X'_2 - is the rotor leakage reactance referred to the stator, and represents the flux linkage of the rotor due to the rotor currents.

R'_2 – is the equivalent rotor resistance referred to the stator that gives the correct rotor current when the rotor is rotating at slip *s*.

4.3 The IEEE Recommended Equivalent Circuit

In practice, it is usual to make an approximation in the equivalent circuit of Fig. 4.2. The modified equivalent circuit is shown in Fig. 4.3 below.

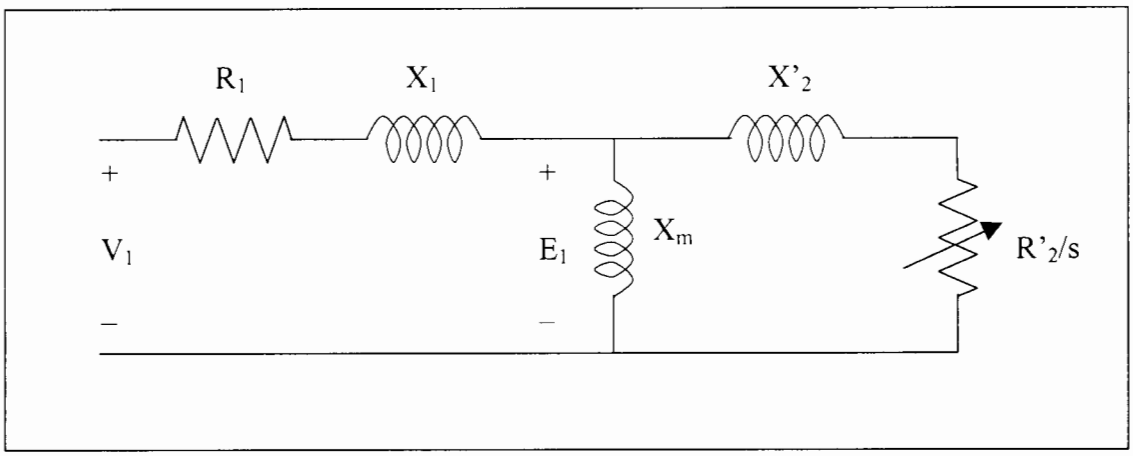

Figure 4.3 IEEE recommended per phase equivalent circuit of a three-phase induction motor

The simplification consists of removing R_c, which represents the core loss. When the resistance R_c is eliminated from the equivalent circuit, the core loss that it represents is included in the rotational power loss due to friction and wind resistance.

4.4 The Per Phase Phasor Diagram of the Motor

The phasor diagram based on the equivalent circuit of Fig. 4.3 is drawn in Fig. 4.4.

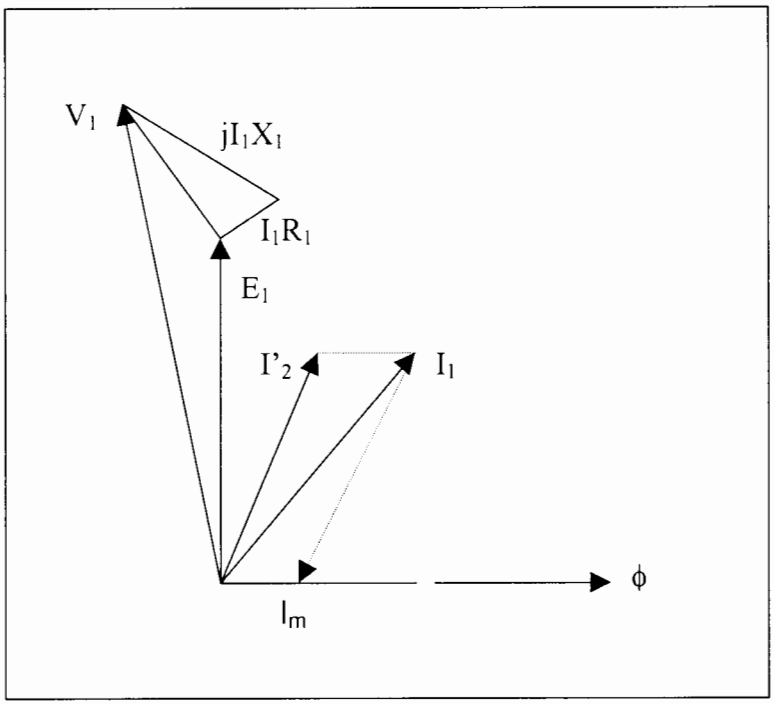

Figure 4.4 Phasor diagram for one phase of the motor

In this diagram the mutual flux labeled ϕ is taken along the horizontal reference direction. The magnetising current that is responsible for this mutual flux is labeled I_m and is drawn in phase with the mutual flux ϕ. The induced e.m.f. in the stator phase due to the mutual flux is labeled E_1, and leads the flux phasor by 90°. This is called the air-gap voltage, and is the voltage across the terminals of the reactor X_m in the equivalent circuit of Fig. 13. The rotor current I'_2 lags this voltage by the phase angle of the impedance $R'_2/s+jX'_2$. The stator phase current is the phasor sum of I'_2 and I_m. All quantities are as referred to the stator.

4.5 The No-Load Test

The no-load test of an induction machine gives information about the exciting current and the rotational losses. This test is performed by applying balanced 3ϕ voltages to the stator windings at the rated frequency. The rotor is kept uncoupled from any mechanical load. The small power loss in the machine at no load is due to the core loss and the friction and windage loss. The total rotational loss at the rated voltage and frequency under load is usually considered to be constant and equal to its value at no load. The equivalent circuit at no-load is shown below in Fig. 4.5.

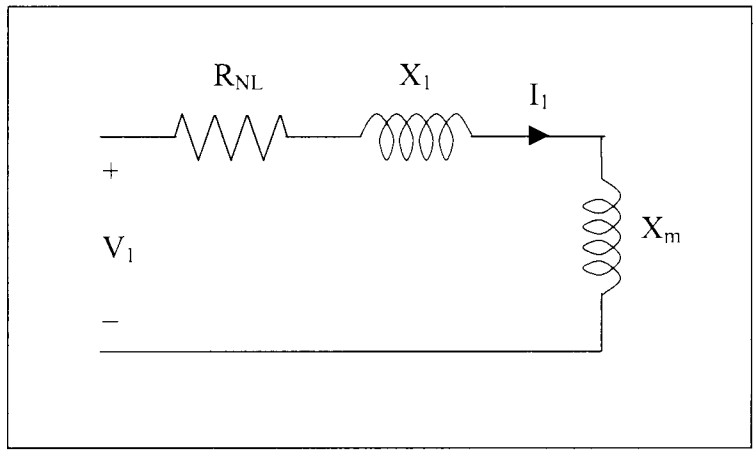

Figure 4.5 The no-load equivalent circuit

For no-load conditions R'_2/s is very high. Therefore, in the equivalent circuit of Fig. 4.5, the magnetising reactance X_m is in parallel with a very high resistance representing the rotor circuit. The total reactance of this combination is almost the same as X_m. The total reactance X_{NL}, measured at the stator terminals, is essentially $X_1 + X_m$. Test results obtained from the no-load test are given in the table below

Supply frequency	50 Hz
Line voltage [V_1]	380 V
Line current [I_1]	14.3 A
Input power [P_{NL}]	1400 W

Table of results from no-load motor test

The calculations are as follows:

The no-load impedance is:

$$Z_{NL}=\frac{V_1}{\frac{I_1}{\sqrt{3}}}=\frac{380\cdot\sqrt{3}}{14.3}=46.03\cdot\Omega$$

The no-load resistance is:

$$R_{NL}=\frac{P_{NL}}{3\cdot\left(\frac{I_1}{\sqrt{3}}\right)^2}=\frac{P_{NL}}{I_1^2}=\frac{1400}{14.3^2}=6.846\cdot\Omega$$

The no-load reactance is:

$$X_{NL}=\sqrt{Z_{NL}^2-R_{NL}^2}=\sqrt{46.03^2-6.846^2}=45.51\cdot\Omega$$

Note that:

$$X_1+X_m=X_{NL}=45.51\cdot\Omega$$

4.6 The Locked-Rotor Test

The locked-rotor test on an induction machine gives information about the leakage impedances. In this test the rotor is locked so that the motor cannot rotate, and balanced 3ϕ is applied to the stator terminals. The test is performed at a reduced voltage and rated current. Normally the frequency is also be reduced, because the effective rotor resistance and leakage inductance at the reduced frequency, corresponding to lower slip values, may differ appreciably from their values at rated frequency. However, the IEEE recommends that for normal motors of less than or equal to 15kW, the effects of frequency are negligible and the locked-rotor test can be performed directly at the rated frequency. The equivalent for the locked-rotor circuit is shown below in Fig 4.6.

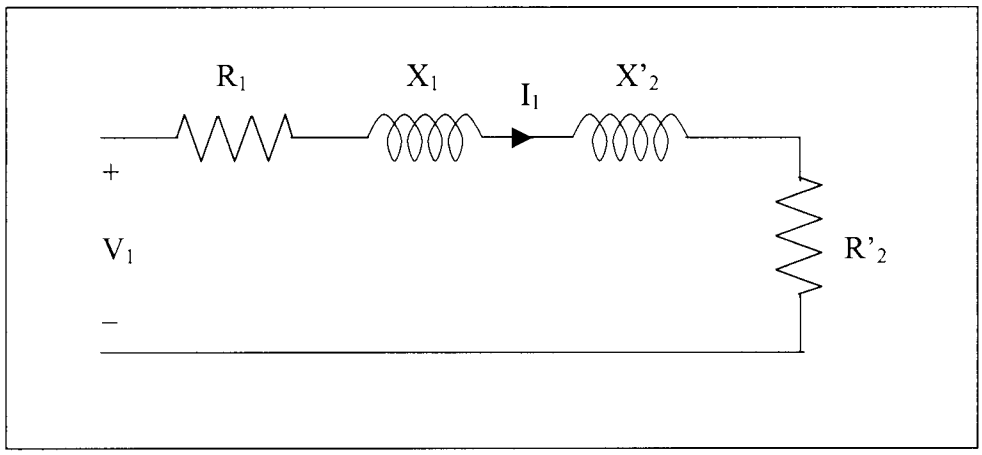

Figure 4.6 The locked-rotor equivalent circuit

For the locked-rotor test the slip is 1. The magnetising reactance X_m is in parallel with the low impedance branch $jX'_2 + R'_2$. Because $|X_m| >> |R'_2 + jX'_2|$, it can be neglected and the equivalent circuit for the locked-rotor test reduces to the form shown above in Fig 4.6.

Test results obtained from the locked-rotor test are given in the table below.

Supply frequency	50 Hz
Line voltage [V_1]	73.4 V
Line current [I_1]	30 A
Input power [P_{LR}]	1620 W

Table of results from locked-rotor motor test.

The calculations are as follows:

The locked-rotor resistance is:

$$R_{LR}=\frac{P_{LR}}{3\cdot\left(\frac{I_1}{\sqrt{3}}\right)^2}=\frac{P_{LR}}{I_1^2}=\frac{1620}{30^2}=1.8\cdot\Omega$$

Therefore:

$$R_2'=R_{LR}-R_1=1.8-0.7=1.1\cdot\Omega$$

The locked-rotor impedance is:

$$Z_{LR}=\frac{V_1}{\frac{I_1}{\sqrt{3}}}=\frac{V_1\cdot\sqrt{3}}{I_1}=\frac{73.4\cdot\sqrt{3}}{30}=4.238\cdot\Omega$$

The locked-rotor reactance is:

$$X_{LR}=\sqrt{Z_{LR}^2-R_{LR}^2}=\sqrt{4.238^2-1.8^2}=3.836\cdot\Omega$$

Note that:

$$X_{LR}\approx X_1+X_2'$$

Hence:

$$X_1=X_2'=X_{LR}=\frac{3.836}{2}=1.918\cdot\Omega$$

The magnetising reactance is therefore:

$$X_m=X_{NL}-X_1=45.51-1.918=43.59\cdot\Omega$$

The IEEE recommends a more accurate determination of R'_2. This is due to $R'_2 + jX'_2$ being in parallel with X_m . The following calculation is then used to determine R'_2 more accurately:

$$R_2=\left(\frac{X_2+X_m}{X_m}\right)^2 \cdot R=\left(\frac{1.918+43.59}{43.59}\right)^2 \cdot 1.1=1.199\cdot\Omega$$

4.7 The Complete Equivalent Circuit with Parameters

The calculations provide the information necessary to furnish the per phase equivalent circuit diagram with parameter values as shown below in Fig. 4.7.

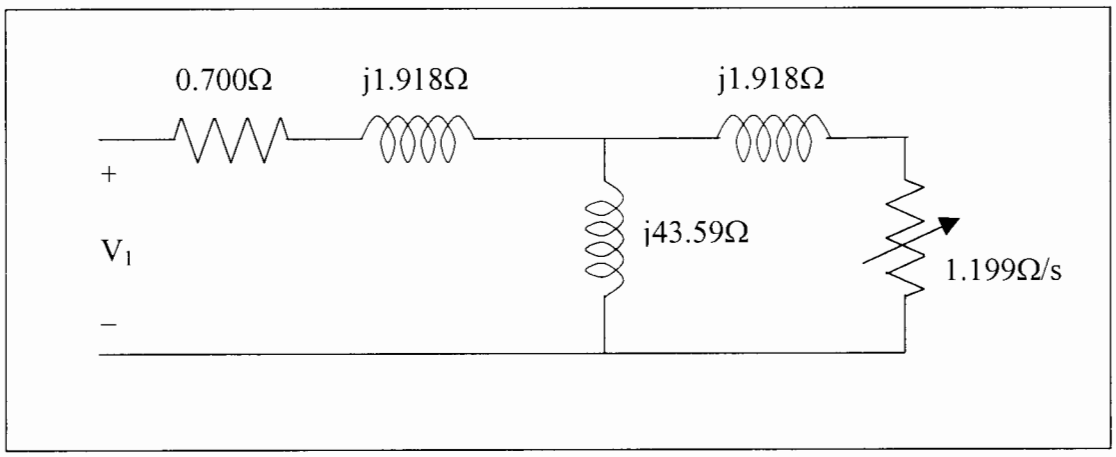

Figure 4.7 ***The complete IEEE recommended per phase equivalent circuit, with parameter values, for the 15kW motor***

With a full mathematical model of the motor available, it is now possible to analyse the motor and predict its performance.

5 Calculation of Compensating Elements

5.1 Introduction

In this chapter the compensating elements required to achieve balanced motor currents are calculated. The equations used are those derived by Holmes [5] and confirmed by Malengret [9], in chapter 2, section 2.2.3, for a two element phase converter.

The equations are repeated below for clarity:

$$Z_a = -\frac{j(X_l^2 + R_l^2)}{X_l - \sqrt{3} \cdot R_l} \qquad Z_b = -\frac{j(X_l^2 + R_l^2)}{X_l + \sqrt{3} \cdot R_l}$$

If stray series resistance is neglected, the above equations will ensure the conditions required for exact phase balance. In order to find the correct values of X and R for each of the above equations we need to solve the following equation over the full slip range of the motor.

$$Z = R + jX$$

Where Z is the per phase impedance, R the per phase resistance and X the per phase reactance, of the motor for a particular value of slip. This is achieved by reducing the equivalent circuit of the induction motor.

5.2 Reducing the Equivalent Circuit of the Induction Motor

The equivalent per phase circuit of the induction motor is shown below in Fig. 5.1.

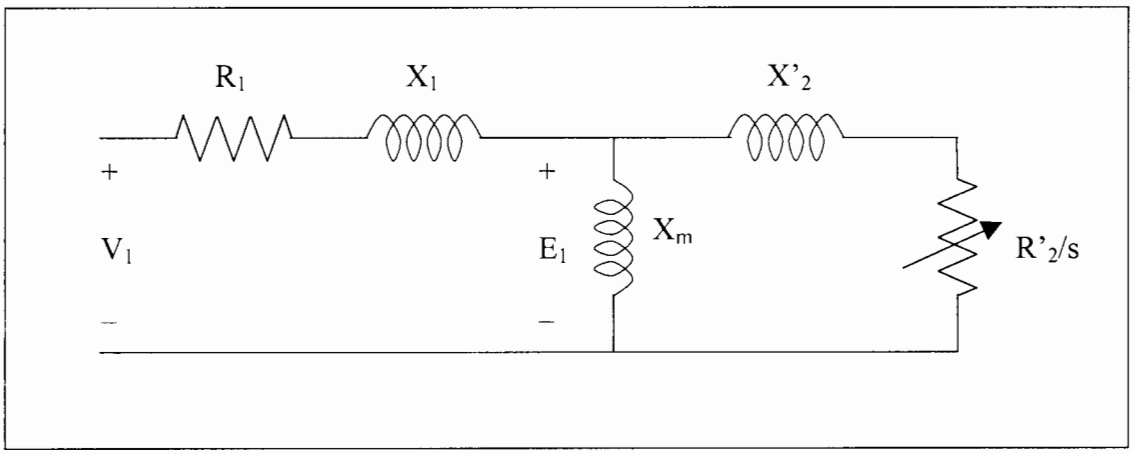

Figure 5.1 Per phase equivalent circuit of the induction motor

It is possible to reduce the above circuit to a single resistance in series with a reactance equivalent as shown in Fig. 5.2.

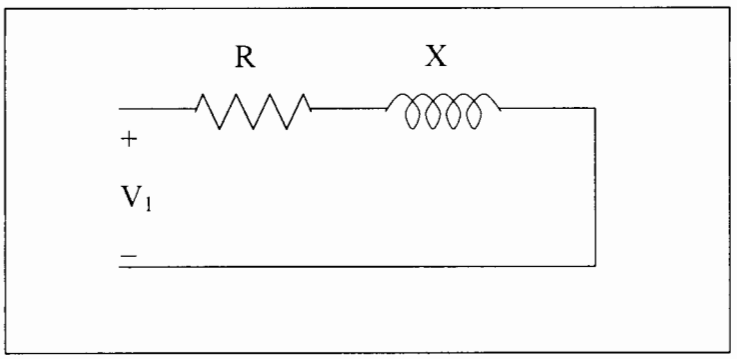

Figure 5.2 Reduced per phase equivalent circuit of the induction motor

Mathematically it is reduced as follows:

Being in series R'_2/s is added to X'_2:

$$\frac{R_2'}{s} + jX_2'$$

This combination is then placed in parallel with X_m:

$$\frac{1}{\frac{1}{\frac{R_2'}{s}+jX_2'}+\frac{1}{0+jX_m}}$$

Being in series R_1 is added to X_1, which is added to the combination:

$$R_1+jX_1+\frac{1}{\frac{1}{\frac{R_2'}{s}+jX_2'}+\frac{1}{0+jX_m}}$$

R is found by taking the real part, and X the imaginary part, of this equation.

$$R=\Re\left(R_1+jX_1+\frac{1}{\frac{1}{\frac{R_2'}{s}+jX_2'}+\frac{1}{0+jX_m}}\right) \qquad X=\Im\left(R_1+jX_1+\frac{1}{\frac{1}{\frac{R_2'}{s}+jX_2'}+\frac{1}{0+jX_m}}\right)$$

If external components are added such as staring resistors, to limit the initial inrush current, and compensating capacitors, to improve the power factor, as shown in Fig. 5.3, the circuit can be reduced in the same manner as shown previously.

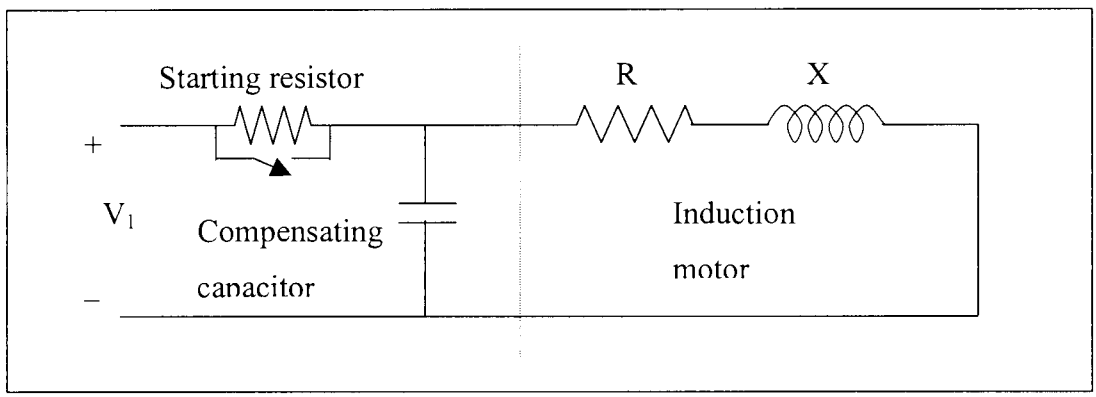

Figure 5.3 Equivalent per phase circuit of the induction motor with additional components

The circuit is reduced and the equations for R and X become:

$$R=\Re\left(\frac{1}{\frac{1}{R_1+jX_1+\frac{1}{\frac{1}{\frac{R_2'}{s}+jX_2'}+\frac{1}{0+jX_m}}}+\frac{1}{0+jX_{comp}}}+R_{start}\right)$$

and

$$X=\Im\left(\frac{1}{\frac{1}{R_1+jX_1+\frac{1}{\frac{1}{\frac{R_2'}{s}+jX_2'}+\frac{1}{0+jX_m}}}+\frac{1}{0+jX_{comp}}}+R_{start}\right)$$

5.3 Calculating the Compensating Element Values

The equations determined are used in a spreadsheet to determine the values of R and X for the slip range of the motor. The values of R and X for every slip value are then substituted into the following formulae.

$$Z_a=-\frac{j\left(X_1^2+R_1^2\right)}{X_1-\sqrt{3}\cdot R_1} \qquad Z_b=-\frac{j\left(X_1^2+R_1^2\right)}{X_1+\sqrt{3}\cdot R_1}$$

The calculated reactances from these formulae are then converted to corresponding values of inductance and capacitance for the compensating elements.

The following well-known expressions are used:

$$X_L = j \cdot w \cdot L \qquad X_c = \frac{1}{j \cdot w \cdot C}$$

Where L is in Henries and C is in Farads.

It is found that a capacitor of 50uF placed across each phase of the motor results in the most favourable spread of values for the compensating elements. The graph of these results is shown in Fig. 5.4.

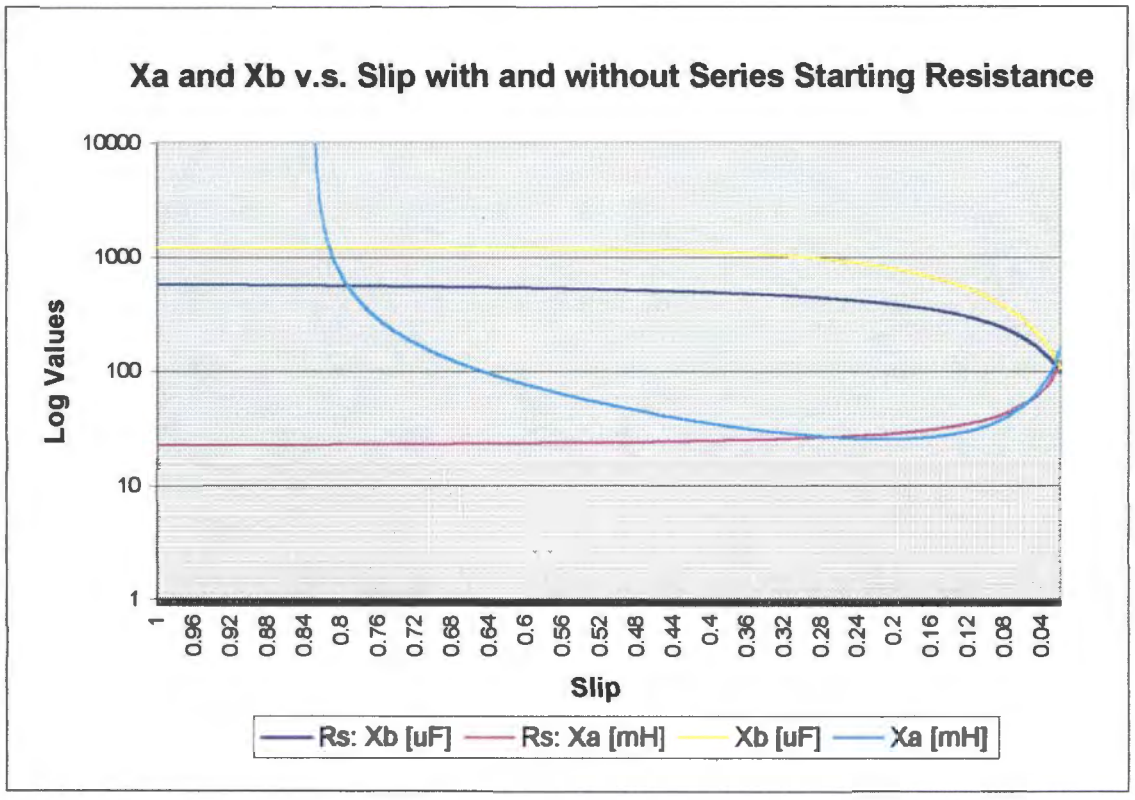

Figure 5.1 Graph of compensating elements vs. slip with and without starting resistance

To limit the initial inrush current to 200% of the rated motor current, a 2.5Ω 60 Amp resistor is placed in series with each of the supply lines of the motor. The resistors are constructed from quarter inch, stainless steel, band strapping, supported from brass cup-hooks, mounted on rectangular wooden frames. Digital images of the actual constructed resistors are shown in Fig 5.5 and 5.6. The resistors have the additional affect of not only lowering the values of compensating elements required, but also flattening out the curve, thus requiring less change in these values.

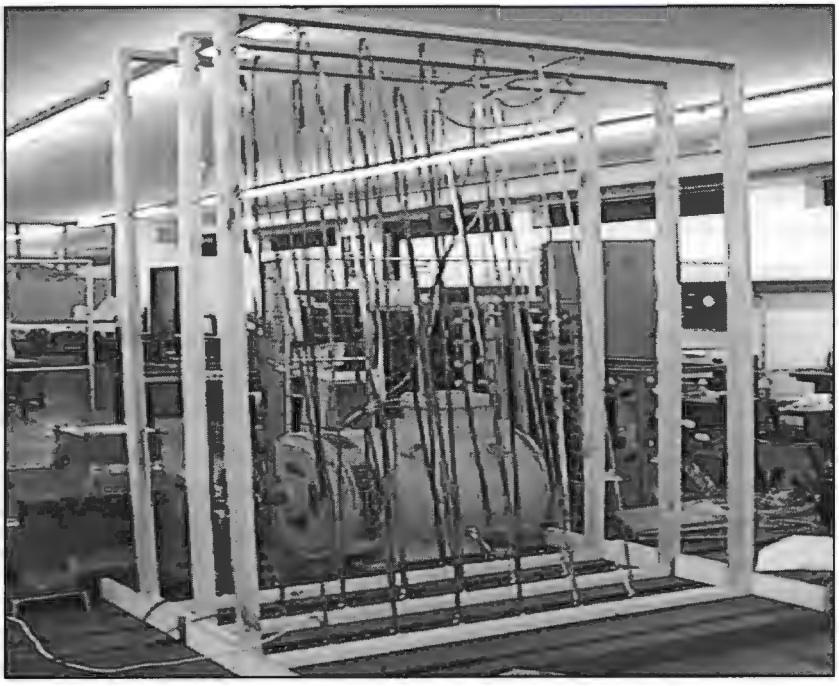

Figure 5.5 Constructed power resistors

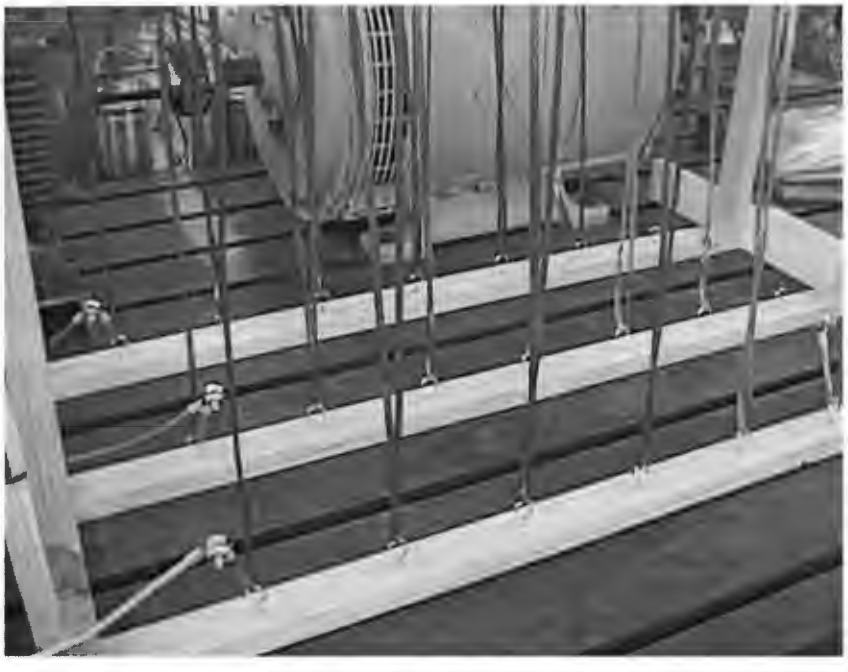

Figure 5.6 Close-up of frame and connections of constructed resistors

6 The Saturable-Core Reactor

6.1 Introduction

This section, which is largely based on Matsch [10], introduces the concept of the saturable-core reactor. The principle of operation is then discussed together with the various configurations that can be employed. Finally the advantages, disadvantages and limitations are addressed.

6.2 Principle of Operation of the Saturable-Core Reactor

The saturable-core reactor is an iron-core inductor, the inductance of which is a function of the current in a separate, d-c control winding. It is therefore possible to obtain a variable inductance, simply by altering a d-c control current. The effect of the control current is to vary the permeability of the core by saturating it with a constant magnetic field. Varying the degree of saturation alters the relative inductance of the reactor. The higher the saturation, the lower the inductance and vice versa. It should be made clear from the beginning that the saturable-core reactor does not act as a transformer.

6.3 The Single-Core Saturable Reactor

This is the simplest form of saturable reactor, with a d-c winding that provides premagnetisation and with an a-c winding to which the current is controlled by varying the amount of premagnetisation.

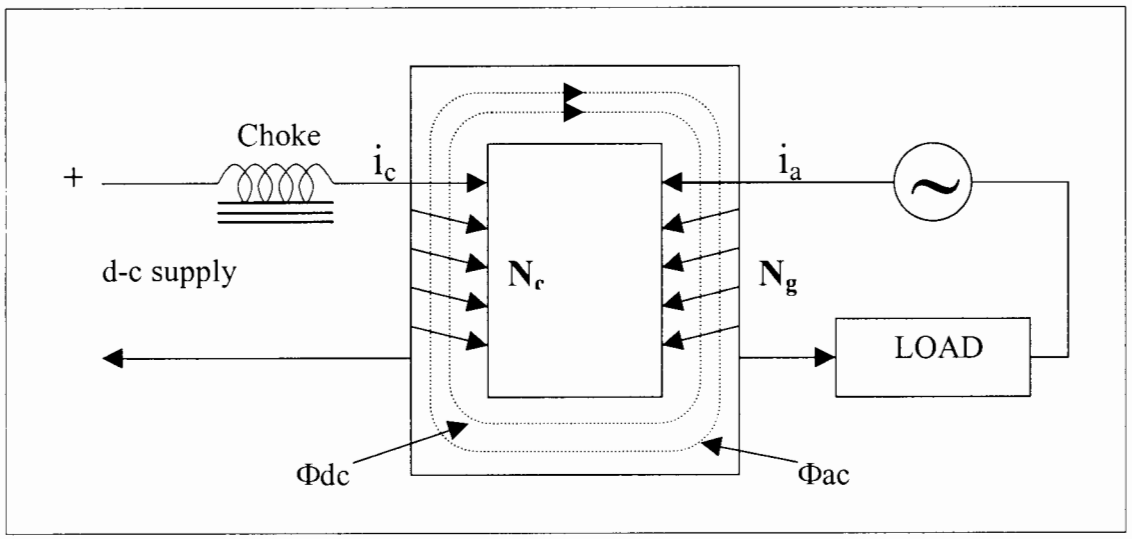

Figure 6.1 Single-core saturable reactor circuit

Fig. 6.1 is a schematic diagram of a single-core reactor with a d-c winding of N_c turns and an a-c winding, also known as the gate winding, of N_g turns. Although the core in the diagram above is rectangular, it may, however, be toroidal or any other convinient shape. To ensure good efficiency and regulation, the resistance of the gate winding must be low when referred to the load impedance. In this case it is necessary to keep the impedance of the control circuit high by inserting an external choke in series with the control winding, in order to prevent the control circuit acting as a short circuited secondary with the a-c winding as the primary. Without this high impedance in the control circuit, the impedance of the reactor, as seen from the a-c winding, would be low, being practically equal to the leakage impedance. Consequently, the controle current would lose most of its effect on the output current, since the leakage flux paths are mainly throught the air.

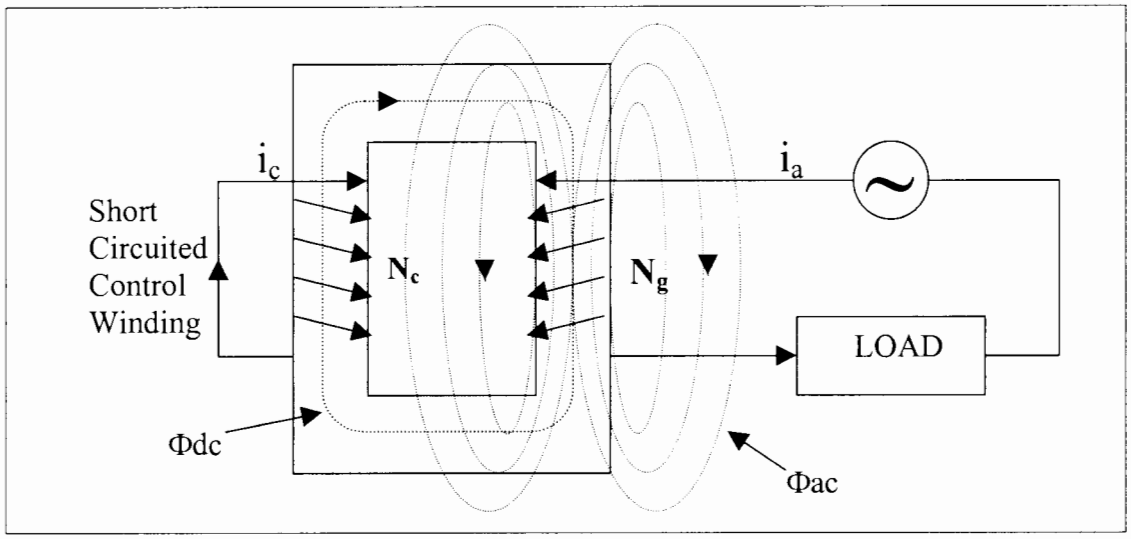

Figure 6.2 Single-core saturable reactor with short-circuited control winding, showing flux paths through the air

Fig. 6.2 shows the effect of not having the choke present in the control winding circuit. The series choke provides a means not only for preventing the a-c component of the current in the control winding from damaging the d-c control power supply, but also from causing the situation in Fig. 6.2 explained earlier. In order for the choke to provide a high impedance , it must have an inductance of several Henries. To obtain this it must have an iron core and an air gap to prevent saturation from the direct current. A choke meating these criteria will in many cases be as large as the saturable core reactor.

If core losses are neglected;

- The reactance is infinite when the a-c flux is confined to the unsaturated region. This occurs when there is no premagnetisation, hence no control current.
- The reactance is zero when the a-c flux is confined entirely to the saturated region. This occurs when a sufficiently large d-c premagnetising current is applied.

In the unsaturated interval, the total mmf in the reactor must be zero. If N_G and N_C are the turns in the output and control windings with i_A and i_C being the respective currents flowing in them, then for the current directions shown in Fig. 6.1, the output current i_a is:

$$i_a = -\frac{N_C}{N_G} i_c$$

During the saturated interval the voltage in the a-c winding is zero, and the current i_a in a noninductive load with a resistance of R_L would be:

$$i_a=\frac{\sqrt{2}\cdot V}{R_L+R_G}\sin(w\cdot t)$$

Where R_G is the resistance of the a-c winding of the reactor and the voltage of the a-c source is:

$$v=\sqrt{2}\cdot V\sin(w\cdot t)$$

The saturable reactor can therefore adjust the output current from a very low value to a maximum of:

$$I=\frac{V}{R_L+R_G}$$

Although a large variation in inductance is possible, the waveform of the current, while almost sinusoidal at maximum inductance, is quite distorted at smaller values.

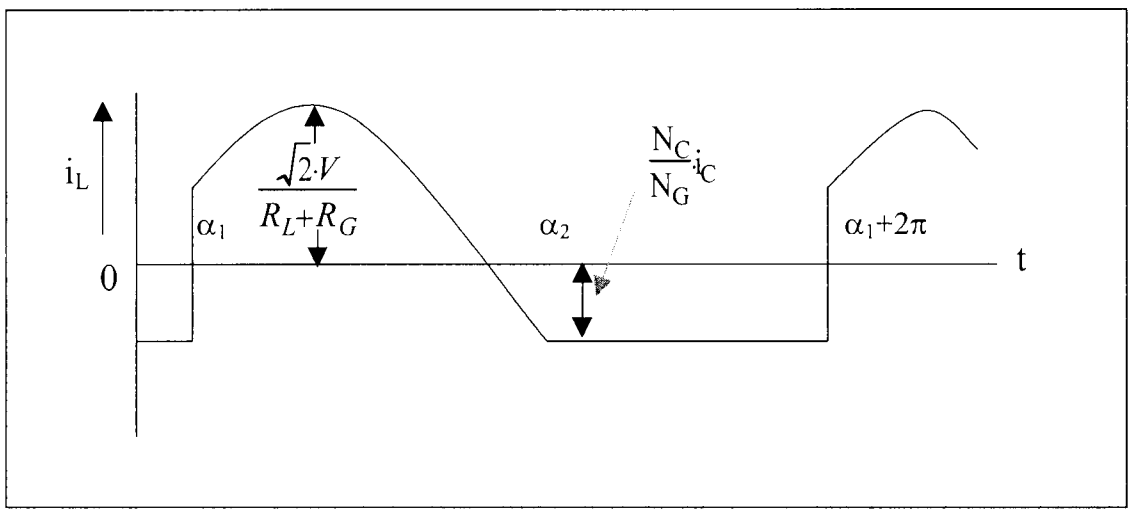

Figure 6.3 Typical output current wave shape from a single-core reactor

As is seen in Fig. 6.3, the waveform of the output current is unsymmetrical over a large part of the operating range.

It is for this reason that the single-core premagnetised saturable reactor is seldom used. In addition, were speed of response is important, there is the disadvantage of a high time constant due to the choke in the control circuit.

6.4 The Twin-Core Saturable Reactor

The disadvantages of the unsymmetrical current waveform and the need for a choke in the control circuit of the single-core saturable reactor are overcome in the twin-core saturable reactor of Fig. 6.4.

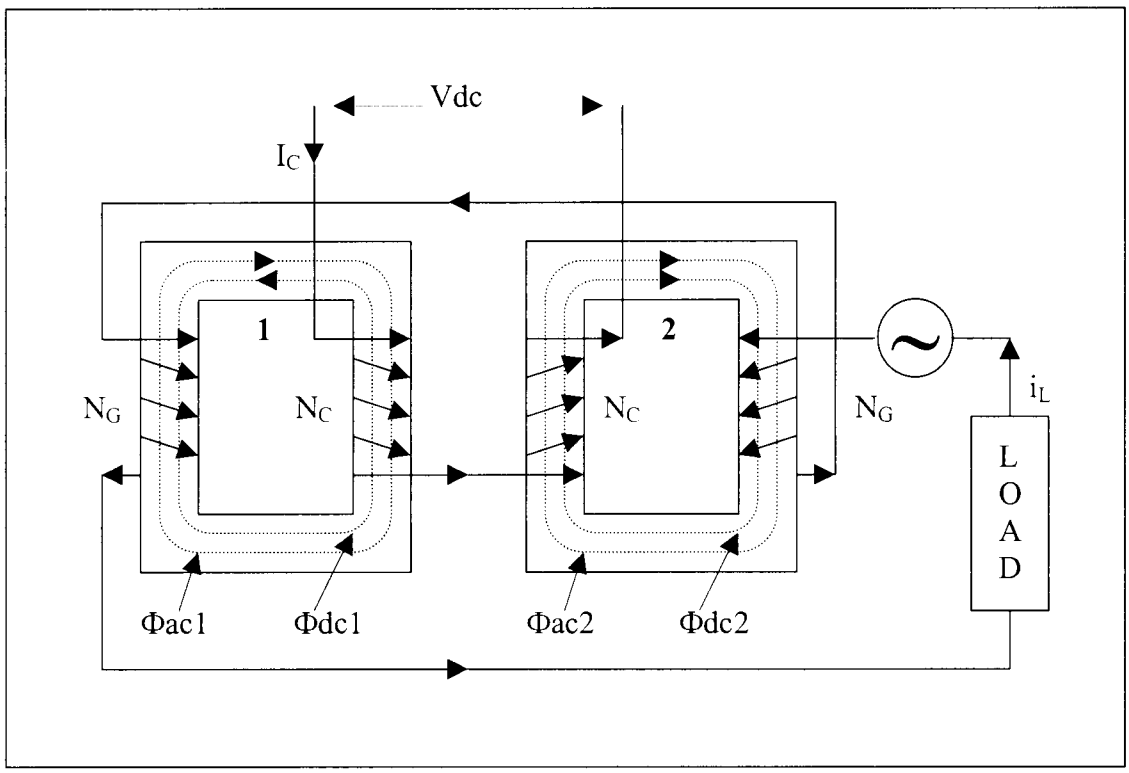

Figure 6.4 Twin-core saturable reactor with series connected a-c windings

The twin-core reactor in Fig. 6.4 is comprised of two identical transformers, 1 and 2, each having a control winding of N_C turns and an output winding of N_G turns. The d-c control windings are connected in series with the same polarity. The a-c output windings are connected with opposite polarity in order to produce fluxes of opposite orientation within the two cores. The reason for this is to cancel out the otherwise

high a-c voltage induced in the control windings, by transformer action, by ensuring that they are of opposite polarity. The result of this is zero net a-c voltage on the control windings. This simplifies the control circuitry by no longer requiring a choke to block the a-c voltage as is necessary in the single-core reactor.

In Fig. 6.4 the a-c output windings are connected in series, however parallel connection is also possible as is shown in Fig. 6.5 below.

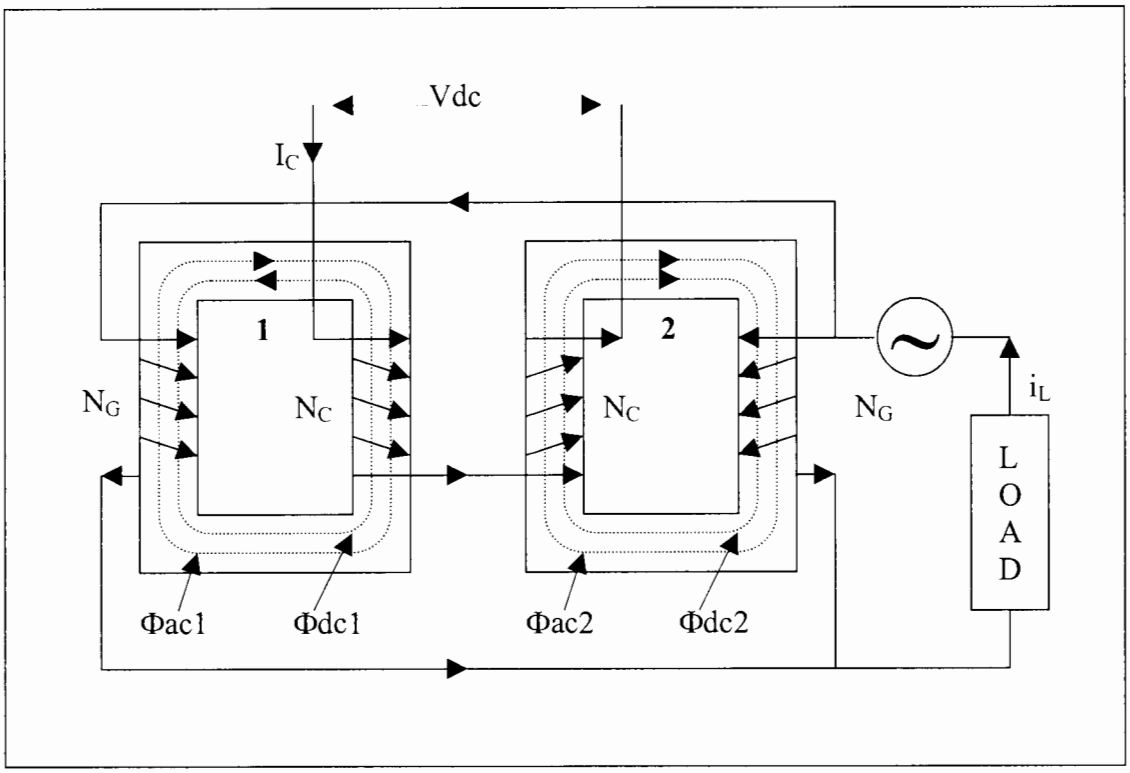

Figure 6.5 Twin-core saturable reactor with parallel connected a-c windings

In both cases extreme caution must be taken to observe that the correct polarity is maintained. Failing to do this will result in hazardous voltages being generated at the terminals of the control winding through transformer action.

The principle of operation of the series- and parallel-connected reactors is identical, producing the same current output waveform shown in Fig. 6.6.

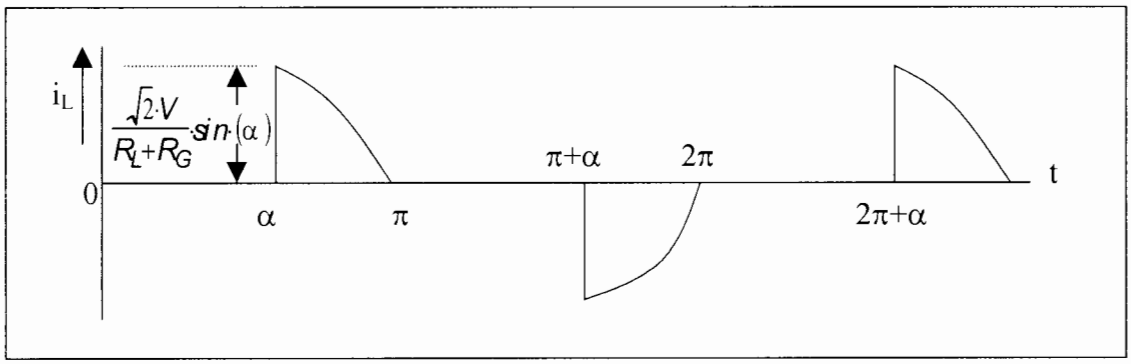

Figure 6.6 Typical current output wave shape from a twin-core reactor

In the table below the advantages and disadvantages of series- and parallel-connected a-c windings are summarised.

	Series	Parallel
Advantages	Larger overall inductance	Smaller overall inductance
Disadvantages	Higher internal resistance	Lower internal resistance

6.5 Three-Legged Core Saturable Reactor

As for the twin-core reactor the disadvantages of the unsymmetrical current waveform and the need for a choke in the control circuit of the single-core saturable reactor are overcome in the three-legged core saturable reactor of Fig. 6.7.

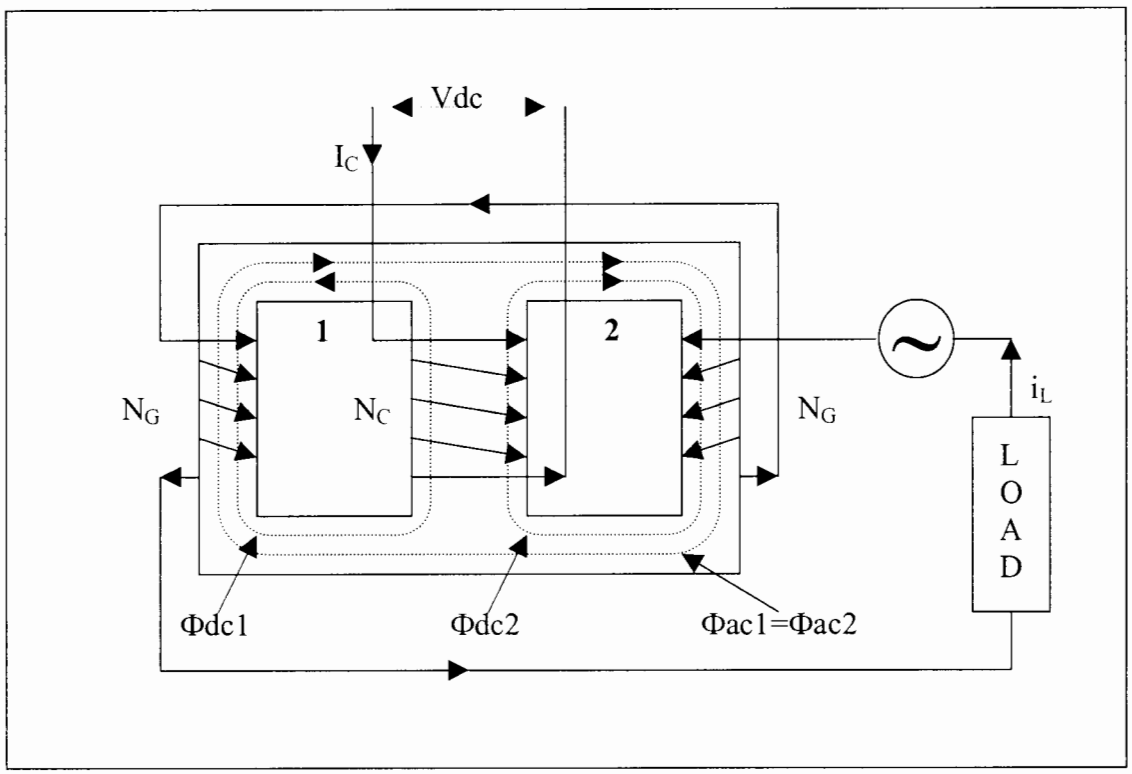

Figure 6.7 Three-legged core saturable reactor with series connected a-c windings

The three-legged core reactor in Fig. 6.7 is comprised of two main output windings on the outer legs of the core, each of N_G turns, and a control winding on the centre leg, of N_C turns. The output windings, as for the twin-core reactor, are connected in opposition so that the alternating fluxes act around the outer path of the core as shown by the arrows. These fluxes do not enter the centre leg under balanced conditions, and so no voltage at the supply frequency is induced in the control winding. This eliminates the need for a choke in the control circuit.

In Fig. 6.7 the a-c output windings are connected in series, however parallel connection is also possible as is shown in Fig. 6.8 below.

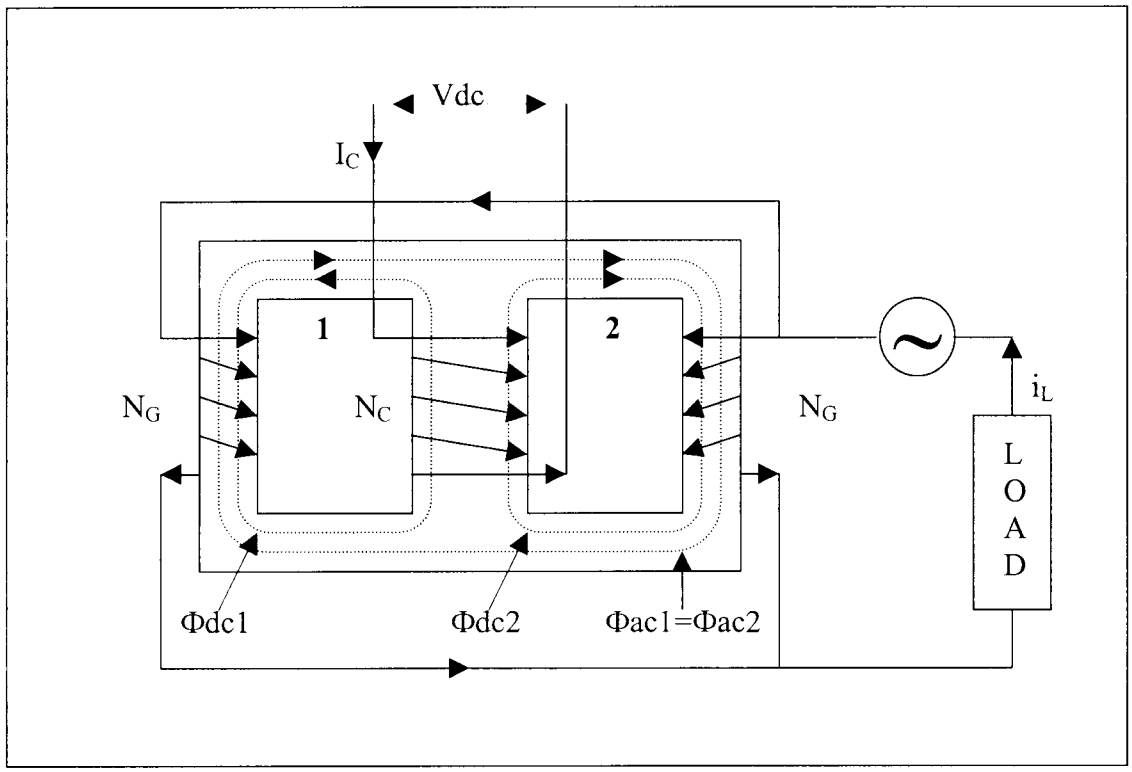

Figure 6.8 Three-legged core saturable reactor with parallel connected a-c windings

The principle of operation of the series- and parallel-connected reactors is identical, producing the same current output waveform shown in Fig. 6.9 below.

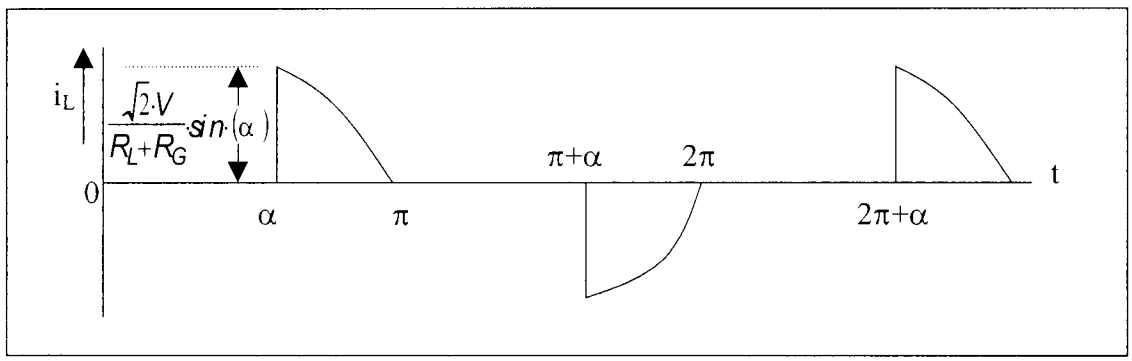

Figure 6.9 Typical current output wave shape from a three-legged core reactor

It should be noted that the twin-core and three-legged core reactors produce the same current output waveform.

However, for practical reasons associated with centre-leg residual d-c magnetisation effects, it is preferable to use the twin-cores as described in the previous section.

7 Design and Construction of the Saturable-Core Reactor

In this chapter a saturable-core reactor is physically realised through design, construction and testing.

7.1 Introduction

The saturable reactor is not a common device and was used mainly before the advent of the thyristor or silicon controlled rectifier (SCR), to control power to loads such as heaters and motors. After the semiconductor devices were invented, the saturable reactor was slowly replaced and dwindled out of existence. There are very few of these devices in existence today and even less knowledge of there operation or construction. It is for these reasons that the design of the saturable reactor has not been entirely scientific, but rather empirical.

7.2 Limitations

Initially it was thought that a 10kVA-reactor core would be necessary in order to prevent saturation of the reactor occurring at motor start-up. However, due to the budget of this project and availability of supplies, the core size of the saturable reactor is limited to a 5kVA.

The cores used are AMC type 5kVA, M5, 0.3mm lamination, grain oriented silicon steel (GOS Steel). Additional information is provided in Appendix B.

7.3 Initial Criteria for Reactor Design

The twin-core saturable reactor was chosen for this design.

The reasons are as following:

- Unlike the three-legged core saturable reactor, the twin core reactor does not suffer from centre-leg residual d-c- magnetisation effects.
- The main windings can be connected in series in order to increase the amount of inductance.

The saturable reactor has the following ratings:

E=380V, I=60Amp, f=50Hz

The voltage of the reactor is rated for the line voltage of the system. The current is rated at the maximum current that the reactor has to carry at any one time, in this case the start-up current of the motor, which is limited to 60Amp by the starting resistors. The frequency is rated at line frequency.

Of primary importance is the thickness of the copper wire to be used on the main windings. The following rule of thumb guide is used:

Continuous current rating of copper wire [Amps/mm^2]	Typical Application
2.5	Inner winding of large core, all windings on one bobbin.
4.0	Nominal
6.0	Single bobbin winding on outer core.

The main windings are on an outer core and thus the 6 A/mm^2 category is used.
The size of the wire needed is:

$$\frac{60\,A}{6\,\frac{A}{mm^2}} = 10\,mm^2$$

Thus 2x5mm, flat copper wire is used.

7.4 Calculating the Number of Turns on the Main Windings

The approximate number of turns for each main winding needs to be determined. This is done with the aid of the following calculation:

$$4.44 f N A B = E$$

Where: f - Frequency of operation.

N - Number of turns.

A - Cross-sectional area of core.

B - Maximum magnetic flux density

E - Voltage across inductor

Rearranging the formula we get:

$$N = \frac{E}{4.44 f A B}$$

Substituting the following values:

f- 50hz

A- 38mm x 90 mm (from core measurements)

B- 1.6 Tesla (recommended by core manufacturer)

E- 190 V (two windings in series each shares half the line voltage)

We get the following:

$$N = \frac{E}{4.44 f A B} = \frac{380}{\frac{2}{4.44 \cdot 50 \cdot 0.038 \cdot 0.09 \cdot 1.6}} = 156.4 \, turns$$

Due to limited inner core space, 145 turns were wound.

Thus the total number of turns on the main winding is 2*145=290.

7.5 Calculating the Number of Turns on the Control Winding

To correctly determine the number of turns on the control winding, and hence maximise the control of the reactor, the law of equal ampere-turns must be adhered to. Thus the number of ampere turns on the control winding must be greater than or equal to the number of ampere turns on the main control windings.

This results in the following equation:

$$N_c \cdot A_c = N_m \cdot A_m$$

Where: N_c – Number of control winding turns.

A_c – Maximum current in control winding.

N_m – Total number of turns on main winding.

A_m – Maximum current in main windings.

Rearranging the formula we get:

$$N_c = \frac{N_m \cdot A_m}{A_c}$$

Substituting the following values:

N_m – 290 turns

A_m – 60 Amps

A_c – 2.5 Amps (maximum desired control current)

We get the following:

$$N_c = \frac{N_m \cdot A_m}{A_c} = \frac{290 \cdot 60}{2.5} = 6960 \cdot turns$$

We therefore require approximately 7000 turns on the control winding that can carry a continuous current of 2.5 Amps. Unfortunately a maximum of 3000 turns, of 0.65mm, round copper wire could be accommodated within the limited inner core space.

7.6 Calculating the Air Gap

The theoretical air gap can be calculated as follows. Assuming that the reluctance of the core is negligible in comparison to that of the air gap, the following equation can be used:

$$B=\mu H=\frac{\mu N I}{l}$$

Where: l – Path length [m]

μ - Permeability of free space

N – Number of turns

I – Peak Current [A]

B – Flux density [T]

Rearranging the formula results in:

$$l=\frac{\mu N I}{B}$$

Substituting the following values:

μ – 4π*10e-7

N – 290

I_{rms} – 60 A

We get the following:

$$l\approx\frac{4\pi\cdot10^{-7}\cdot290\cdot\sqrt{2}\cdot60}{1.6}=19.33\,mm$$

Thus the total air gap length is calculated to be 19.33mm. Therefore each air gap is half of this value. Thus

$$l\approx\frac{19.33}{2}=9.7\,mm$$

However, due to fringing fields and non-uniform core distribution, the air gap is best determined experimentally. The best results are obtained with an air gap of 0.75mm per side.

7.7 The Constructed Saturable Reactor

The diagram of the constructed saturable reactor is shown below in Fig. 7.1.

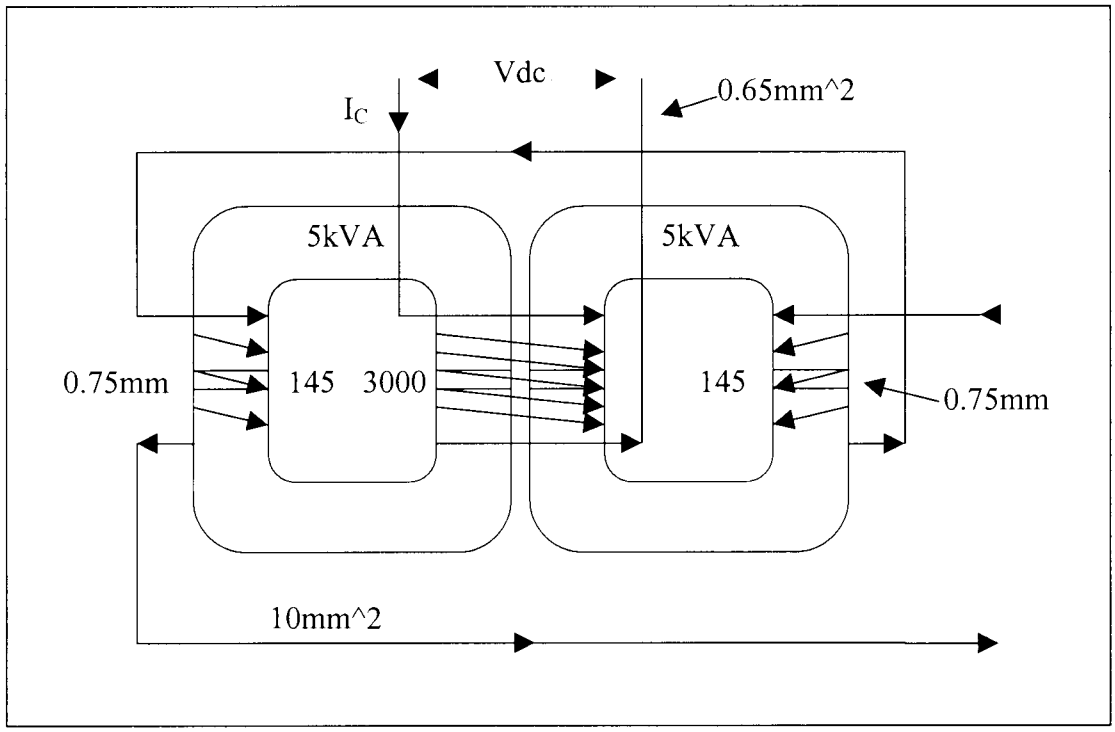

Figure 7.1 Diagram of constructed twin-core saturable reactor

Additional data:

- Resistance of main windings in series ≈ 100mΩ
  (This measurement is taken with a Wheatstone bridge.)
- Resistance of control winding ≈ 43Ω

A number of digital images, Fig 7.2 and 7.3, of the actual reactor are included on the following page:

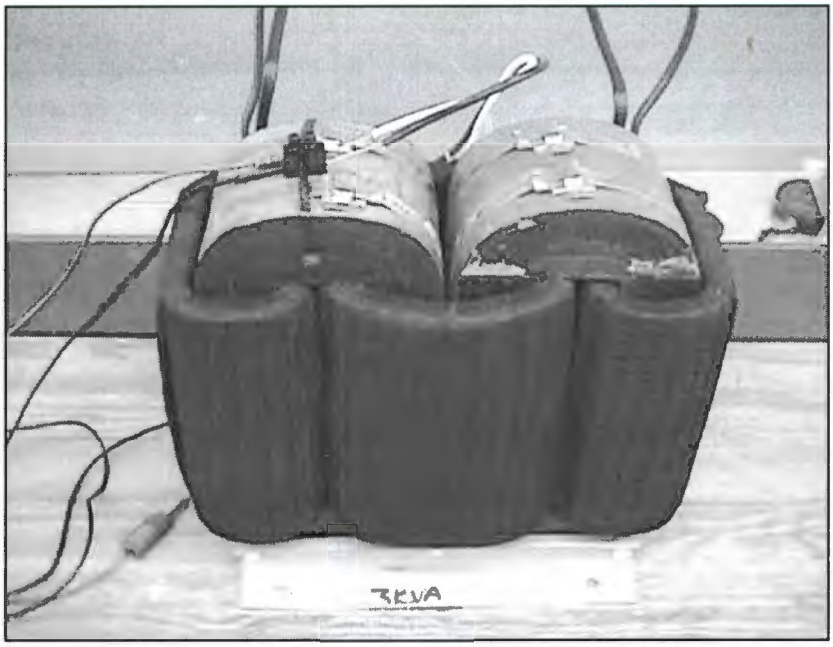

Figure 7.2 Top view of constructed saturable-core reactor

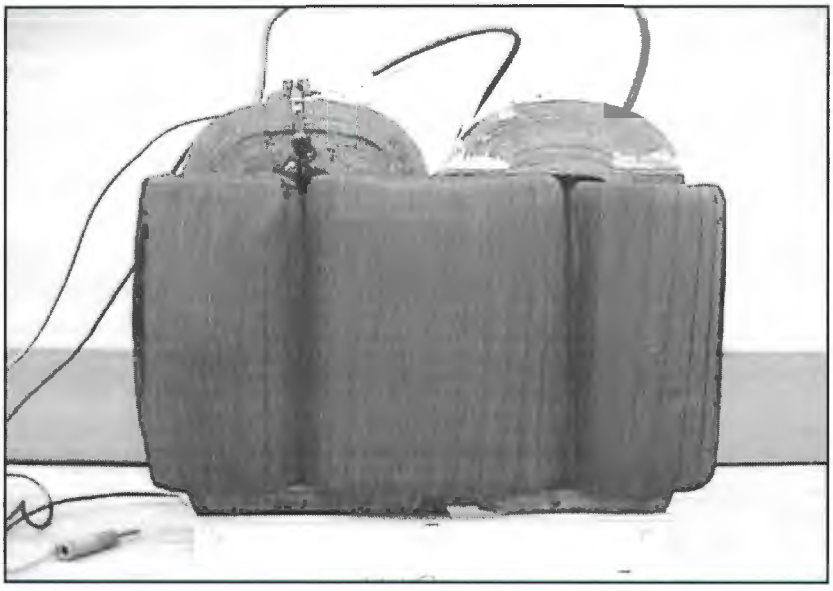

Figure 7.3 Front view of constructed saturable reactor

7.8 *Experimental Test Results*

The saturable reactor is tested as follows:

- 380V is applied across the main windings of the reactor.
- The current into the reactor and voltage across it are noted as the control current is increased in steps.

The values recorded from this test, with the aid of the Fluke 39 Power Meter, are illustrated in a Fig. 7.4 below.

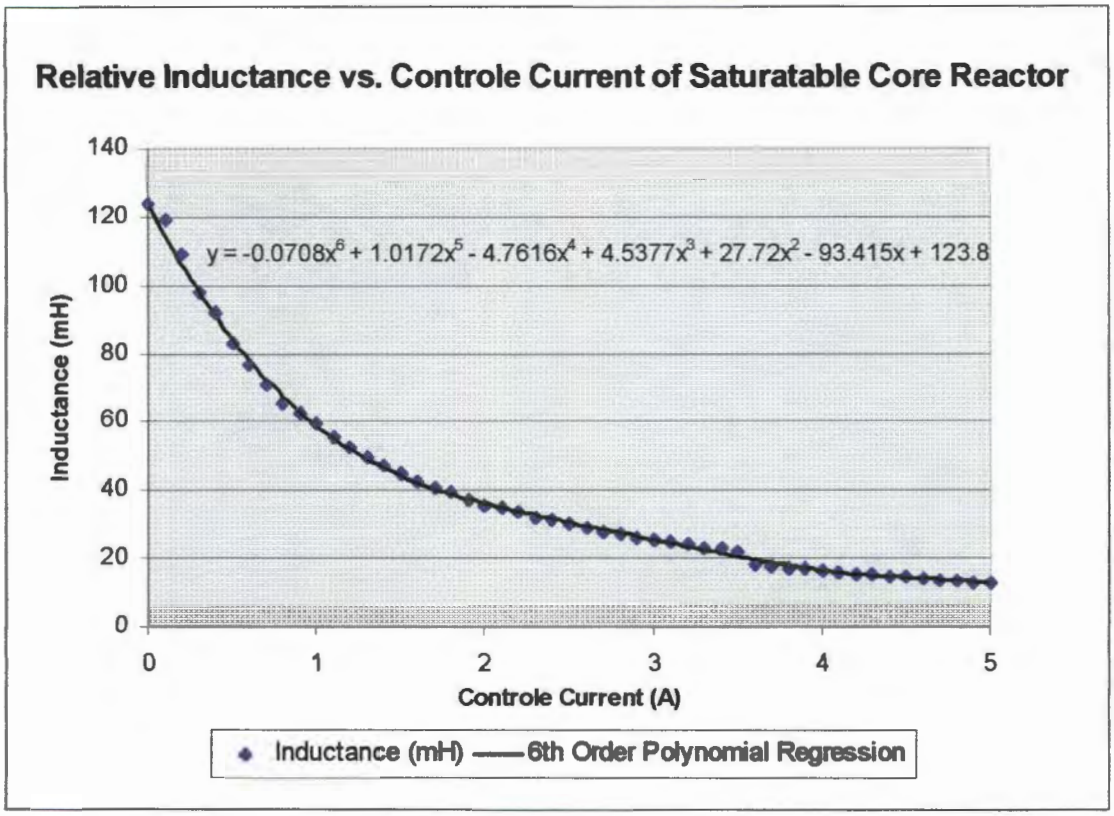

Figure 7.4 Graph of inductance verses control current for the designed saturable core reactor

As shown in Fig. 7.4 above, a change in inductance from 120mH to 30mH is possible over the rated control current range, a variation in inductance of 4 to 1. However, if the control current is doubled, which is acceptable for brief intervals, an inductance of 12mH is achievable, a variation in inductance of 10 to 1.

8 Converter Design

8.1 Introduction

In this section the design process and the ideas behind the development of the converter are covered. An initial proposal is made and progressively refined in stages, with issues of importance being addressed, ultimately resulting in the final converter design. The final design is then discussed in detail.

8.2 Initial Proposal for Converter Design

As shown previously in chapter 5, section 5.3, a simple form of reactive phase shifting network, as shown in Fig. 8.1 below, with appropriate values of Z_α and Z_β, can give balanced phase conversion for one particular load phase impedance Z.

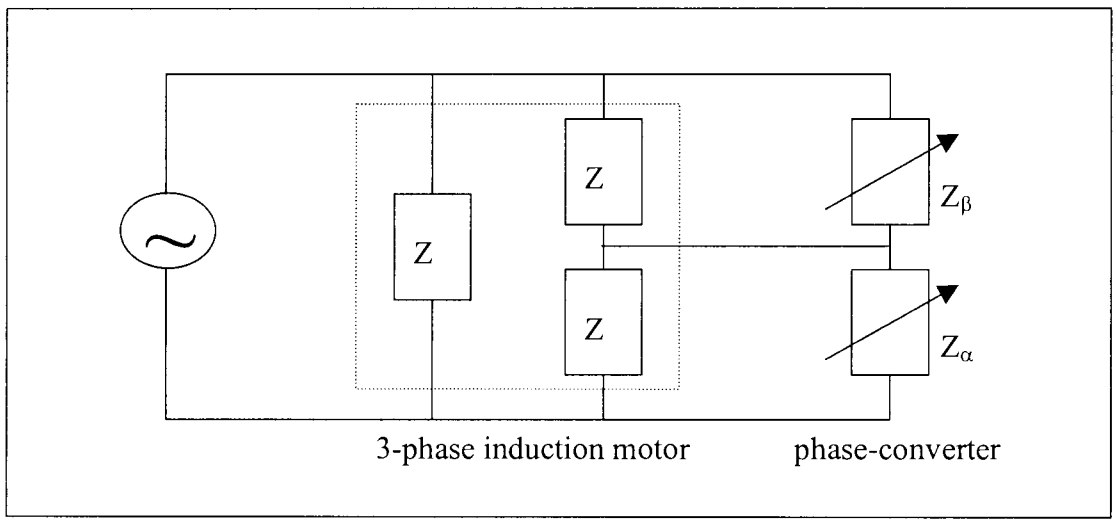

Figure 8.1 Reactive phase-converter

The impedance of a three-phase cage-induction motor is slip-dependent. Thus, if exact phase balance is to be maintained at a range of operating slips, Z_α and Z_β must vary as functions of slip.

It can also be arranged through the appropriate use of current limiting starting resistors in series with the motor, that elements Z_α and Z_β remain purely inductive and purely capacitive, respectively, over the full motor slip range.

With this in mind the initial idea of a rough controller that only balanced at certain critical slip points of motor operation was proposed and is shown in Fig. 8.2 below.

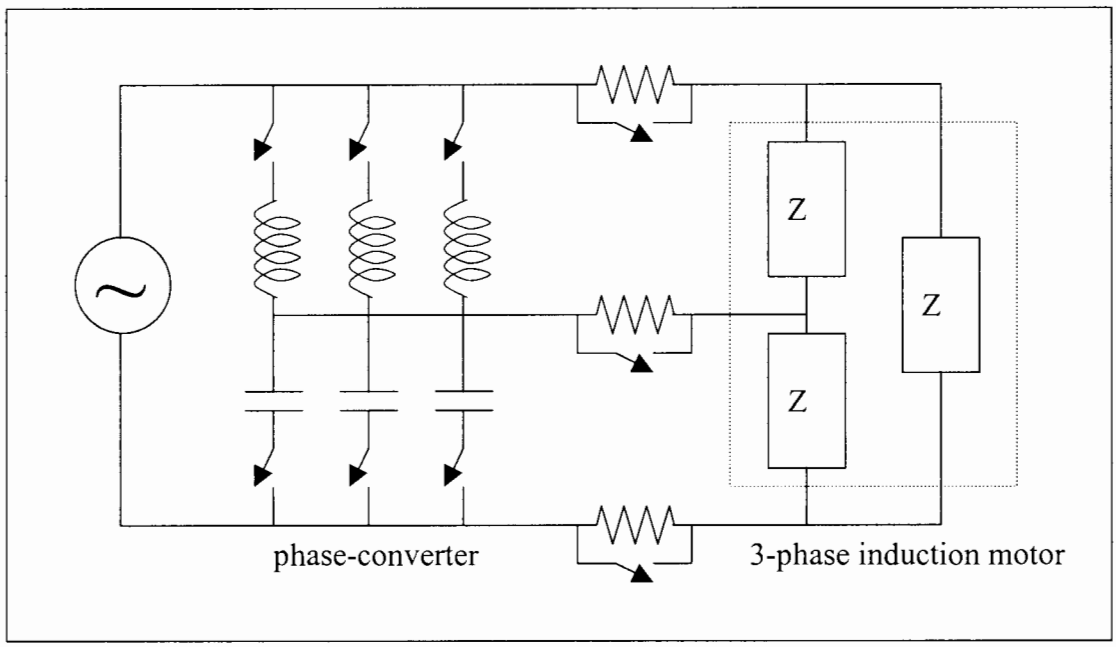

Figure 8.2 Proposal for initial converter design

The principle idea behind the controller is to maintain rough current balance at motor start-up, full-load, 2/3 of full-load, 1/3 of full-load and no-load. This is achieved through selectively switching in various fixed capacitors and inductors as illustrated in Fig. 8.2 above.

Unfortunately for the particular motor in question this method is not economically viable. The inductance's necessary, as calculated in chapter 5, need to be rated at 380 V, range from 20 to 100mH and are required to handle currents from 60 to 10A, respectively. Inductors of this nature would have iron cores that would render them not only very expensive, but also bulky and heavy. This fact alone renders this approach impractical.

8.3 *Improved Converter Design with One Saturable-Core Reactor*

The limitation of using fixed inductors of various sizes is overcome with the use of a twin-core saturable-reactor as shown below in Fig. 8.3.

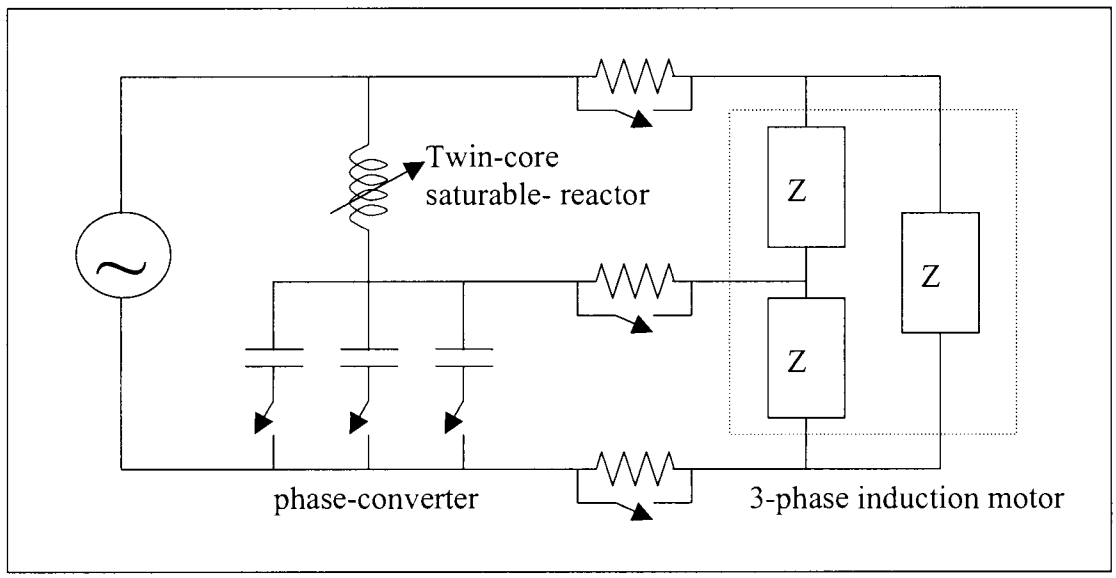

Figure 8.3 Proposal for improved converter design using a twin-core saturable-reactor

The saturable reactor, used as a variable inductor, provides two major improvements to the converter design, namely:

1 **The replacement of several inductors of fixed values with one variable inductor.** This has the effect of not only reducing the cost of the converter, but also its weight, size and complexity. It also provides the ability for a power inductance that is easily controlled and continually variable. This should result in a more fine control of the converter and hence more stable current balance of the motor.

2 **The elimination of inductor switching.** The saturable-core reactor is in circuit continually, as shown in Fig. 8.3 above, and thus eliminates the need for switching of inductance. This reduces the cost of the converter and its complexity. In the situation where electro-mechanical relays are used for switching, the risk of failure is also increased.

8.4 Switching of Capacitors

Special attention needs to be paid when switching capacitors in and out of circuit, especially in high voltage applications. If capacitors are subjected to excessive inrush currents, by allowing them to be switched directly onto the supply lines without consideration of where exactly in the mains cycle they are connected, the consequences can be dire. These range from capacitor plate or dielectric damage, which reduces the effective working lifetime of the capacitor, through to capacitor failure by means of explosion, fire or worse still, explosion and fire.

The greater the voltage difference that exists between what is stored on the plates of the capacitor and the supply voltage, the greater the inrush current of the capacitor will be. The greatest inrush currents are thus caused by the following three switching scenarios when capacitors are switched directly onto the supply lines:

1. When a discharged capacitor is directly connected to the supply lines and the supply voltage, at the instant of connection, is either at a maximum or minimum. In this case, as illustrated in Fig. 8.4, the instantaneous voltage change across the capacitor is equal to the peak line voltage.

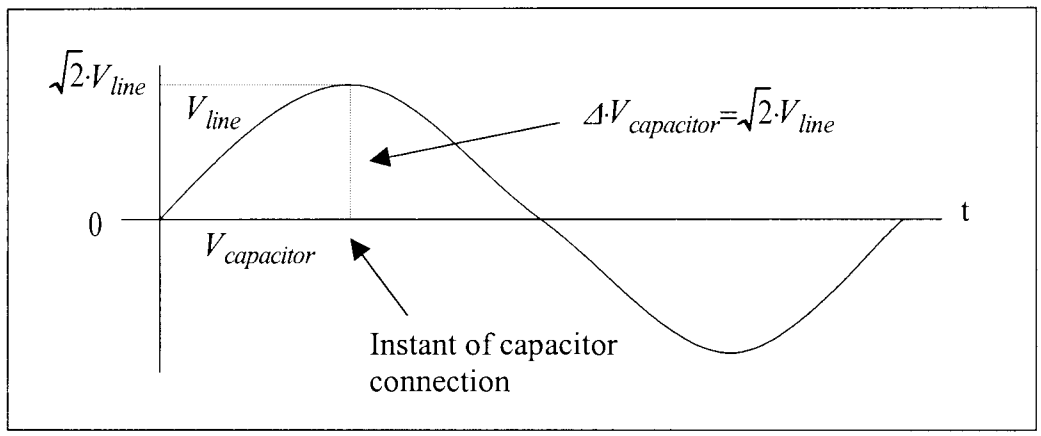

Figure 8.4 Connection of discharged capacitor to line at peak line voltage

2. Equally dangerous is when a fully charged capacitor is directly connected to the supply lines and the supply voltage, at the instant of connection is zero. In this case, as illustrated in Fig. 8.5 below, the instantaneous voltage change across the capacitor is equal to the peak line voltage.

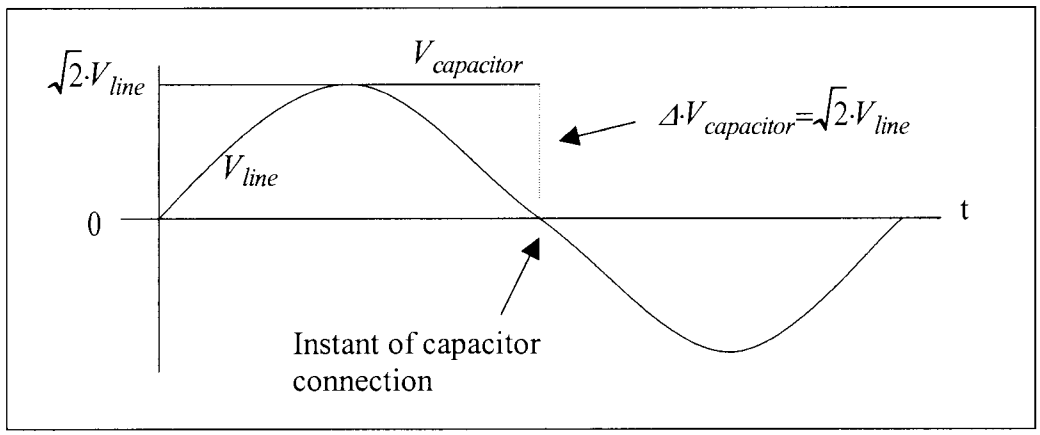

Figure 8.5 Connection of fully charged capacitor to line at zero line voltage

3. The worst possible situation arises when a fully charged capacitor is directly connected to the supply lines, and the supply voltage, at the instant of connection, is either at a maximum or minimum and of opposite polarity to the charge of the capacitor. In this case, as illustrated in Fig. 8.6, below, the instantaneous voltage change across the capacitor is equal to twice the peak line voltage.

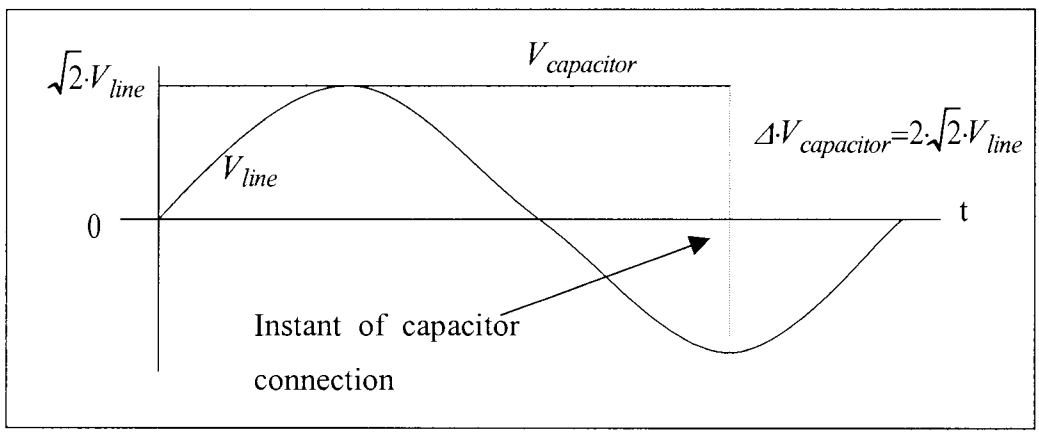

Figure 8.6 Connection of fully positively charged capacitor at peak negative line voltage

Thus in order to prolong the effective working lifetime of a capacitor, it is necessary to minimise capacitor stress at switching instants. This is accomplished by minimising the instantaneous voltage difference between the capacitor and the supply at the instant that the capacitor is connected to the lines. The ideal switching instant is thus when the voltage of the capacitor equals the voltages of the supply, as is shown below in Fig. 8.7.

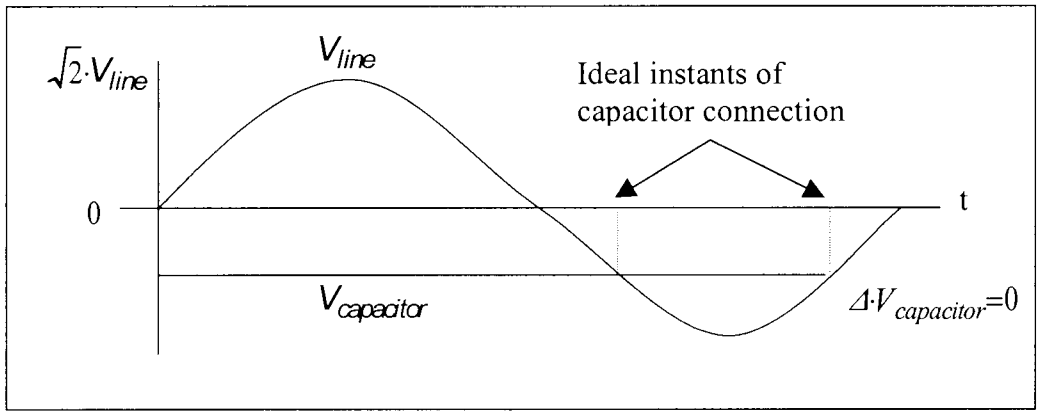

Figure 8.7 Ideal switching instant for connection of partially charged capacitor

Switching of capacitors in this situation can be accomplished either electro-mechanically by capacitor switching contactors, or electronically by thyristors.

8.5 Capacitor Switching by means of Capacitor Switching Contactors

A capacitor switching contactor is a relay, specially modified for the switching of capacitive loads, see Appendix C. The relay, as is shown in Fig. 8.8 below, incorporates two sets of contacts and an inrush current limiting resistor that is shorted out after a set period of time.

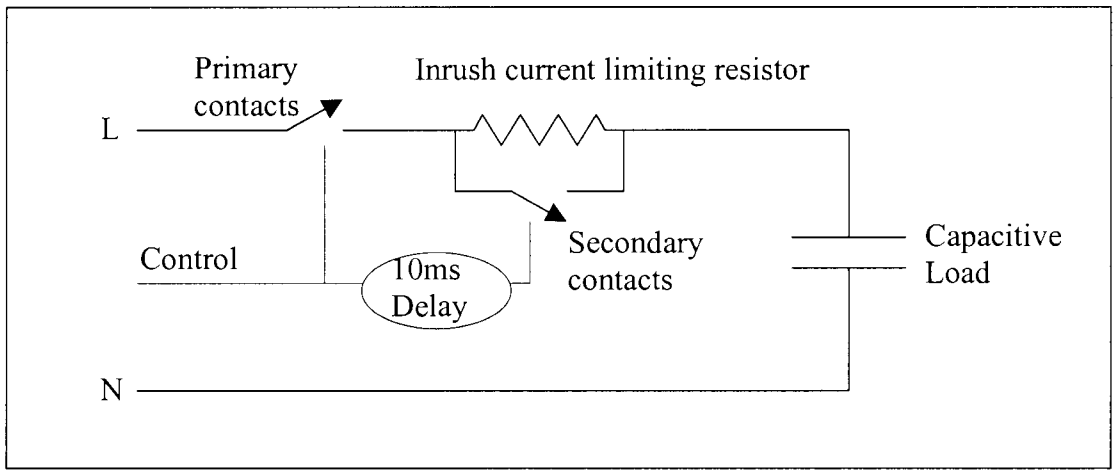

Figure 8.8 Internal circuit diagram of capacitor switching contactor

The relay operates as follows. When voltage is applied to the control input, the primary contacts are energised, and the inrush current limiting resistor is placed in series with the capacitive load. This allows the load to initially charge or discharge at a significantly reduced rate, as opposed to direct on line switching, and synchronises the load voltage with the supply. After approximately 10 milliseconds the secondary contacts are energised, shorting out the resistor and thus placing the load directly across the supply lines. This method significantly reduces the voltage stress placed on the capacitor during switching.

Thus making use of capacitor switching contactors allows repetitive switching of capacitive loads without consideration of where exactly in the supply cycle they are connected. However, they are inherently slow, being electro-mechanical, and are therefore not suitable for applications that are cycle-by-cycle dynamic where fast repetitive switching is required. It is for this reason that this method of switching capacitors is not used.

8.6 Capacitor Switching by means of Thyristors

The thyristor is a power semiconductor-switching device that has the capability for controlled switching for only one direction of current flow. However, using two thyristors in a "anti-parallel" or "back-to-back" configuration, as shown in Fig. 8.9 below, it is possible to use them as bi-directional switches in a-c circuits.

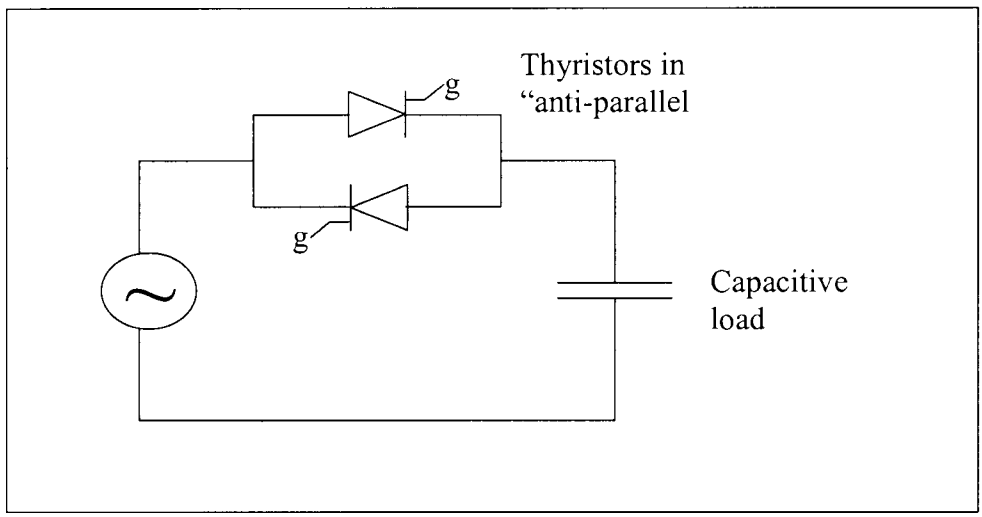

Figure 8.9 Circuit diagram of "anti-parallel" thyristors used as an a-c switch

The gate, labelled 'g', is the control terminal. In its normal or "off" state the thyristor will block current from flowing in either direction, however, if a positive current pulse is applied to the gate while the thyristor is forward biased, it will turn "on" and start conducting as a diode. It will continue to allow current to flow irrespective of whether the gate current is removed or not and will only return to its "off" state if either the current source is removed or the flow of current is reversed. Thus with two thyristors in "anti-parallel" and appropriate gate pulsing, a load can be switched onto the supply lines at any point in the cycle.

Unlike the capacitor switching contactor, care must now be taken to ensure that the thyristors are only allowed to switch on when there is no voltage difference between the capacitor and the supply. However, this presents a unique problem when a capacitor is switched out of circuit and then needs to be reconnected.

Due to the nature of capacitive loads, the current through them lags the voltage across them by 90°. Thus when the thyristor turns off at a current minimum, the voltage across the capacitor is always at a maximum or minimum and this charge remains on the capacitor. The positive case is shown below in Fig. 8.10.

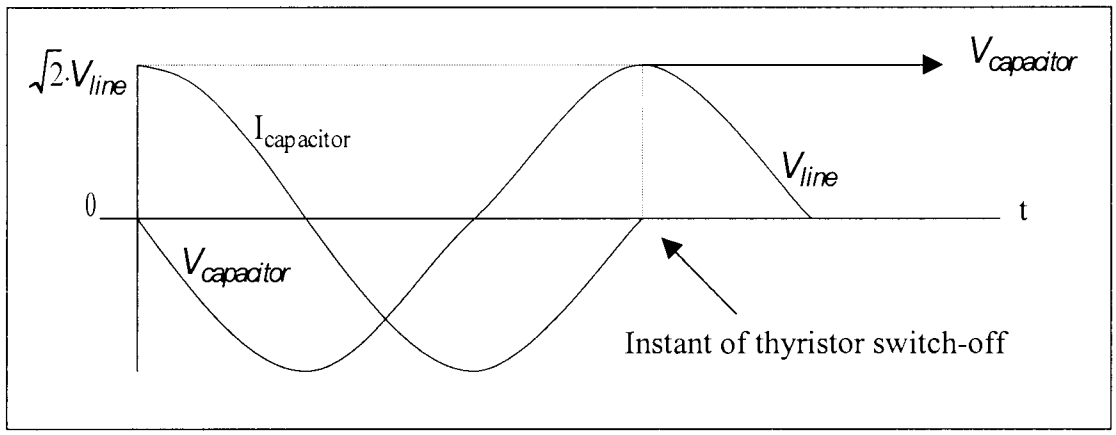

Figure 8.10 Waveforms of capacitor voltage and current at thyristor switch-off

Due to the capacitor being fully charged to either $\pm\sqrt{2}\cdot V_{line}$ the net voltage across the thyristor becomes a sinusoid that fluctuates between zero and either $\pm 2\cdot\sqrt{2}\cdot V_{line}$ .The positive case is shown in Fig. 8.11 below.

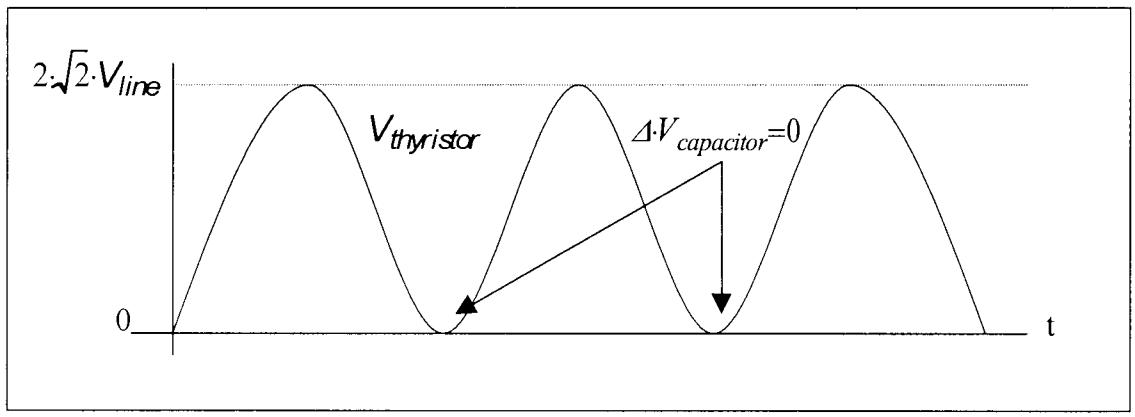

Figure 8.11 Waveform of voltage across switching thyristor when capacitor is fully charged

This waveform represents the difference in voltage between the capacitor and the supply. It is the voltage zero's on this waveform that represent the ideal instants for the capacitor to be switched onto the supply lines.

At these instants the voltage difference between the capacitor and the supply is zero, thus if connected to the supply lines at these instants, the capacitor will experience no stress.

This presents no difficulty at low voltages, 230V and below. The peak voltage across the thyristor, as shown in Fig. 8.11, for 230V is:

$$V_{peak}=2\cdot\sqrt{2}\cdot V_{line}=2\cdot\sqrt{2}\cdot 230\approx 650\cdot V$$

Standard 800V thyristors and zero-crossing detectors that are available "off-the-shelf" handle this voltage. However for higher voltages, 380V and above, it presents a problem. The peak voltage across the thyristor, as shown in Fig. 8.11, for 380V increases to:

$$V_{peak}=2\cdot\sqrt{2}\cdot V_{line}=2\cdot\sqrt{2}\cdot 380\approx 1075\cdot V$$

Thyristors are readily available in voltage ratings that range up to 1600V, however, zero-crossing detectors are not. Thus to correctly switch capacitors in and out of circuit at such high voltage requires complex additional zero-crossing circuitry.

It is for this reason that this method of switching capacitors is not used.

8.7 The Saturable-Core Transformer

8.7.1 Introduction

This section introduces the concept of the saturable-core transformer, proposed by Malengret [9]. The principle of operation is then discussed together with the various configurations that can be employed to obtain a variable source of capacitance. Finally conclusions are made.

8.7.2 Principle of Operation of the Saturable-Core Transformer

The saturable-core transformer is an iron-core transformer, the coupling of which is a function of the current in a separate, d-c control winding. It is therefore possible to vary the coupling between the primary and secondary windings, of the transformer, simply by altering a d-c control current. The effect of the control current is to vary the permeability of the core by saturating it with a constant magnetic field. Varying the degree of saturation alters the coupling between the primary and secondary windings of the transformer. The higher the saturation, the less the coupling and vice versa. It should be made clear that the principle of operation of the saturable-core transformer is in many ways similar to that of the saturable-core reactor. Thus, if required, a greater understanding of its operation may be obtained by reviewing the material found in chapter 6.

8.7.3 Variable Capacitance by means of the Saturable-Core Transformer

The limitation of using fixed capacitors of various sizes can be overcome with the use of a saturable-core transformer, proposed by Malengret [9], as shown below in Fig. 8.12.

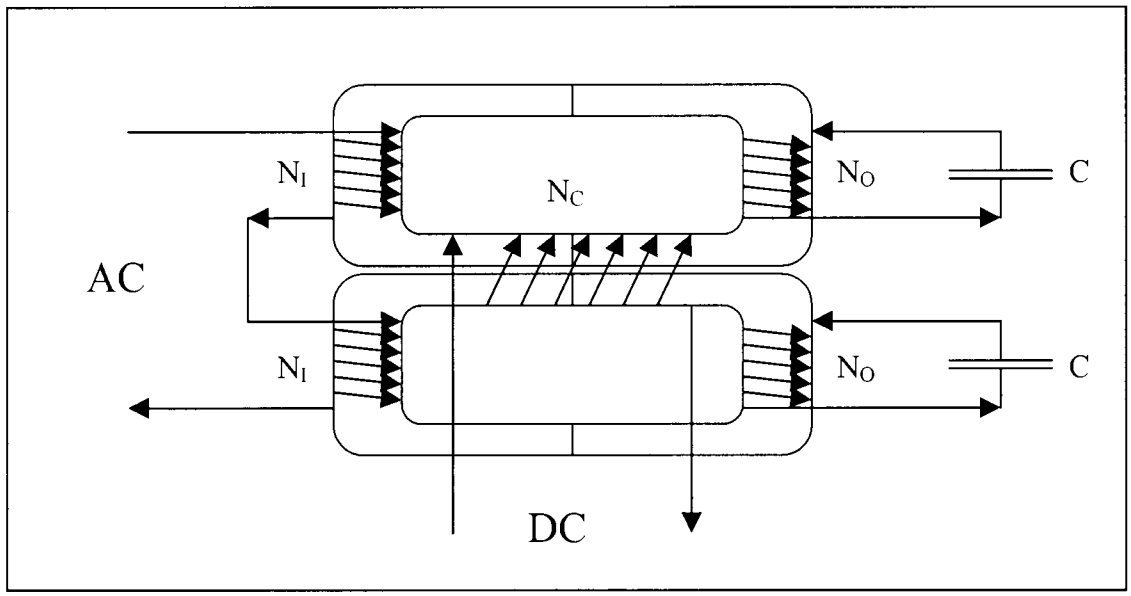

Figure 8.12 Saturable-core transformer with isolated secondary windings

The twin-core transformer in Fig. 8.12 is comprised of two identical transformers, 1 and 2, each consisting of an input winding of N_I turns and an output winding of N_O turns. The d-c control winding, of N_C turns, is common to both cores. The a-c input windings are connected in such a way as to produce fluxes of opposite orientation within the two cores. This ensures that the control winding experiences zero net flux and hence zero net a-c voltage is induced in it. Each output winding has a capacitor placed across it.

Under normal operation the load on the output of the transformer is reflected to the input, thus the supply sees the full capacitive load. However as d-c current is injected into the control winding, reducing the permeability of cores, two effects are noted.

- Firstly the coupling between the input and output windings decreases. This reduces the amount of the capacitive load, on the secondary, as seen by the primary of the transformer and hence the supply.
- Secondly, due to a reduction in core permeability, the inductance of the primary windings decreases.

These two factors result in a fairly low control current being required in order to reduce the effective capacitance, as seen by the supply, to zero. If suitable values of capacitor are selected the effective impedance of the transformer, as seen by the supply, can be made to swing from fully capacitive through to fully inductive.

In Fig. 8.12 the a-c output windings of the transformer are isolated, each having a capacitor placed across them. This configuration, however, requires both capacitors to be of identical value if symmetrical operation of the transformer is required. If they are of unequal values (typically capacitors have tolerances of only 20%), fluxes of unequal magnitudes will be generated in each core. The d-c control winding therefore experiences a net flux which induces an a-c voltage in it. This is extremely undesirable as mentioned in chapter 6.

This problem is overcome by series connection of the output windings as is shown in Fig. 8.13 below.

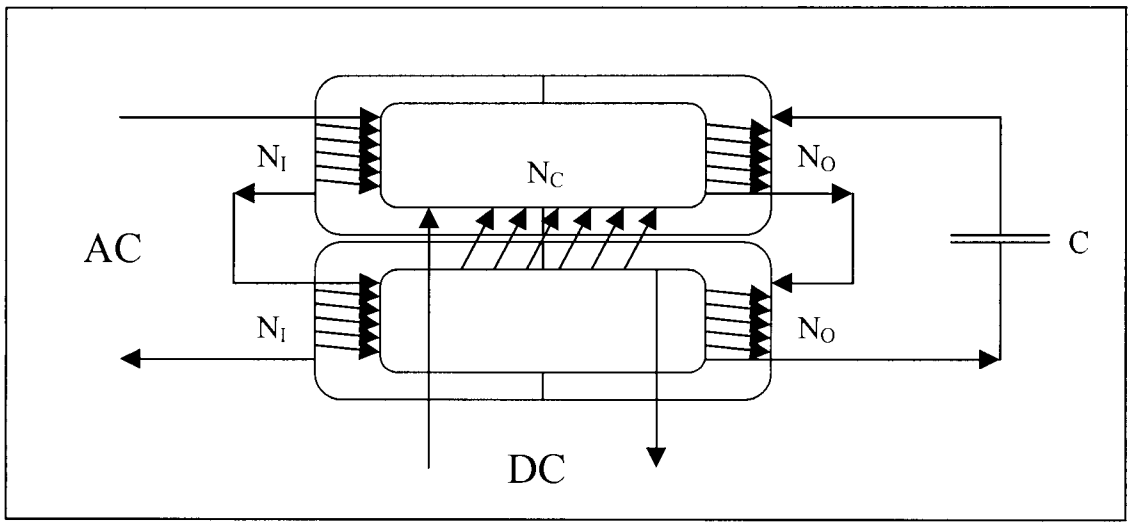

Figure 8.13 Saturable-core transformer with series connected secondary windings

Thus by varying the control current of the transformer it is possible to obtain a variable source of capacitance. The saturable transformer, used to vary effective capacitance, provides two major improvements over switched methods, namely:

1. **The replacement of several switched capacitors of fixed values with one effectively variable capacitor.**

   This provides the ability for a power capacitance that is easily controlled and continually variable, unlike the rough switched capacitance methods.

2. **The elimination of capacitor switching.**

   The saturable-core transformer and the capacitors are in circuit continually and thus eliminate the need for capacitor switching. In the case of semiconductor switching this reduces the complexity of the control by not requiring complex zero-crossing circuitry to correctly switch in the capacitors, as described in chapter 7, section 7.5. In comparison to electro-mechanical switching this method decreases the risk of failure, due to the robustness of the components and lack of moving parts.

The saturable-core transformer, used to vary capacitance, thus not only provides a viable alternative to, but also improves on the previously discussed switched capacitor methods.

8.7.4 Experimental Designs

In this section various saturable-core transformers are physically realised through construction and testing. This is in order to determine the feasibility of using a saturable transformer to vary capacitance as described in the previous section.

The saturable transformer is not a common device and as yet the author has found no reference to any material pertaining to this topic. If this is the case then Malengret's concept of a saturable transformer is unique. There are also no guidelines for design or construction. It is for these reasons that the design of the saturable transformers has not been entirely scientific, but rather empirical.

Various core layouts were considered by the author in an attempt to improve on Malengret's design. Illustrated below are a host of brainstormed ideas each accompanied by a brief explanation of why they were not adopted.

In the case were an ideal transformer is placed between the supply and a capacitor, as shown below in Fig. 8.14, the input of the transformer behaves as a capacitor of value C.

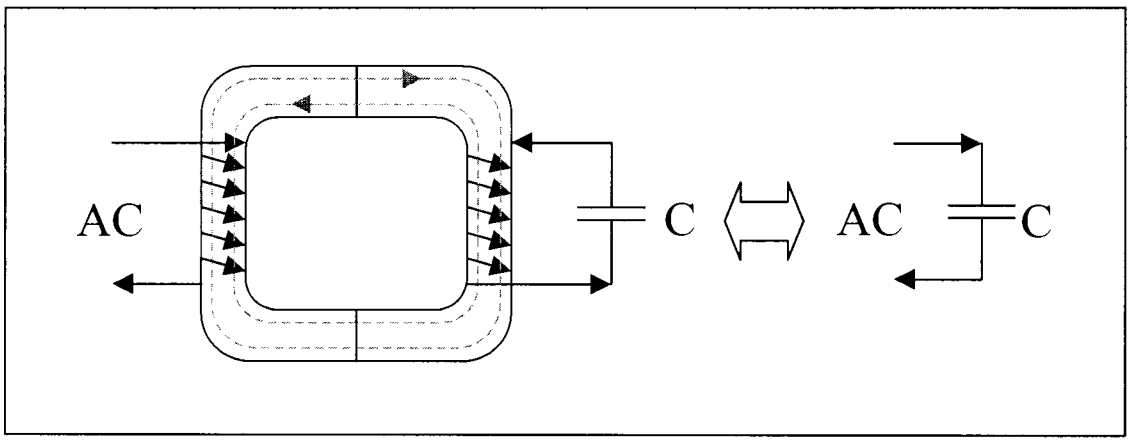

Figure 8.14 Ideal transformer with capacitor output

The supply does not see the transformer, which serves only to couple the magnetic field induced by the primary winding through the core to the secondary winding.

Design 1

Two d-c saturation windings are placed as shown in Fig. 8.15, below, in order to obtain variable coupling between the primary and secondary windings.

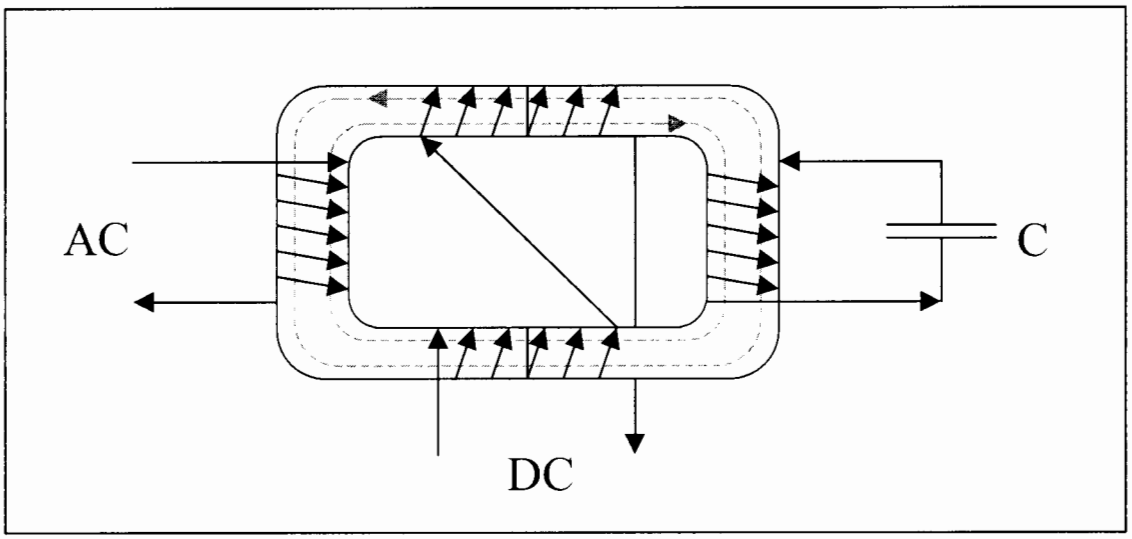

Figure 8.15 Saturable transformer with two d-c series connected control windings

By altering the degree of saturation in the core, it is possible to restrict the flow of magnetic flux in both directions, thereby effectively reducing the coupling between the primary and secondary windings of the transformer.

This idea, however, is not pursued due to high voltages being induced in the control windings. Although the control winding as a whole experiences a zero net a-c voltage, because each winding is connected with opposite phase orientation, each winding is still subject to a very large a-c voltage which could result in insulation breakdown.

Design 2

The core of the transformer is distorted, as shown below in Fig. 8.16, in order for a single control winding to be wound.

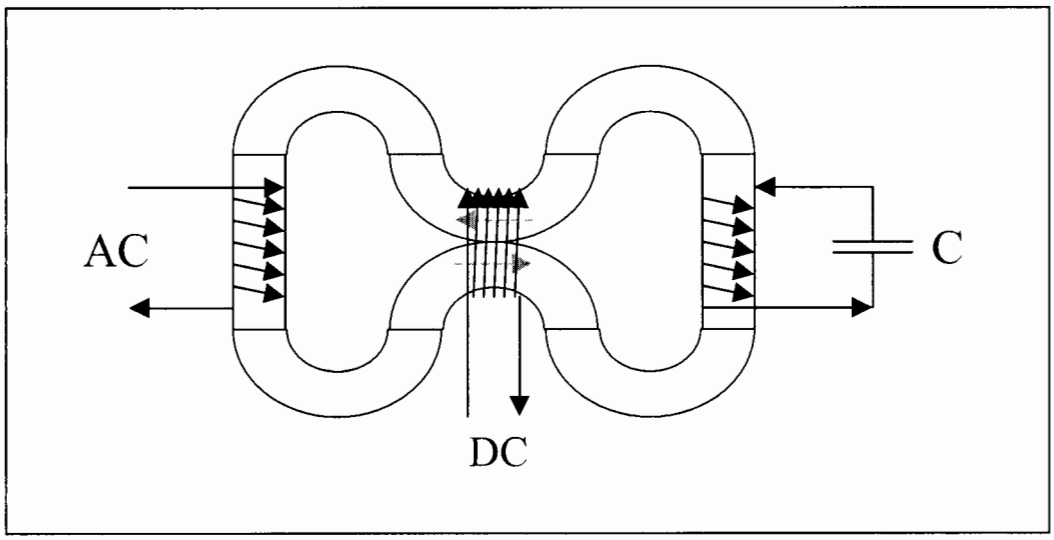

Figure 8.16 Saturable transformer with distorted core and single d-c control winding

The control winding now encloses the opposing flux paths, which cancel one another, resulting in no voltage being induced in the d-c control winding. The principle of operation of this design is identical to that of design 1, and differs only in core shape.

The idea, however, is taken no further due to the difficulty of constructing core of this nature, since they are not available commercially.

Design 3

Two e-cores are placed side-by-side as shown below in Fig. 8.17. (An exploded view for visual clarity)

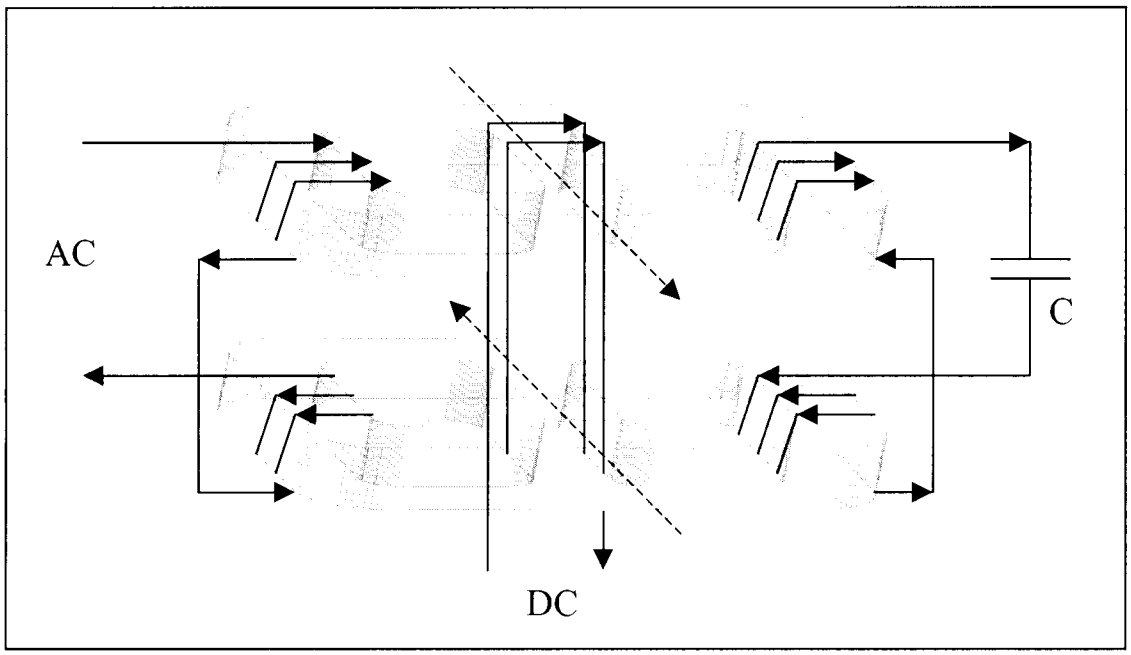

Figure 8.17 Saturable transformer with dual e-core and single d-c control winding

This arrangement allows for the use of standard "off-the-shelf" cores and incorporates flux cancellation within the d-c control winding.

Under normal operation, the flux created by the primary a-c winding travels through the path of least reluctance or shortest magnetic circuit. In this instance the flux travels through the centre leg of the e-core and thus the coupling between the primary and secondary windings is poor. This occurs in both cores, however, due to the opposite phase orientation of the primary windings, as shown above, the fluxes generated are always of equal magnitude and opposite direction. The result is zero net flux, within the control winding, and hence zero net a-c voltage is induced.

By injecting a d-c current into the control winding, the permeability of the centre legs of both cores decreases, resulting in magnetic paths of high reluctance. The flow of flux within the centre legs is therefore restricted, forcing it to travel in the outer ring

of the transformer and effectively increasing the coupling between the primary and secondary windings. It is therefore possible to control the coupling of the transformer by altering the degree of saturation. The higher the control current the greater the coupling and visa versa.

In Fig. 8.19, below, it is shown how a second d-c control winding is added to further decrease the coupling under normal operating conditions. The two control windings now work in opposition to one another acting like magnetic valves. By varying the degree of saturation in the respective portions of the cores, it is possible to restrict the flow of flux, forcing it to flow either through the centre or outside legs of the transformer.

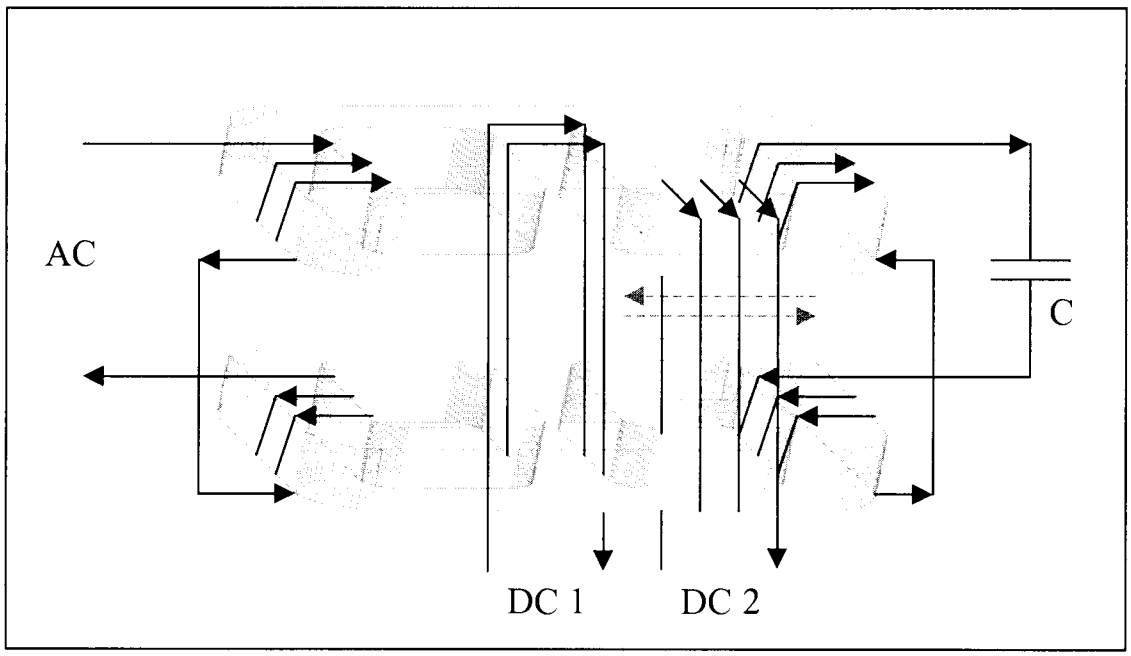

Figure 8.18 Saturable transformer with dual e-core and dual d-c control winding

The idea, however, is discarded due to its large and cumbersome nature. A large amount of iron and copper are required. Firstly, because two cores are used and secondly, because the control winding, which is common to both cores, is separated by a minimum distance of approximately twice the thickness of the primary or secondary windings. This results in a large amount of copper being used to construct the d-c control winding. The extended control winding suffers not only from increased resistance but also, consequently, from increased power (I^2R) losses.

8.7.5 Experimental Construction and Testing

A number of variations of these three designs were considered, however, all suffered from similar problems to those mentioned above. This resulted in Malengret's proposal being adopted for the design of the saturable transformer.

Fig. 8.19, below, outlines the construction details of the saturable transformer.

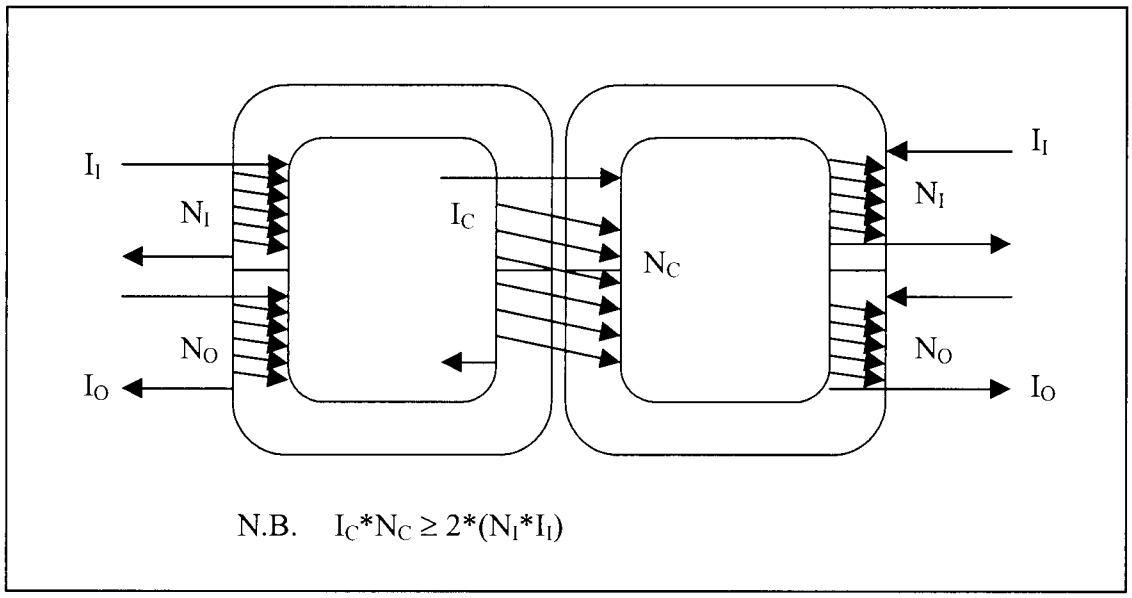

Figure 8.19 Saturable-core transformer construction details

Various combinations were experimented with in order to obtain a rough idea of what type of construction would yield optimal results. As seen later in Figs. 8.19-8.21, all designs followed the same basic format, as shown above, in Fig. 8.18.

The design guidelines for saturable transformers are common both to conventional transformers and saturable reactors.

The following list highlights the fundamental guidelines:

1. To fully utilise the power rating of the transformer core, the window area of the core (the space encompassed by core) should be filled with copper wire.

2. In order for the transformer not to saturate under normal operating conditions, the ampturns specified for each core, I_I*N_I, should not be exceeded by the respective input winding, N_I.
3. In order to obtain full control of the core, the ampturns of the control winding, I_A*N_C, should be greater than or equal to twice that of the input ampturns, I_I*N_I.

The digital images, Figs. 8.20, 8.22 and 8.24 that follow are of various saturable transformers constructed for testing purposes. Each image is accompanied by a short explanation.

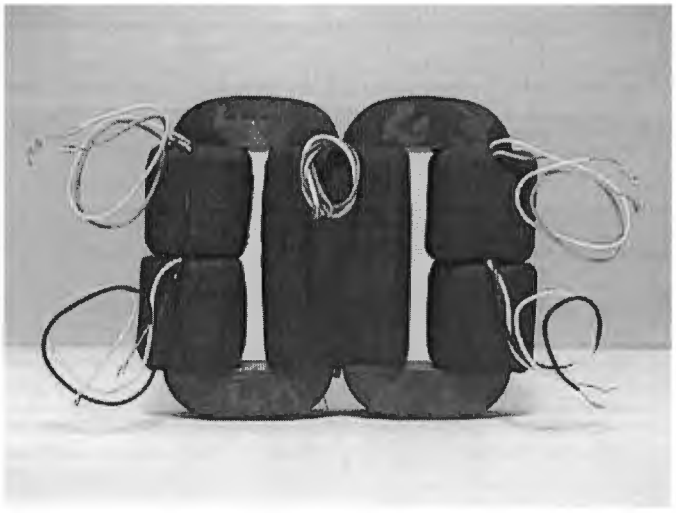

Figure 8.20 First constructed saturable-core transformer

In Fig 8.20, above, the first attempt to realise Malengret's proposal of a saturable transformer can be seen. Two sets of c-cores are utilised with the windings placed as shown above. The input and output windings are of an equal number of turns, while the control winding consists of a considerably greater number turns. Exact transformer specifications can be found in Appendix D.

The transformer is tested and the readings taken are illustrated in Fig. 8.21, below.

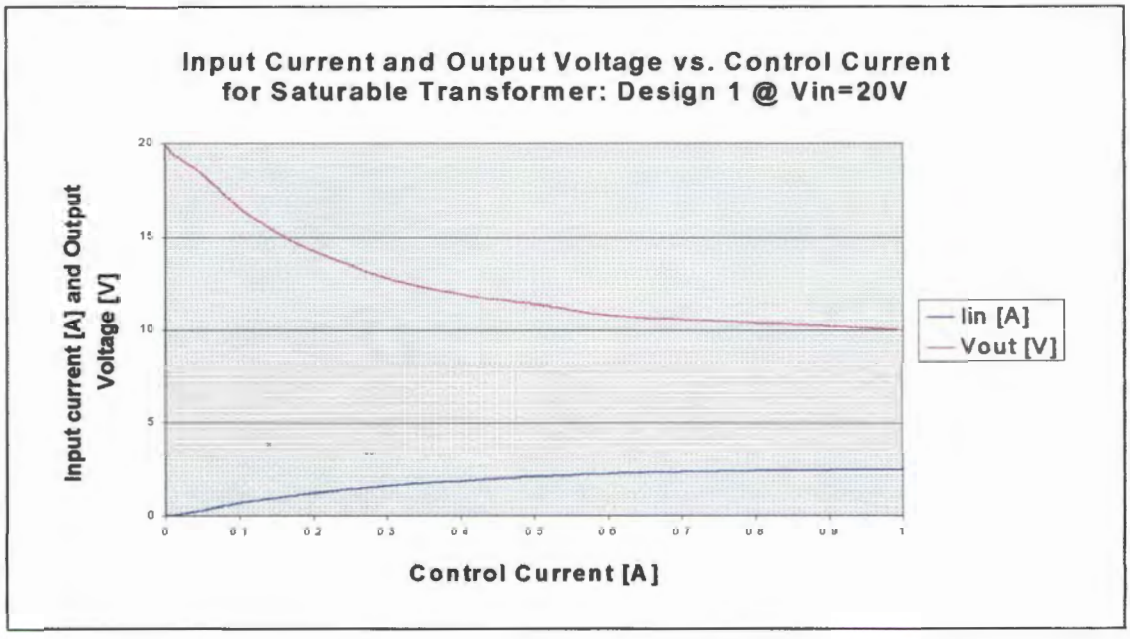

Figure 8.21 Graph of test results for first saturable-core transformer construction

From Fig. 8.21, above, it is seen that for a linear increase in control current, two effects take place, namely:

1. The coupling between primary and secondary windings decreases exponentially resulting in a 50% decrease in output voltage.
2. The input current rises exponentially, indicating an exponential drop in transformer input inductance from approximately 1.6H to 25mH.

The results are favourable, however, it is found that the wire thickness used for the input and output windings is of too small a cross-sectional area. The resistance of the windings is thus high, resulting in excessive I^2R losses. This not only causes the core temperature of the transformer to rise to unacceptable levels, but also results in an inefficient transformer. The window areas within the cores are also not fully utilised, resulting in inefficiencies.

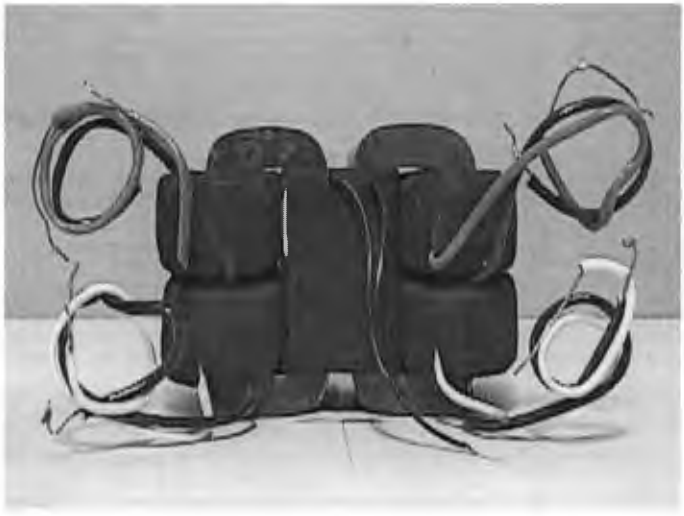

Figure 8.22 Second constructed saturable-core transformer

In the second saturable transformer to be constructed, as shown above in Fig 8.22, the excessive losses experienced in the first construction are overcome through more efficient use of window area and through the use of conductors of larger cross-sectional area. This significantly reduces the losses within the transformer windings and helps to maintain the core temperature to within the recognised limits. In this way a more efficient transformer is designed.

The transformer is tested and the readings taken are illustrated in Fig. 8.23, below.

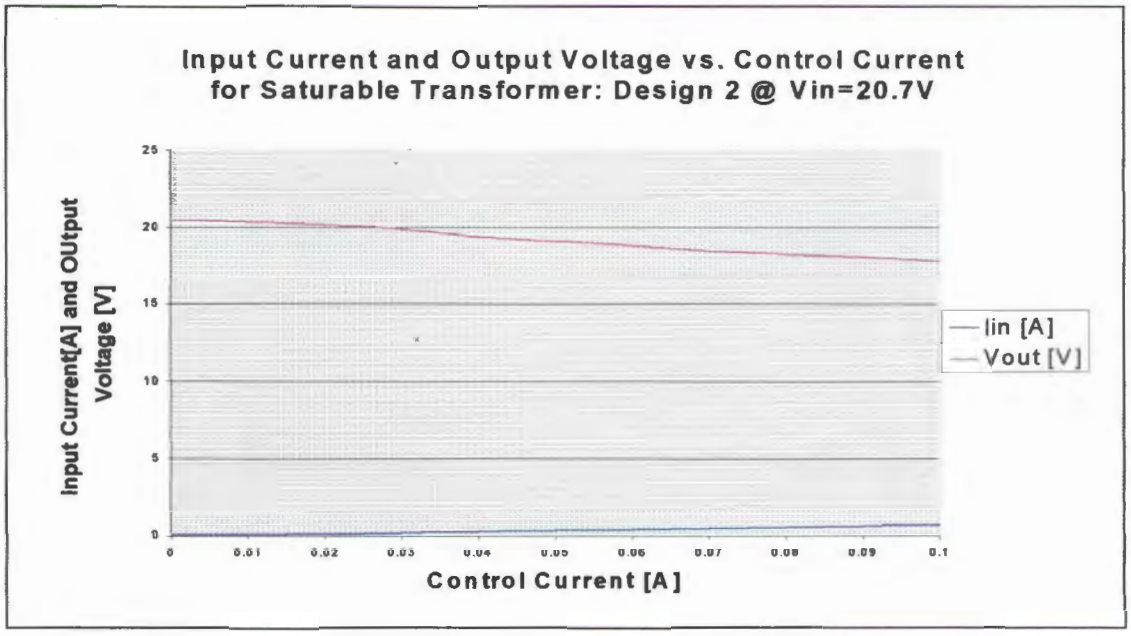

Figure 8.23 Graph of test results for second saturable-core transformer construction

As seen in Fig. 8.23, above, only a very small variation in both input current and output voltage is achieved. The poor control, in comparison to the first design, is thought to result from following three factors, namely:

1. Lack of adequate control current. This is due to the control winding consisting of many turns of relatively thin wire (after construction of the a-c windings not much window area was left for the control winding – hence the use of much thinner wire) resulting in a high internal resistance.
2. Coupling from input- to output windings. Stray flux, resulting from fringing fields caused during core saturation, easily couples between the input and output windings due to their close proximity to one another.
3. Coupling from core to core. Stray flux, resulting from fringing fields caused during core saturation, easily couples between both cores due to their close proximity to one another.

It is therefore found that, in this particular design, even at full saturation of the core, the coupling between the primary and secondary windings is still significant.

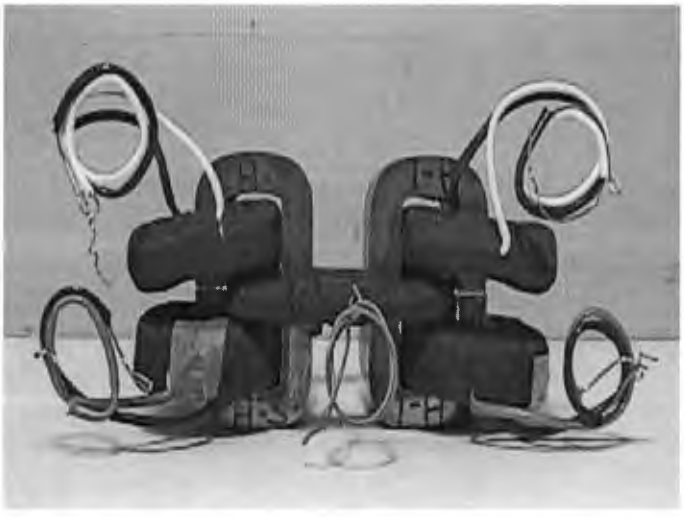

Figure 8.24 Third constructed saturable-core transformer

In the third saturable transformer to be constructed, as shown above in Fig 8.24, an attempt is made to reduce the coupling between the primary and secondary windings during core saturation. This takes on two forms, namely:

1. Physical separation of the windings.
2. Physical separation of the cores.

The transformer is tested and the readings taken are illustrated in Fig. 8.25, below.

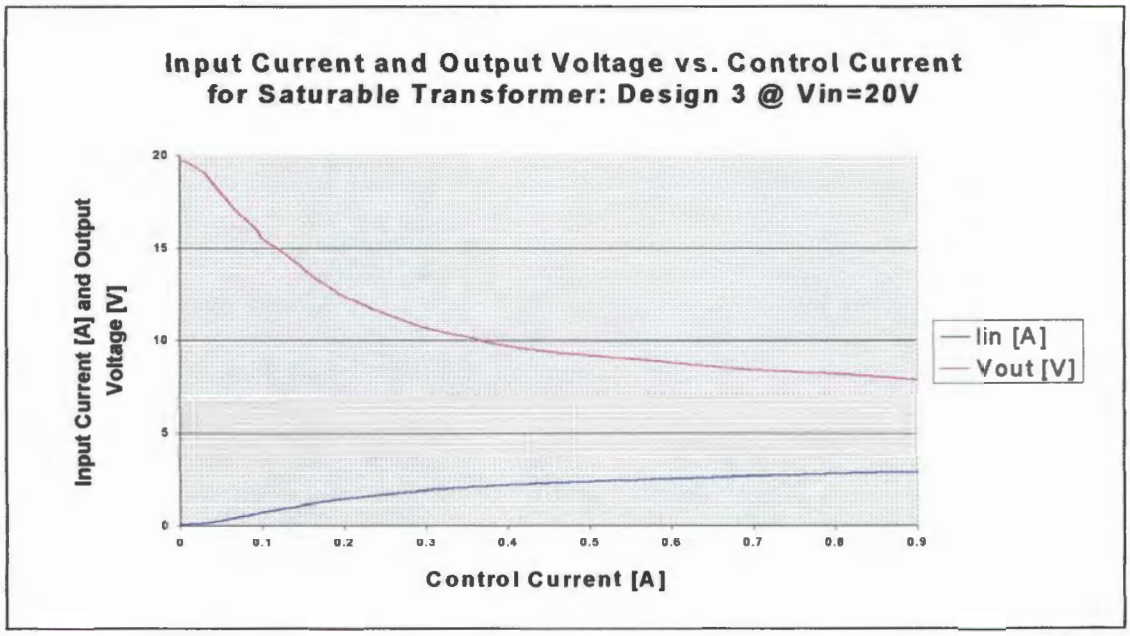

Figure 8.25 Graph of test results for third saturable-core transformer construction

The readings illustrated in Fig. 8.25, above, are virtually identical to those obtained from testing of the first saturable transformer construction, as seen earlier in Fig. 8.21. Both curves posses the same exponential decay in output voltage and exponential rise in input current with respect to a linear increase in control current.

From these results the following conclusions are made:

1. Adequate amp-turns are required in order for the control winding to effectively alter the coupling between the primary- and secondary windings of the transformer.
2. The proximity of the input windings to the output windings is of little importance. In comparison to the effect of the control current on coupling, the position of the primary- and secondary windings seems to have a negligible effect.

3. The proximity of two cores is of little importance. In comparison to the effect of the control current on coupling, the position of the two cores seems to have a negligible effect. It is therefore preferable to keep the cores next to one another, as in the first and second constructions shown in Figs. 8.20 and 8.22, in order to minimise the length of the control winding and in so doing lower its resistance.

8.7.6 Conclusions

Through experimental construction and testing the principle of operation of the saturable-core transformer is verified. The results correlate with the theory presented, however, differences are present which render this method for varying capacitance not viable. They are as follows:

1. The coupling is not as controllable as expected. Instead of the output voltage falling to zero, when the control current is increased, it tends to some constant value above zero, which is undesirable for this application. It must be noted, however, that the designs considered are of relatively simple construction and improvements could result from more elaborate designs as discussed earlier in section 8.7.4 Experimental Designs.
2. The design of the saturable transformer is not well established and hence more groundwork is necessary in order to establish their potential and limitations.
3. The transformer is not ideal and hence is subject to losses. Under normal operation these present themselves as winding losses, core losses and coupling losses.

Thus a more reliable technique for varying capacitance is sought after.

8.8 Improved Converter Design with Two Saturable-Core Reactors

The problems associated with the saturable-core transformers and the switching of capacitors are overcome once again with the use of a twin-core saturable-reactor as shown below in Fig. 8.26.

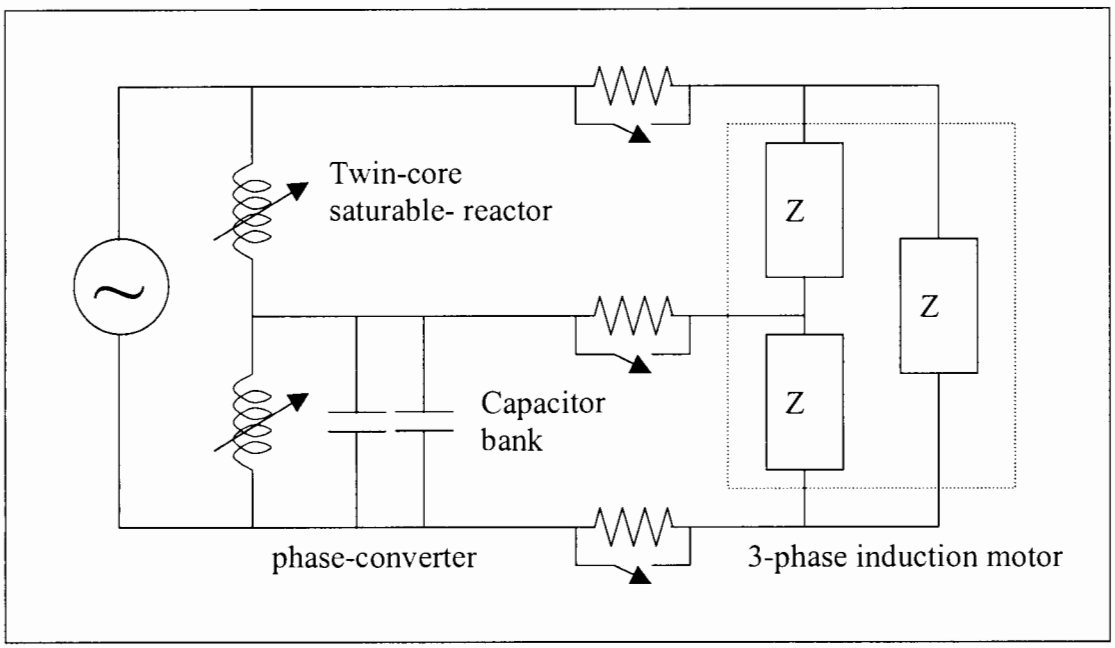

Figure 8.26 Proposal for improved converter design using two twin-core saturable-core reactors

The saturable reactor, again used as a variable inductor, is placed in parallel with a fixed bank of capacitors, effectively creating a variable source of capacitance. As the inductance is decreased, assuming appropriate capacitor and inductor values, the overall effective capacitance, as seen by the rest of the circuit, is also decreased.

The effective capacitance required, as calculated in chapter 5, ranges from approximately 600uF at start up to 150uF while running at no load. It is also seen from the chapter on "Design of the Saturable-Core Reactor" that the reactor designed is capable of varying in inductance from 120mH to 12mH.

With a bank of 700uF of capacitance placed in parallel with the reactor, the following variation in effective capacitance, as shown in Fig. 8.27, is obtained.

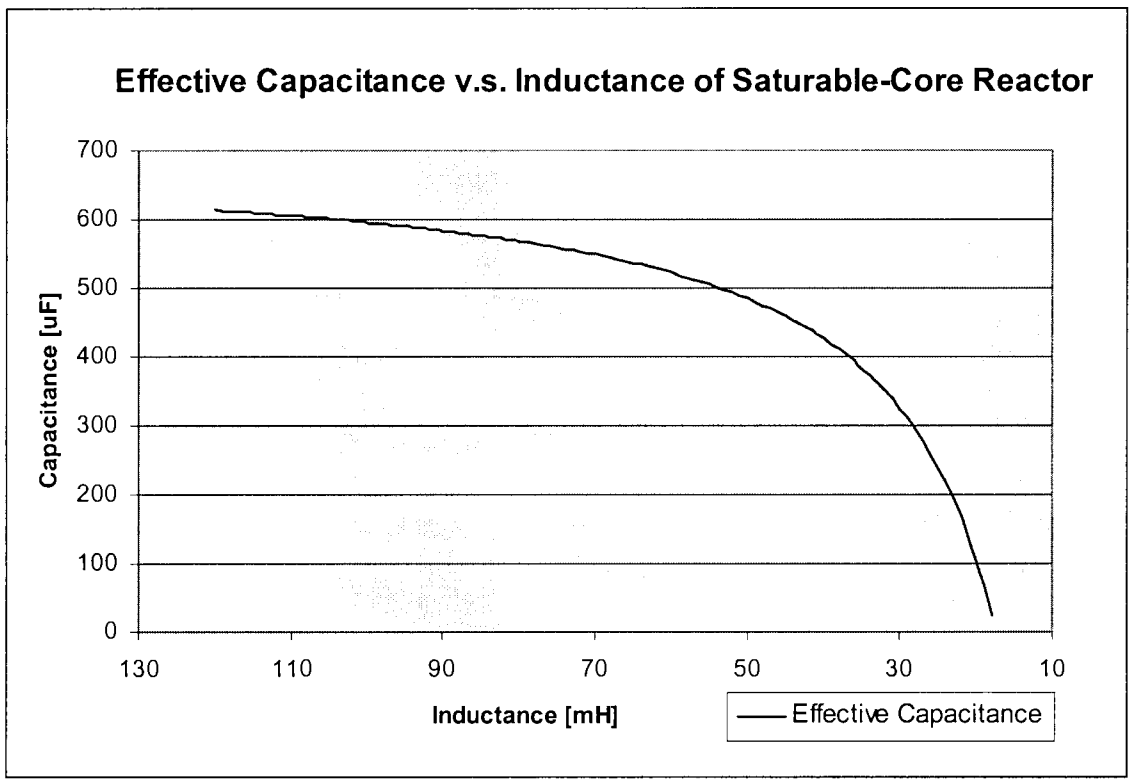

Figure 8.27 Graph of effective capacitance vs. inductance for saturable reactor in parallel with fixed 700uF capacitor bank

Thus by varying the inductance of the reactor it is possible to obtain a variable source of capacitance. The saturable reactor, used to vary the effective capacitance, provides two major improvements to the converter design, namely:

1. **The replacement of several switched capacitors of fixed values with one effectively variable capacitor**

   This provides the ability for a power capacitance that is easily controlled and continually variable, unlike the rough switched capacitance methods. This should result in a more fine control of the converter and hence more stable current balance of the motor.

2. The elimination of capacitor switching

The saturable-core reactor and the capacitors are in circuit continually, as shown in Fig. 8.26, and thus eliminate the need for capacitor switching. This reduces the complexity of the converter by not requiring complex zero-crossing circuitry to correctly switch in the capacitors, as described in chapter 7, section 7.5. If capacitor switching contactors are used, the risk of failure is also increased.

From a price perspective this method neither increases nor decreases the overall cost of the converter dramatically, in comparison with capacitor switching contactors or thyristor a-c switching and all the necessary circuitry associated with it. The saturable-core reactor is rather a compact method of altering the effective capacitance, however, it does slightly increase the amount of capacitance required, by about 100uF, and substantially alters the overall weight of the converter.

8.9 Further Improvements to Converter Design

8.9.1 Improvement 1

The first improvement to the converter design concerns the parallel inductor-capacitor network used to obtain a variable source of capacitance. The network is shown below in Fig. 8.28.

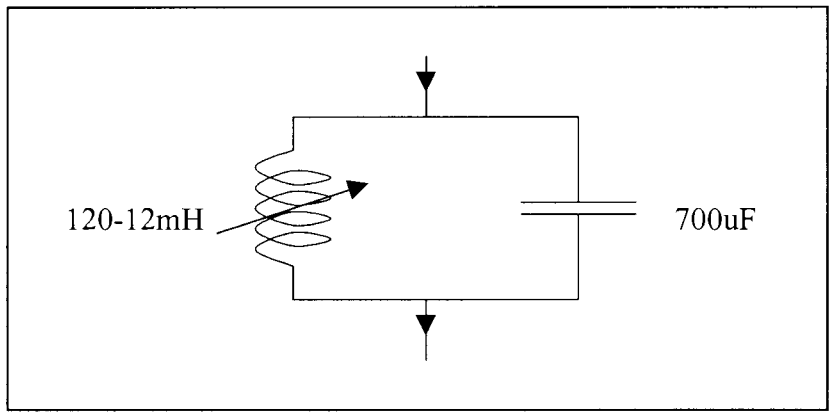

Figure 8.28 Circuit diagram of the parallel capacitor-inductor network

If the converter is to maintain current balance of the motor, then the voltage across all three motor phases must be equal. The inductor-capacitor network is placed directly across one of the motor phases and thus should always have a voltage equal to the line potential across it. Thus, on a 380V system, the inductor-capacitor network should always have approximately 380V across it, if adequate current balance is to be maintained. Therefore, irrespective of what effective capacitance the inductor-capacitor network has, as seen by the system, it will always have 380V across it.

If, for example, the inductance value of the saturable reactor is low, then the effective capacitance, as seen by the system, is also low. Thus the capacitor-inductor network will draw very little current from the system. However, the inductance value of the saturable reactor is low, and it has 380V across it, thus large circulating currents flow between the capacitor bank and the saturable reactor as shown below in Fig. 8.29.

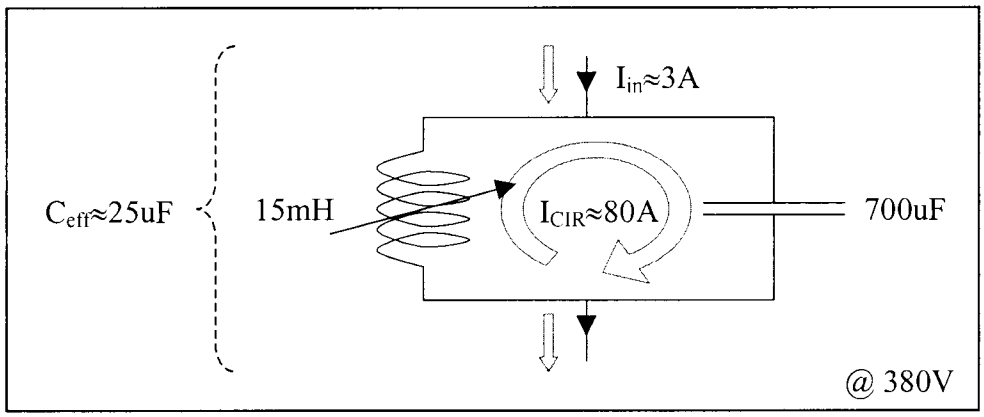

Figure 8.29 Circuit diagram of inductor-capacitor network showing large circulating currents

These large circulating currents cause local heating in the saturable reactor windings. Although the internal resistance is low, $R_{IN}\approx 100m\Omega$, at 80A the losses, which manifest themselves as heat, are substantial as shown.

$$I^2 R = 80^2 0.1 = 640 W$$

If the reactor is subjected to these conditions for extended periods of time, thermal failure of the windings will result.

At start-up the slip of the motor is high, requiring a large effective capacitance to achieve balance. The reactance required from the saturable reactor, in the inductor-capacitor network, to achieve this, is high and thus only small circulating currents flow. However, when the slip of the motor is low, a low effective capacitance is required to achieve balance. The reactance required from the saturable reactor, is thus low and large circulating currents result.

In order to relieve the problem of circulating currents, one of three steps can be taken.

1. Either the motor needs to be heavily loaded continuously. However, this defeats the purpose of a controller that can handle wide variations of motor load.
2. Or the saturable reactor can be increased in size in order to handle the large circulating currents. However, this not only increases the size, but also the cost of the converter substantially.
3. Or a switched capacitor method needs to be employed. Although adding to the electronic complexity of the converter, this appears to be the best solution.

The third idea is adopted and illustrated below in Fig. 8.30.

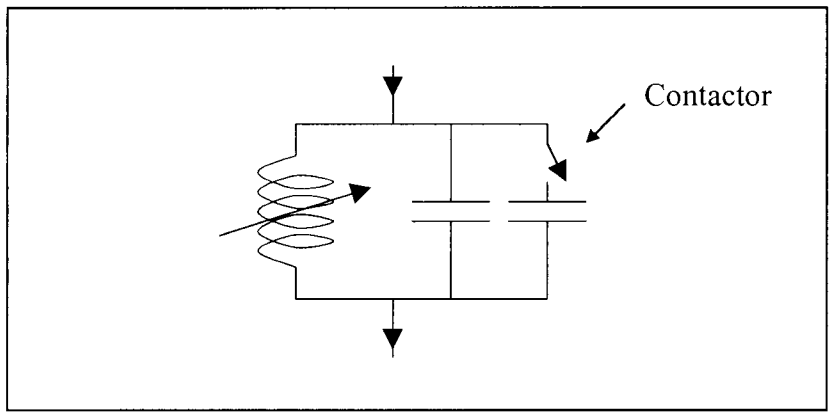

Figure 8.30 Circuit diagram of improved parallel capacitor-inductor network

At motor start-up, the contactor is activated, thus providing the full amount of capacitance required by the system in order to maintain current balance of the motor. However, once the motor is running, this excess capacitance, which is responsible for the large circulating currents in the inductor-capacitor network, is no longer required. Therefore, at some predefined point after motor start-up, the contactor is released, reducing the amount of capacitance placed across the inductor. This reduces the circulating currents in the network significantly, which not only places less electrical stress on the system as a whole, but also makes it viable as a means for varying capacitance in this particular application.

8.9.2 Improvement 2

The second improvement to the converter design revolves around the quality of supply to the converter. The reasons for the improvement are best conveyed via the following experiment, illustrated below, in Fig. 8.31.

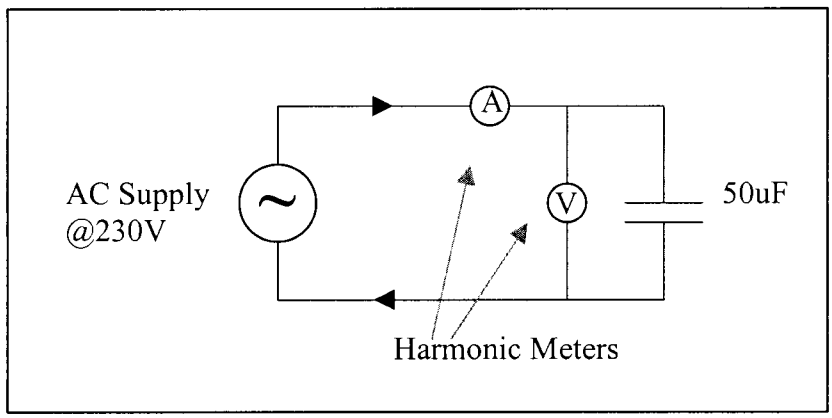

Figure 8.31 Circuit diagram of test set-up for quality of supply demonstration

In the above test a 50uF capacitor is placed directly across the supply and the voltage and current harmonics are measured. The results, taken from a Fluke 43 Power Quality Analyser [see Appendix E for details], can be seen in the figures that follow.

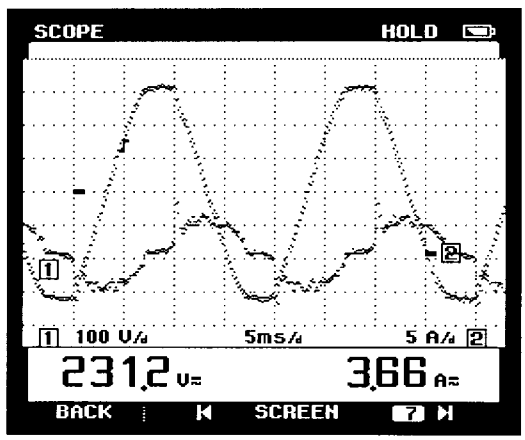

Figure 8.32 Waveforms of voltage and current for the 50uF capacitor

In Fig. 8.32, above, the distorted supply voltage (flattened peaks) and the even more distorted capacitor current, drawn as a result of this, can be seen.

The reason for the poor supply voltage waveform is as a result of a large number of fullbridge rectified capacitive loads, such as are found in most switch-mode power supplies of computers etc., being present on the supply. Due to the nature of these circuits, current is only drawn when the supply voltage is greater than the d-c voltage present on the capacitor, to "top-up" the charge on the capacitor. This process naturally only occurs at the peaks of the a-c supply waveform resulting in a large current being drawn for a short period of time about these points. The accumulated effect of many of these devices, such as are present in most modern institutions, results in a very large pulse current being draw from the supply at the peak of its cycle. This effect of this is to causes a greater than usual volt drop through the supply cables at these instants, which results in a sinusoidal supply waveform with flattened peaks as seen. The voltage harmonics that are present in the supply under these circumstances are shown in Fig. 8.33, below.

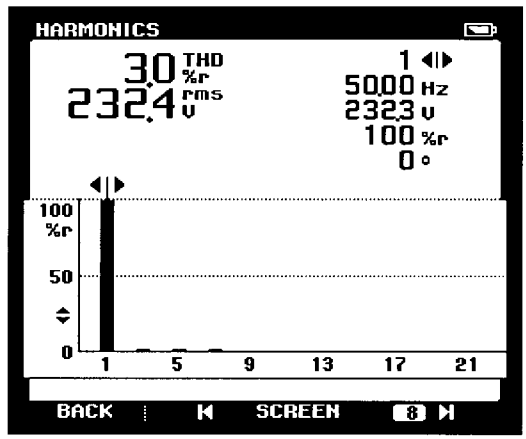

Figure 8.33 Harmonic content of the supply voltage

As is seen in Fig. 8.33 above, the total voltage harmonic distortion is only 3.0%, which falls well within acceptable limits. The problem, however, arises due to the nature of capacitive loads whose impedance falls with rising frequency. This is verified with the capacitor equation shown below:

$$X_c = \frac{1}{j w C}$$

Thus the higher the frequency, the lower the effective impedance of the capacitor.

It is for this reason that the current drawn by the capacitor is so distorted. Any higher frequency voltage components present in the supply result in correspondingly large harmonic currents being drawn from the it. Readings taken of the supply current harmonics drawn under these circumstances, are shown below in Fig. 8.34.

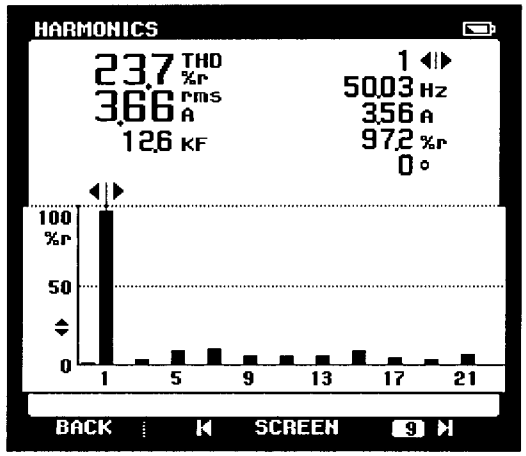

Figure 8.34 Harmonic content of the supply current

The total current harmonic distortion, as shown above in Fig. 8.34, is 23.7%. Current harmonics of this magnitude will severely reduce the working lifespan of a motor [1].

The inductor-capacitor network, used in the converter, is placed directly across one phase of the motor. It is therefore subject to voltage distortions that result in large harmonic currents. For this reason it is necessary to improve the network in order to reduce the magnitude of these harmonic currents drawn by the capacitors.

An inductor of fixed value is therefore inserted in series with the capacitors in order to introduce an impedance that increases with frequency. This is verified with the inductor formula shown below:

$$X_L = j \cdot w \cdot L$$

The inductor acts to restrict the flow of higher frequency current components through the capacitors.

The further improved inductor-capacitor network is shown, below, in Fig. 8.35.

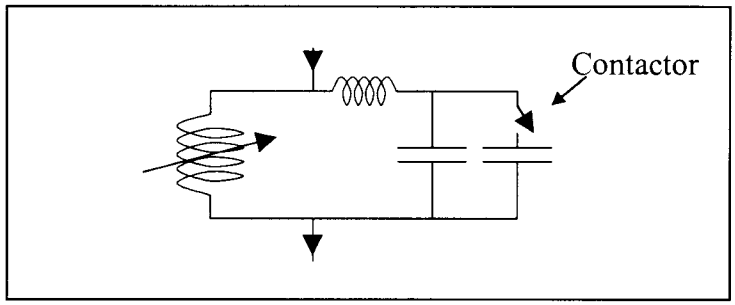

Figure 8.35 Circuit diagram of improved parallel capacitor-inductor network with series inductor

8.9.3 Improvement 3

The third improvement, previously mentioned in chapter 5, involves the power factor of the motor. The reduced, per phase, equivalent circuit of an induction motor is shown in Fig. 8.36, below. In this instance all the equivalent circuit parameters are lumped together forming a single resistance in series with a reactance equivalent as shown.

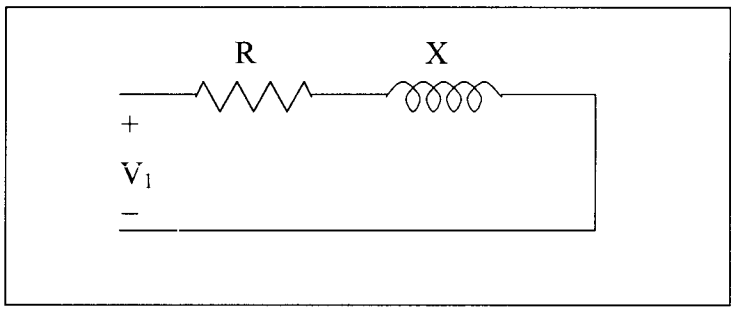

Figure 8.36 Reduced per phase equivalent circuit of an induction motor

The inherent inductive nature of the motor determines the supply power factor, given by:

$$PF = \cos \theta_1$$

Where θ_1 is the phase angle of the stator current I_1. The supply power factor will therefore always be lagging, which is not ideal.

This is partially corrected for by the addition of a compensating capacitor, per phase, as shown below in Fig. 8.37, which not only help to improve the power factor of the motor, but also help to reduce the compensating element values.

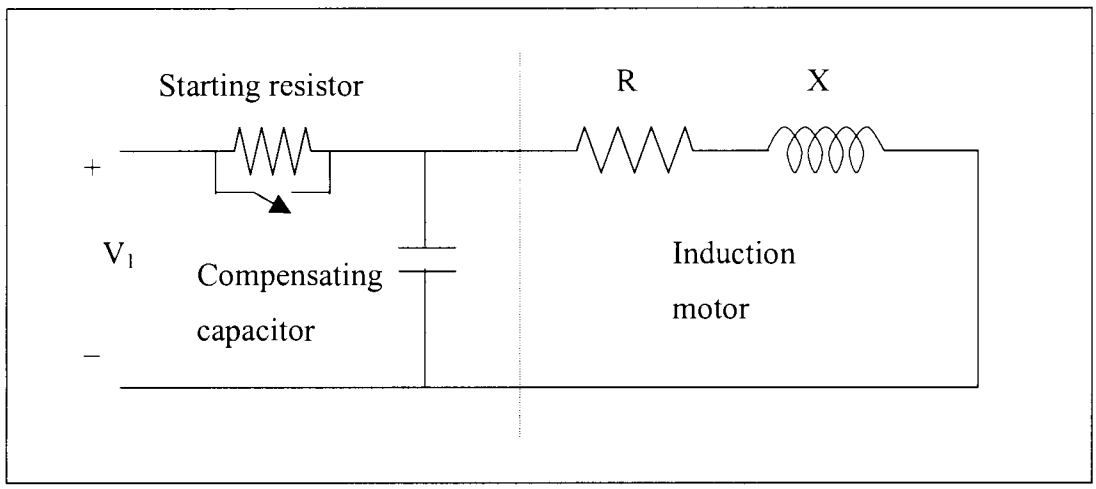

Figure 8.37 Equivalent per phase circuit of the induction motor with compensating capacitor

The above three improvements are now implemented in the final converter design.

8.10 Final Converter Design

The final converter design is thus established and is shown below in Fig. 8.38.

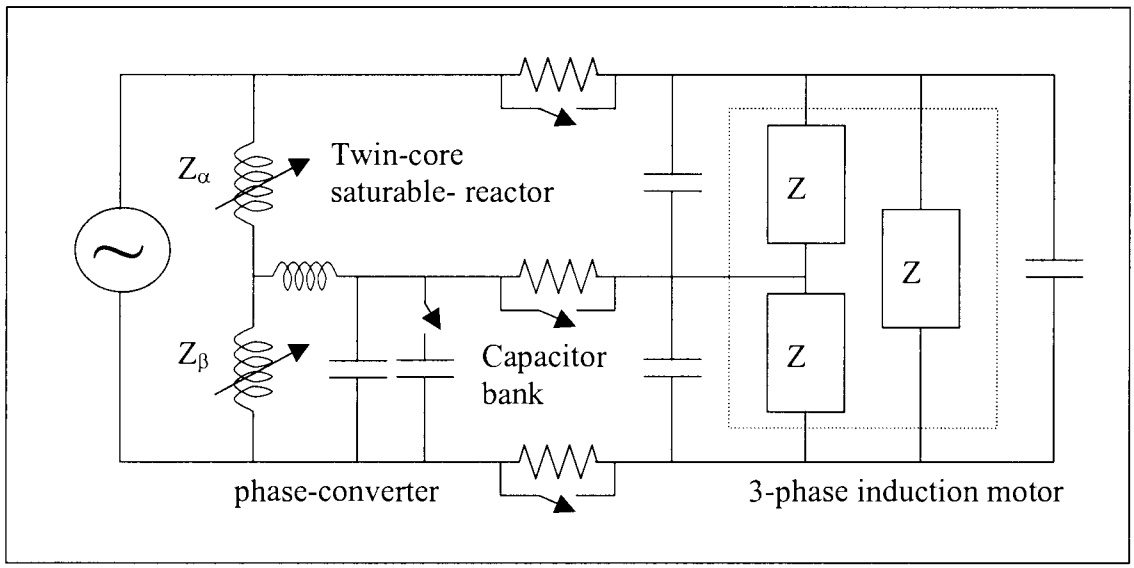

Figure 8.38 Final converter design using two twin-core saturable reactors and improved capacitor bank

The circuit in Fig. 8.38 is shown **complete** with the following:

- **Switched capacitor bank** used to reduce the overall capacitance and hence minimise circulating currents.
- **Series inductance** to reduce harmonic currents drawn by the capacitor bank.
- **Compensating capacitors** that are placed directly across the motor phases in order to reduce the compensating element values and improve the overall power factor of the system.
- **Starting resistors** that limit the inrush currents at motor start-up to 60A.
- **Contactors** used to switch out the starting resistors and a proportion of the capacitor bank, both of which are not required once the motor has run up.

Together these components form the reactive phase shifting network required to obtain balanced phase conversion for the motor over its full slip range.

As the slip of the induction motor changes, either while running up from stand still or due to load variations, the compensating elements, Z_α and Z_β, can be varied to maintain exact phase balance. The values of inductance, Z_α, and capacitance, Z_β, verses slip for the motor are shown in Fig. 8.39 below.

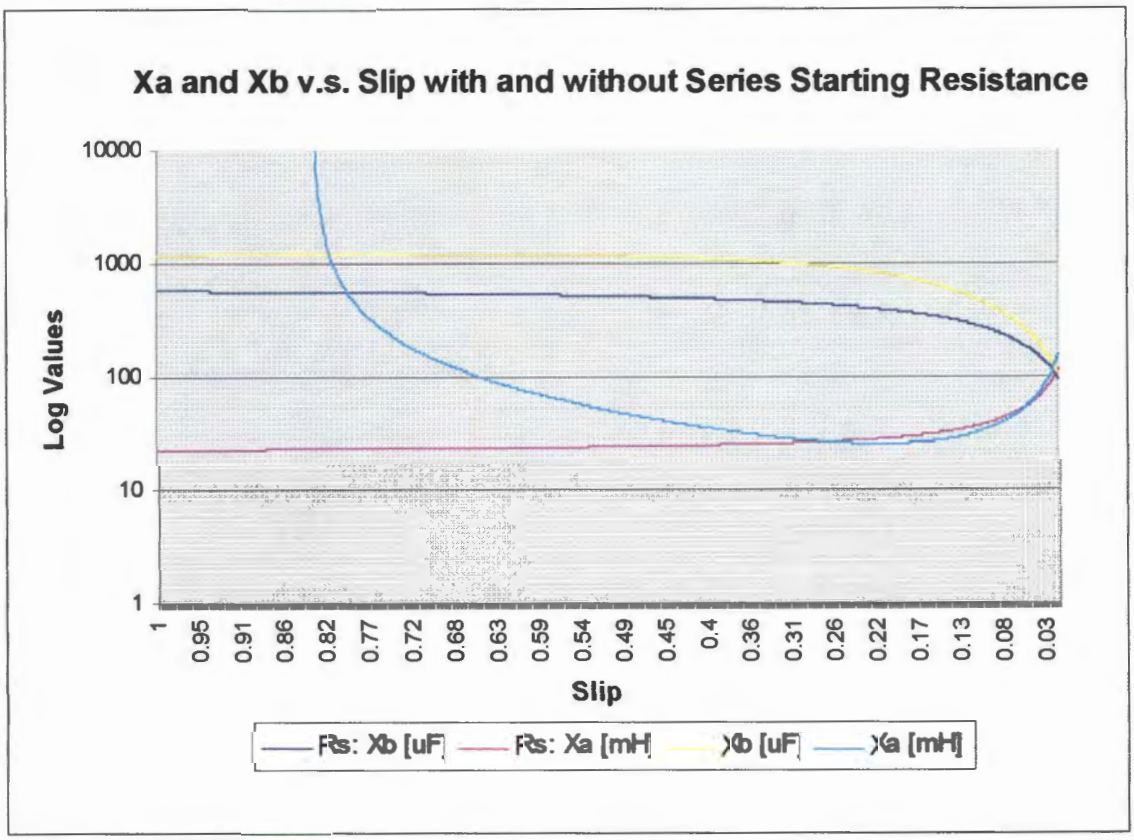

Figure 8.39 Graph of inductance and capacitance vs. slip required to achieve phase balance

Thus for different values of motor slip, both saturable reactors have to be adjusted in order to achieve the values as shown in Fig. 8.39.

At high slip values, corresponding to motor startup, low inductance and the large capacitance is required. Thus the first saturable reactor is driven hard into saturation in order to obtain this low value of inductance. The second reactor, in parallel with the capacitor bank, is hardly saturated at all, in order to obtain a high effective capacitance.

As the slip values decrease, corresponding to an increase in motor speed, the inductance required increases and the capacitance required decreases. The first saturable reactor is driven less into saturation, in order to obtain this higher inductance. The second reactor, however, is driven harder into saturation, in order to lower the effective capacitance of the capacitor bank.

It is therefore observed that the two reactors perform opposite roles to one another. While the one is saturated the other is not and visa versa.

The next chapter deals with how automatic selection of values for the compensating element can be accomplished.

9 Control Theory

9.1 Introduction

In this chapter the design process and the ideas behind the development of the control of the converter are covered. Several control methods are proposed, with issues of importance being addressed. One of these methods is utilised and applied to the final converter design. The final control method is then discussed in detail.

Due to the physical nature of the motor-pumping system, it is neither practical nor economically viable to attach any speed-monitoring device, such as a taco-generator, to the system. It appears that measuring motor slip, which is accomplished by measuring motor speed, is the ideal method for controlling the converter, seen that compensating element values are calculated as functions of motor slip. However, the scope of this project does not allow for this, thus other methods of control are investigated.

9.2 *Single Variable Control Methods*

9.2.1 Introduction

As seen in the chapter 3, section 3.8, it is possible to calculate, for a particular motor at a certain slip, the values of the compensating elements required to achieve exact current balance. Thus for every value of slip, both compensating element values are known. In this way it is possible to tie both of the variable compensating elements together. This reduces a multi-variable control problem to a function of one variable, significantly simplifying the control strategy.

9.2.2 Digital Phase Control Method

This method of control is based on monitoring the phase angle of the manufactured phase voltage. A block diagram of the control circuit is shown below in Fig. 9.1.

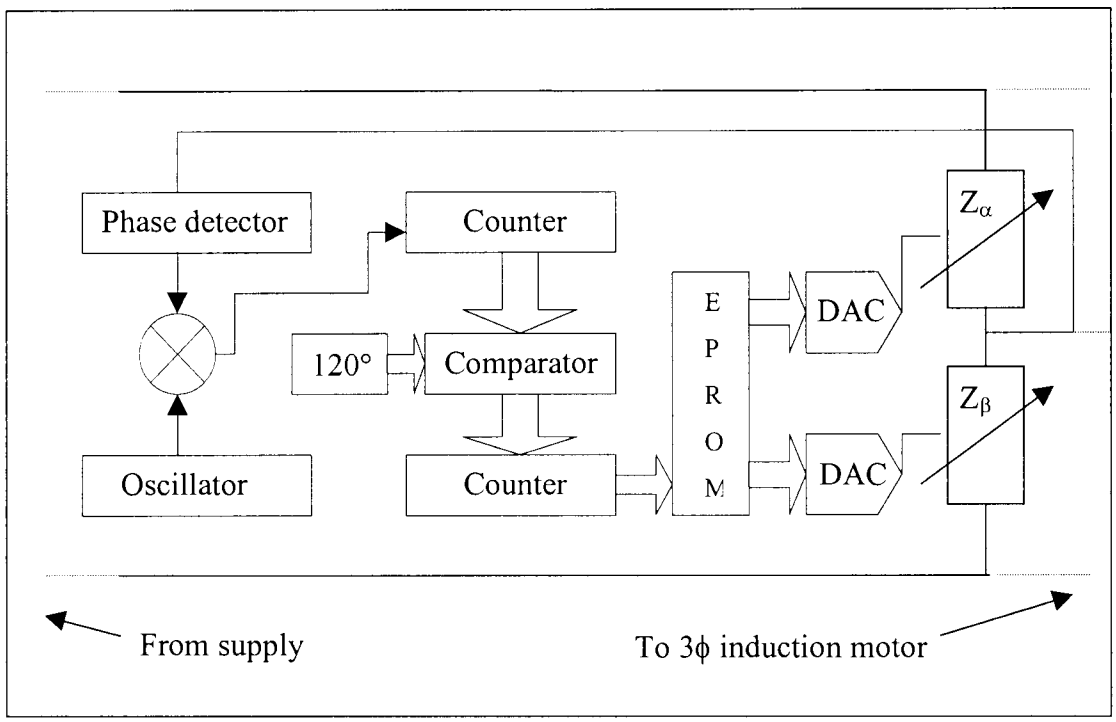

Figure 9.1 Block diagram of digital phase control method for converter

This digital controller makes use of the fact that the two compensating element values can be linked, resulting in a single variable control function, to simplify the control strategy.

The controller operates as follows:

1. The phase of the manufactured voltage is monitored by two, polarity sensitive, zero-crossing detectors. Their output pulses are differentiated and fed into an R-S flip-flop. The output of the flip-flop is a pulse, the width of which corresponds to the phase of the manufactured voltage.
2. The pulse is then gated with a digital oscillator, the result being a gated number of pulses proportional to the phase of the manufactured voltage.
3. These pulses are sent to a binary counter, which outputs a binary number proportional to the phase of the manufactured voltage.
4. The binary number is then compared with a known binary reference of 120°, the output of which is a greater than, less than or equal to signal.
5. The output signal is used to controls an up/down synchronous counter which then either steps up or down or stays the same based on this signal. The output of the synchronous counter drives the address lines of two EPROM's.
6. The values of the currents that are required to control the two saturable-core reactors, so that they create the correct inductance and capacitance, are stored as voltage pairs in the two EPROM's. The output lines of the EPROM's are used to drive two digital-to-analogue (DAC) converters.
7. The DAC output voltages are then used to drive two switch-mode power supplies (SMPS) which convert the voltages into the required currents for the saturable reactors.

This method of control is suitable for the converter, however, it does have some drawbacks. The advantages and disadvantages are listed below:

Advantages:

- This method links the two variable compensating elements together, forming a single variable control problem that significantly simplifies the control strategy.
- The zero-crossing voltage detectors are optically isolated from the supply lines. This not only eliminates the need for voltage transformers, but also improves the isolation and safety of the control circuitry.
- The zero-crossing detectors have digital outputs, thus there is no need to convert the feedback signals from analogue to digital using an ADC.
- The motor characteristics are stored in two EPROM's. Reprogramming of the EPROM's is all that is required for the controller to operate on another motor.
- This control method requires no external sensors, such as tacho-generators, to be attached to the motor.

Disadvantages:

- The controller is motor specific and would have to be reprogrammed for various makes of motor.
- The system, being digital, is inherently slower than its analogue equivalent.
- The controller is sensitive to variations in the line frequency. This is due to the compensating element values that are pre-stored in the EPROM's, being calculated for a 50 Hz system.

9.2.3 Combined Analogue and Digital Voltage Control Method

This method of control is based on monitoring the manufactured phase voltage. A block diagram of the control method is shown below in Fig. 9.2.

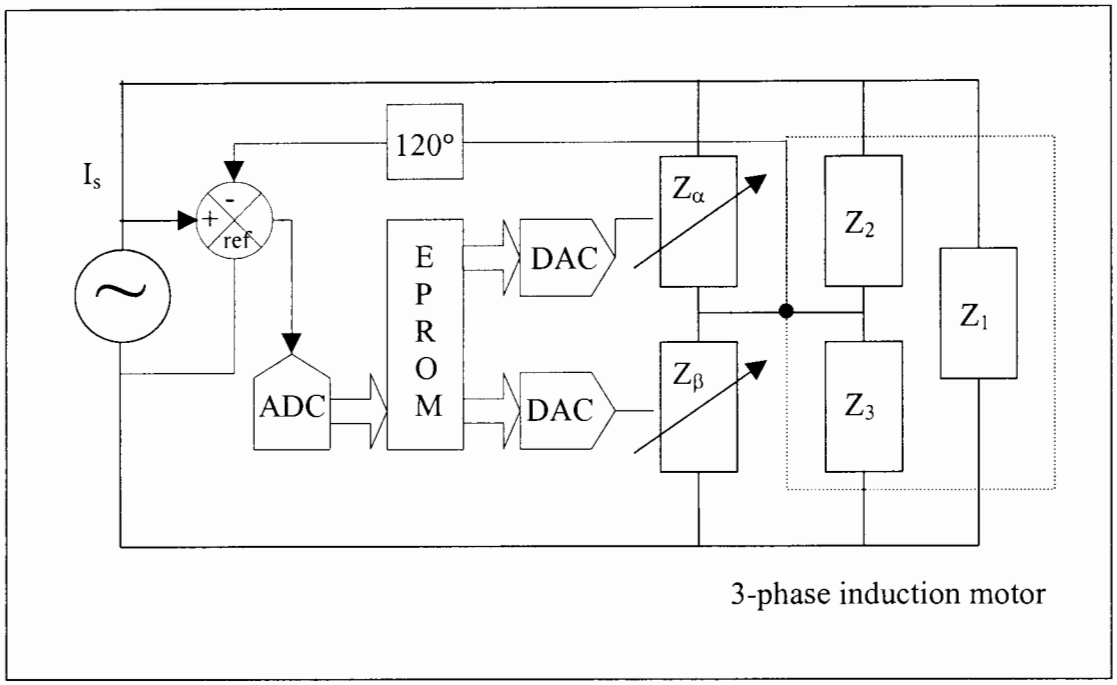

Figure 9.2 Block diagram of combined analogue/digital control method

The controller operates as follows:

1. The manufactured phase voltage is monitored and shifted by 120° in order to bring it into phase with the supply voltage.
2. This voltage is then subtracted from the monitored supply voltage and an error voltage produced.
3. An analogue-to-digital converter then digitises the error voltage.
4. The digital signal is used as an address for a lookup table.
5. The pairs of calculated compensating element values, for the complete slip range of the motor, are stored sequentially in the lookup table.
6. The corresponding digital values stored in the lookup table are converted to analogue values by two digital-to-analogue converters.

7. These analogue values are used to drive the saturable reactors to obtain the desired results.

The advantages and disadvantages of this method of control are listed below.

Advantages:

- This method links the two variable compensating elements together, forming a single variable control problem that significantly simplifies the control strategy.
- The motor characteristics are stored in two EPROM's. Reprogramming of the EPROM's is all that is required for the controller to operate on another motor.
- This control method requires no external sensors, such as tacho-generators, to be attached to the motor.

Disadvantages:

- The need for isolating transformers in order to monitor the two desired voltages.
- Converting from analogue-to-digital increases the amount of hardware. This process can be slow and could result in additional errors being introduced into the control loop.
- The controller is motor specific and would have to be reprogrammed for various makes of motor.
- The whole system is frequency sensitive, seen that all stored values are calculated based on a 50 Hz operating frequency.

9.3 Multi-Variable Control Methods

9.3.1 Analogue Current Control Method

On initial inspection the control of the converter appears trivial as shown in Fig. 9.3 below.

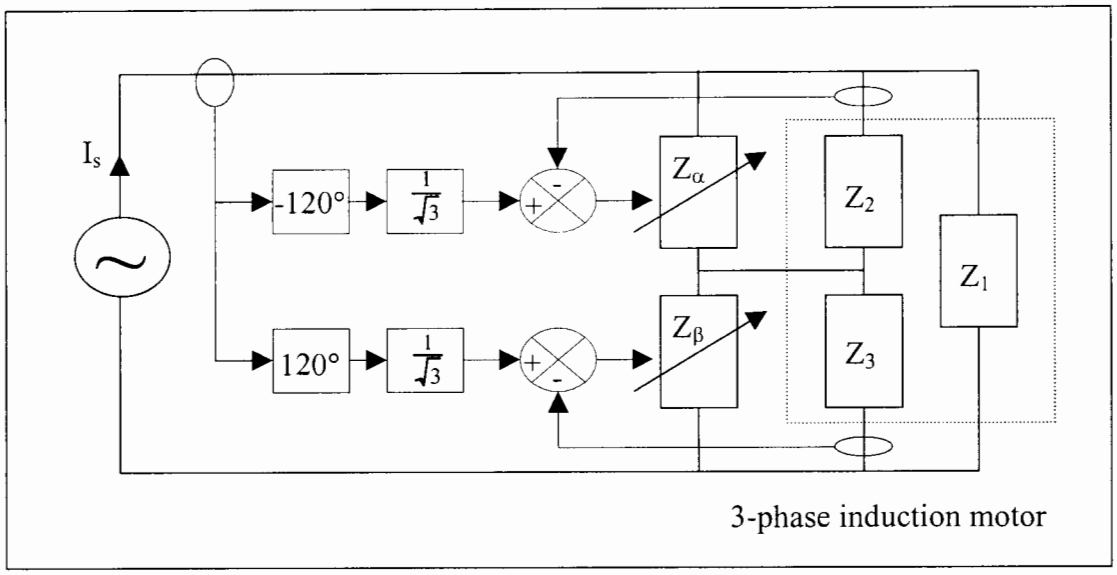

Figure 9.3 Analogue current control method proposed for the converter

By studying the current vector diagram, Fig. 9.4, of the converter, a clearer understanding of the expected principle of operation of the controller is gained.

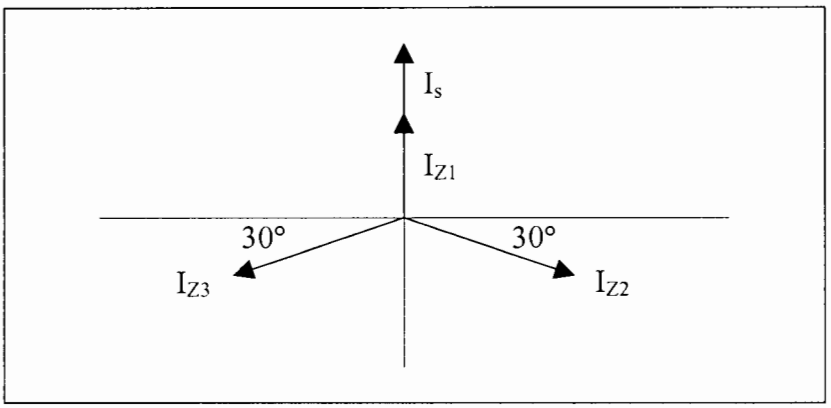

Figure 9.4 Ideal current vector diagram for the converter

As is shown in Fig. 9.4, ideally for a balanced system, all three motor phase currents are not only equally spaced by 120°, but also equal in magnitude. If there is no power loss in the converter, the magnitude of the supply is root three times greater than the phase currents.

Each half of the converter, being symmetrical, works as follows:

1. The supply current is monitored and shifted by 120° to bring it into phase with the I_{Z2} the current that is to be controlled.
2. This current is divided by root three in order reduce its magnitude to that of I_{Z2}.
3. This current is then subtracted from the monitored value of I_{Z2} and the error is used to drive the compensating element in order to correct for any imbalance in I_{Z2}.

Unfortunately this proposed control method will not work due to inherent instability. The problem is explained as follows:

- If any one of the compensating elements alters its value, more or less current will flow through it.
- This results in a variation in the current drawn from the supply.
- This alters the setpoint, which is common to both halves of the controller.
- Thus both halves of the controller will attempt to correct for the imbalance, resulting in instability.

A new method of control is thus required.

9.3.2 Improved Analogue Current Control Method for Converter

An attempt is made to remove the instability by moving the current sensor from the supply line to the motor phase that is placed across the supply lines. This is shown in Fig. 9.5 below.

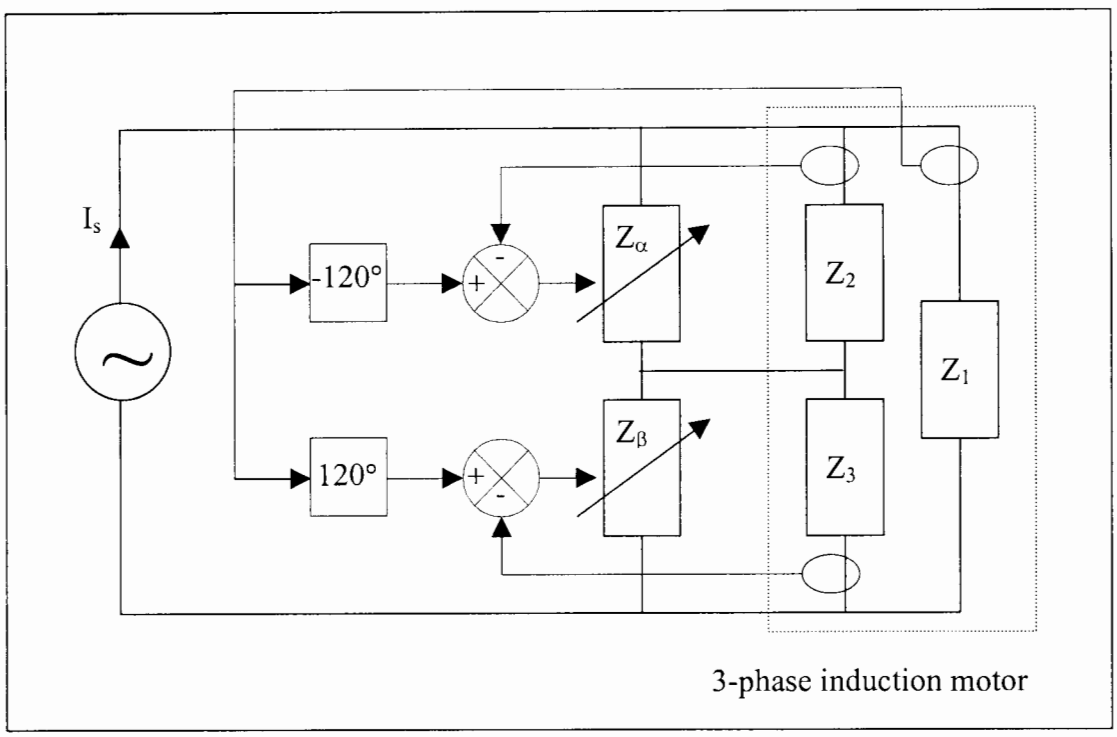

Figure 9.5 Improved analogue current control method for converter

The current that is sensed in this arrangement is independent of supply current variations. The impedance of monitored phase, Z_1, and hence the current drawn through it, I_{Z1}, varies only as a function of motor slip.

As is shown in Fig. 9.4 ideally under balanced supply conditions, all three motor phase currents are not only equally spaced by 120°, but also equal in magnitude.

Each half of the converter, being symmetrical, works as follows:

1. The supply current is monitored and shifted by 120° to bring it into phase with the I_{Z2} the current that is to be controlled.
2. This current is then subtracted from the monitored value of I_{Z2}, and the error is used to drive the compensating element in order to correct for any imbalance in I_{Z2}.

Unfortunately this proposed control method, although an improvement, suffers from two drawbacks. They are as follows:

- Either an extra set of wires needs to be brought out from the motor or the current sensors need to be mounted on the motor and the signal wires taken back to the converter in order to monitor the phase currents of the delta connected motor.
- The control circuitry is sensitive to harmonics and frequency shift, because it relies on sinusoidal input voltages.

Thus further refinements to the control method are required.

9.3.3 Refined Analogue Current Control Method for Converter

The control method discussed in 9.3.2 is improved upon in order to remove some of the disadvantages associated with it. The refined control method for the converter is shown below in Fig. 9.6.

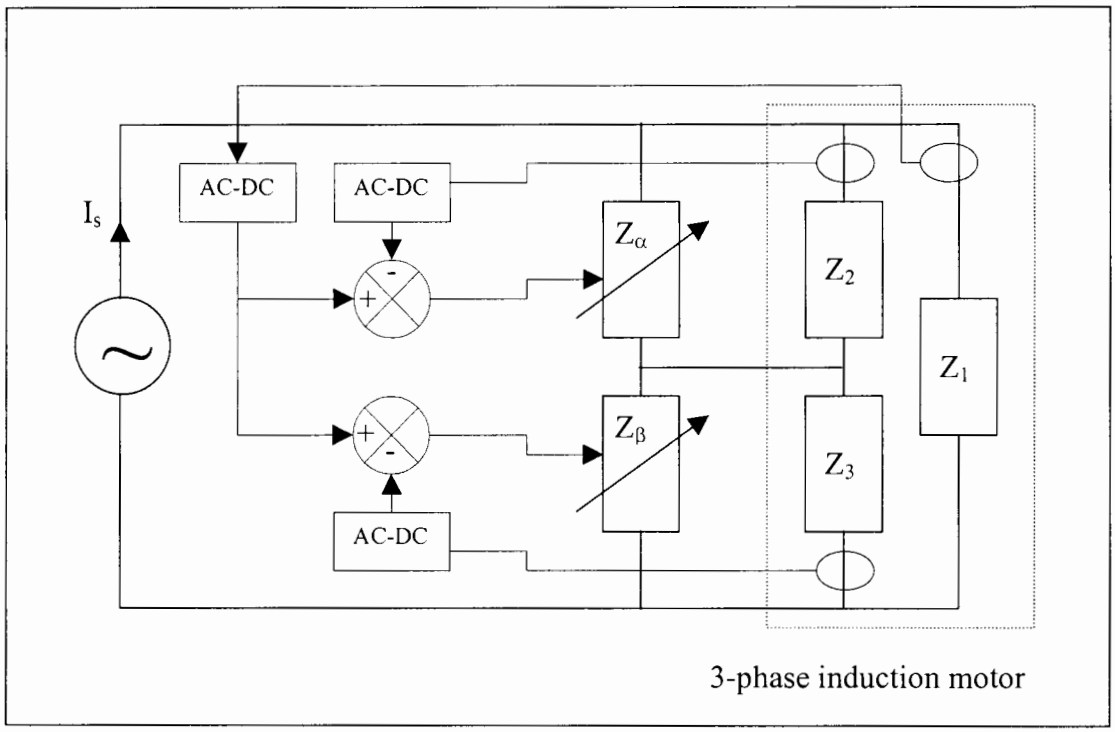

Figure 9.6 Refined analogue current control method for converter

As is seen in Fig. 9.6 above, the basic topology of the control method remains unchanged. The phase currents of the motor are still monitored, however, they are now converted to dc values. It is these dc signals that are used to control the converter as explained.

Each half of the converter, being symmetrical, works as follows:

1. The supply current is monitored and the ac signal is precision rectified and smoothed, converting it to a dc value.
2. I_{Z2}, the current that is to be controlled, is also monitored and converted to a dc value as explained above.
3. This second dc voltage is subtracted from the first and the difference or error voltage is used to drive the compensating element in order to correct for any imbalance in I_{Z2}.

This control method is implemented in the final converter design, however, it still suffers from the problem associated with monitoring of the motor phase currents. The sensitivity to current harmonics and frequency changes are removed with the introduction of the averaging circuits.

10 Controller Simulation

10.1 Introduction

In this chapter the control method that is to be implemented in the final converter design is verified through simulation. The results of the simulation are then used to determine the suitability of the controller to the converter. The software used for simulation was the industry standard MicroSim (PSpice) Release Version 8.0 – July 1997.

10.2 Test Circuit

A test circuit is first simulated, before attempting to simulate the entire controller, in order verify the theory of the two element compensator, as derived by Malengret [9] and discussed in detail in chapter 3 section 6-8. The test circuit, shown below in Fig. 10.1, consists of a purely resistive, balanced, three-phase load.

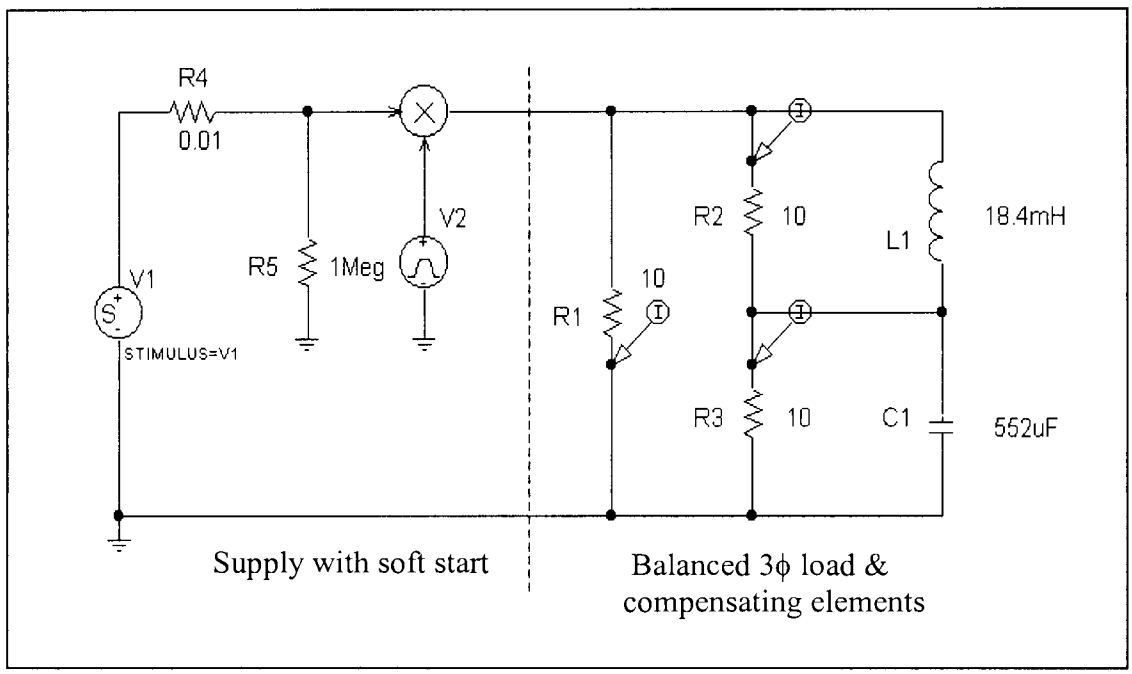

Figure 10.1 Test circuit used to verify simulator operation

The compensating element values are derived from the equations obtained in chapter 3 as follows:

$$Z_a = -\frac{j(X_l^2+R_l^2)}{X_l-\sqrt{3}\cdot R_l} \qquad Z_b = -\frac{j(X_l^2+R_l^2)}{X_l+\sqrt{3}\cdot R_l}$$

Substituting the values of X_l and R_l we get:

$$Z_a = -\frac{j\cdot 10^2}{-\sqrt{3}\cdot 10} \qquad Z_b = -\frac{j\cdot 10^2}{\sqrt{3}\cdot 10}$$

$$Z_a = j\cdot 5.77 \qquad Z_b = -j\cdot 5.77$$

Now converting to component values, remembering that $\omega=2\pi f$, we get:

$$Z_a = j\cdot w\cdot L \qquad Z_b = \frac{1}{j\cdot w\cdot C}$$

$$j\cdot 5.77 = j\cdot 2\pi\cdot 50 L \qquad -j\cdot 5.77 = \frac{1}{j\cdot 2\pi\cdot 50 C}$$

$$L = 18.4\,mH \qquad C = 552\,uF$$

Simulating the test circuit, as seen in Fig. 10.1, results in the graph shown below in Fig. 10.2.

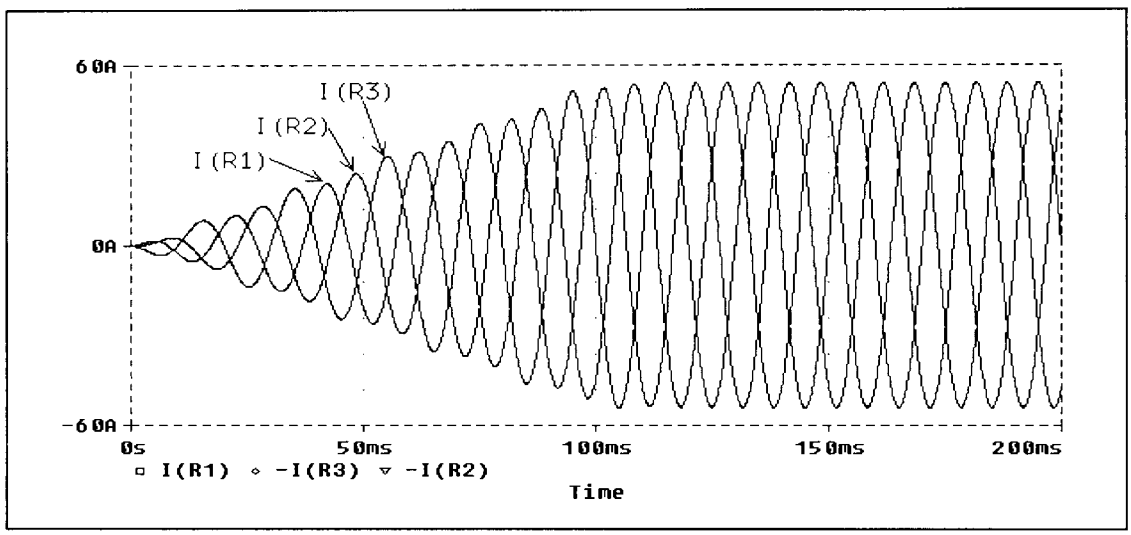

Figure 10.2 Graph of phase currents resulting from test circuit simulation

As seen in Fig. 10.2, the phase currents of the load are completely balanced and 120° apart. The soft start is responsible for the linear rise in voltage for the first 100ms. This is achieved, as seen in Fig. 10.1, by multiplying the incoming supply waveform with a voltage pulse that starts from a value of zero and rises linearly to a value of one over 100ms. This is done in order to prevent convergence errors from occurring during the simulation.

10.3 Control Circuit

Through first simulating a test circuit, a clearer understanding of the simulator is obtained. In this way the intricacies, capabilities and boundaries of the program are also established well in advance.

The circuit used to verify the control theory proposed in chapter 9 and to model the converter with controller, is illustrated below in Fig. 10.3.

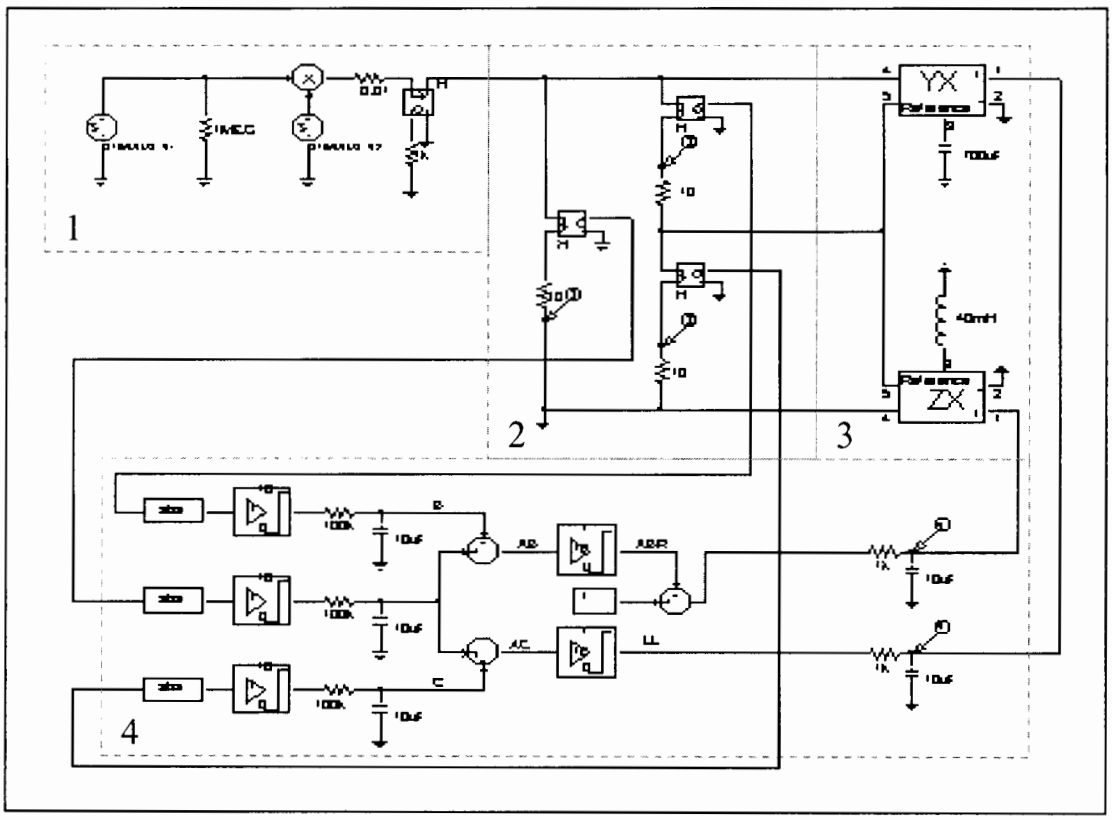

Figure 10.3 Converter simulation circuit

Various portions of Fig 10.3 are numbered for explanation:

1. 380V Power supply with soft start.
2. Balanced, resistive, delta-connected, three-phase load with current sensors.
3. Variable compensating elements.
4. Proportional controller with limiting.

The phase currents and control voltages obtained from simulating the circuit shown in Fig. 10.3 are shown in Fig 10.4, below.

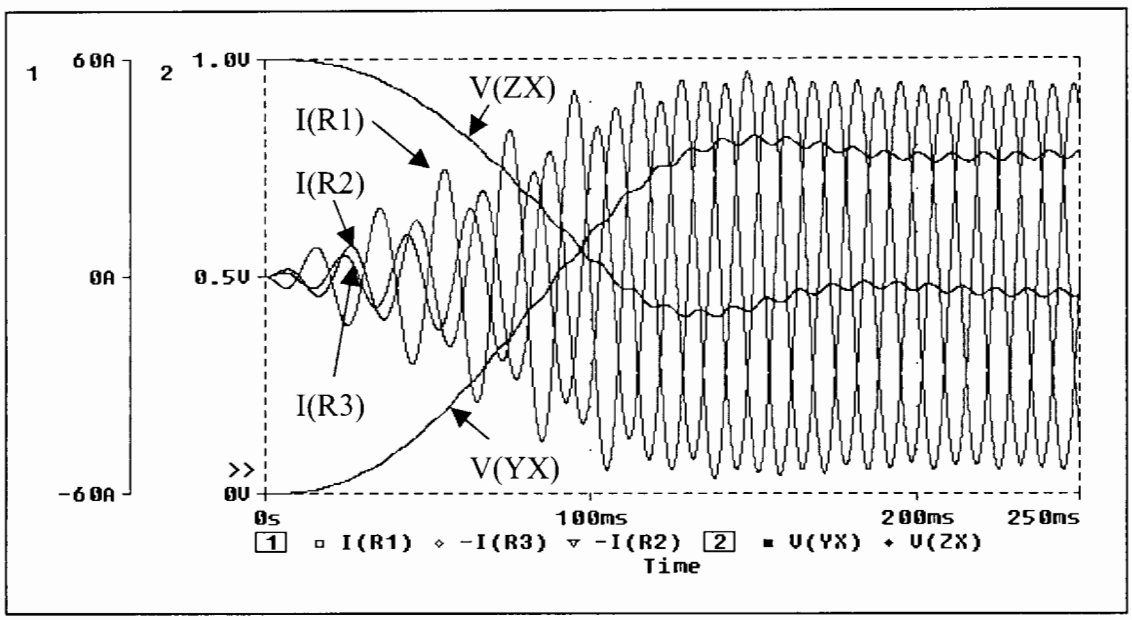

Figure 10.4 Graph of phase currents and control voltages for converter

From the graph in Fig. 10.4, above, several points are noted, namely:

1. **Balanced three-phase currents**. Initially, there is a degree of imbalance, however, after a certain settling time, full balance is achieved.
2. **Stable control voltages**. There is a marginal amount of overshoot, however, both voltages converge and remain stable. The control voltages contain a certain amount of ripple due to the 100Hz component present after rectifying and smoothing of the monitored phase currents.

This is more clearly seen in Fig 10.5, below, an expanded portion of the trace, from 200ms to 250ms, shown in Fig. 10.4.

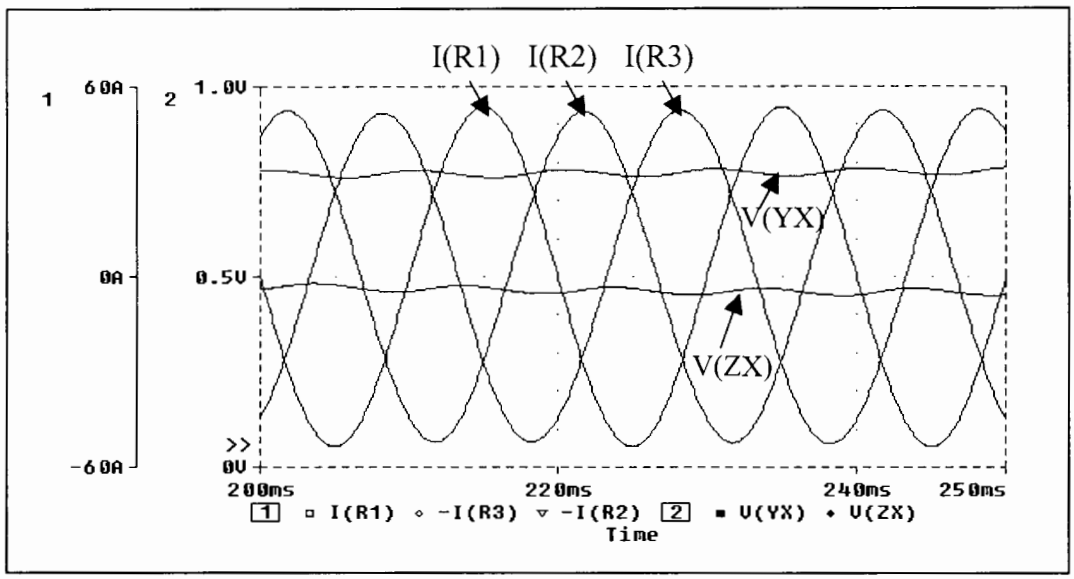

Figure 10.5 Expanded trace of phase currents and control voltages

The ripple can be reduced by increasing the time constants of the smoothing circuitry, however, this increases the delays in the control loop and introduces instability.

3. **Similarity between Fig. 10.3 & Fig.10.4.** The graphs of results obtained from the initial test circuit and the converter controller circuit are comparable.

Next the controller is subject to a step response in order to evaluate its stability under varying load conditions. The circuit used to perform the step test is shown in Fig. 10.6, below.

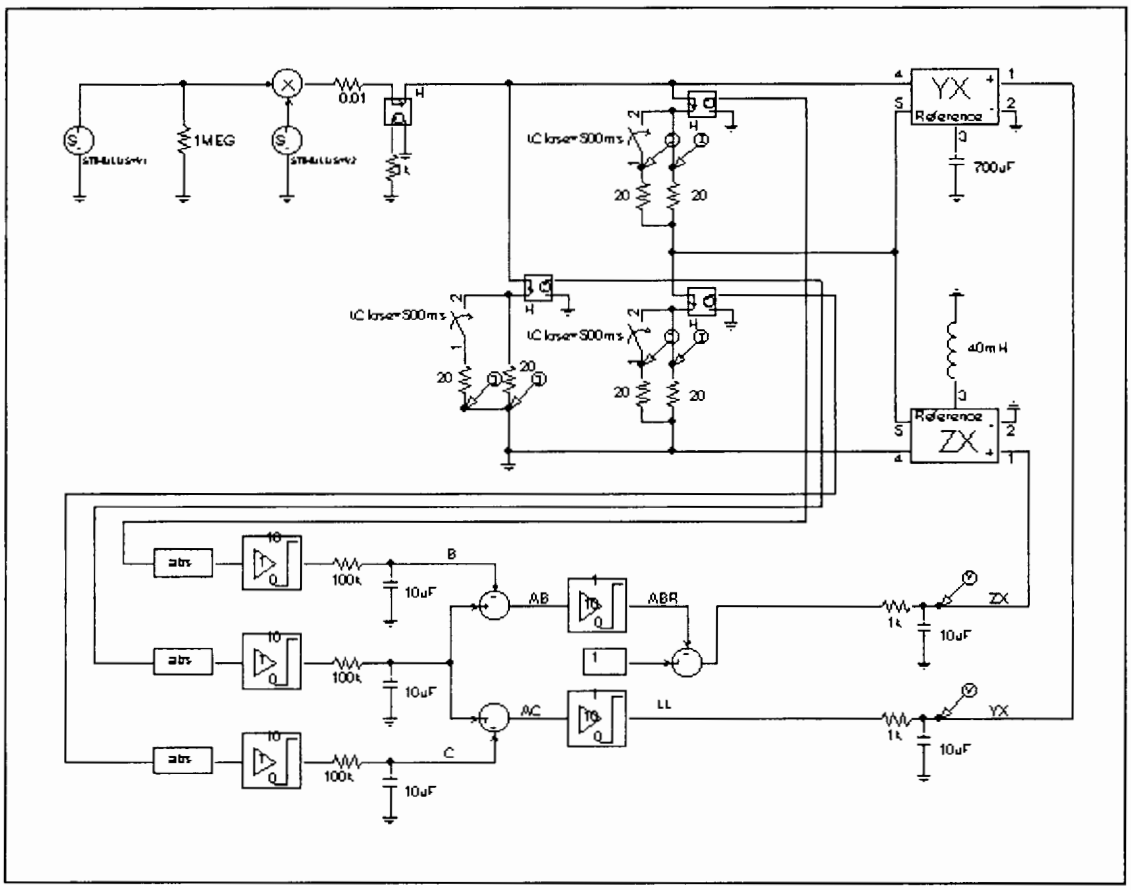

Figure 10.6 Converter simulation circuit with switchable load

As is seen in Fig. 10.6, above, the circuit differs only in load from the circuit in Fig. 10.3. The load is made discretely variable, through the addition of timed switches that bring in additional loads after 500ms. This has the effect of simulating a step change in load to the motor.

The results of the simulation are shown in Fig 10.7.

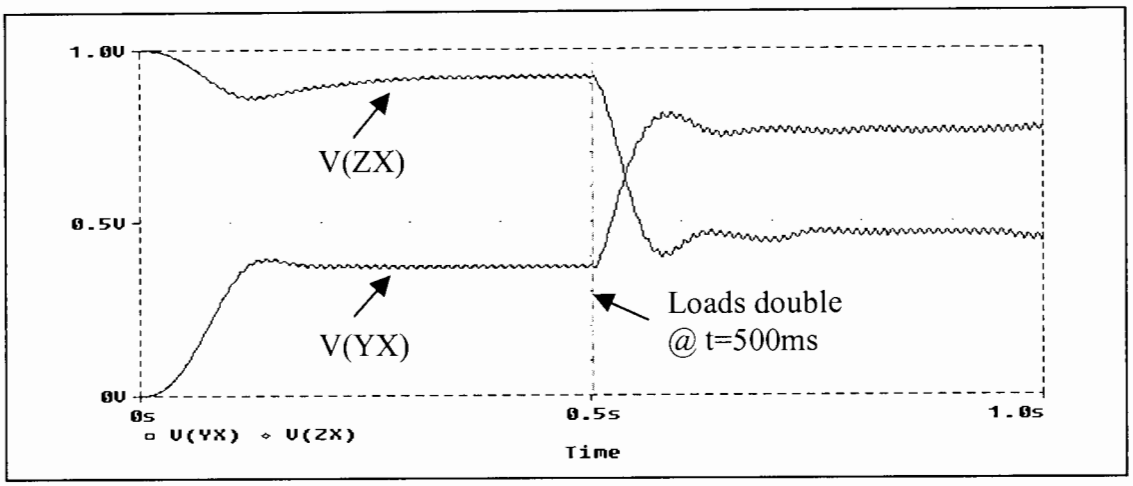

Figure 10.7 Graph of converter control voltages under changing load conditions

As is seen in Fig. 10.7, above, stable control voltages are produced. There is a marginal amount of overshoot after the step load change as with start up, however, both voltages converge and remain stable after a certain settling time. During the finite settling time, a degree of current imbalance results, however, full balance is restored once the control voltages settle. This is shown more clearly in Fig. 10.8, below, an expanded portion of the trace in Fig. 10.7, from 450ms to 650ms, including load currents.

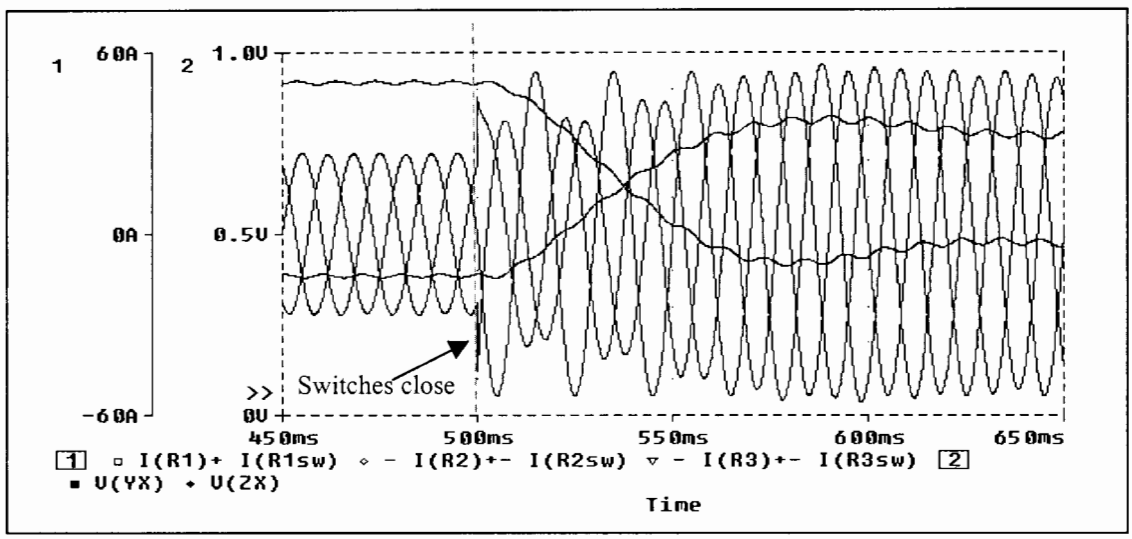

Figure 10.8 Expanded trace of phase currents and control voltages about switching point

The simulation circuit is now modified to more accurately model the converter. The following changes are made:

1. The load is made exponentially resistive to approximate a motor accelerating from standstill, at start up, to full speed, at no load. The resistance of each phase varies (from 10Ω to 50Ω) as a function of an input voltage stimulus, V3, (from 0V to 1V). The function is shown below:

$$R_{123}=10+40 \cdot V_3$$

The graph of V3 is shown in Fig. 10.9, below.

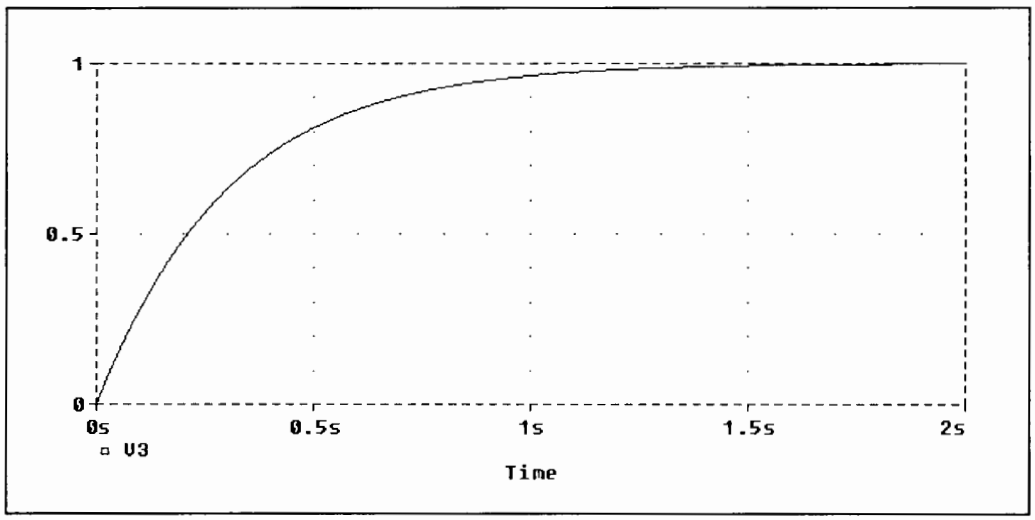

Figure 10.9 Graph of exponentially varying input voltage stimulus, V3

2. The controller is modified to take "real life" initial conditions into account. When initially powered up, the control voltages into the compensating elements start from 0V and rise to their desired values. The rise and fall times of these signals are limited by the time constants of the out put low-pass filters. Thus the control voltages cannot change their values instantaneously.

The modified circuit can be seen in Fig. 10.10, below.

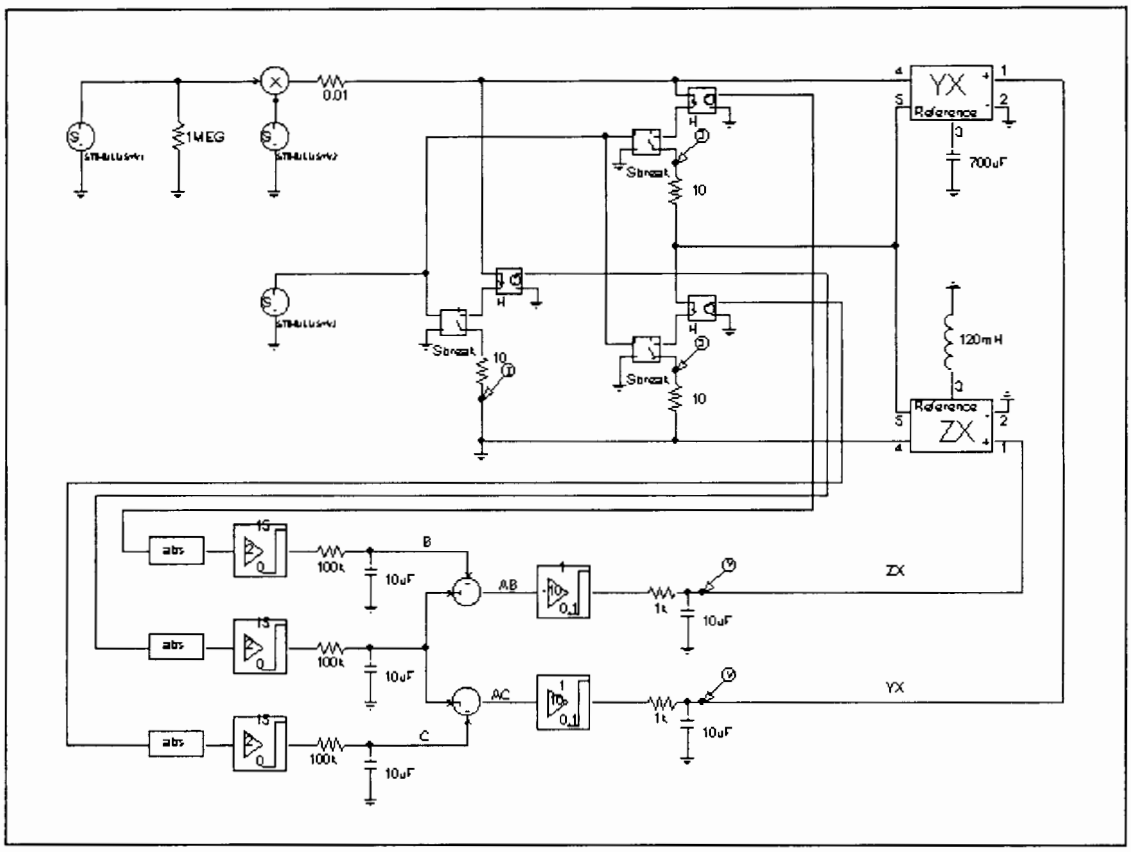

Figure 10.10 Modified simulation circuit with motor load

As with an induction motor, the loads are present from converter switch on and begin to increase in resistance immediately. This is shown in Fig. 10.9, the graph of input voltage stimulus V3.

The results of the simulation are shown in Fig 10.11, below.

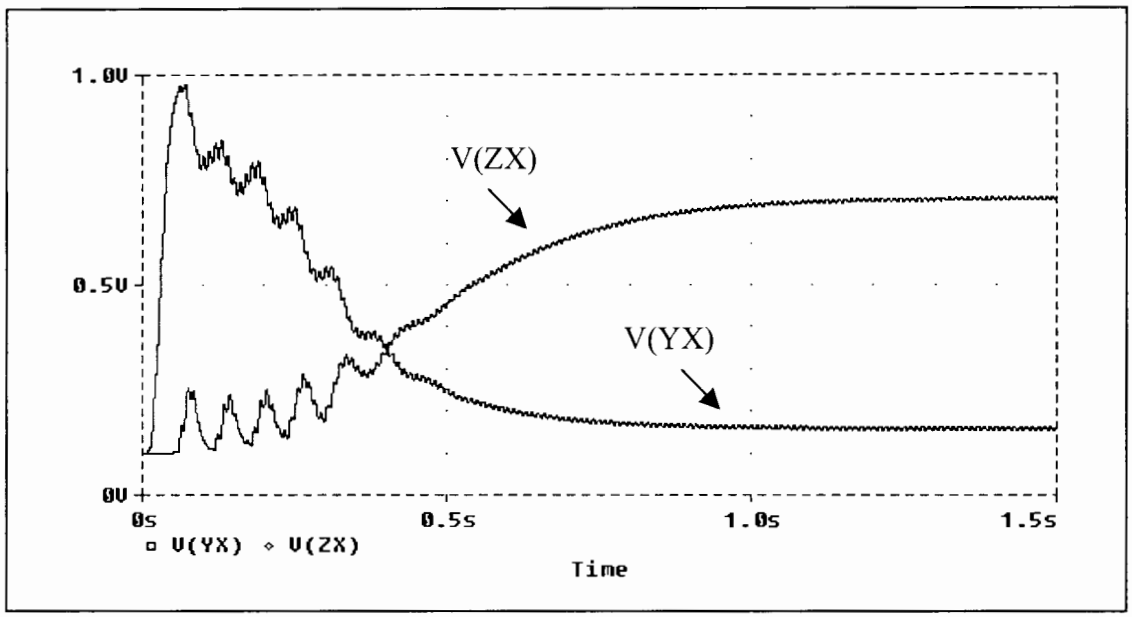

Figure 10.11 Graph of modified converter control voltages under exponentially decreasing load conditions

As is seen in Fig. 10.11, above, stable control voltages result. There is a marginal amount of instability just after start up, due to hunting[1], however, both voltages "lock on" to the varying load, track it, and soon settle. As with the previous simulation a degree of current imbalance occurs during the settling time, however, full balance is restored once the control voltages settle.

[1] Hunting – The two halves of the controller are not fully independent. Thus the two compensating elements have an effect on each other. If one overshoots, the other is effected and tries to compensate. Due to the time delays associated with the smoothing filters, these oscillations take some time to decay, thus the two control voltages hunt each other in an attempt to regain stability.

This is shown more clearly in Fig. 10.12 and Fig 10.13, below. These show expanded portions of the trace in Fig. 10.11, from 0 to 150ms and from 1,25s to 1,35s, respectively, including load currents.

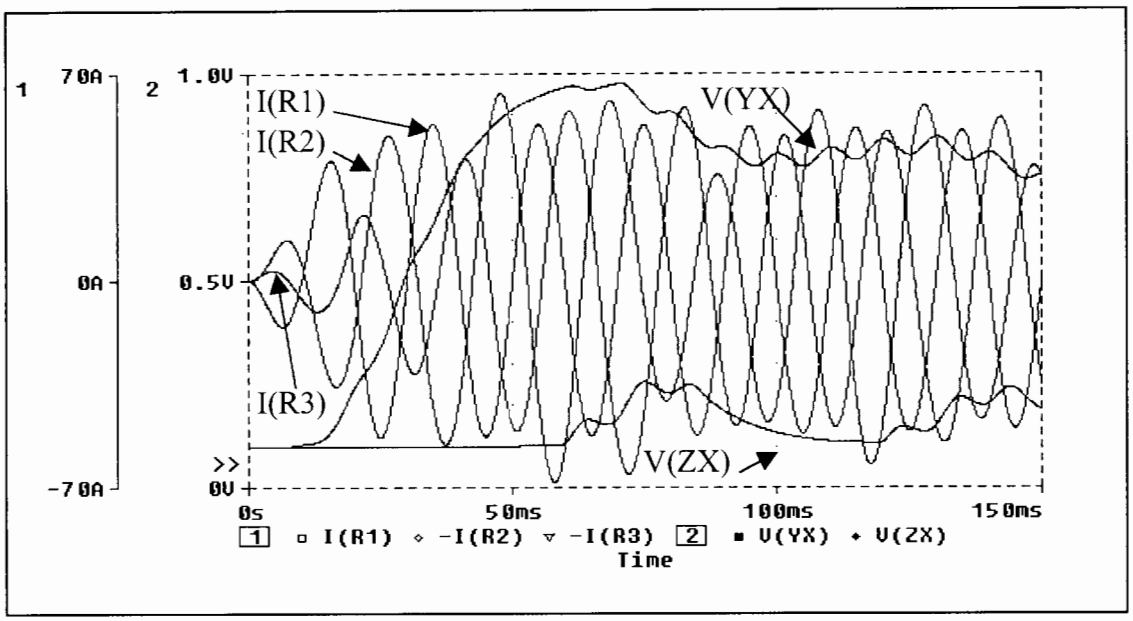

Figure 10.12 Expanded trace of initial phase currents and control voltages for modified converter

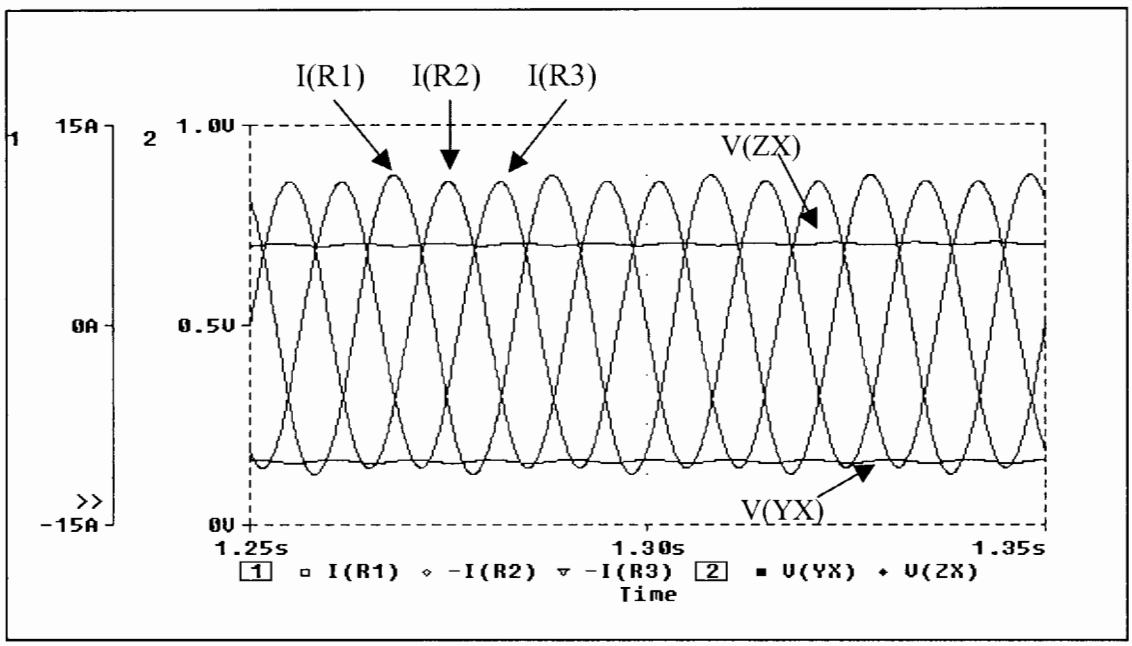

Figure 10.13 Expanded trace of phase currents and control voltages, after settling period, for modified converter

After careful consideration the simulation circuit is altered to more accurately model the motor load and hence the response of the converter.

The load is modified to take the inductance, as well as the resistance, of the motor into account while accelerating from standstill to full speed. The per phase values of these parameters vary as a function of an input voltage stimulus, V3+V4, the graph of which is shown in Fig. 10.14, below.

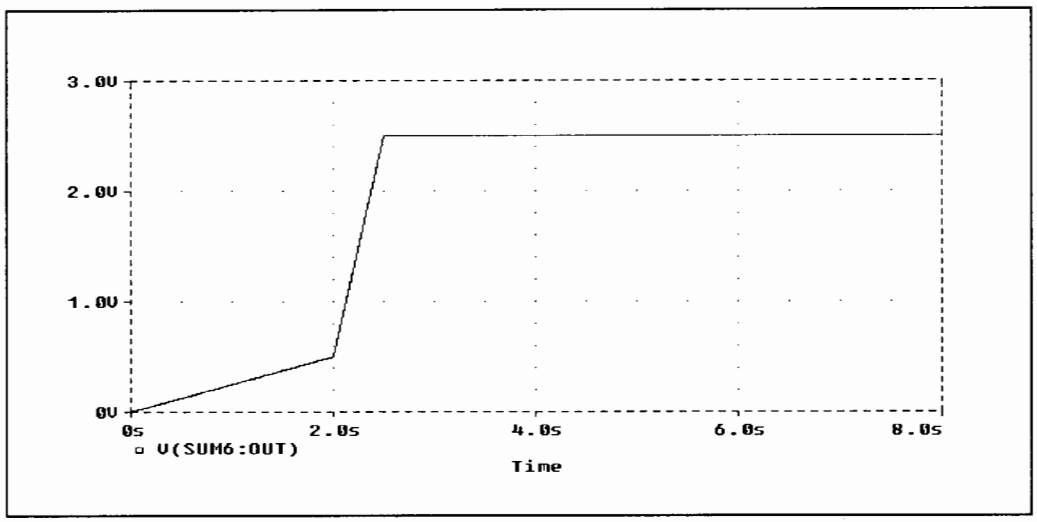

Figure 10.14 Graph of modified input voltage stimulus, V3+V4

It is noted that the per phase currents of the motor stay almost constant throughout acceleration, decreasing slightly, and decrease rapidly close to full speed. It is for this reason that the stimulus profile shown in Fig. 10.14, above is used.

The resistance and inductance of each phase vary from 1.9Ω to 20Ω and from 0mH to 75mH respectively. The functions are shown below:

$$R_{123}=1.9+20\cdot\left(V_3+V_4\right)^{\max(1)}$$

$$L_{123}=30\cdot\left(V_3+V_4\right)$$

The improved circuit can be seen in Fig. 10.15, below.

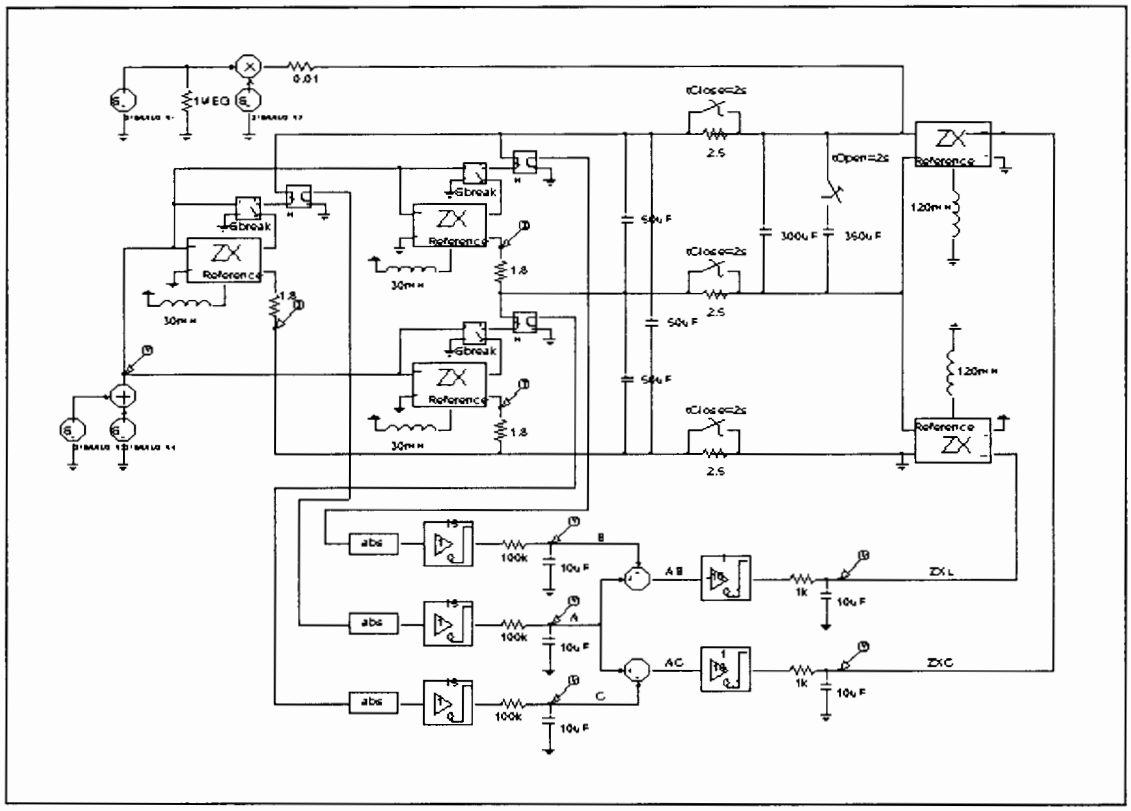

Figure 10.15 Improved simulation circuit with modified motor load

The improved simulation circuit shown in Fig. 10.15, above, thus more accurately models an induction motor as it accelerates from standstill, at start-up, to full speed at no load, by taking the varying internal resistance and inductance of the motor into account over its full slip range.

The results of the simulation are shown in Fig 10.16, below.

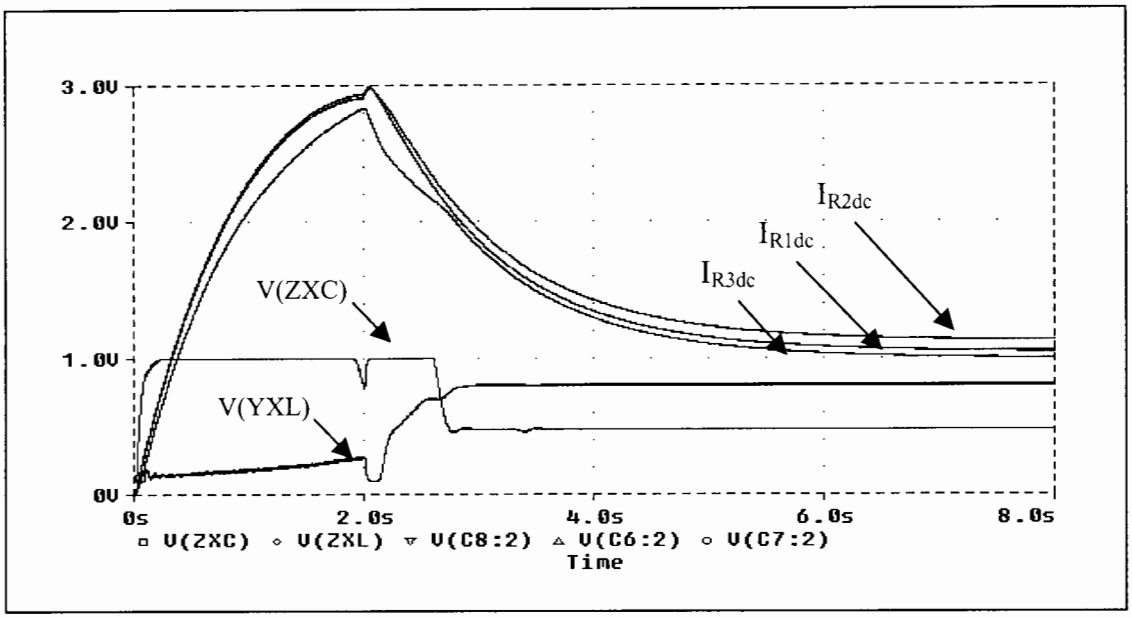

Figure 10.16 Graph of converter control voltages and equivalent dc motor phase currents for improved motor load

As is seen in Fig. 10.16, above, stable control voltages result. There is a marginal amount of instability just after switchover, however, both voltages "lock on" to the varying load, track it, and soon settle. As with the previous simulation a degree of current imbalance occurs during the settling time, however, full balance is restored once the control voltages settle.

The controller thus maintains balanced motor currents over the full slip range of the motor.

The results obtained from simulating the converter under various load conditions are favourable and indicate that implementation of the proposed control theory will work. The next two chapters involve the design and physical construction of the controller as a whole.

11 Design and Construction of Controller Circuitry

11.1 Introduction

In this chapter the ideas behind the development and actual construction of the control circuitry are covered. The overall design is discussed briefly, followed by a detailed description of each subsection. The switch-mode-power-supplies (SMPS), although strictly part of the control circuit, will be dealt with, in detail, in chapter 12.

11.2 Overview of Controller

A general block diagram overview of the controller is shown in Fig. 11.1, below.

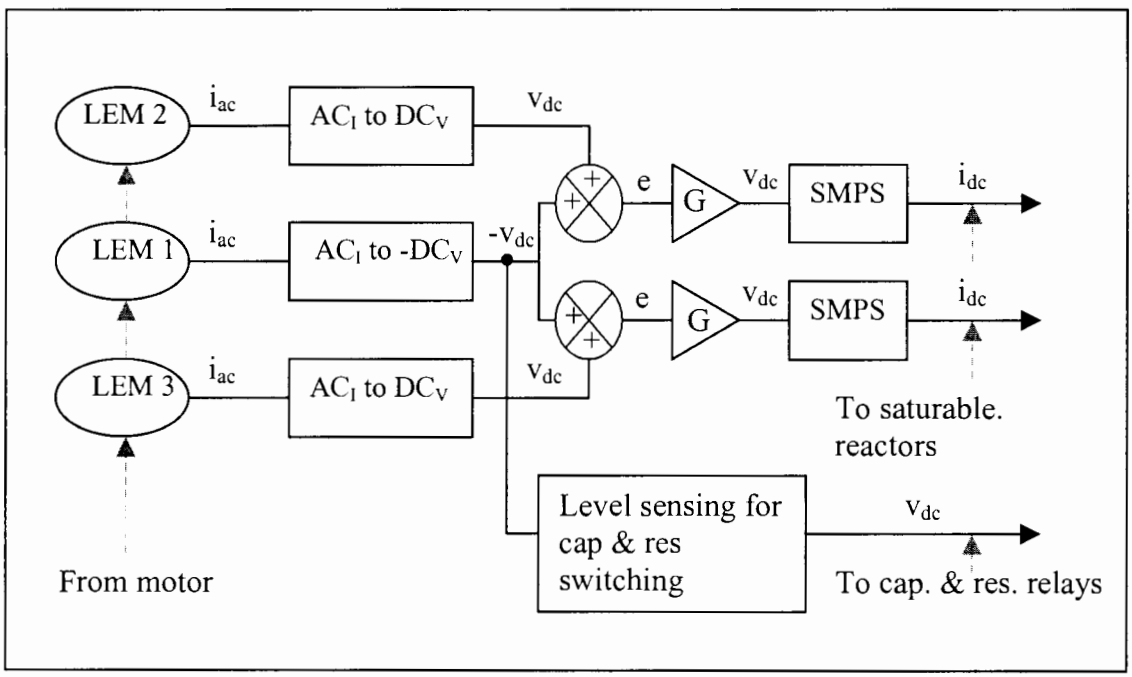

Figure 11.1 Controller block diagram overview

The motor phase currents are monitored using LEM current transducers. The output currents of LEMs 2 &3 are converted to equivalent positive dc values. The output of LEM 1, the primary phase current of the motor, is converted to a negative equivalent

dc value and used as the current setpoint. These values are then summed, as shown, to form error signals. The error signals are then amplified and used as demand voltages to control the SMPS's.

Simultaneously the average dc value derived from the output of LEM 1 is used to determine when to switch out the starting capacitors and resistors.

11.3 Current Acquisition

The phase currents of the motor are monitored using LEM LA 100-P closed loop current transducers [for specifications see Appendix F]. An illustration of a LEM sensor is shown in Fig. 11.2, below.

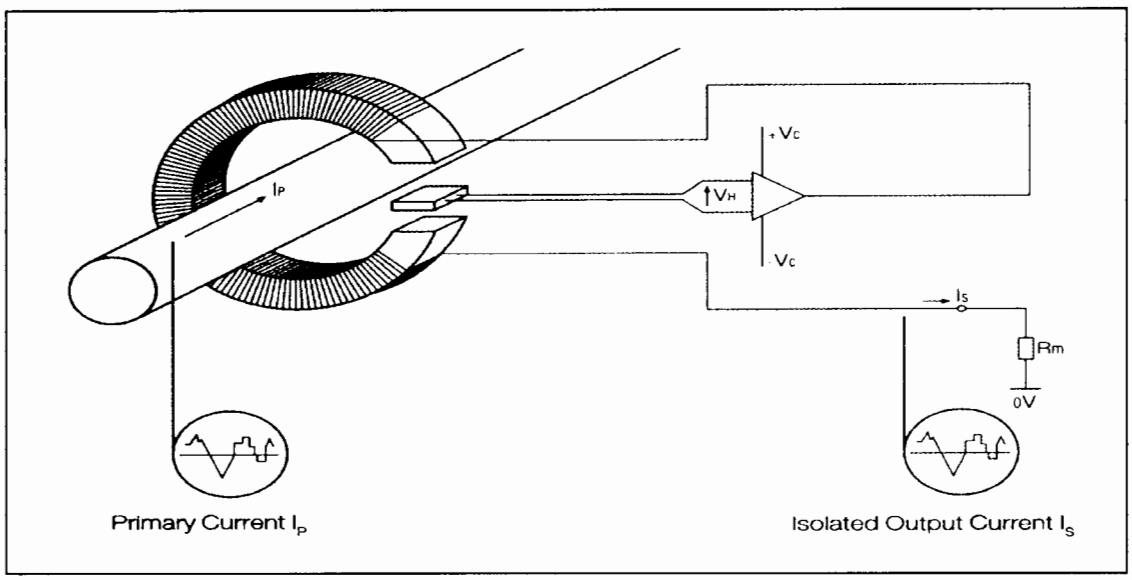

Figure 11.2 LEM current transducer

The module is rated at $100A_{RMS}$ ac or dc and has a current ratio of 2000:1. Thus for a sinusoidal current of 100A, the LEM will output a sinusoidal current of 50ma. Similarly, for a current of +100A dc, the LEM will source 50ma.

The advantages of using sensors with current as opposed to voltage outputs are as follows:

1. Long signal cables can be used between the sensors and the control circuitry. This is because, within practical limits, any voltage dropped across the cable, due to internal resistance, has no effect on the output current being driven by the module.
2. Current signals are less prone to interference often prevalent in electrically noisy environments.
3. Current signals are less prone to interference from magnetic fields such as are generated by the saturable reactors.

11.4 Current to Voltage Conversion

The small current output, I_S, from the LEM is converted to a voltage by allowing it to flow through a current sense resistor, R_M. The sense voltage generated is small due to the low resistor value specified by the manufacturer and for this reason it is buffered and amplified. The circuit used is shown in Fig. 11.3, below.

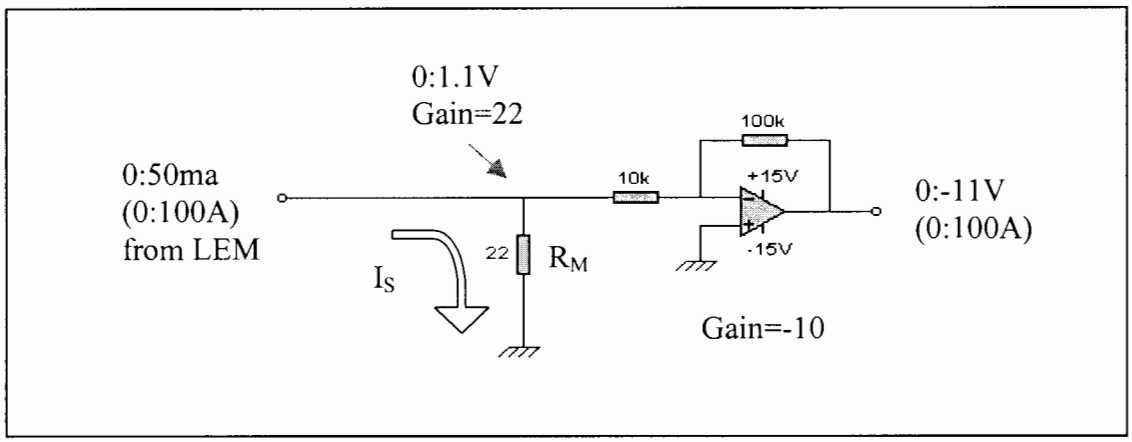

Figure 11.3 Current to voltage converter

The overall gain of the circuit is fixed at -220 and therefore for a 0 to 50ma input an output voltage of 0 to –11V is achieved, as shown in Fig. 11.3, above.

11.5 Signal Conditioning

The monitored phase currents of the motor are sinusoidal in nature, thus the output currents of the LEM's are sinusoidal. The resulting sinusoidal voltage produced by the current to voltage converter stage is precision rectified and the ac component is averaged out to obtain a dc voltage that is the average dc of the input. Thus a dc representation of the monitored phase current is obtained. The circuit used, courtesy of S.Schire, Dep. of Elec. Eng., UCT, is shown in Fig. 11.4, below.

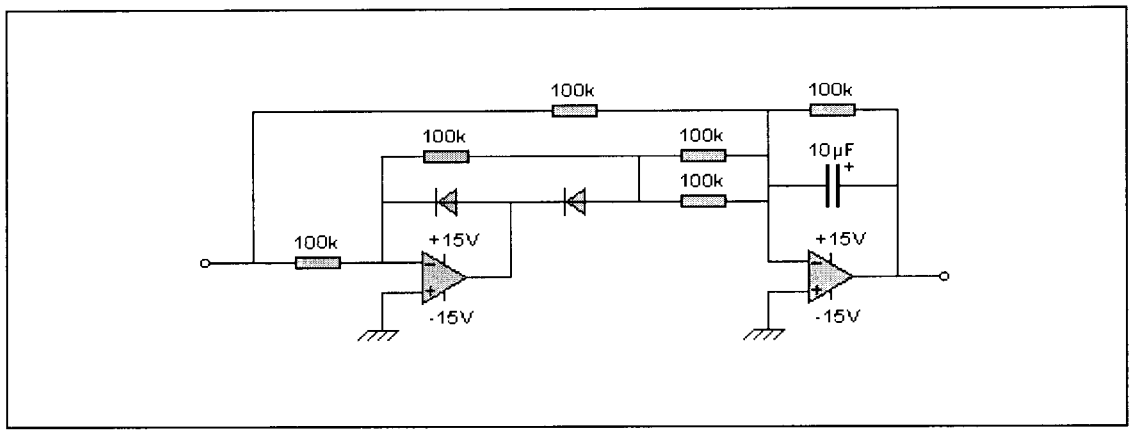

Figure 11.4 Circuit diagram of the precision rectifier with smoothing

An example input and output waveform are shown in Fig. 11.5, below.

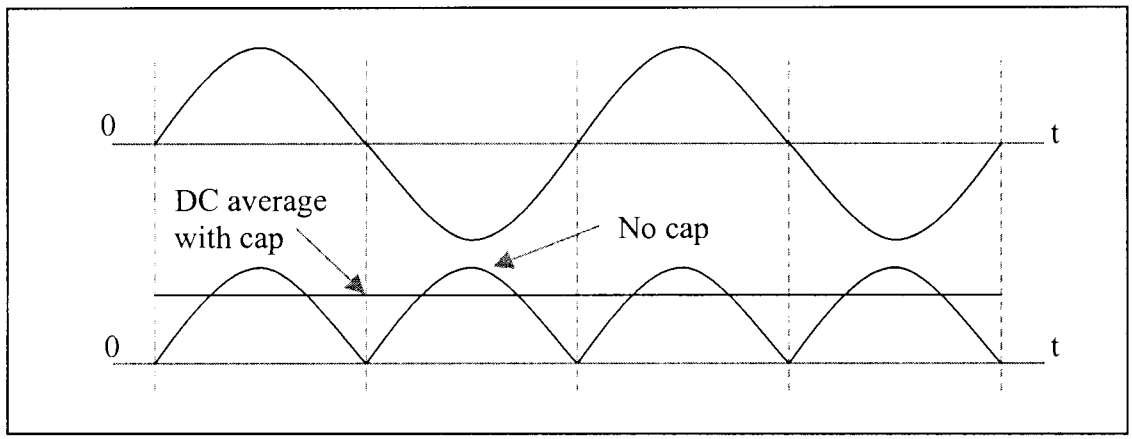

Figure 11.5 Example input and output waveforms of the precision rectifier with smoothing

A negative output is obtained by reversing the polarity of the diodes and capacitor.

11.6 Signal Combination

The dc voltages representing the phase currents of the motor are now summed, remembering that the setpoint voltage is negated, to from error voltages. These error voltages represent the difference between the setpoint current and the other monitored phase currents. The error voltages are then amplified to produce the demand voltages required to drive the SMPS's.

The gain of this section is made as large as possible in order to reduce the overall error of the control system, however, if the values are made too large the system becomes unstable. It is for this reason that a gain of |10| is used. The circuit used to implement this is shown in Fig. 11.6, below.

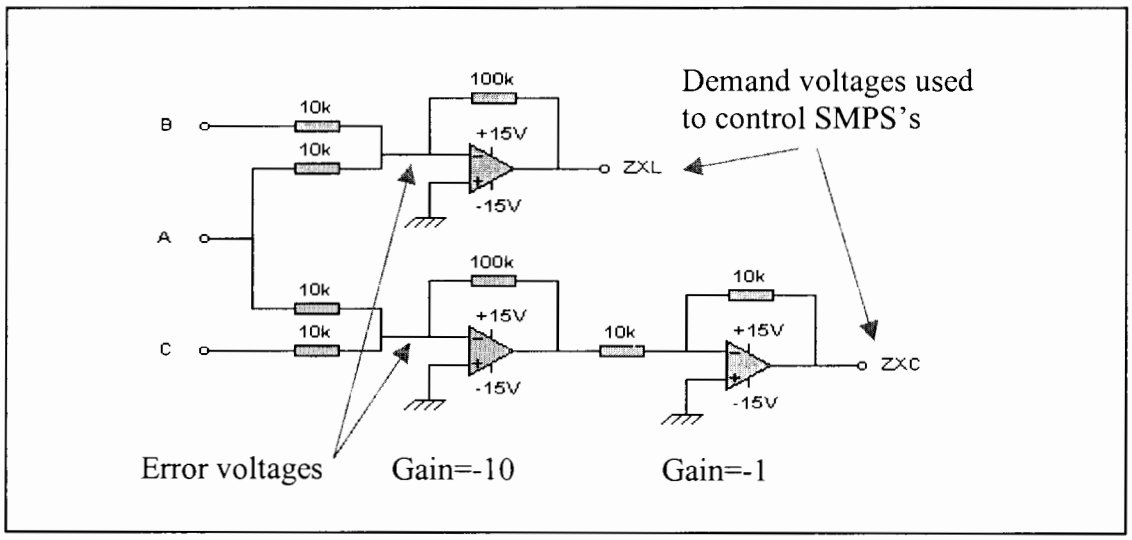

Figure 11.6 Circuit diagram of error amplifiers

As seen above in Fig. 11.6, the control loop containing the capacitor bank has an extra inverting stage. This is to ensure that the two demand voltages always move in opposition so as to converge. If this is not done the demand voltages will always diverge resulting in an unstable controller.

11.7 Switching Circuitry

The circuit used to switch out the starting resistors and additional capacitance required for motor startup is shown in Fig11.7, below. The circuit utilises the average dc representation of the primary phase current of the motor in order to determine the status of the switching relays.

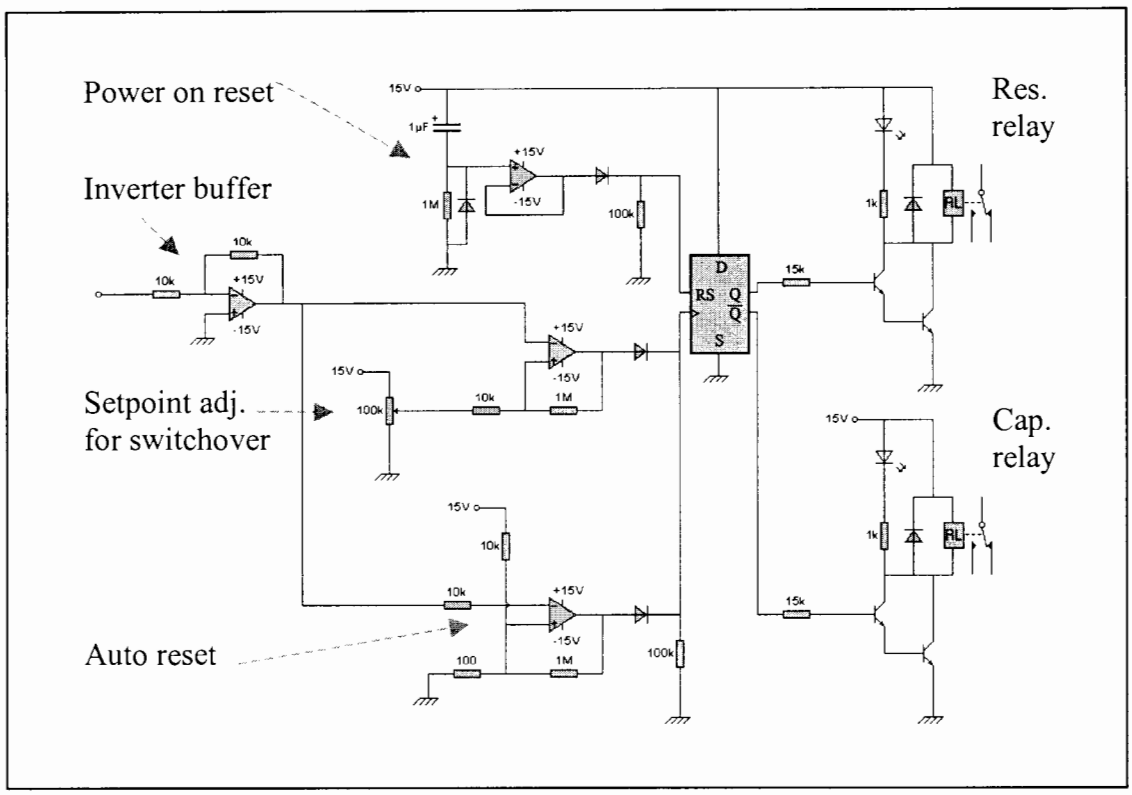

Figure 11.7 Circuit diagram of automatic capacitor and resistor switching circuit

As seen, above, the important sections of the circuit are labelled for clarity. A short description of each section is given below:

1. **Power on reset.** Generates a pulse to return the switching circuit to its start-up status in the event of a power failure to the converter.
2. **Auto reset.** Automatically generates a pulse to return the switching circuit to its start-up status once the monitored phase current has dropped below a minimum threshold value.

3. **Setpoint adjust for switchover.** Automatically generates a pulse to change the status of the switching relays based on the primary phase current of the motor. The switchover only occurs on the falling edge of the current signal, i.e. when the current signal crosses the setpoint and it is decreasing. This is done, because when the motor is started the primary phase current almost instantaneously rises to the value set by the limiting resistors, crossing the setpoint. The phase currents of the motor are inversely proportional to its shaft speed, and therefore only decrease with an increase in speed. It is only while the speed is increasing that the current drops and this is when the switchover must occur.
4. **Inverter buffer.** The input signal is inverted and buffered in order to prevent loading.

Other points to note are as follows: a D-type flip-flop is used to generate the switching logic and Darlington power transistors are used to switch the relays.

A complete circuit diagram of the control circuitry is included in Appendix G.

12 Design and Construction of Switch-Mode Power Supplies

12.1 Introduction

In this chapter the circuit topology, principal of operation, design process and construction of the SMPS's are discussed. The SMPS's perform the important function of interfacing between the low voltage, low power, produced by the control circuits and the medium power at medium voltage, required to control the saturable reactors.

12.2 Circuit Requirements

As seen in chapter 7, sections 7.7 and 7.8, the control winding has the following characteristics:

- Resistance of control winding: 43Ω
- Current required: $0 \sim 5A_{DC}$

In order for this to be achieved a controllable current source with the following specifications is required:

Input:	V(control)	$0 \rightarrow 10V_{DC}$	
Outputs:	V(out)	$0 \rightarrow 250V_{DC}$	To drive max. current into control coil.
	I(out)	$0 \rightarrow 5A_{DC}$	Corresponding to $0 \rightarrow 10V_{DC}$ control voltage.

The power rating of the supply is thus 1.25kW (250*5). A linear power supply capable of this would be large, bulky and very inefficient due to the large amounts of power that would be dissipated. For these reasons, although more complex, a switch-mode power supply is opted for, being smaller, more efficient and with very little heat dissipation requirements.

12.3 Converter Topology

The step-down (buck) converter is chosen, because the output voltage required (0-250 V_{DC}) is lower than the dc input voltage, V_D, (±300V_{DC}) derived directly from rectified mains (230V). The converter topology is shown in Fig. 12.1, below.

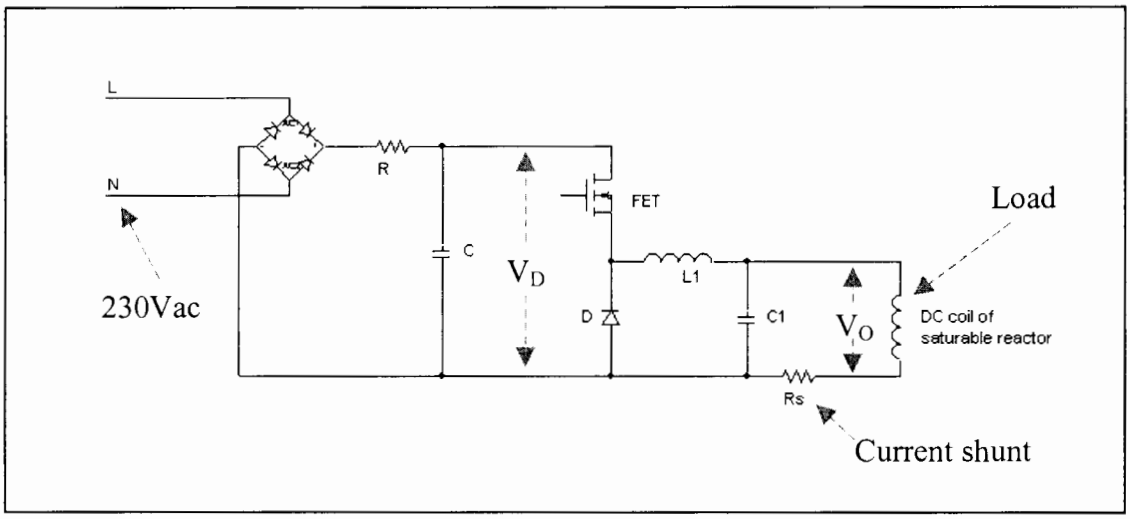

Figure 12.1 Diagram of standard step-down (buck) converter

The incoming mains voltage is full-wave rectified and smoothed by capacitor, C, to form a dc bus voltage, V_D. The current limiting resistor, R, limits the initial inrush current into the discharged capacitor, C.

By varying the duty ratio (the ratio of the on duration to the switching time period), δ, of the FET, V_O can be controlled. The relationship is shown in the formula below:

$$V_O = \delta \cdot V_D$$

The problem of stored inductive load energy is overcome by using a freewheel diode, D, as shown in Fig. 12.1. The output voltage fluctuations are very much reduced by using a LPF (low-pass filter), consisting of an inductor, L_1, and a capacitor, C_1. The corner frequency of this LPF is selected to be much lower than the switching frequency, thus essentially eliminating the switching frequency ripple in the output voltage. For more information refer to "Power Electronics Converters, Applications, and Design (second edition)", Mohan, Underland, Robins, Chapter 7, pp161-172.

The converter topology can be simplified for the following two reasons:

- A variable current as opposed to voltage is required as an output to the load.
- The large inductance inherent to the DC control coil of the saturable reactor essentially eliminating the switching frequency current ripple through the load.

For these reasons the LPF of the standard step-down converter can be illiminated.
The simplified converter topology is shown in Fig 12.2, below.

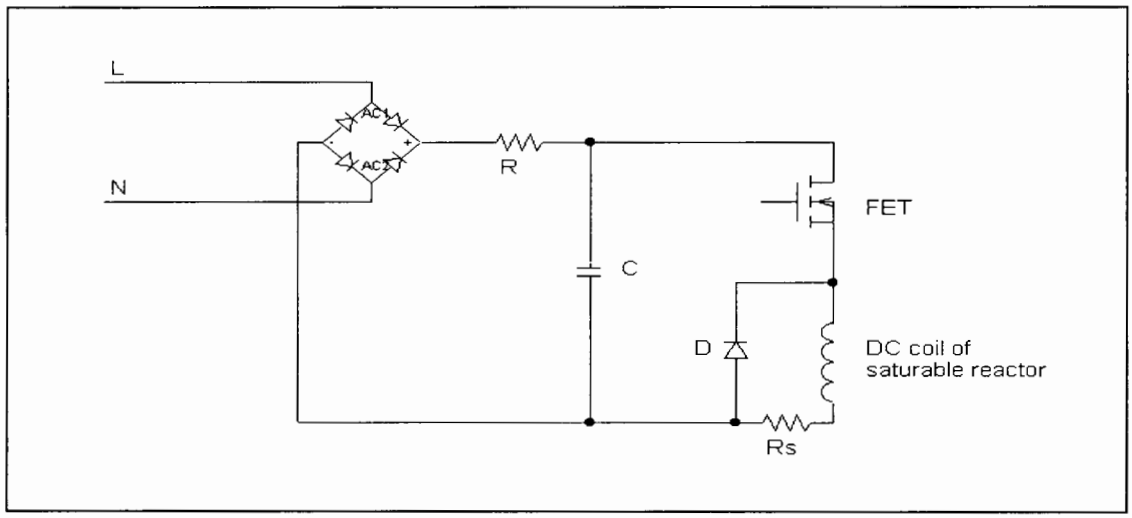

Figure 12.2 Diagram of simplified step-down (buck) converter

This design offers simplicity at reduced cost due to a lower component count and is used for both SMPS's.

The control of the FET switching is discussed next.

12.4 Switching Scheme

Standard pulse-width modulation (PWM) switching at a constant frequency is used to control the duty ratio of the FET. A block diagram of the pulse-width modulator is shown in Fig.12.3, below.

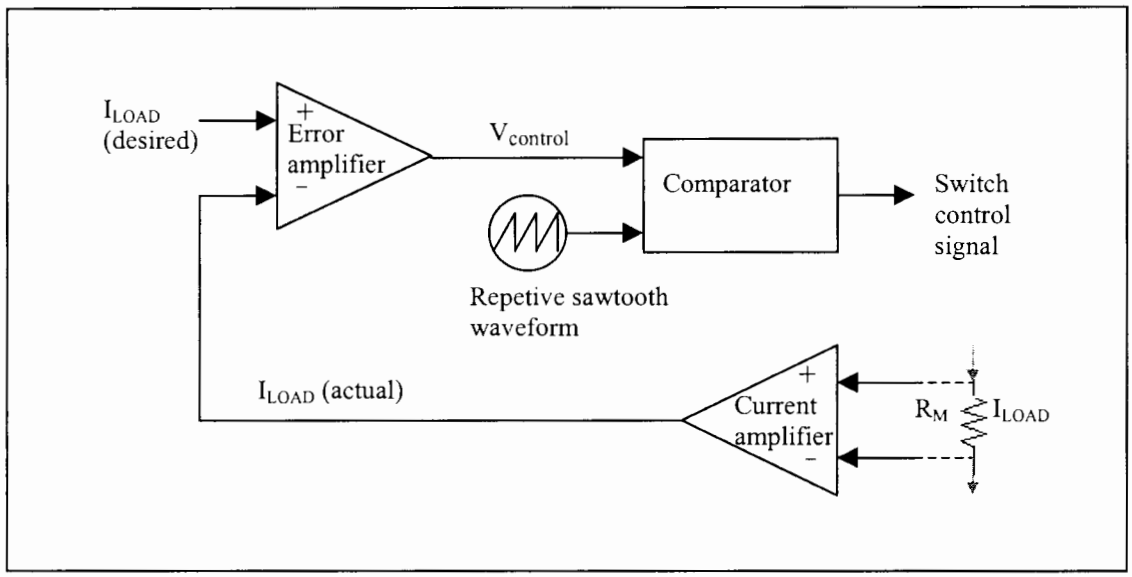

Figure 12.3 Block diagram of pulse-width modulator

The switch control signal, which controls the state (on or off) of the switch, is generated by comparing a signal-level control voltage, $V_{control}$, with a repetitive sawtooth waveform as shown in Fig. 12.3. The control voltage signal is obtained by amplifying the error, or difference between the actual output current and the desired value. The frequency of the sawtooth waveform, with a constant peak, establishes the switching frequency. This frequency is kept constant and chosen to be a few kilohertz. When the amplified error signal, which varies very slowly with time relative to the switching frequency, is greater than the sawtooth waveform, the switch control signal becomes high, causing the FET to turn on. Otherwise, the FET is off.

The result of this is an average output current that varies linearly with control voltage.

The signals mentioned and seen in Fig. 12.3 are illustrated in Fig. 12.4, below.

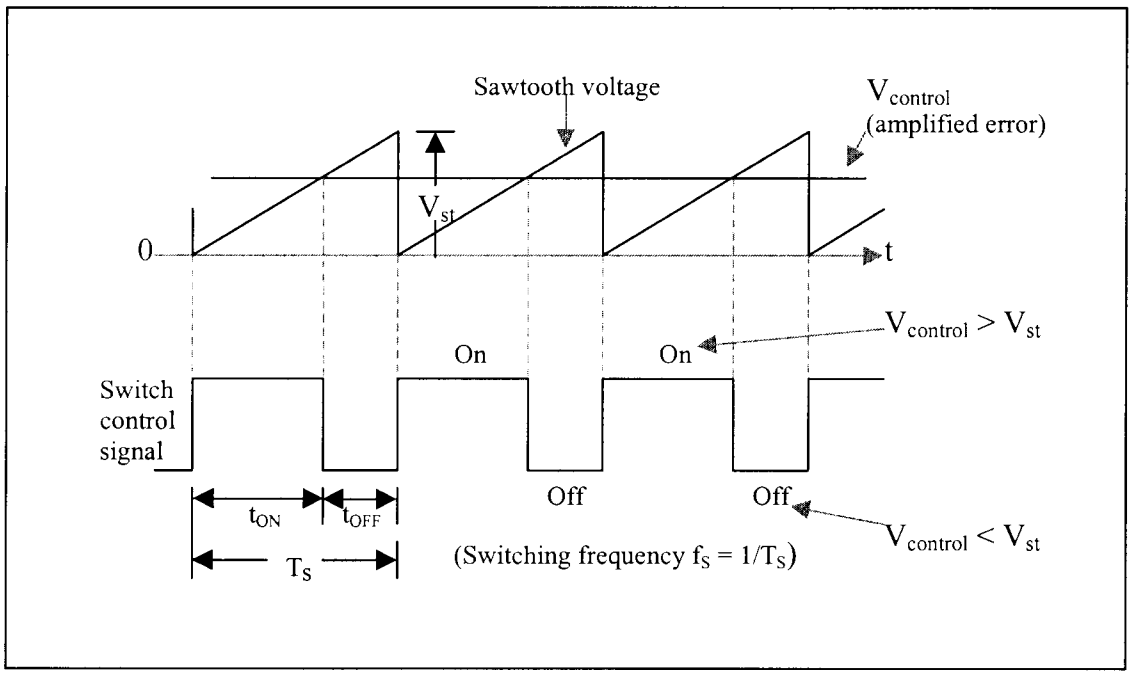

Figure 12.4 Pulse-width modulator signals

12.5 Circuit Design and Construction

Much experimentation was done with the controller design once an initial prototype was constructed on breadboard. It is, found, however, that in practise due to large common mode voltage differentials, current loops, noise, capacitive coupling, switching spikes and other problems not mentioned in the theory that practical implementation is rather specialised and therefore time consuming if never attempted before. It is in this light and with much gratitude that an existing design by Dan Archer was adapted for this particular task.

A complete circuit diagram of the adapted switch-mode power supply is included in Appendix G.

A digital image of the authors constructed SMPS's is shown in Fig.12.5, below.

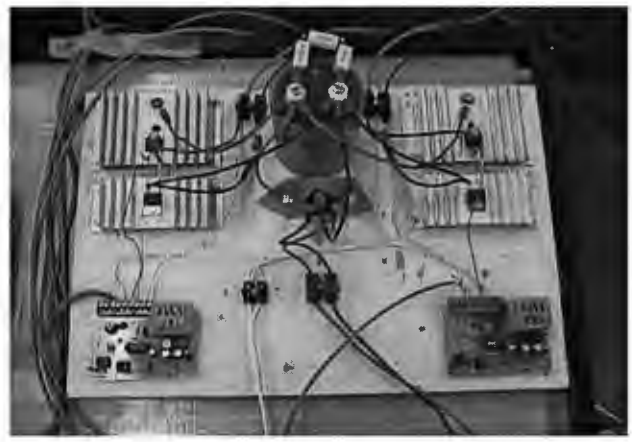

Figure 12.5 Constructed SMPS's

The diode bridge (centre) and smoothing capacitor (top centre) are common to both supplies. The FET's (top left and right) are mounted on heatsinks for cooling as well as the freewheel diodes (just below FET's). The adapted controller boards (bottom left and right) for controlling the FET switching are also shown.

13 Experimental Construction, Testing and Results

13.1 Introduction

This chapter is ideally aimed at testing the final converter design together with the implemented controller as a single system. Testing, however, is done progressively, in stages, for the following reasons:

- In order to verify mathematically derived values.
- To establish that each section of the converter is functioning correctly. This helps to determine, more easily, the exact cause of any problems that might occur when the system is tested as a whole in feedback.
- In order to confirm simulations.

The final converter design is then tested. The results of the testing are discussed in detail and based on these results and the knowledge obtained throughout the course of the research, conclusions are draw and recommendations are made.

13.2 Testing Values for Compensating Elements

Firstly the principle of the converter design, without the controller, is tested in order to confirm, experimentally, the calculated values of the compensating elements. The following test set up, as shown below in Figure 13.1, is used for testing the converter design.

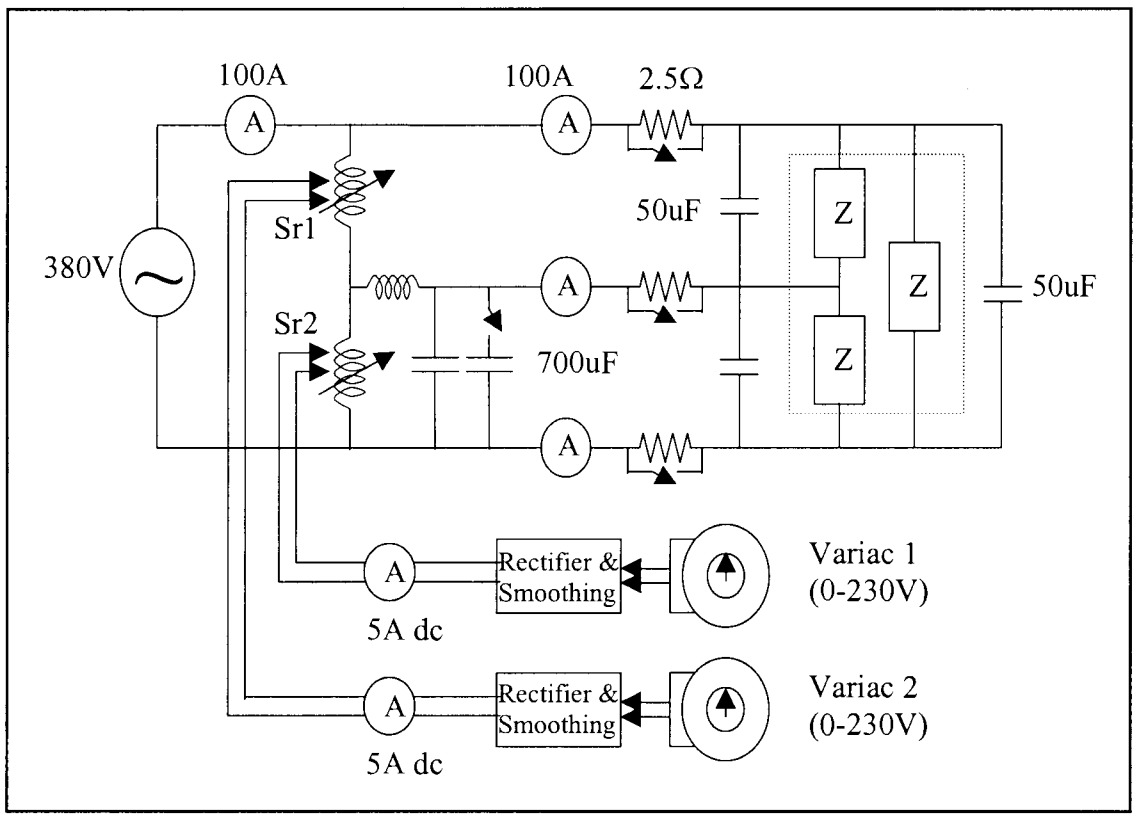

Figure 13.1 Diagram of experimental test set-up for the converter

Images of the test set-up described by Fig. 13.1 are shown below in Fig 13.2 through 13.4.

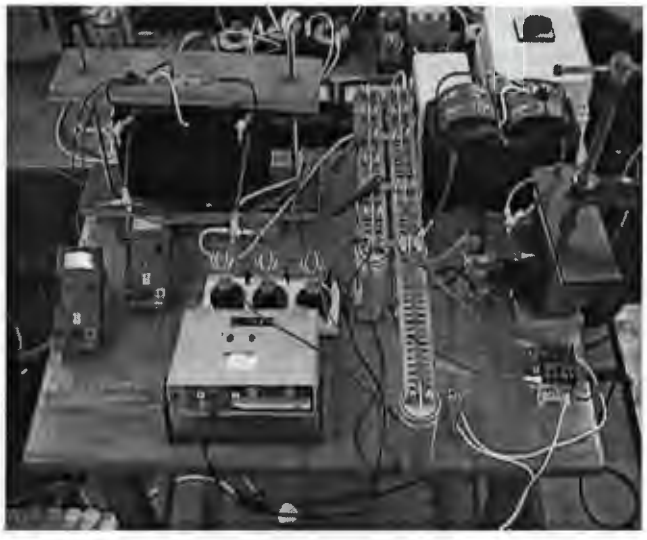

Figure 13.2 Fixed and switched capacitor banks (centre) with both saturable reactors (top left &right) and inductor (right centre). Also shown are both ammeters (centre left), a voltmeter to measure the capacitor voltage, light bulbs used to discharge the capacitors that are switched out of circuit and the auxiliary and main contactors used to switch the capacitors.

Figure 13.3 Converter test set-up: Induction motor (right) connected to a DC generator (left) that is used to both run up and load the motor. Variacs (bottom left) to vary the incoming line voltage to the converter. Motor line voltmeters and other magnetic circuit breaker protection can be seen (centre).

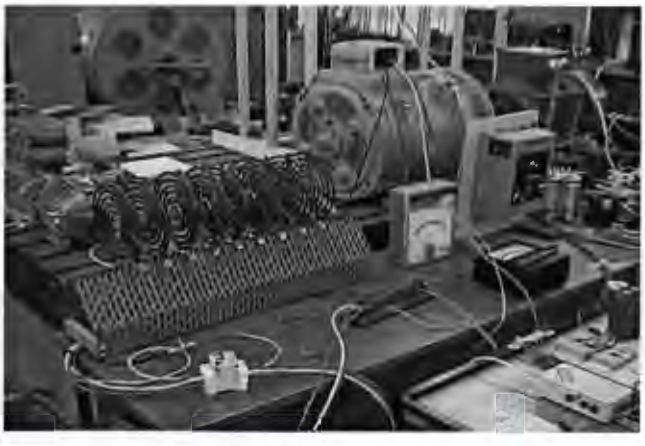

Figure 13.4 Converter test set-up. Switchable resistive block (left) used for loading the motor with volt- and ammeter connected. DC supply for armature and field of generator (right center). Current limiting resistors can just be made out in the background.

From the graph of currents vs. slip for both saturable reactors, shown in Fig. 13.5, below, the current for each reactor is established and set up using the variacs and ammeters.

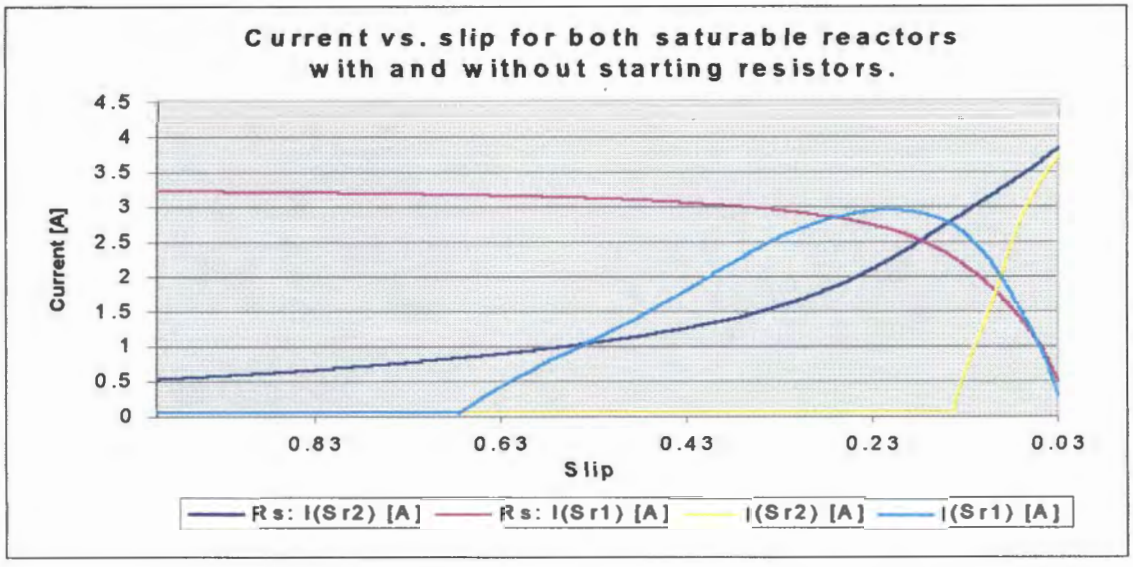

Figure 13.5 ***Graph of current vs. slip for both saturable reactors with starting resistors in and out of circuit***

Initially the shaft of the motor is locked. The current values for the saturable reactors corresponding to a motor slip of 1, as read off the graph in Fig. 13.5, are set up using the respective variacs. Voltage is applied to the set up and balanced currents are observed.

Next the motor is allowed to accelerate to no-load speed and the above experiment is repeated. Full balance could not be achieved at no-load, however, with a small amount of load balance is established. This indicates that at slip values approaching 0 the values of the compensating elements required escalate and become unpredictably larger than calculated. In this way, by increasing the load, various values are attempted over the working slip range of the motor and confirmed.

Next the SMPS's are added and the above experiment repeated. The currents required for both saturable reactors are now established by applying the appropriate control voltages to the SMPS's. Again the values in Fig. 13.5 are confirmed.

13.3 Testing the Controller

By applying 380V, three-phase, to the motor, it is accelerated from standstill to full speed. It is verified that the current acquisition produces the correct average dc voltages, corresponding to the motor phase currents, and that the switching circuitry switches the resistors and capacitors out of circuit at an appropriate moment.

Images of the controller construction are shown in Figs. 13.6 through 13.9, below.

Figure 13.6 The LEM current transducers are mounted inside the terminal box, housed on top of the motor, in order to sense the individual phase currents.

Figure 13.7 The controller (left) and the switching circuitry (right) as implemented on breadboard. The relay LED status indicators (far right) can also be seen.

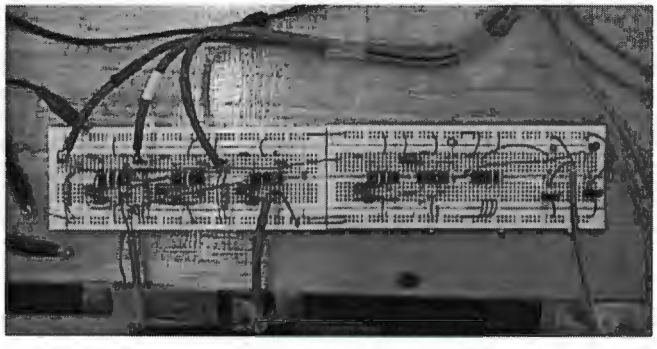

Figure 13.8-9 Auxiliary and main relays for resistor (right) and capacitor (left) switching. MOV's are used on the relay coils to suppress voltage spikes caused by during switching.

13.4 Testing the Converter

The final converter design, together with the implemented controller, is now tested as a single system. A block diagram of the converter is show in Fig. 13.10, below.

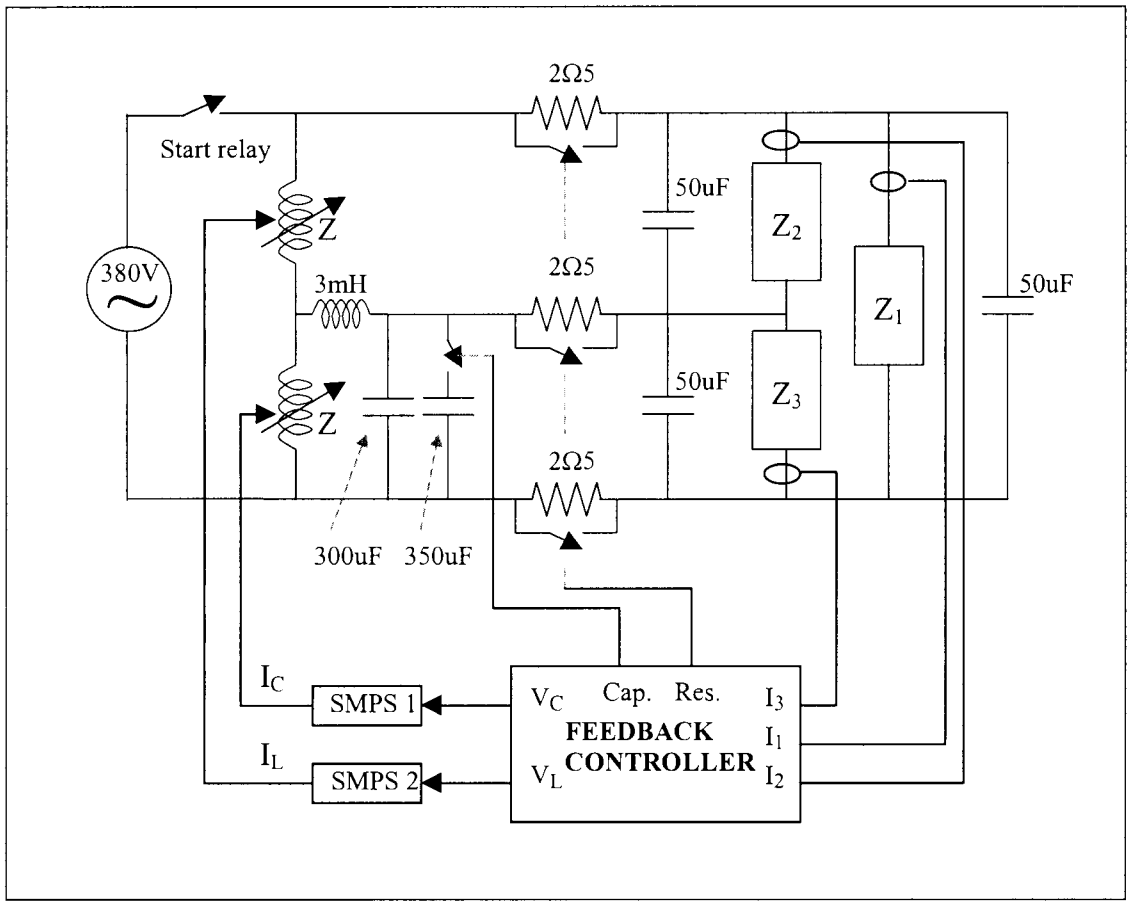

Figure 13.10 Diagram of final converter design test set-up

The control loop is now completed, implementing closed loop feedback control of the compensating elements.

A partial load is placed on the generator and the start relay is energised applying full mains voltage to the converter. The results of the test are shown graphically in Fig. 13.11, below.

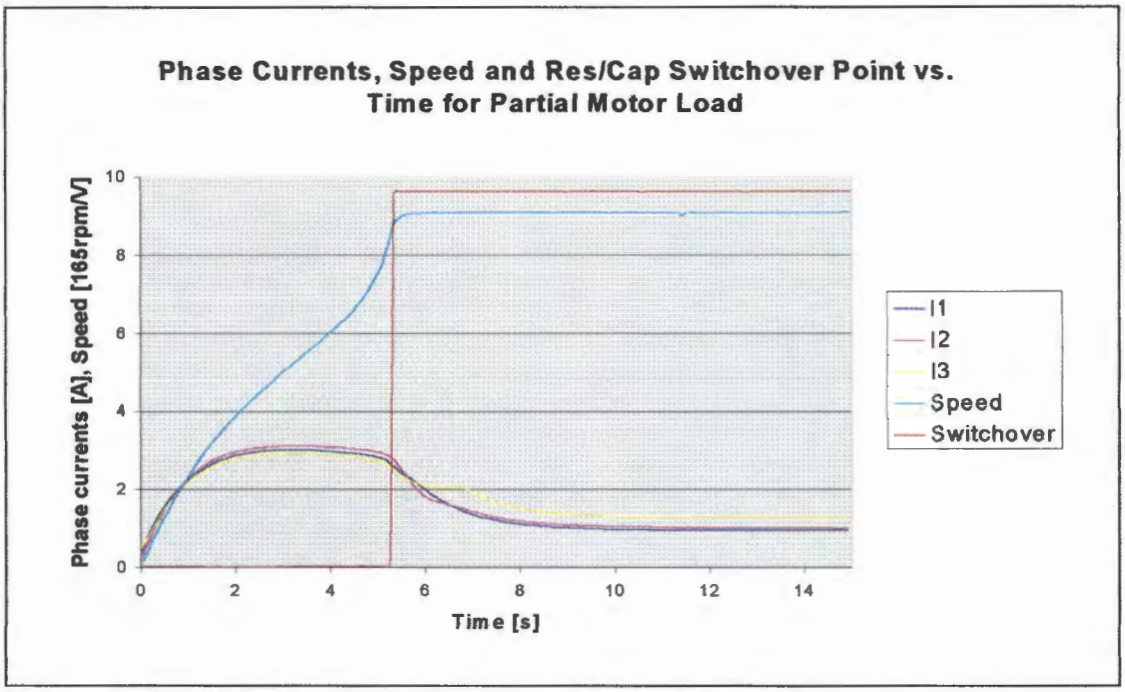

Figure 13.11 Graph of results for partial motor load test

As is seen in the graph shown in Fig. 13.11, above, the phase currents of the motor, I2 and I3, track the primary phase current, I1, and remain approximately equal over the full slip range of the motor from standstill at start up to running speed at the rated load.

The starting resistors and capacitors switch out approximately 5 seconds after switch on. This switchover causes momentary loss of current balance, however, after an adjustment period, the controller begins to track the primary phase current again.

The test is repeated, however, this time no load is placed on the generator. The start relay is energised and readings are taken. The results of the test are shown graphically in Fig. 13.12, below.

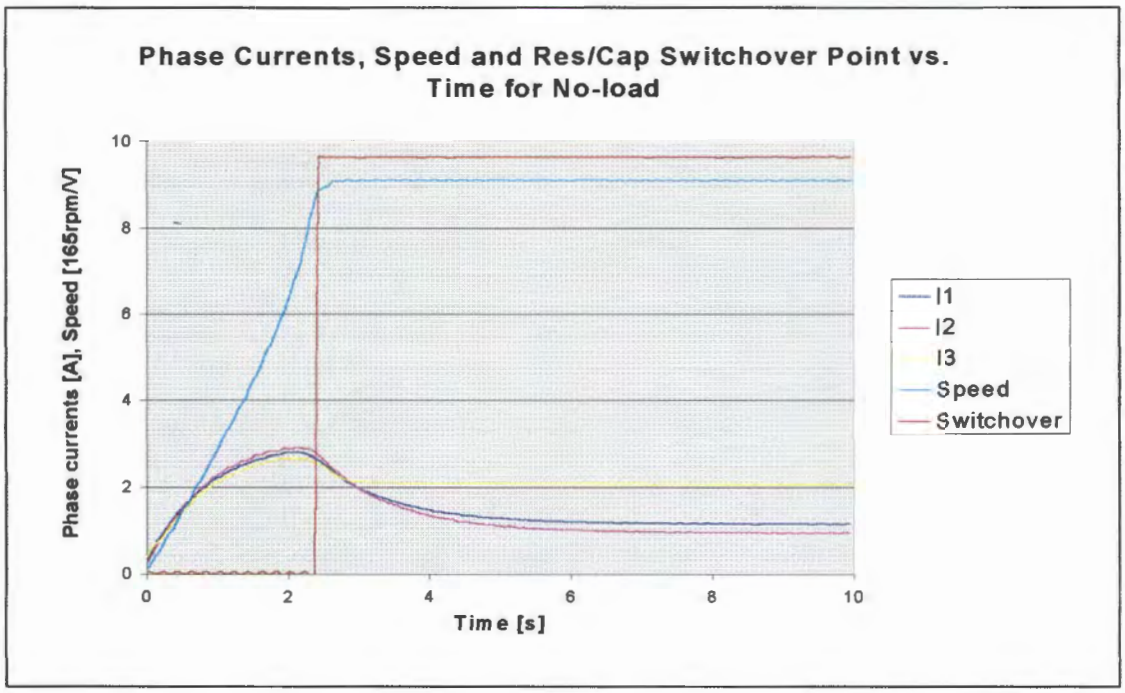

Figure 13.12 Graph of results for no-load motor test

Again the phase currents of the motor, I2 and I3, track the primary phase current, I1. However, shortly after the resistors and capacitors are switched out of circuit, I3, stops tracking and balance is lost.

This confirms the result obtained from the no-load test performed in section 13.2, which indicated, that at slip values approaching 0 the values of the compensating elements required escalate and become unpredictably larger than calculated. This explains why the converter is unable to maintain current balance under these conditions.

The converters ability to maintain current and voltage balance under varying load conditions is tested by applying different loads to the motor. The results are seen in Fig. 13.13 and Fig.13.14, below.

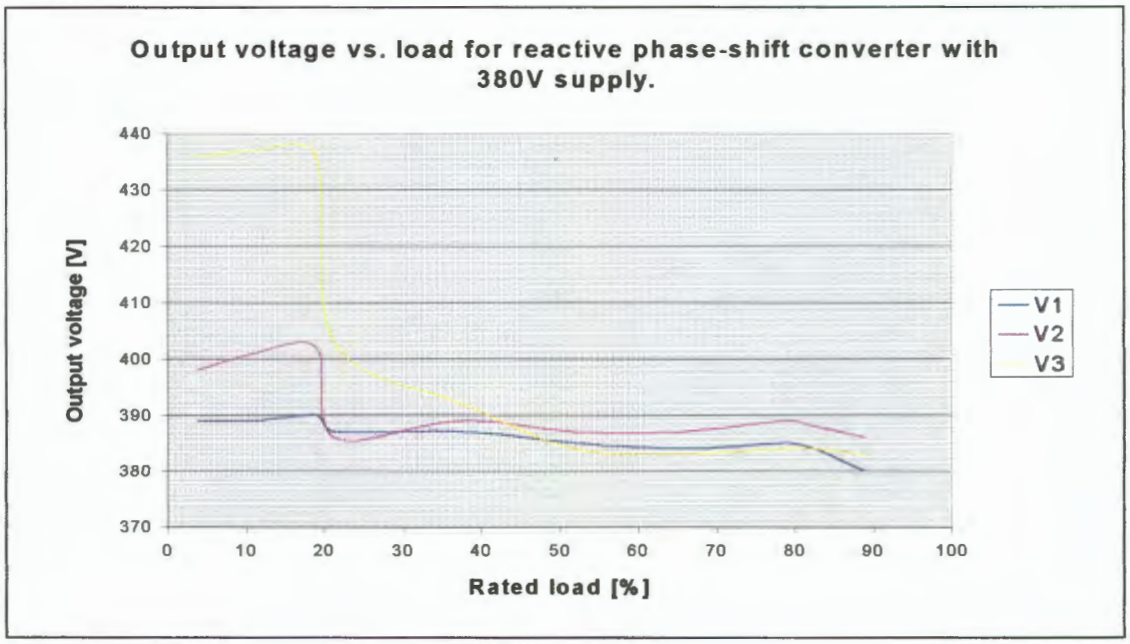

Figure 13.13 Graph of converter output line voltages vs. motor load

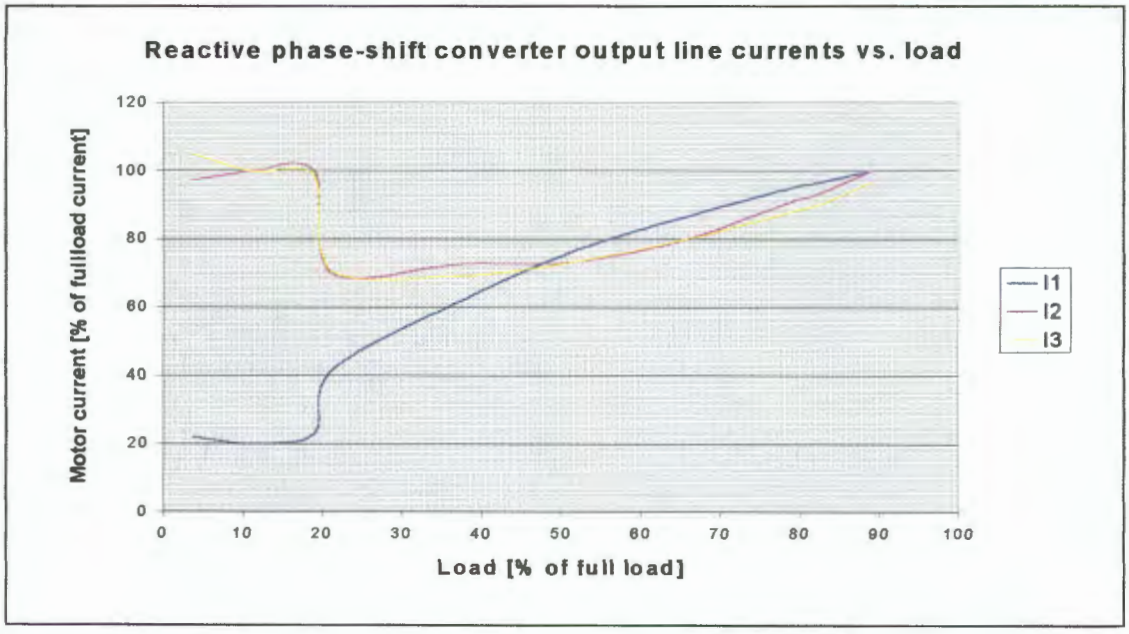

Figure 13.14 Graph of motor line currents vs. load

As seen in the Fig. 13.13&14 the converter starts to maintains both current and voltage balance from 20/30% of full load upwards. The inability of the converter to maintain balance at light loads, due to the limited ranges of the compensating elements, is again confirmed by both graphs.

Next the torque vs. speed curve for the converter driven motor is obtained. This is a two step procedure, namely:

1. Obtain speed vs. time graph for unloaded motor. The generator and motor are uncoupled and rated voltage is applied to the converter. The appropriate signals are then captured while the motor is allowed to accelerate.
2. The inertia of the motor is obtained and together with the results from the above test the torque vs. speed curve, at rated voltage, for the converter driven motor, is calculated.

Step 1, above, is carried out resulting in the graph shown in Fig. 13.15, below.

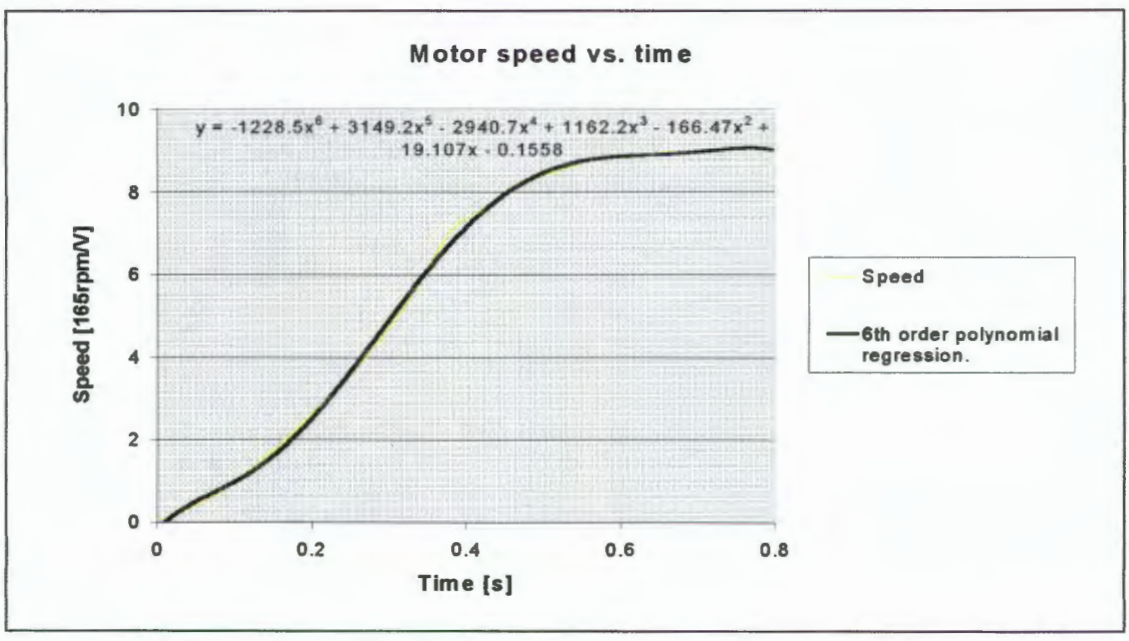

Figure 13.15 Graph of speed vs. time for converter driven unloaded motor

A polynomial regression is also performed to obtain a best-fit solution, the equation of which is shown in Fig. 13.15.

Step 2: the inertia of the motor, 0.059kgm^2, is obtained from the manufacturers specifications, see Appendix H for details. This together with the speed vs. time information is substituted into the following equation to derive the torque vs. speed graph:

$$M_A = \frac{Jn}{9.55 t_A}$$

Where:

M_A - Acceleration torque in Nm

t_A - Acceleration time in seconds

J - Moment of inertia in kgm^2

N - Rotational speed in rpm

The derived torque vs. speed graph for the converter driven motor is shown in Fig. 13.16, below.

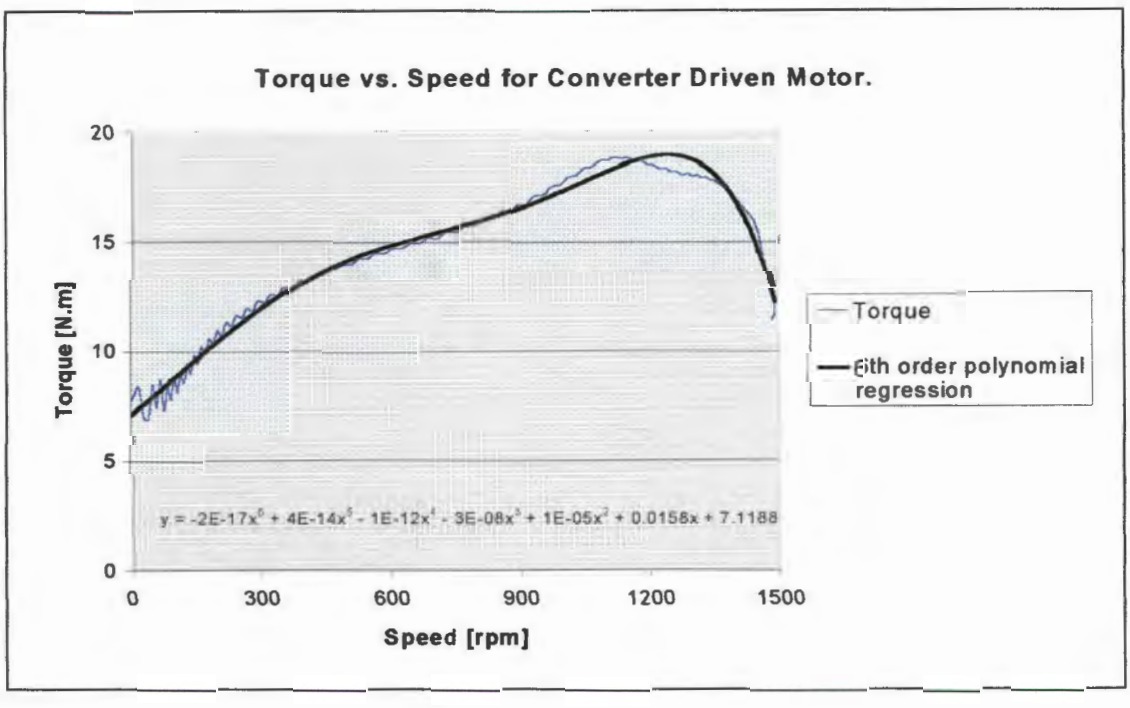

Figure 13.16 Graph of torque vs. speed for converter driven unloaded motor

Again a polynomial regression is performed to obtain a best-fit solution, the equation of which is shown in Fig. 13.16.

The torque generated by the motor is substantially less than that specified by the manufacturer [see Appendix H for details]. This is due to the following reasons:

1. There is a fundamental trade-off between starting torque and compensating element size. As seen in chapter 5, the current limiting resistors help to maintain the values of the compensating elements within reasonable limits, over the full slip range of the motor. They achieve this by reducing the maximum motor current, however, torque is proportional to current and therefore, by doing this, the starting torque of the motor is also reduced. If the greater starting torque is required, larger compensating elements must be used at increased expense.
2. The controller, due to inherent time delays associated with averaging, takes a finite amount of time to respond to the control signal. Thus under no load conditions, as experienced in the above test, the motor may respond more quickly than the controller, resulting in reduced output torque, due to lack of control. When under load, the motor-load is slow to respond, allowing the controller to maintain balance and hence increased output torque.

Images of the test set-up described by Fig. 13.10 are shown below in Fig 13.17 through 20.

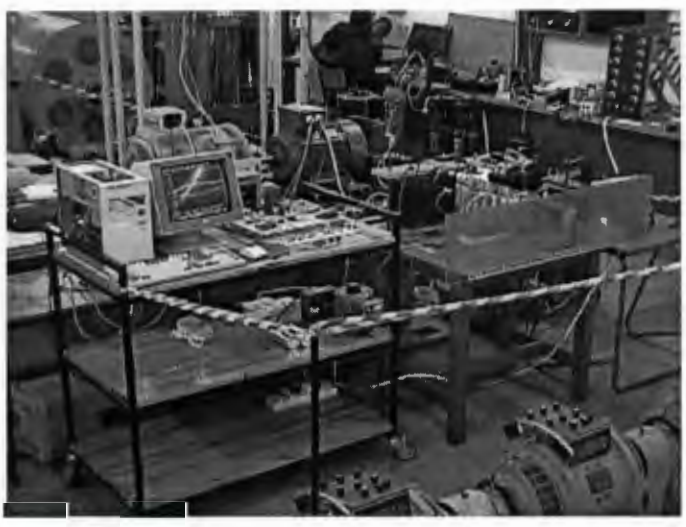

Figure 13.17 Converter test set-up. Various safety measures taken throughout the course of the project are visible, such as danger tape and a perspex shield, used to prevent accidental contact with any live componentry.

Figure 13.18 Data acquisition set up. The PC is fitted with an Eagle Technology PC 30B card used to capture and store the necessary waveforms.

Figure 13.19 Motor shaft speed is recorded with the aid of a Johannes Hubner DC Tacho-Generator, kindly donated by Alstom, Small Motors, South Africa. Details of the tacho-generator can be found in Appendix J.

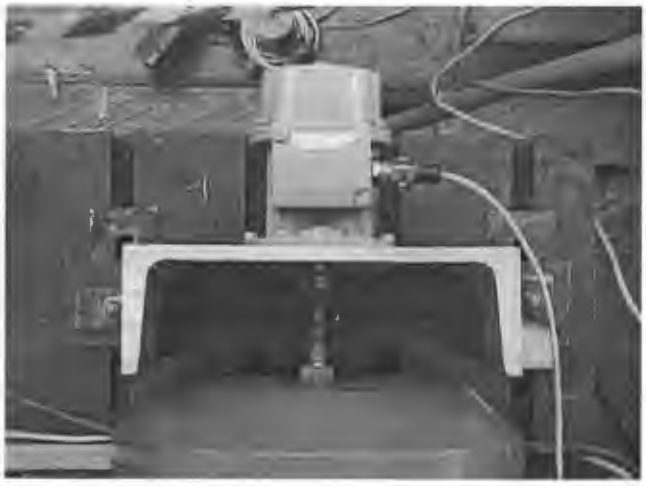

Figure 13.20 The motor shaft is extended, as shown, to allow for connection of the tacho-generator. Connection is made via a flexible coupling, to allow for misalignment, consisting of a short piece of garden hose and two jubilee clamps.

14 Conclusions

Passive element conversion, with the use of the saturable-core reactor, offers the user an economical and reliable method of converting from single- to three-phase. However the use of this technique is by no means restricted to phase conversion only. The area of load balancing of three-phase systems is becoming an area of great interest, not only for the small three-phase user, but also from a complete power system perspective. Based on the findings, the following conclusions can be made:

1. It is possible to achieve single- to three-phase conversion, for an induction motor load, with the use of passive storage elements only.
2. It is possible to design this converter with variable reactances that can be altered in order to maintain balanced currents for the motor under varying load conditions.
3. It is possible to design a controller, that does not require any speed sensing devices to be attached to the motor, to dynamically vary the reactances of the converter in order to maintain balanced motor currents under varying load conditions.
4. The saturable-core reactor provides an excellent means of altering a power inductance with small control currents while still providing full galvanic isolation between the two.
5. The use of a saturable-core reactor in parallel with an inductor and fixed bank of capacitors is a plausible method of achieving a variable source of capacitance.
6. The analogue control method used forms a stable control loop for the converter. This approach provides a simple, cost effective and reliable controller.
7. The converter is simple, robust and reliable, requiring no maintenance. This enables quick and easy repair, in the event of failure, by semiskilled persons, with minimum downtimes involved.

8. The converter is ideally suited to rural/remote water pumping applications where a centrifugal type pump, requiring low initial starting torque, is used.
9. It is possible to increase the starting torque of the motor, however, larger compensating elements are required, which increases both the cost and weight of the converter
10. This method can be scaled up indefinitely, thus making it possible to achieve single-to three-phase conversion for motor loads in the megawatt region, or to achieve load balancing on high voltages power systems.

15 Recommendations

It is recommended that the following steps be taken to improve on the design and performance of the converter.

1. The topology of the voltage to current converters, used to drive the saturable core reactors, should be changed from step-down (buck) to full-bridge configuration, as shown in Fig. 15.1, below.

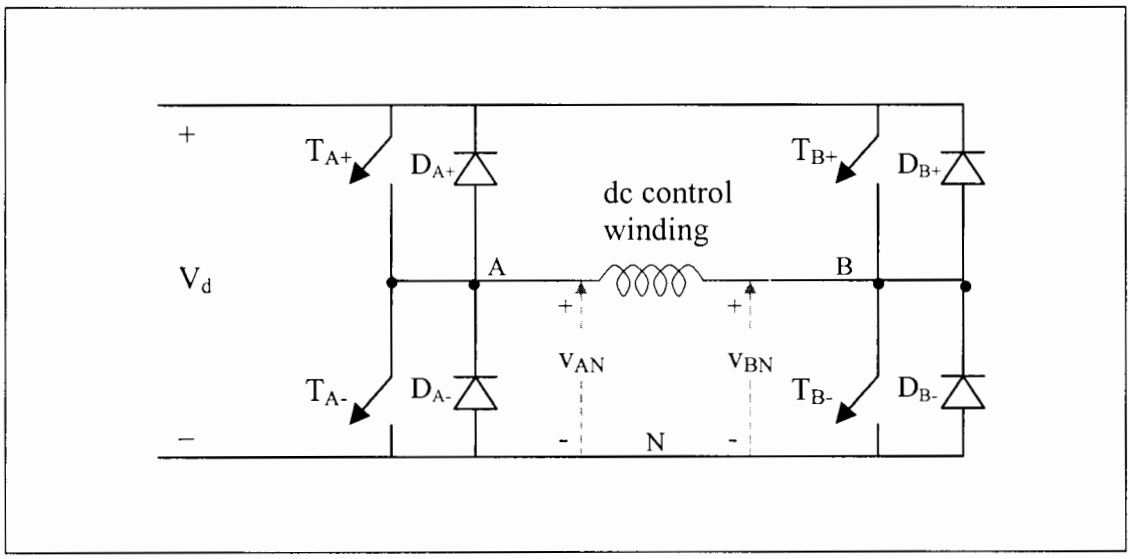

Figure 15.1 Full-bridge dc-dc converter

The bi-directional ability of the converter allows for equally fast current rise and fall time, as opposed to the fast rise and slow fall time associated with the freewheeling diode action of the buck converter. This converter configuration will improve on the converter design by improving the response time of the saturable reactors and hence reducing the overall system response time.

2. The averaging method, used to obtain average dc representations of the ac current signals, for control purposes, should be replaced by an integrating and sampling method, such as is shown in Fig 15.2, below.

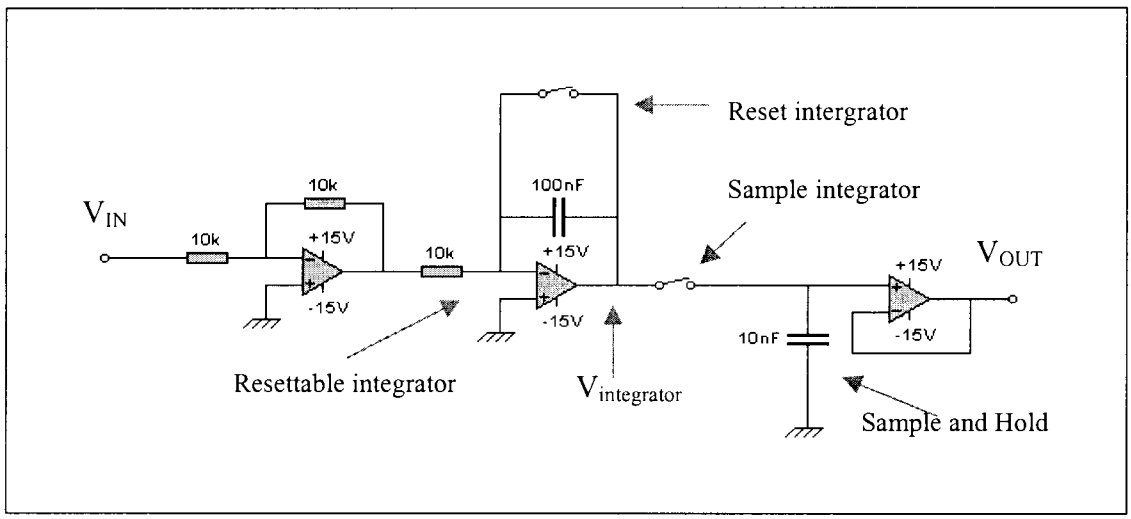

Figure 15.2 Resettable integrator with sample and hold output

The expected waveforms of which are shown in Fig. 15.3, below.

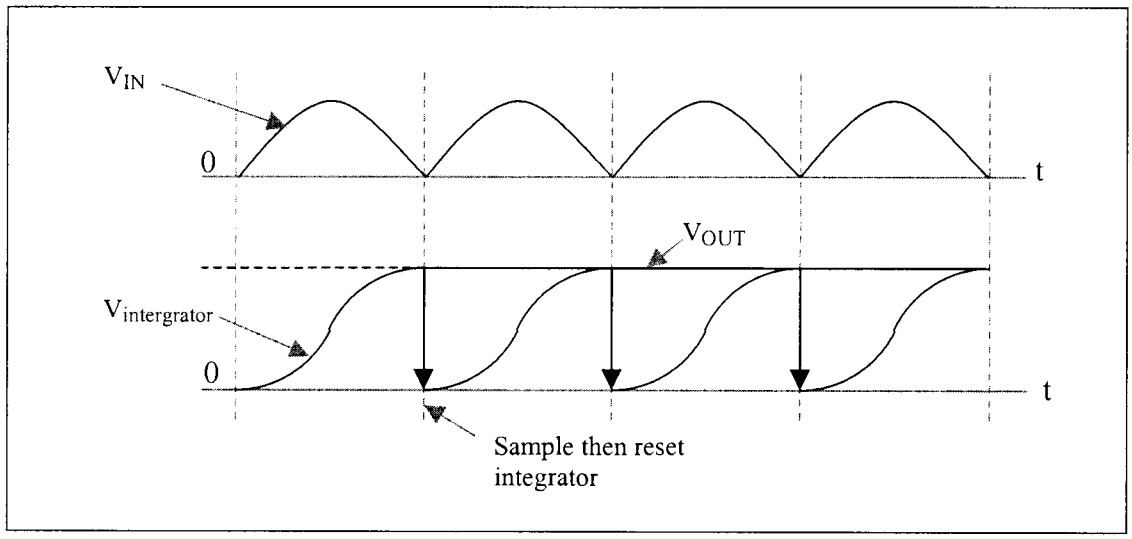

Figure 15.3 Waveforms of integrator method

In this way it is possible to reduce the settling time and the ripple of the output dc control voltages. This reduces the controller response time, decreasing overall system response time, and hence improving on the converter design.

The following two recommendations will not necessarily improve converter performance, however, they simplify the converter design and controller implementation and reduce the overall cost of the system.

3. The current feedback should be replaced by voltage feedback as shown in Fig. 15.4, below.

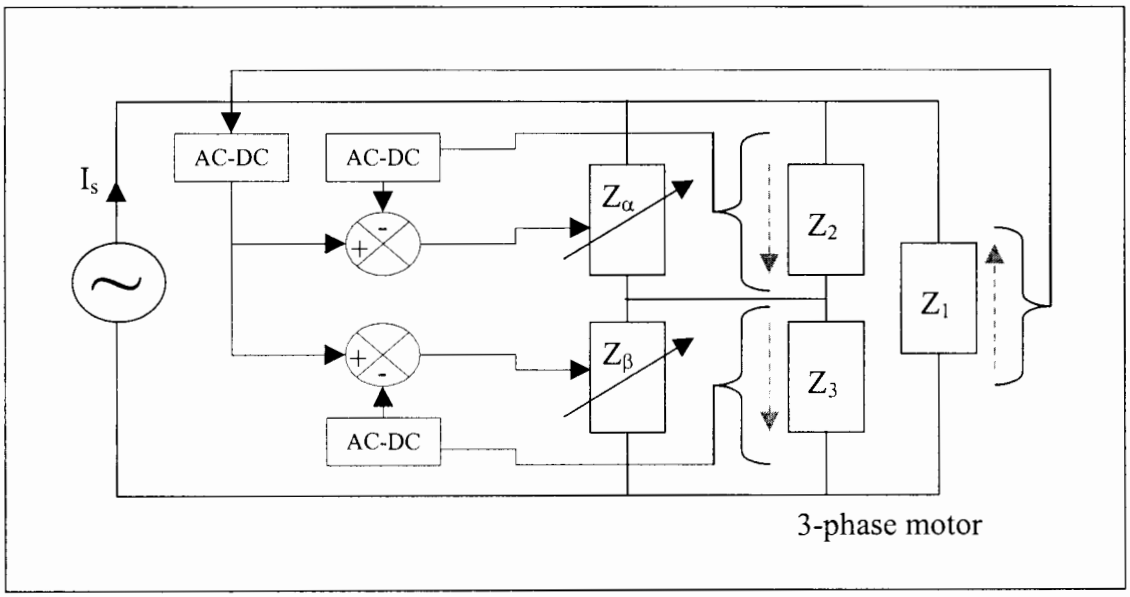

Figure 15.4 Analogue voltage control method for converter

This presents two distinct improvements to the converter design, namely:

- As seen in Fig.15.4, above, the LEM current transducers are no longer required which reduces the overall converter cost. They can be replaced by either differential amplifiers or by voltage transformers, if complete galvanic isolation is required.
- The sensors are no longer required to being mounted on the motor (to monitor the individual phase currents) and can be moved from the motor into the converter.

4. The entire controller can be implemented digitally in a PIC microcontroller, such as the PIC 16C73, as opposed to discrete analogue components. The analogue signal conditioning is still be required, however, the PIC is even capable of generating the PWM waveforms required to drive both switch-mode power supplies.

Implementing a digital control scheme adds flexibility to the controller that the analogue equivalent cannot offer. An example of this would be an LCD display for user interfacing. It is not only easier to implement integral and differential control action in a digital controller, but also to change the time constants associated with these functions while in the tuning process.

There is much scope for further development in the area of phase conversion and load balancing by means of passive elements and saturable-core reactors.

16 Bibliography

1. Bhavaraju, V. Enjeti, P. (1996) "An Active Line Conditioner To Balance Voltages In A Three – Phase System," IEEE Transactions On Industry Applications, vol. 32, no. 2. Pages 287 – 292.

2. Enjeti, N. Rahman, A. (1993) "A New Single-Phase to Three-Phase Converter with Active Input Current Shaping for Low Cost AC Motor Drive," IEEE Transactions On Industry Applications, vol. 29, no 4. Pages 806 – 813.

3. Czarnecki, L. Hsu, S. (1995) "Adaptive Balancing Compensator," IEEE Transaction on Power Delivery, vol. 10, no. 3. Pages 1663-1669.

4. He, J. Mohan, N. (1987) "Input Current Shaping In Line Rectification by Resonant Converter," In Proceedings IEEE PESC Conf. Pages 990-995.

5. Holmes, P. (1985) "Single- to Three-Phase Transient Phase Conversion in Induction Motor Drives," IEEE Proceedings, vol. 132, Pt.B, no. 5.

6. Katz, L (?) "How Phase Converters Help Apply Motors," Power Transmission Design Review. Pages 17-23. & 65-69.

7. Kohlmeir, H. Niermeyer, O. & Schroder, D. (1987) "Higher Dynamic Four Quadrant AC Motor Drive with Improved Power Factor and Online Optimised Pulse Pattern with PROMC," IEEE Transactions On Industry Applications, vol. 1A-23, no. 6. Pages 1001-1009.

8. Maggs, A. (1945) "Single-Phase to Three-Phase Conversion by the Ferraris-Arno System," British Thomson-Houston Co., Ltd. Pages 133-136.

9. Malengret, M. (1998) Preliminary Ph.D. Research.

10. Matsch, L (1964) Capacitors, Magnetic Circuits & Transformers. Prentice-Hall. Pages 309-338.

11. Mohan, N. Underland, T. Robbins, W. (1984) "Power Electronics," John Wiley & Sons, Inc. Second Edition. Page 98.

12. Mohan, N. Underland, T. & Ferraro, R. (1984) "Sinusoidal Line Current rectification with a 100kHz B-SIT Step-Up Converter," IEEE PESC Conf. Rec. Pages 92-98.

13. Mulkern, J. Mohan, N. (1988) "A Sinusoidal Line Current Rectifier using a Zero Voltage Switching Step-Up Converter," IEEE IAS Conf. Rec. Pages 767-771.

14. Richardson, D (1978) Rotary Electric Machinery and Transformer Technology. Reston Publisher Co. Pages 580-585.

15. Sen, P. (1989) Principles of Electric Machines and Power Electronics. John Wiley & Sons. Pages 229-257.

16. Sugimoto, H. Moromoto, S. Yano, M. (1988) "A High Performance Control of a Voltage Type PWM Converter," IEEE PESC Rec. Pages 360-368.

17. Thiyagarajah, K. Ranganathan, V. Ramakrishna, I. (1991) "A High Switching Frequency System for AC Motor Drives Operating from Single-Phase Supply," IEEE Transaction on Power Electronics. vol. 6, no. 4.

18. Wagner, C. Evans, R. (1933) Symmetrical Components as Applied to the Analysis of Unbalanced Electrical Circuits. McGraw-Hill Book Company Inc. Pages 345-387.

19. Wu, R. Dewan, S. Slemon, G. (1988) "A PWM AC to DC Converter with Fixed Switching Frequency," IEEE IAS Annual Meeting. Pages 706-711.

17 Appendices

A : Malengret - Mathematical Derivation

B : AMC Steel Core - Data

C : Capacitor Switching Contactor - Data

D : Saturable-Core Transformer – Specifications

E : Fluke 43 Power Meter - Technical Specifications

F : LEM Current Transducer - Technical Specifications

G : Circuit Diagrams

H : Induction Motor – Technical Specifications

I : Water Pump – Data

J : Tacho-Generator – Technical Data

A : Malengret - Mathematical Derivation

Derivation of Currents I_{NS}, I_{NT}, I_{NR} for Two Element Compensator with Pure Resistive Single-phase Load.

The single-phase load is a pure resistor, therefore assume $B_1=0$, Eq. 2.4 becomes:

$$T_{RS}=\frac{-1}{\sqrt{3}}G_1 \qquad T_{ST}=0 \qquad T_{TR}=\frac{1}{\sqrt{3}}G_1$$

Referring to Fig. 2.10 the compensator currents $\underline{i}_{NS}$, $\underline{i}_{NT}$, $\underline{i}_{NR}$ can be calculated as follows:

Assuming that the three-phase supply voltages V_{TS}, V_{SR}, V_{RT} are balanced sinusoids and of positive sequence direction.

$\underline{V}_{TS}= V\angle 0$, $\underline{V}_{SR} =V\angle +120$, $\underline{V}_{RT} = \angle +240$,

if $I = VG_1$, then:

$\underline{i}_{NS} = -\underline{V}_{SR}\, j\,(T_{RS}) = -V\angle 120 * (-j\, G1/\sqrt{3}) = I/\sqrt{3}\angle 120 +90$ **$\underline{i}_{NS} = I/\sqrt{3}\angle 210$**

$\underline{i}_{NT} = \underline{V}_{RT}\, j\,(T_{RT}) = V\angle 240 *(j\, G1/\sqrt{3}) = I/\sqrt{3}\angle +240 +90$ **$\underline{i}_{NT} = I/\sqrt{3}\angle 330$**

$\underline{i}_{NR} = -\underline{i}_{NS} - \underline{i}_{NT} = -I/\sqrt{3}\angle 210 - I/\sqrt{3}\angle 330$ **$\underline{i}_{NR} = I/\sqrt{3}\angle 90$**

The magnitude of the negative sequence current is $1/\sqrt{3}$ of the single phase load current I_S.

It is observed that this is a balanced negative sequence current.

It follows that that the 3 phase supply currents are:

$\underline{i}_{PR} = -\underline{i}_{NR} = -I/\sqrt{3}\angle 270$ **$\underline{i}_{PR} = I/\sqrt{3}\angle -90$**

$\underline{i}_{PS} = \underline{I}_s - \underline{i}_{NS} = I\angle 0 - I/\sqrt{3}\angle 210$ **$\underline{i}_{PS} = I/\sqrt{3}\angle 30$**

$\underline{i}_{PT} = -\underline{I}_s - \underline{i}_{NT} = I\angle 0 - I/\sqrt{3}\angle 330$ **$\underline{i}_{PT} = I/\sqrt{3}\angle 150$**

The three phase supply magnitude is $1/\sqrt{3}$ the single phase load current. which is a balanced positive sequence current. The negative and positive sequence current add up to make $\underline{I}_s, 0, -\underline{I}_s$. These are the currents seen in Fig. 2.12.

B : AMC Steel Core - Data

- **Physical core sizes**
- **B-H curve**
- **Magnetising characteristics**
- **Core losses**

amc

Table of Physical Sizes: Single phase cores for shell type transformers in GOSS

Tabelle physikalischer Groessen: Einphasige Kerne fuer Manteltransformator in GOSS

Tabla de Dimensiones Físicas: Núcleos de una-fase para transformadores de tipo revestido en ASGO (GOSS)

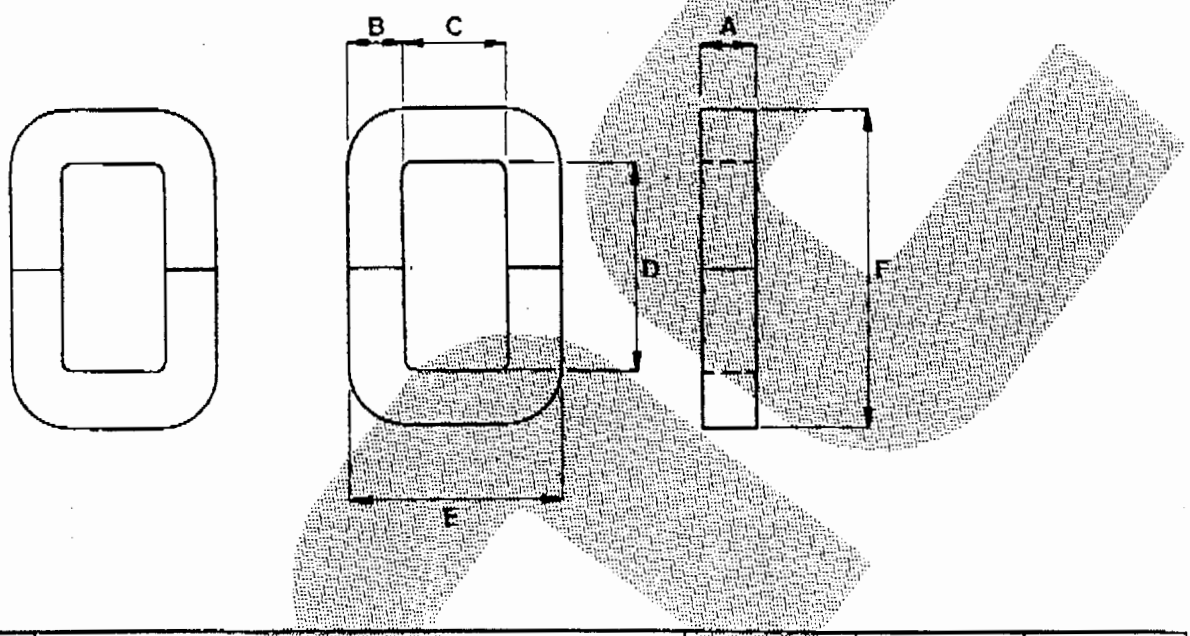

Code or VA/ Set Code oder VA/ Set Código o VA/ Set	V/T at 1.7 Tesla V/T bei 1.7 Tesla V/T a 1.7 Tesla	Nominal Dimensions (mm) Nennabmessungen (mm) Dimensiones Nominales (mm)						Length of Flux Path (cm) Laenge des Kraftfluss-weges (cm) Longitud de camino de Flujo (cm)	Nett Area/ Set (cm²) Netto-flaeche/ Set (cm²) Area Neta/ Set (cm²)	Nominal Weight/ Set (kg) Nenn-gewicht/ Set (kg) Peso Nominal/ Set (kg)
		A	B	C	D	E	F			
50	0.258	40	9	13	38	33	59	12.4	6.84	0.72
100	0.344	40	12	19	54	46	83	17.7	9.12	1.36
250	0.430	40	15	26	64	59	100	22.1	11.40	2.10
350	0.537	50	15	26	64	59	100	22.1	14.25	2.61

[redacted]
302130
0.30mm

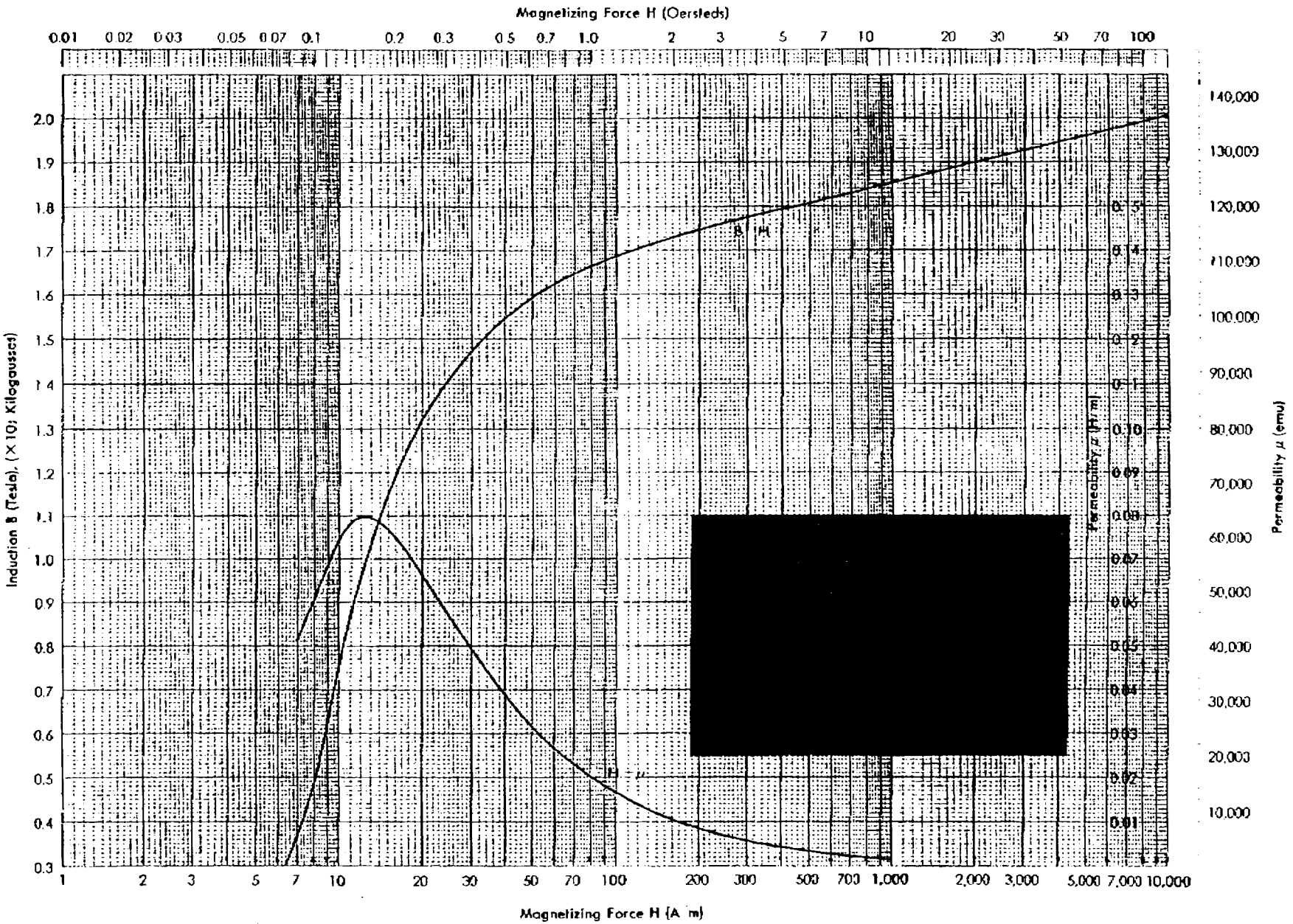

Magnetising Characteristics - Toroids in 0.3 mm GOSS - Tested at 50Hz

Magnetisierung Eigenschaften - Ringkerne mit 0,3 mm GOSS - Getestet bei 50Hz

Caracteristicas Magnétizantes - Toroidales en 0,3 mm ASGO (GOSS) - Copelado a 50Hz

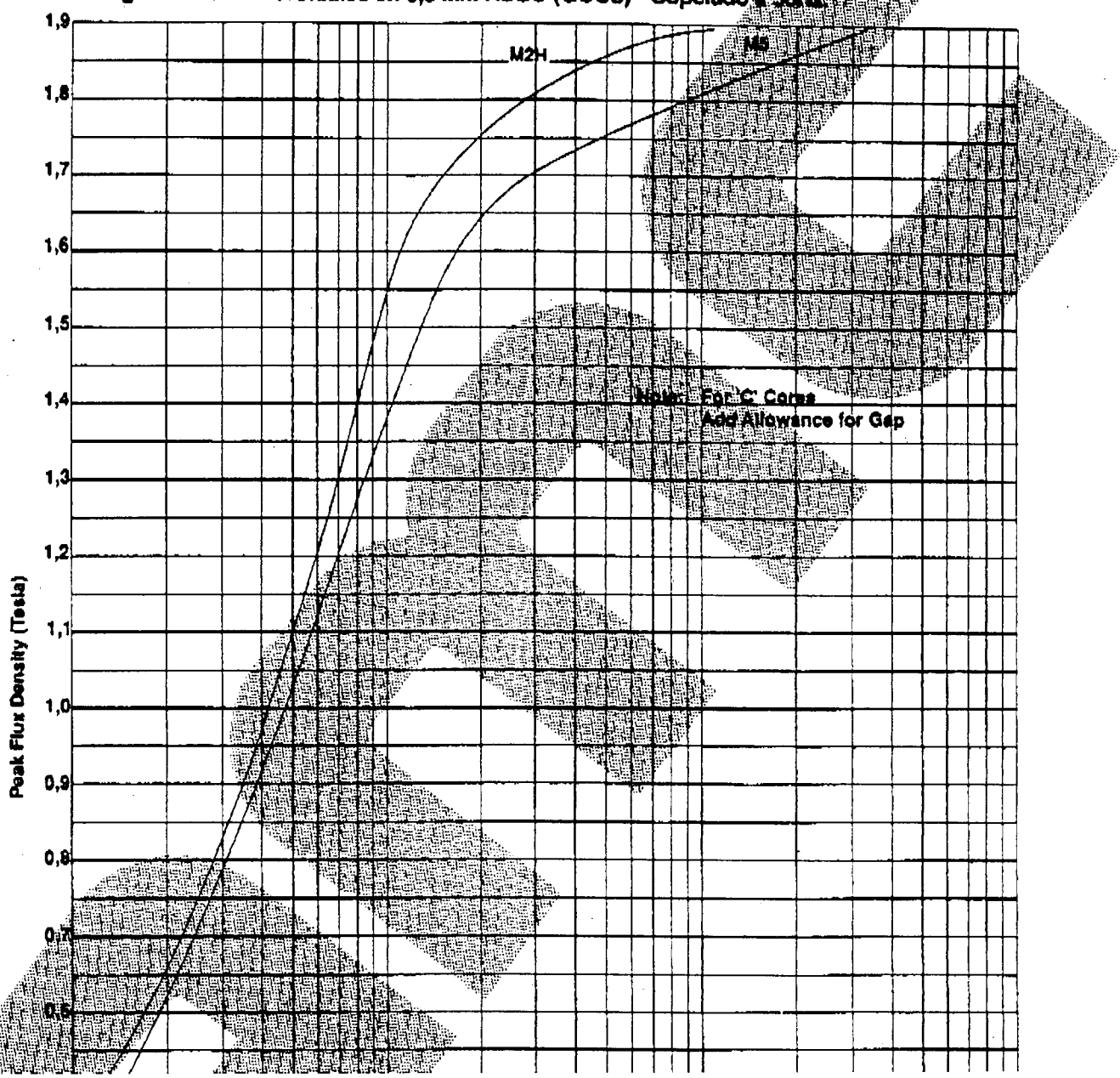

Core Loss (Iron Losses) - 0.3 mm GOSS - Tested at 50Hz

Kern Verlust (Eisenverlust) - 0,3 mm GOSS - Getestet bei 50Hz

Pérdidas de núcleo (Pérdidas de Hierro) - 0.3 mm ASGO (GOSS) Copelado a 50Hz

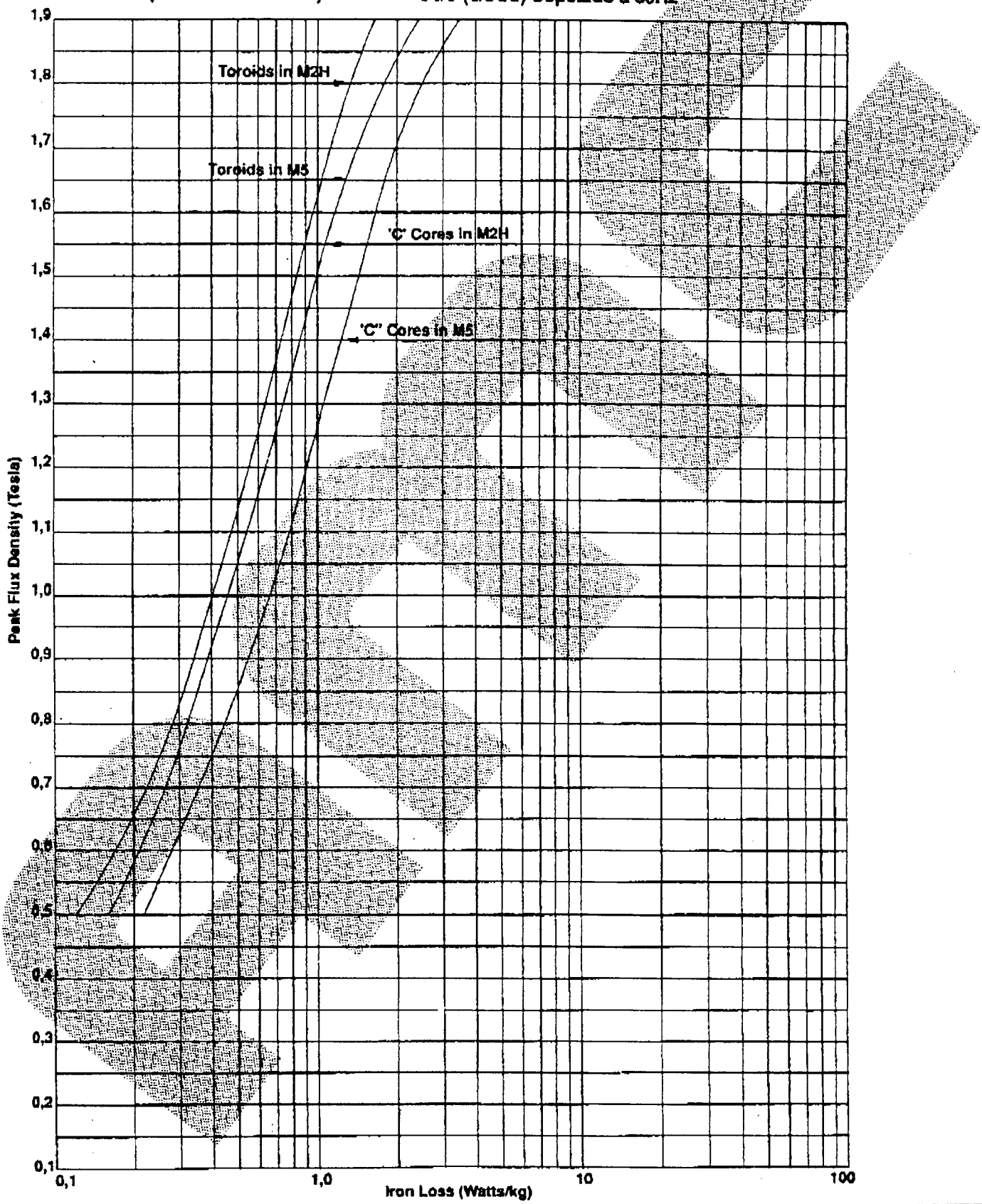

C : Capacitor Switching Contactor - Data

- **Wiring diagrams**
- **Contactor operation**
- **Performance graph**

Wiring diagrams

K2-16K10
K2-23K10
K2-30K10

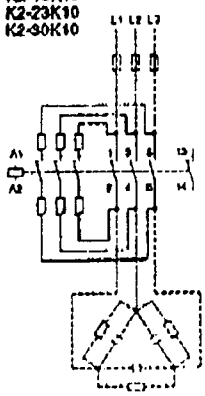

K2-16K01
K2-23K01
K2-30K01

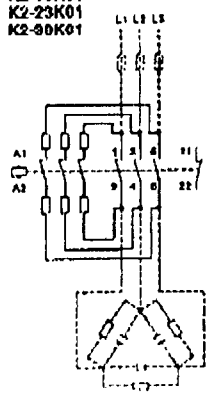

K2-45K00
K2-60K00

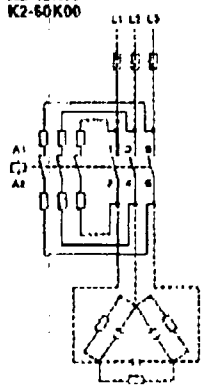

K2-45K01
K2-60K01

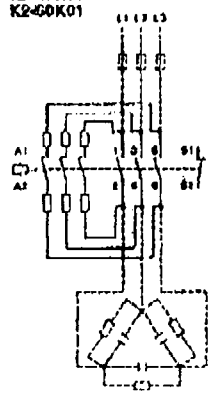

Dimensions (mm)

K2-16K10
K2-16K01

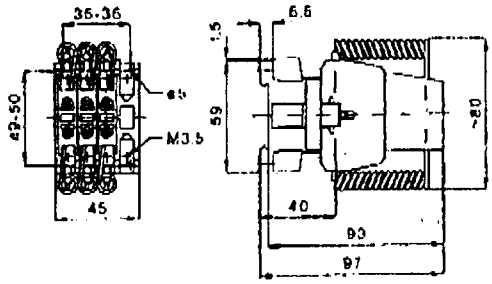

K2-23K10, K2-23K01
K2-30K10, K2-30K01

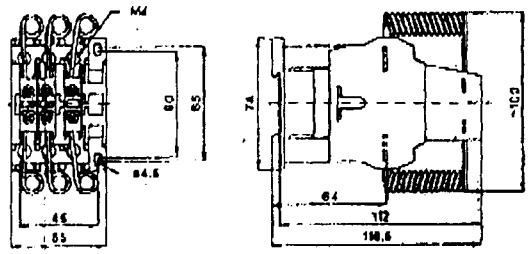

K2-45K00
K2-60K00

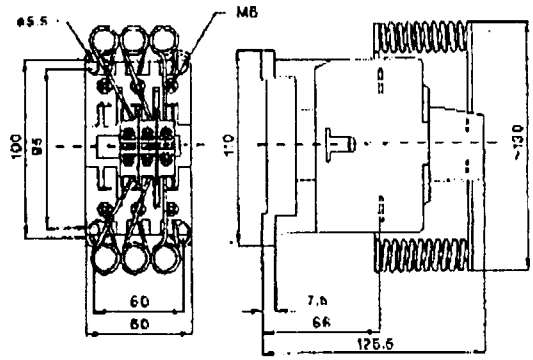

K2-45K01
K2-60K01

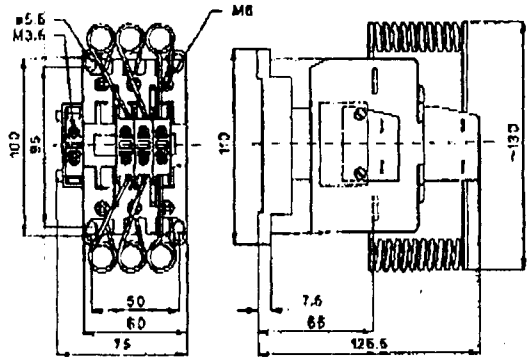

K2-45K01S
K2-60K01S

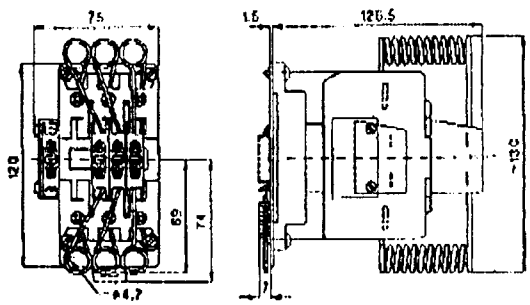

1.2) Contactor operation at direct switching of capacitors

1.2.1) Theoretic view of function

Make

In case of the pre-contacts during make, the current peaks are attenuate by resistor wires.
These current peaks would weld the main-contacts of contactor and they are also not good for the capacitors.

The total resistance of the resistor wires is mostly ohmic, the inductive one can be ignored.
The looking like a coil is only a case of construction.

Devices of Benedikt & Jäger use pre-contacts with snap function, that means each pre-contact block is connected with a permanent magnet to the contactor. The pre-contacts are opening at a time, at which the main contacts are surely closed.

The single controlled pre-contacts are increasing the safety of operating, in opposite of contamination during operation.

Operation:

During operation the resistor wires are not getting warmer, because the are not in the circuit.

Break:

Important: these contactors can be used for both installations, because the pre-contacts have no function during break, thus means that the peaks of the break-over voltage (power) of the chokes can't make any damage.

make **with** pre-contacts (B&J\Oszi13)

K2-16K 12.5kVAr (18A / 400V)

vertical: 250A / div horizontal: 0.5ms / div

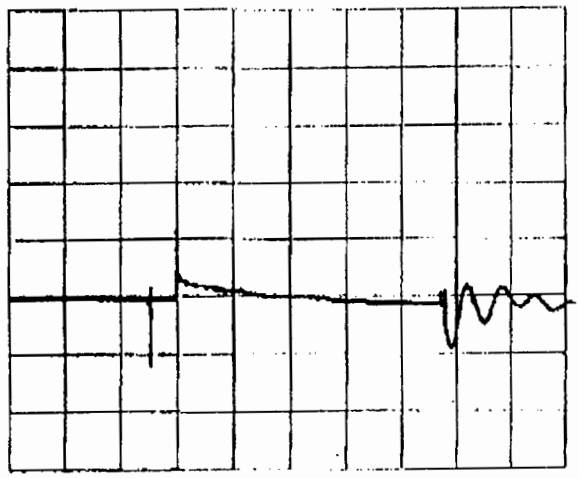

make **without** pre-contacts (B&J\Oszi12)

K2-16K 12.5kVAr (18A / 400V)

vertical: 250A / div horizontal: 0.5ms / div

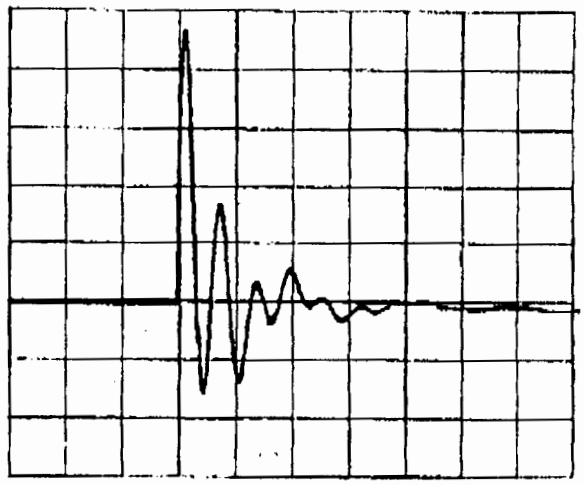

The difference of the left picture to the others before is the time scale.
The peak before the first current peak can be seen as a measuring failure.

The right picture shows a make current peak without pre-contacts with about 1200A with high power in opposite to 280A with low power (power = integrated area).
Of course, the contactors endure a few switches without pre-contacts.

D : Saturable-Core Transformer – Specifications

- **Core and winding data**

Design 1

Core	:	750VA "GOS Steel" c-cores	
N_I	:	250 turns	0.8mm ϕ (wire diameter)
N_O	:	250 turns	0.8mm ϕ
N_C	:	2500 turns	0.1mm ϕ

Design 2

Core	:	500VA "GOS Steel" c-cores	
N_I	:	250 turns	1.25mm ϕ (wire diameter)
N_O	:	250 turns	1.25mm ϕ
N_C	:	2500 turns	0.1mm ϕ

Design 3

Core	:	500VA "GOS Steel" c-cores	
N_I	:	250 turns	1.25mm ϕ (wire diameter)
N_O	:	250 turns	1.25mm ϕ
N_C	:	2500 turns	0.25mm ϕ

E : Fluke 43 Power Meter - Technical Specifications

- **Safety specifications**
- **Function specifications**
- **Current probe**
- **Scope**
- **Miscellaneous**
- **Electromagnetic immunity**

FLUKE®

Power Quality Analyzer

43

Users Manual

Safety Specifications

Safety Characteristics

Designed and tested for measurements on 600 V rms Category III, Pollution Degree 2 in accordance with:

- EN 61010.1 (1993) (IEC 1010-1)
- ANSI/ISA S82.01-1994
- CAN/CSA-C22.2 No.1010.1-92 (including approval)
- UL3111-1 (including approval)

Installation Category III refers to distribution level and fixed installation circuits inside a building.

⚠ **Maximum Input voltage Input 1 and 2**

Direct on inputs or with test leads TL24 (see Figure 11)
0 to 66 kHz ..... 600 V rms
> 66 kHz ..... derating to 5 V rms
With Shielded Banana-to-BNC Adapter Plug BB120 (see Figure 11)
0 to 400 kHz ..... 300 V rms
> 400 kHz ..... derating to 5 V rms

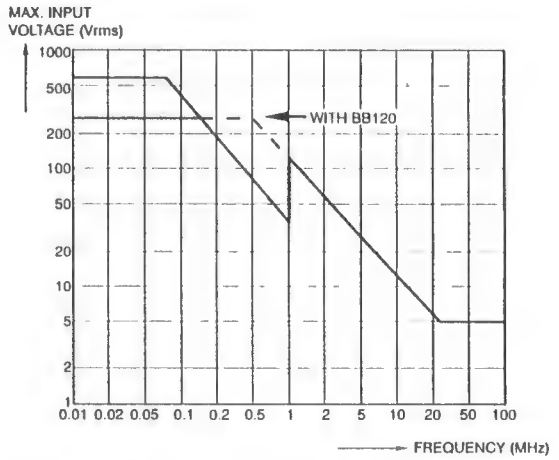

Figure 11. Max. Input Voltage v.s. Frequency

⚠ **Maximum floating voltage**

From any terminal to ground
0 to 400 Hz ..... 600 V rms

Function Specifications

For all specifications, probe specifications must be added.

Electrical functions

Specifications are valid for signals with a fundamental between 40 and 70 Hz.

Minimum input voltage ..... 4 V peak-peak
Minimum input current ..... 10 A peak-peak (1 mV/A)

Input bandwidth ..... DC to 15 kHz (unless specified otherwise)

Volts / Amps / Hertz

Readings ..... V rms (AC+DC), A rms (AC+DC), Hz
- Voltage ranges (auto) ..... 5.000 V to 500.0 V, 1250 V ±(1 % + 10 counts)
- Current ranges (auto) ..... 50.00 A to 500.0 kA, 1250 kA ±(1 % + 10 counts)
- Frequency range ..... 10.0 Hz to 15.0 kHz
  - 40.0 to 70.0 Hz ..... ±(0.5 % + 2 counts)

Power

Readings ..... Watt, VA, VAR, PF, DPF, Hz
- Watt, VA, VAR ranges (auto) ..... 250 W to 250 MW, 625 MW, 1.56 GW
  - when selected: total (%r): ±(2 % + 6 counts)
  - when selected: fundamental (%f): ±(4 % + 4 counts)
- DPF ..... 0.00 to 1.00
  - 0.00 to 0.25 ..... not specified
  - 0.25 to 0.90 ..... ± 0.04
  - 0.90 to 1.00 ..... ± 0.03
- PF ..... 0.00 to 1.00 ± 0.04
- Frequency range ..... 10.0 Hz to 15.0 kHz
  - 40.0 to 70.0 Hz ..... ±(0.5 % + 2 counts)

Harmonics

Number of harmonics ..... DC..21, DC..33, DC..51

Readings / Cursor readings
- V rms / I rms ..... fund. ±(3 % + 2 counts)
  31st ±(5 % + 3 counts)
  51st ±(15 % + 5 counts)
- Watt ..... fund. ±(5 % + 10 counts)
  31st ±(10 % + 10 counts)
  51st ±(30 % + 5 counts)
- Frequency of fundamental ..... ± 0.25 Hz

Current Probe

⚠ Safety Characteristics

Designed for measurements on 600 V rms Category III. Protection class II, double or reinforced insulation requirements in accordance with:
- IEC 1010-1
- ANSI/ISA S82
- CSA-C22.2 No.1010.1-92
- UL1244

Electrical Specifications

Current range ..... 1A to 500 A rms
AC current over range limit ..... 700 A rms
Maximum 10 minutes, followed by removal from current carrying conductor for 30 minutes.
Output Signal ..... 1mV AC/A AC

Accuracy

5 to 10 Hz
- 1 to 500 A ..... -3 dB typically

10 to 20 Hz
- 1 to 300 A ..... ± 5 %
- 300 to 400 A ..... ± 15 %
- 400 to 500 A ..... ± 25 %

20 to 45 Hz
- 1 to 500 A ..... ± 5 %

45 to 65 Hz
- 1 to 20 A ..... ±5 % of reading + 0.3 A
- 20 to 100 A ..... ±5 % of reading ± 3° phase shift
- 100 to 500 A ..... ±2 % of reading ± 5° phase shift

65 Hz to 3 kHz
- 1 to 50 A ..... ±(5 % + 0.4 A)
- 50 to 500 A ..... ± 5 %

Influence of temperature on accuracy ..... <0.15 % per 10 °C (18 °F)

Altitude

During operation ..... 2.0 km (6560 feet)
While stored ..... 12 km (40 000 feet)

Scope

Input Impedance

Input 1 ..... 1 MΩ // 12 pF (± 2 pF)
Input 2 ..... 1 MΩ // 10 pF (± 2 pF)

Horizontal

Time base modes (selectable) ..... Normal, Single, Roll

Ranges (selectable within modes)
In Normal ..... 5 s to 20 ns/div
In Single shot ..... 5 s to 1 µs/div
In Roll mode ..... 60 s to 1 s/div

Time base error ..... < ±(0.4 % + 1 pixel)

Maximum sampling rate
10 ms to 60 s ..... 5 MS/s
20 ns to 10 ms ..... 25 MS/s

Trigger source (auto) ..... Input 1 or Input 2

Vertical

Voltage ranges ..... 5.0 mV/div to 500 V/div
Trace accuracy ±(1 % + 2 pixels)

Bandwidth input 1 (voltage)
excluding test leads or probes ..... DC to 20 MHz (-3 dB)
with test leads TL24 ..... DC to 1 MHz (-3 dB)
with 10:1 probe PM8918 (optional) ..... DC to 20 MHz (-3 dB)
with shielded test leads STL120 (optional) ..... DC to 12.5 MHz (-3 dB)
DC to 20 MHz (-6 dB)
Lower transition point (AC coupling) ..... 10 Hz (-3 dB)

Bandwidth input 2 (current)
with Banana-to-BNC adapter ..... DC to 15 kHz
Lower transition point (AC coupling) ..... 10 Hz (-3 dB)

Scope readings

The accuracy of all scope readings is valid from 18 °C to 28 °C with relative humidity up to 90 % for a period of one year after calibration. Add 0.1 x (the specified accuracy) for each °C below 18 °C or above 28 °C. More than one waveform period must be visible on the screen.

V DC, A DC ..... ±(0.5 % + 5 counts)

V AC and V AC+DC (True RMS) input 1
DC to 60 Hz ..... ±(1 % + 10 counts)
60 Hz to 20 kHz ..... ±(2.5 % + 15 counts)
20 kHz to 1 MHz ..... ±(5 % + 20 counts)
1 MHz to 5 MHz ..... ±(10 % + 25 counts)
5 MHz to 20 MHz ..... ±(30 % + 25 counts)

A AC and A AC+DC (True RMS) input 2
DC to 60 Hz ..... ±(1 % + 10 counts)
60 Hz to 15 kHz ..... ±(30 % + 25 counts)

Frequency (Hz), Pulse width, Duty cycle (2.0 % to 98.0 %)
1 Hz to 1 MHz ..... ±(0.5 % + 2 counts)
1 MHz to 10 MHz ..... ±(1 % + 2 counts)
10 MHz to 30 MHz ..... ±(2.5 % + 2 counts)

Phase (Input 1 to Input 2)
1 Hz to 400 Hz ..... ±2°

Peak voltage
Peak max, Peak min ..... ± 5 % of full scale
Peak-peak ..... ± 10 % of full scale

Crest
Range ..... 1.0 to 10.0
±(5 % + 1 counts)

Miscellaneous

Display

Useful screen area ..... 72 x 72 mm (2.83 x 2.83 in)
Resolution ..... 240 x 240 pixels
Backlight ..... Cold Cathode Fluorescent (CCFL)

⚠ Power

External

Power Adapter PM8907
Input Voltage ..... 10 to 21V DC
Power ..... 5 W typical

Internal

Rechargeable Ni-Cd battery pack BP120
Voltage range ..... 4 to 6 V DC
Operating Time ..... 4 hours
Charging Time ..... 4 hours with Fluke 43 off
12 hours with Fluke 43 on
Refresh cycle ..... 8 to 14 hours

Memory

Number of screen memories 10
Number of transient memories (temporary) 40

Mechanical

Height x width x depth ..... 232 x 115 x 50 mm (9.1 x 4.5 x 2 in)
Weight (including battery pack) ..... 1.1 kg (2.5 lbs)

Interface ..... RS232, optically isolated
Supported Printers ..... HP Deskjet®, Laserjet®, PostScript and Epson FX80

Serial via PM9080 (optically isolated RS232 Adapter/Cable).
Parallel via PAC91 (optically isolated Print Adapter Cable, optional).

To PC ..... Dump and load settings and data

Serial via PM9080 (optically isolated RS232 adapter/cable),
using SW43W (FlukeView® Power Quality Analyzer software).

Electromagnetic Immunity

The Fluke 43, including standard accessories, conforms with the EEC directive 89/336 for EMC immunity, as defined by IEC1000-4-3, with the addition of the following tables.

Disturbance with test leads TL24 or Current Clamp 80i-500s

- Volts / amps / hertz
- Resistance, Capacitance
- Power
- Harmonics

Table 1

No visible disturbance	E = 3 V/m	E = 10 V/m
Frequency: 10 kHz - 27 MHz Frequency: 27 MHz - 1 GHz	(-) (-)	(-) (-)

(-): no visible disturbance

Disturbance with test leads TL24 in scope mode

- V AC+DC (True RMS)

Table 2

Disturbance less than 1 % of full scale	E = 3 V/m	E = 10 V/m
Frequency: 10 kHz - 27 MHz Frequency: 27 MHz - 200 MHz Frequency: 200 MHz - 1 GHz	2 V/div - 500 V/div 500 mV/div - 500 V/div (-)	10 V/div - 500 V/div 2 V/div - 500 V/div 5 mV/div - 500 V/div

(-): no visible disturbance

Table 3

Disturbance less than 10 % of full scale	E = 3 V/m	E = 10 V/m
Frequency: 10 kHz - 27 MHz Frequency: 27 MHz - 200 MHz Frequency: 200 MHz - 1 GHz	1 V/div 200 mV/div (-)	5 V/div 1 V/div (-)

(-): no visible disturbance

Ranges not specified in Tables 2 and 3 may have a disturbance of more than 10 % of full scale.

F : LEM Current Transducer - Technical Specifications

- **Electrical data, accuracy and general data**
- **Dimensions and connections**

LA 100-P

Definition

The «LA 100-P» is a current transducer for the electronic measurement of currents : DC, AC, IMPL., etc., with galvanic isolation between the primary (high power) and the secondary (electronic) circuits.

Electrical data

Nominal current I_N		**: 100 A rms**
Measuring range		**: 0 to ± 150 A**
Measuring resistance		**: R_M min. R_M max.**
with ± 12 V	**at ± 100 A max.**	**: 0 ohm 40 ohm**
	at ± 120 A max.	**: 0 ohm 10 ohm**
with ± 15 V	**at ± 100 A max.**	**: 0 ohm 100 ohm**
	at ± 150 A max.	**: 0 ohm 25 ohm**
Nominal analog output current		**: 50 mA**
Turns ratio		**: 1 : 2000**
Accuracy at +25°C and at ± 15 V (± 5 %)		**: ± 0.65 % of I_N**
Accuracy at + 25°C and at ± 12 to ± 15 V		**: ± 0.9 % of I_N**
Supply voltage		**: + and - 12 to 15 V (± 5 %)**
Isolation		**: between primary and secondary : 2 kV rms/50 Hz/1 min.**

Accuracy - Dynamic performance

Zero offset current at +25°C	: max. ± 0.1 mA
Residual current [1] I_{HC} at I primary after an overload of 3 x I_N	: max. ± 0.15 mA
Thermal drift of offset current (between 0°C and +70°C)	: typical ± 0.05 mA max. ± 0.25 mA
Linearity	: better than 0.15 %
Response time	: better than 500 nS
Rise time	: better than 1 µs
di/dt accurately followed	: better than 200 A/µs
Bandwidth	: 0 to 200 kHz (-1dB)

General data

Operating temperature	: 0°C to +70°C
Storage temperature	: -25°C to +85°C
Current consumption	: 10 mA (at ± 15 V) + output current
Secondary internal resistance	: 130 ohm (at +70°C)
Package	: insulated plastic case qualified according to UL 94-V0
Weight	: 18 g.
Fastening	: for mounting on printed circuit board by 3 pins 0.63 x 0.56 mm, recommended hole size 0.9 mm dia.
Connection to primary circuit secondary circuit	: through-hole 12.7 x 7 mm : on 3 pins 0.63 x 0.56 mm
Polarity markings	: a positive measuring current is obtained on terminal M, when the primary current flows in the direction of the arrow.
EMC 940516/1	: qualified according to IEC 801.3

LEM SA

CASE POSTALE 785
CH-1212 GRAND-LANCY 1
GENEVA, SWITZERLAND

CHEMIN DES AULX 8
CH-1228 PLAN-LES-OUATES
GENEVA, SWITZERLAND

TEL: 022/ 706 11 11
FAX: 022/ 794 94 78
TELEX: 429 422 LEM CH

Notes : 1) The result of the coercive field of the magnetic circuit.
- The temperature of the primary conductor should not exceed 90°C.
- This is a standard model; for different versions (e.g. supply voltages, turns ratios, unidirectional measurements, etc.), please contact us.

Remarks : 1) Dynamic performance (di/dt and response time) is best with a single bar completely filling the primary hole
2) In order to achieve the best magnetic coupling, the primary windings have to pass over the top side of the device.

Dimensions LA 100-P

General tolerance ± 0.2 mm
Recommended hole dia. 0.9 mm

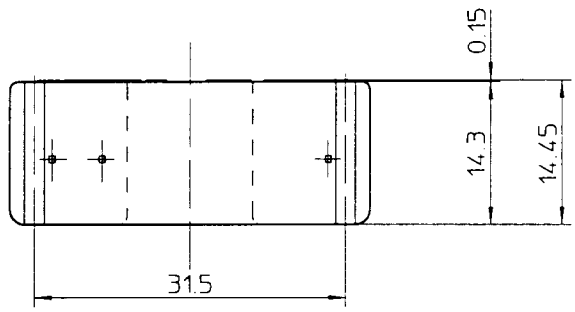

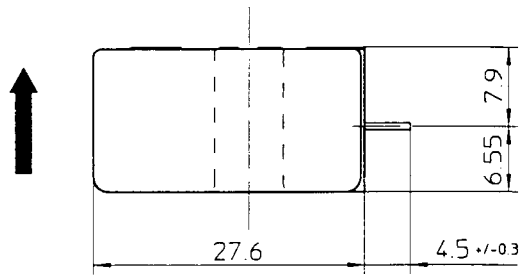

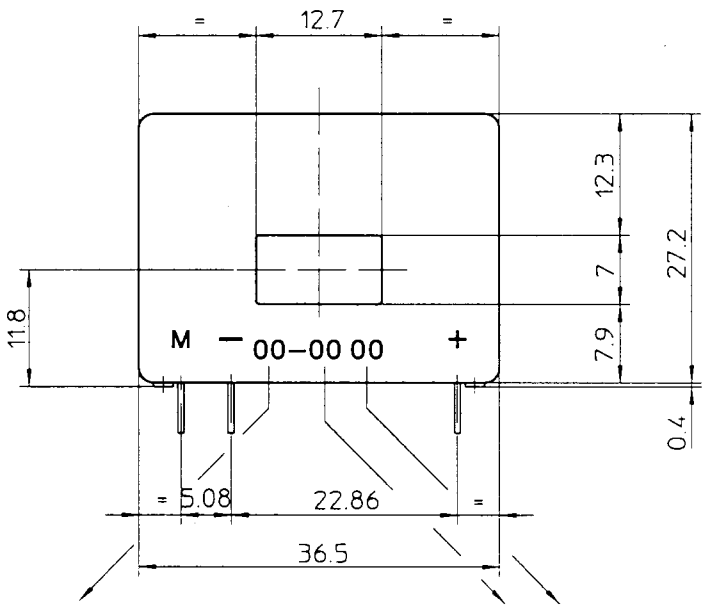

Standard 00
or N° SP..

Week year
Date Code

Secondary terminals :

Terminal + : supply voltage + 12 to 15 V
Terminal - : supply voltage - 12 to 15 V
Terminal M : measure

Connection :

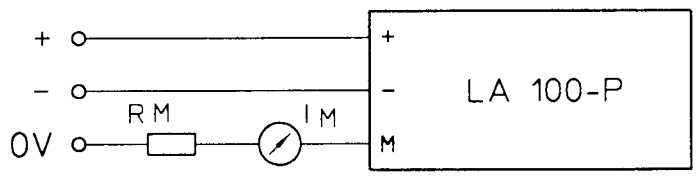

«This data sheet is a translation of the French version which is deemed authentic.»
We reserve the right to carry out modifications on our transducers, in order to improve them, without previous notice.

G : Circuit Diagrams

- **Signal conditioning and error amplifier circuits**
- **Switching circuit**
- **Switch-mode power supply**

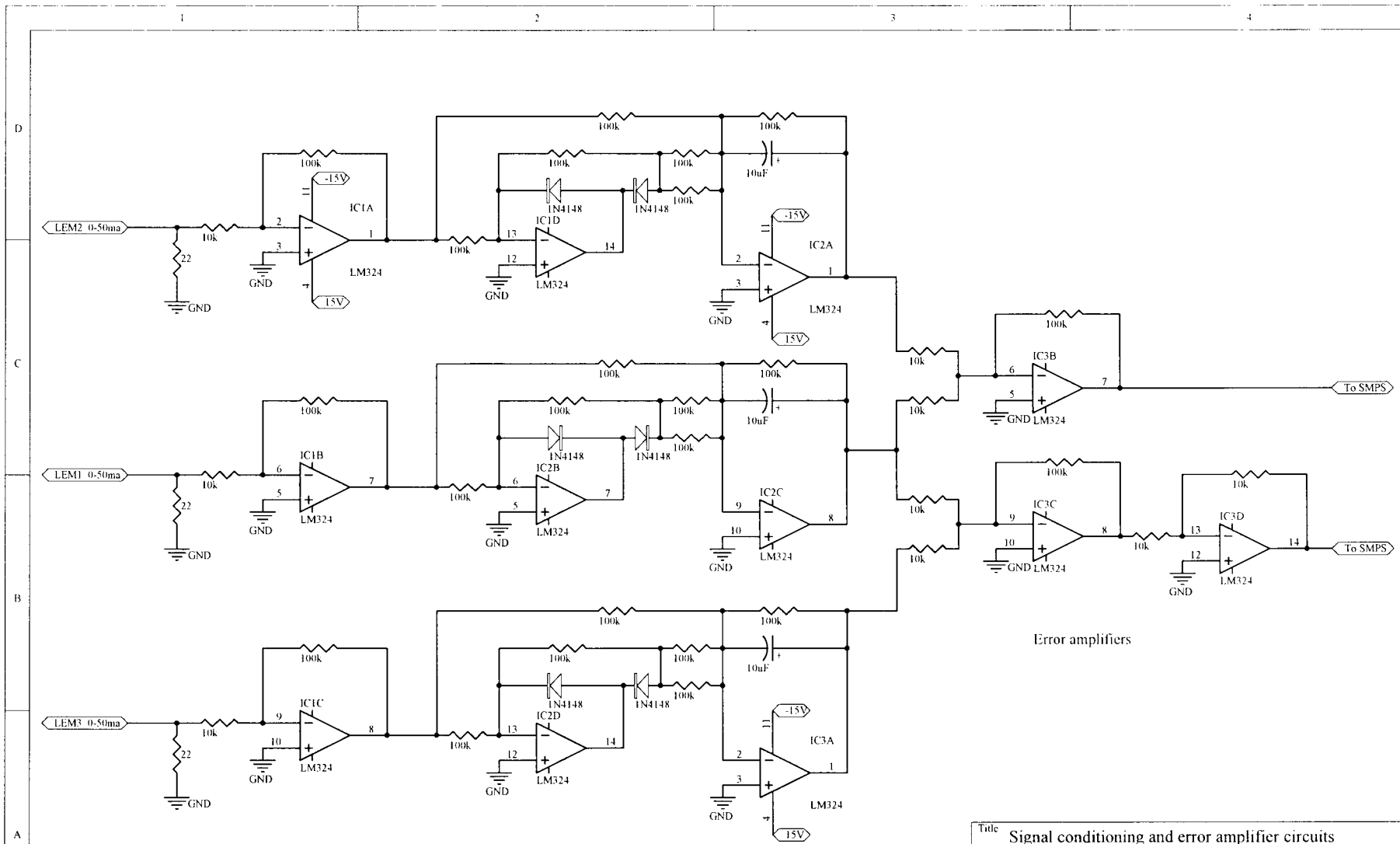
LEM2 0-50ma
LEM1 0-50ma
LEM3 0-50ma
IC1A
IC1B
IC1C
IC1D
IC2A
IC2B
IC2C
IC2D
IC3A
IC3B
IC3C
IC3D
LM324
1N4148
100k
10k
22
10uF
-15V
15V
GND
To SMPS
Current-to-voltage conversion
Precision rectifying and smoothing
Error amplifiers
Title
Signal conditioning and error amplifier circuits
Size
A4
Number
1
Revision
0
Date: 25-Sep-1999
Sheet of 1 of 1
File: D:\Work\...\Controller.sch
Drawn By: Stuart Marinus

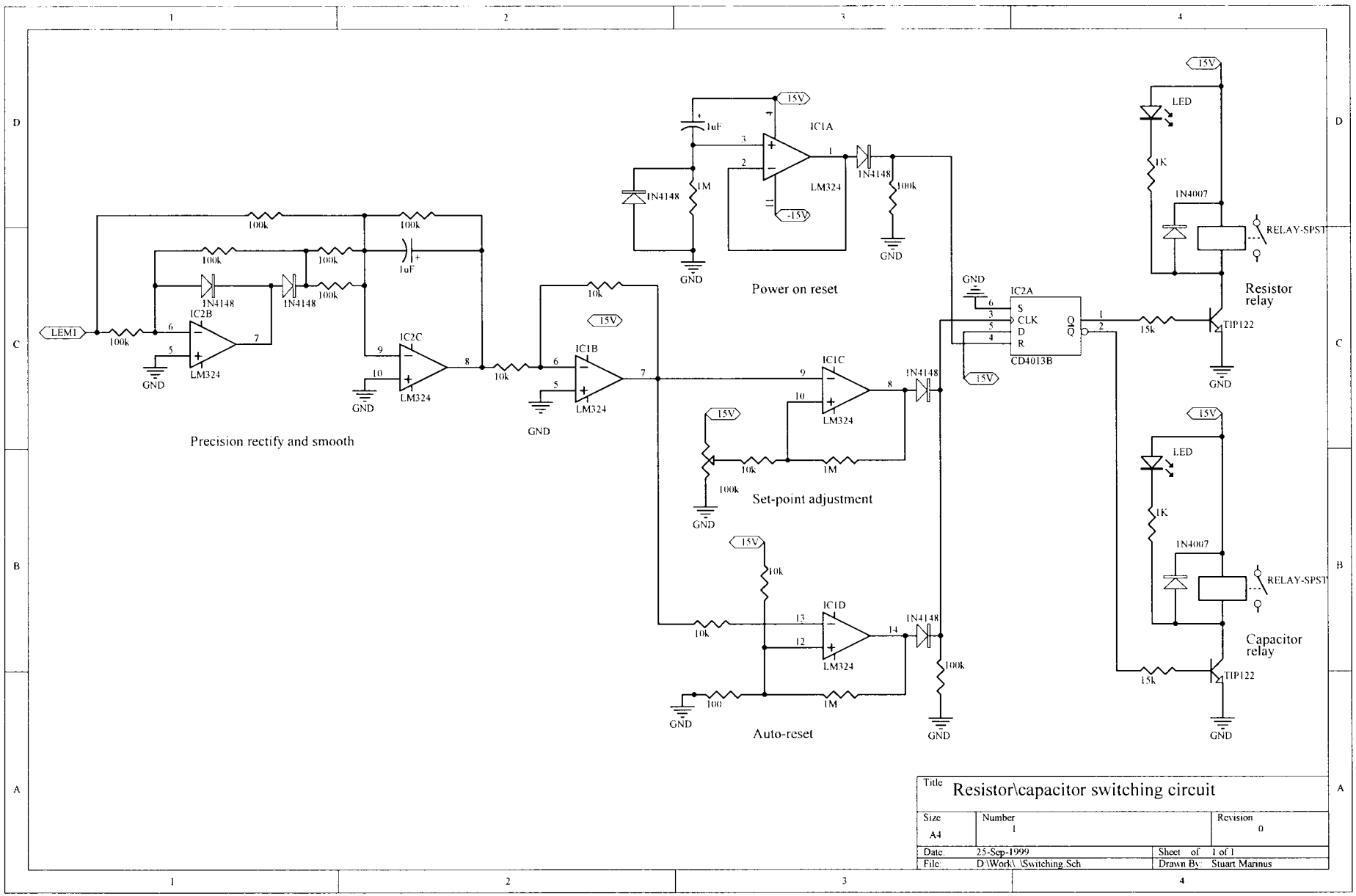
LEM1
100k
IC2B
LM324
GND
1N4148
1uF
IC2C
10k
IC1B
Precision rectify and smooth
15V
IC1A
1M
-15V
Power on reset
IC1C
Set-point adjustment
IC1D
100
Auto-reset
IC2A
CD4013B
S
CLK
D
R
Q
LED
1K
1N4007
RELAY-SPST
Resistor relay
15k
TIP122
Capacitor relay
Title
Resistor\capacitor switching circuit
Size
A4
Number
1
Revision
0
Date:
25-Sep-1999
Sheet of 1 of 1
File:
D:\Work\ \Switching.Sch
Drawn By:
Stuart Marinus

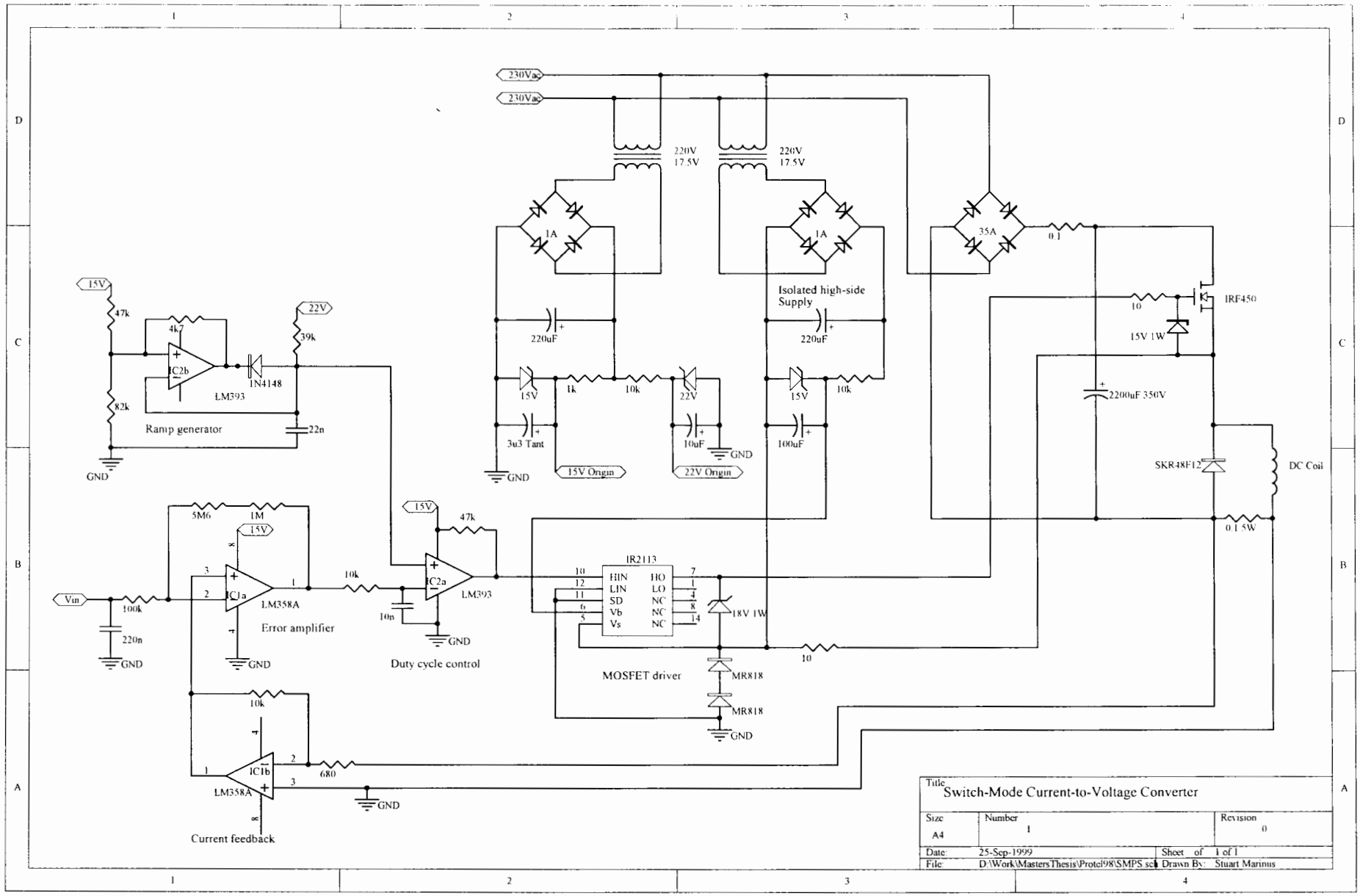

Title: Switch-Mode Current-to-Voltage Converter

Size	Number	Revision
A4	1	0

Date:	25-Sep-1999	Sheet of 1 of 1	
File:	D:\Work\MastersThesis\Protel98\SMPS.sch	Drawn By:	Stuart Marinus

H : Induction Motor – Technical Specifications

- **General information**
- **Physical dimensions**
- **Performance**
- **Equivalent circuit parameters**

Kilowatts	15
Duty	S1
RPM	1450
SUPPLY VOLTS	380
ENCLOSURE	IP55
INS. CLASS TEMP RISE	F/B RISE
AMB © / ALTITUDE	40
MOUNTING	B3
COOLING IC	IC0141
BEARING – DE/NDE	BALL/BALL
SHAFT EXTENSION / SIZE	STD
FRAME SIZE	160L
PRICE NETT EXCL VAT	R 3450-00

CAST IRON FRAME 3 PH 50 HZ CAGE MOTORS
TOTALLY ENCLOSED FAN COOLED IP 55 SIZES 160M TO 315L

PERFORMANCE

to SABS tolerances

RATED OUTPUT	FRAME SIZE	FRAME TYPE	RATED SPEED	POLE	RATED CURRENT AT 380V	RATED TORQUE	EFFICIENCY UNDER DIFFERENT CONDITIONS			POWER FACTOR UNDER DIFFERENT CONDITIONS					LOCKED ROTOR RATIOS AS MULTIPLES OF RESPECTIVE QUANTITIES				NO LOAD CURRENT AT 380V	BREAK DOWN TORQUE	% SLIP AT BDT	ROTOR INERTIA J	MOTOR MASS
															Star		D.O.L.						
							4/4	3/4	2/4	4/4	3/4	2/4	NL	LR	Torque	Current	Torque	Current					
kW		LA6	r/min		A	Nm	%	%	%						p.u.	p.u.	p.u.	p.u.	A	p.u.		kg.m²	kg
4	160M	163	715	8	10.6	53.4	78	77	74	0.73	0.66	0.52	0.13	0.67	0.45	1.29	2.10	4.80	8.1	2.50	20	0.051	110
5.5	160M	164	720	8	14.8	73	81	80	76	0.70	0.62	0.50	0.12	0.61	0.50	1.34	2.30	5.00	11.1	2.70	20	0.068	125
7.5	160M	163	960	6	17.4	74.5	86	86	84	0.76	0.67	0.54	0.09	0.57	0.43	1.32	2.00	4.90	10.7	2.25	27	0.050	120
	160L	166	720	8	18.4	99.5	84	83	80	0.74	0.69	0.58	0.11	0.59	0.49	1.42	2.25	5.30	11.5	2.70.	17	0.11	145
11	160M	163	2920	2	22	36	84	83	79	0.90	0.88	0.80	0.32	0.58	0.57	2.01	2.40	7.20	9.2	3.00	18	0.034	115
	160M	163	1450	4	22.5	72.5	88	88	87	0.85	0.81	0.73	0.13	0.63	0.57	1.80	2.40	6.45	9.5	2.60	14	0.045	125
	160L	166	960	6	25.5	109	87	87	85	0.76	0.70	0.58	0.09	0.56	0.45	1.33	2.10	4.95	15.0	2.30	30	0.072	145
	180L	186	725	8	27	145	86	86	84	0.72	0.66	0.57	0.09	0.49	0.39	1.20	1.80	4.45	14.8	2.05	9.6	0.24	195
15	160M	164	2920	2	29	49	87	86	82	0.90	0.89	0.80	0.29	0.58	0.59	1.98	2.50	7.40	10.2	3.00	18	0.044	130
	160L	166	1450	4	30	99	89	89	88	0.85	0.81	0.70	0.13	0.61	0.53	1.89	2.50	6.75	12.7	2.70	14	0.058	140
	180L	186	970	6	31.5	148	88	88	86	0.82	0.76	0.66	0.09	0.62	0.54	1.64	2.50	6.10	14.8	2.50	11	0.22	195
	200L	207	725	8	34.5	198	87.1	87	85	0.76	0.73	0.63	0.09	0.58	0.44	1.28	2.05	4.75	17.5	2.20	10	0.41	235
18.5	160L	166	2920	2	35.5	60.5	88	87	83	0.90	0.88	0.81	0.25	0.58	0.61	2.18	2.60	7.00	12.0	3.20	17	0.058	150
	180M	183	1460	4	37	121	90	89	87	0.84	0.79	0.71	0.10	0.55	0.57	2.08	2.40	7.45	15.9	2.80	10	0.13	185
	200L	206	975	6	38	181	89.4	89	88	0.83	0.81	0.72	0.09	0.68	0.57	1.69	2.85	6.30	15.8	2.40	8.7	0.32	220
	225S	220	730	8	39.5	242	88.5	88	87	0.80	0.78	0.68	0.10	0.55	0.42	1.33	1.95	4.95	18.5	2.15	8.9	0.53	300
22	180M	183	2940	2	42	71.5	90	90	89	0.88	0.85	0.78	0.15	0.51	0.60	2.08	2.55	7.45	14.5	3.00	11	0.077	185
	180L	186	1460	4	43.5	144	91	91	90	0.84	0.80	0.71	0.09	0.53	0.58	2.14	2.45	7.65	18.2	2.90	10	0.16	200
	200L	207	975	6	44	216	89.8	89	88	0.85	0.84	0.76	0.10	0.57	0.50	1.56	2.30	5.80	16.0	2.10	8.2	0.37	235
	225M	223	730	8	46.5	288	89	89	88	0.81	0.76	0.69	0.09	0.53	0.41	1.30	1.90	4.85	20.5	2.10	9	0.74	325
30	200L	206	2940	2	56	97.5	91.7	91	89	0.88	0.85	0.82	0.21	0.45	0.52	1.94	2.20	6.95	17.2	2.75	8.8	0.13	230
	200L	207	1465	4	58	196	91.5	91.6	89	0.86	0.83	0.75	0.10	0.55	0.60	1.96	2.55	6.90	22.0	2.60	9.3	0.26	240
	225M	223	980	6	58	292	91	91	90	0.86	0.84	0.75	0.10	0.55	0.58	1.79	2.70	6.65	22.0	2.25	6.8	0.63	305
	250S	253	730	8	63	393	90.5	90.5	89.5	0.80	0.78	0.71	0.07	0.52	0.45	1.33	2.10	4.95	25.0	2.05	7.2	1.2	460
37	200L	207	2940	2	69	120	91.7	91	89	0.89	0.87	0.82	0.18	0.46	0.56	2.05	2.35	6.90	20.5	2.95	8.5	0.17	250
	225S	220	1475	4	71	240	91.5	91	89	0.87	0.84	0.74	0.09	0.52	0.66	1.98	2.80	6.90	29.0	2.80	7.5	0.47	300
	250S	253	980	6	73	361	91.9	91	90	0.84	0.81	0.76	0.08	0.53	0.52	1.68	2.40	6.25	24.0	2.05	5.9	0.97	435
	250M	255	730	8	75	484	91.5	91.5	91	0.82	0.80	0.71	0.07	0.50	0.48	1.41	2.20	5.25	29.5	2.30	7.1	1.4	490

CAST IRON STANDARD THREE-PHASE 50HZ T.E.F.C.
SQUIRREL CAGE INDUCTION MOTOR. FRAME SIZE 90-315

CS4
DIMENSIONS

FLANGE & FOOT MOUNTED

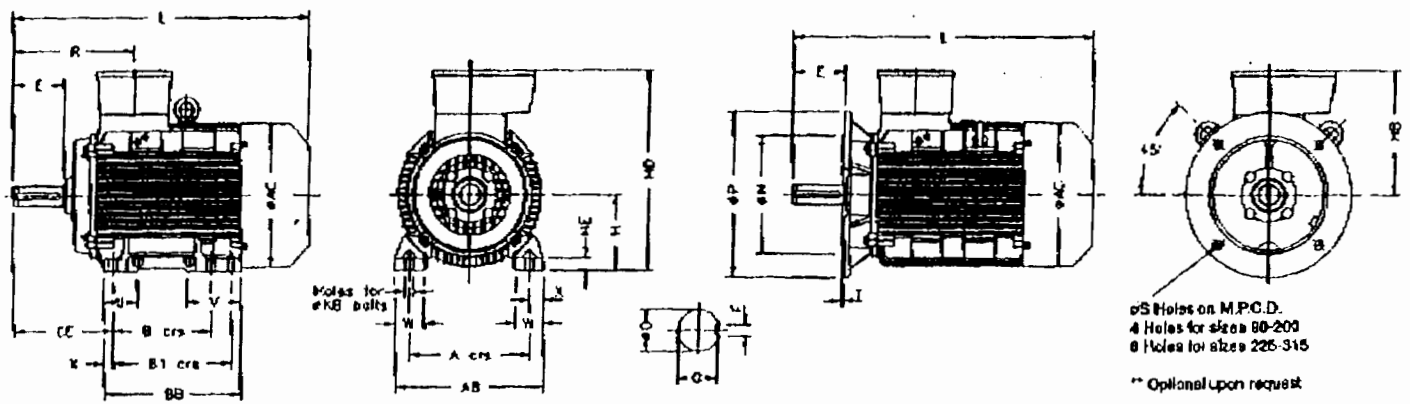

SIZE	POLE	A	AB	AC	B	B1	BB	CE	D	E	F	G	H	HB	HE	HD	K	KB	L	M	N	P	R	S	T	U	V	W	X
90S	2-8	140	175	176	100	-	156	108	24	50	8	20	90	165	13	255	15	8	371	165	130	200	151	12	4	40	65	37.5	17.5
90M	2-8				-	125																							
100L	2-8	160	200	194	140	-	176	123	28	60	8	24	100	170	16	270	18	10	415	215	180	250	164	14	4	40	40	45	20
112M	2-8	190	226	218	140	-	176	130	28	60	8	24	112	185	18	287	18	10	442	215	180	250	164	14	4	40	50	45	18
132S	2-8	216	256	257	140	-	218	169	38	80	10	33	132	202	18	334	20	10	505	265	230	300	201	14	4	50	88	50	20
132M	2-8				-	178																							
160M	2-8	254	314	302	210	-	284	218	42	110	12	37	160	262	26	422	20	12	640	300	250	350	262	19	5	70	116	60	30
160L	2-8				-	254																							
180M	2-8	279	344	347	241	-	319	231	48	110	14	42.5	180	282	26	462	20	12	716	300	250	350	266	19	5	70	108	65	32.5
180L	2-8				-	279																							
200L	2-8	318	398	390	-	305	365	243	55	110	16	49	200	297	34	497	25	16	792	350	300	400	270	19	5	85	85	80	40

15 KW →

225S	4-8	356	436	435	286	-	381	289	60	140	18	53	225	338	34	563	25	16	849	400	350	450	314	19	5	85	110	80	40
225M	2	356	436	435	-	311	381	259	55	110	16	49	225	338	34	563	25	16	819	400	350	450	284	19	5	85	110	80	40
225M	4-8							289	60	140	18	53							849				314						
250S	2	406	506	482	311	-	409	308	60	140	18	53	250	435	42	685	30	20	1020	500	450	550	368	19	5	100	140	100	50
250S	4-8								70		20	62.5																	
250M	2	406	506	482	-	349	409	308	60	140	18	53	250	435	42	685	30	20	1020	500	450	550	368	19	5	100	140	100	50
250M	4-8								70		20	62.5																	
280S	2	457	557	536	368	-	479	330	65	140	18	58	280	459	42	739	30	20	1107	500	450	550	379	19	5	100	151	100	50
280S	4-8							360	80	170	22	71							1137				409						
280M	2	457	557	536	-	419	479	330	65	140	18	58	280	459	42	739	30	20	1107	500	450	550	379	19	5	100	151	100	50
280M	4-8							360	80	170	22	71							1137				409						
315S	2	508	628	602	406	-	527	356	65	140	18	58	315	494	52	809	35	24	1160	600	550	660	390	24	8	125	171	120	60
315S	4-8							386	85	170	22	76							1190				420						
315M	2	508	628	602	-	457	527	356	65	140	18	58	315	494	52	809	35	24	1160	600	550	660	390	24	8	125	171	120	60
315M	4-8							386	85	170	22	76							1190				420						
315L	2	508	628	602	-	508	578	356	70	140	20	62.5	315	494	52	809	35	24	1250	600	550	660	390	24	8	120	120	120	60
315L	4-8							386	90	170	25	81							1290				432						
315L**	2	508	628	602	-	457	527	356	70	140	20	62.5	315	494	52	809	35	24	1260	600	550	660	390	24	8	120	120	120	60
315L**	4-8							386	90	170	25	81							1290				432						
315LX	2	508	628	602	-	508	578	356	70	140	20	62.5	315	494	52	809	35	24	1352	600	550	660	390	24	8	120	120	120	60
315LX	4-8							386	90	170	25	81							1382				420						
315LX**	4-8	508	628	602	-	457	527	386	90	170	25	81	315	494	52	809	35	24	1382	600	550	660	420	24	8	120	120	120	60

ALSTOM

FAX MESSAGE

Low Voltage Motors
Aberdeen Road
Industrial Sites,
Benoni
Private Bag 1026
Benoni
1500

To: Stewart Marinus

Company: UCT

Fax No.: (021) 650 - 3465 *Date:* 28/08/98 *Ref.:* gh-mct

From: G. Halfar *Fax No.:* (011) 899 - 1208 Telephone: (011) 899 - 1028

No. of pages: 1 *(Including cover sheet)*

RE : EQUIVALENT CIRCUIT PARAMETERS REQUIRED

With reference to our telephonic discussion of 28 August 1998 , herewith the information as requested :

i) Stator resistance / phase @ 20 degrees Celsius = 0,7014 Ω / phase

ii) Stator reactance / phase (Running) = 1,6080 Ω/phase

iii) Rotor resistance/phase referred to stator (Running) = 0,7738 Ω/phase

iv) Rotor reactance/phase referred to stator (Running) = 3,3679 Ω/phase

v) Magnetising reactance/phase = 50,5260 Ω/phase - (Running)

vi) Magnetising resistance /phase = 29,1023 Ω/phase (Running)

Trusting that you will find this so in order .

Regards

Signed

G. HALFAR
Electrical Design Engineer - LV

I : Water Pump – Data

- **Torque-speed curves**
- **Performance curves**

SIGMUND
PULSOMETER
PUMPS LTD.

PUMP CLOSED VALVE TORQUE-SPEED CURVE.

DATA SHEET 0908

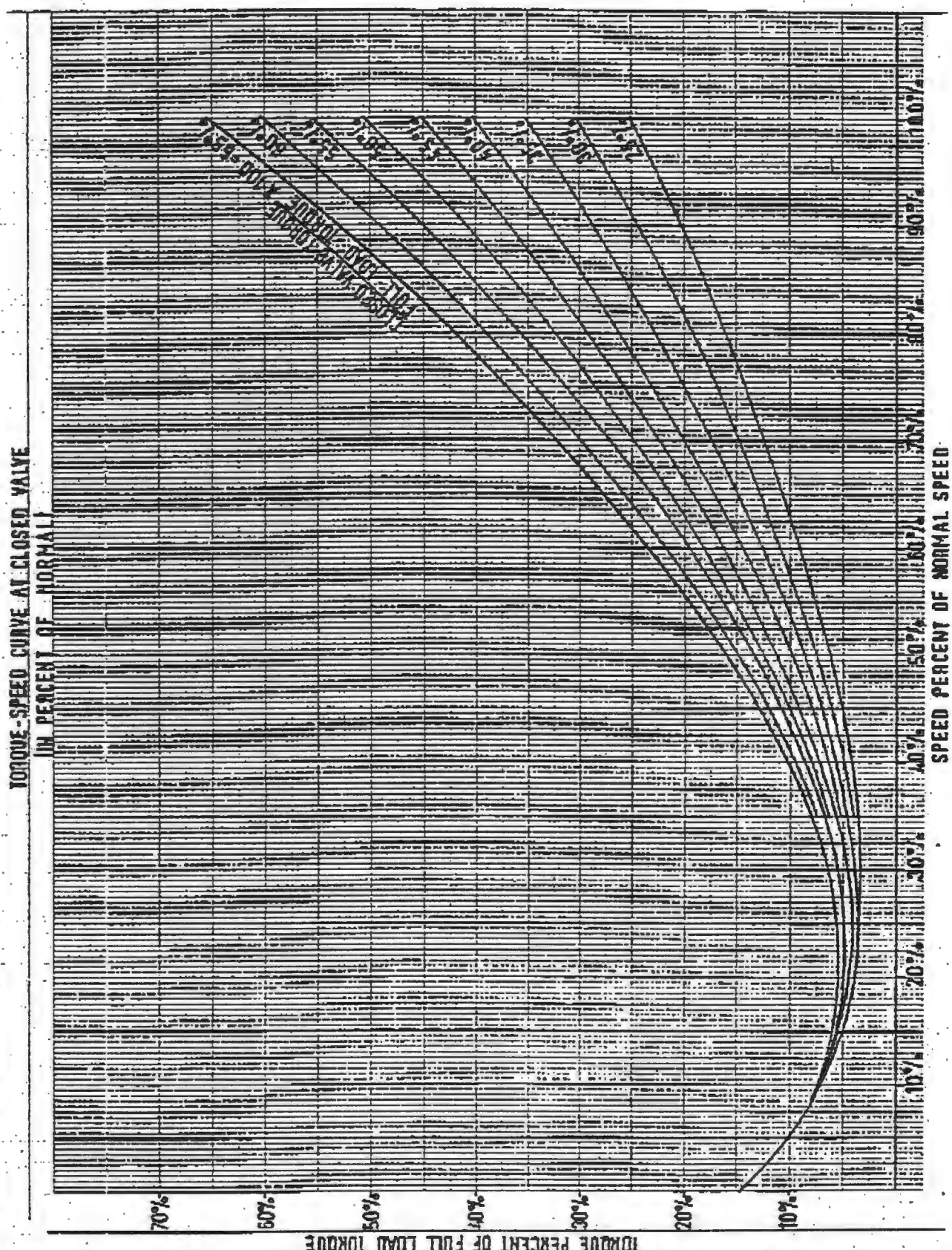

1450 rpm	40-200

Curve No	C - 017 - 06	Pumps Tested to: ISO 2548 - Class 'C' Annexure B	Performance Based on: Water Density 1000 kg/m Viscosity 12 cSt	Impeller Dia	24	Nominal Size	65
Issue Date	94 - 03			Impeller Width	10	Nominal Outlet	40

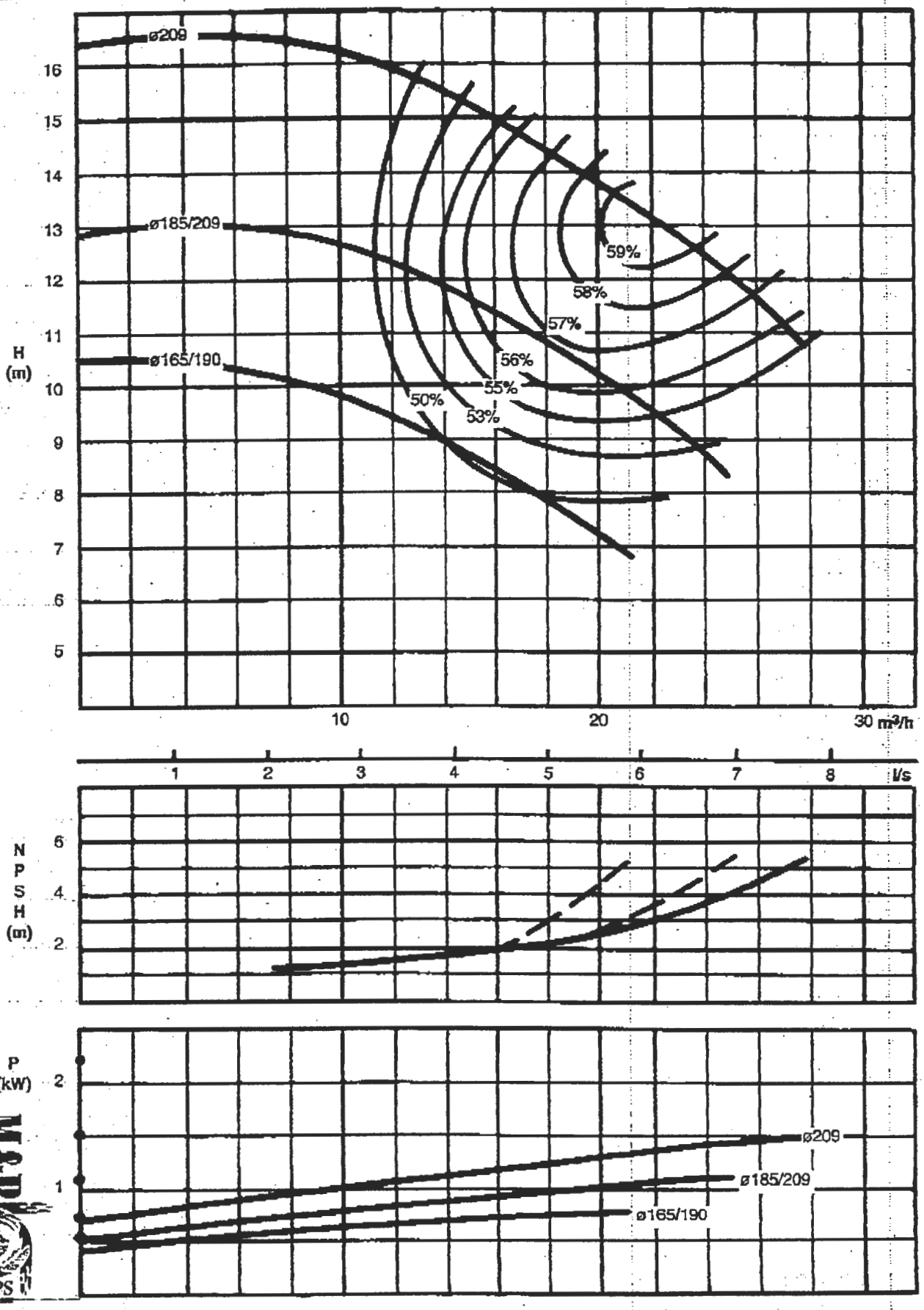

M&B PUMPS

J : Tacho-Generator – Technical Data

- **Selection tables**
- **Technical data**
- **Dimension Drawings**

D.C. Tacho-Generator
Type TDP 0,7

JOHANNES HÜBNER GIESSEN

Selection tables

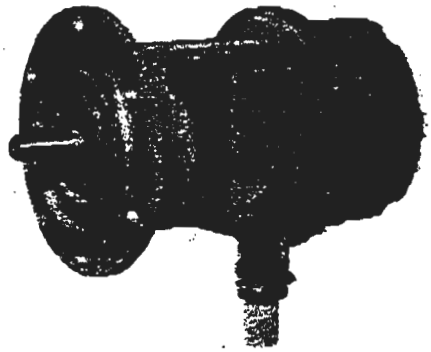

Excitation	**permanent**
Rated voltage tolerance	± 1%
Direction of rotation	reversible
Polarity, terminal connections	dependent on direction of rotation
No. of poles	2
Brushes per machine	2 pairs Quality AG 35 Dimensions 3x5x12
Harmonic voltage ΣU~eff (RMS)	~ 0,3% from 100 up to 3000 rpm from 10 up to 100 rpm approx. 1%
Linearity error	≤ ± 0,1 % at a power rating of approx. 0,1 W
Temperature coefficient	± 0,05 % per 10 K compensated magnet system ± 0,3 % per 10K uncompensated magnet system at a power rating of approx. 0,1 W/ 1000 rpm temperature range up to + 100 °C
Reversing error	± 0,2 %
Insulation	Class B
Winding test	1000 V by manufacturer
Repeat test	max. 800 V
Moment of inertia	approx. 0,440 kgcm²
Weight	approx. 2,5 kg

TDP 0,7 with fitted
overspeed switch type FSE 102

Attachments

All tachos can **be fitted** at NDE with **incremental encoder, overspeed switch, absolute encoders, speed monitors, etc.**

Preferred voltages

Type	Rated voltage at 1000 rpm [V]	Max. speed* [rpm]	Max. permissible current at 1000/9000 rpm [mA]	Optimum load resistance [kΩ]	Armature resistance at 20 °C approx. [Ω]	No-load voltage at 1000 rpm [V]
TDP 0,7 /. . .–1	10	9000	90/810	1,1	5,4	10,5
TDP 0,7/. . .–2	20	9000	45/405	4,4	21	21
TDP 0,7 /. . .–3	30	9000	30/270	10	44	31,3
TDP 0,7/. . .–4	40	9000	22/198	18	93	42
TDP 0,7 /. . .–5	50	9000	18/162	28	128	52
TDP 0,7/. . .–6	60	9000	15/135	40	180	63

Tacho-generators with rated voltage 70 . . . 150 V at 1000 rpm available.

* with degree of protection IP 56: max. 4000 rpm

JOHANNES HÜBNER · Fabrik elektrischer Maschinen GmbH · 35394 Giessen · Siemensstrasse 7
☎ (0641) 7969-0 · Telex 04-82907 · Fax (0641) 73645

JOHANNES HÜBNER GIESSEN

Fabrik elektrischer Maschinen GmbH

D.C. Tacho-Generator for 70-150V at 1000 rpm

TYPE TDP 0,7 ...-SE

Technical Data:

Max. power:	12W ≥ 3000 rpm	degree of protection:	IP 55
Rated power per rev.:	4mW (800-3000 rpm)	construction type	B5 or B3
Tolerance of rated voltage:	± 6 %	Number of slots:	19
Linearity error:	≤ 0,15 %	Number of segments:	38
Direction of rotation:	reversible	No. of poles:	2
Reversing error	± 0,1 %	Weight:	approx. 2,5 kg
Temperature coefficient of the magnet system:	± 0,33 % per 10 K	Moment of inertia:	0,83 kgcm²
Harmonic voltage (RMS).	≤ 0,8 % from 200 to 3000 rpm	Initial break-away torque:	2,5 Ncm
Brushes per tacho:	2 pairs, quality AG 35 dimensions: 3 x 5 x 12	Insulation:	class B
Dimension drawing	see data sheet TDP 0,7		

Advantages:

- can be delivered within a short time
- high voltage max. 150 V at 1000 rpm
- Armature removable without loss of magnetic force/voltage reduction
- High-powered version by means of Rare-earth magnets, 4 W at 1000 rpm

Type	Voltage at 1000 rpm	Max. Speed	Min. Load resistance	Armature Resistance at 20°C	Rated Current
	Volt	rpm	Ohm	Ohm	mA
TDP 0,7 ....7-SE	70	7700	1200	47	57
TDP 0,7 ....8-SE	80	6750	1600	61	50
TDP 0,7 ....9-SE	90	6000	2000	58	44
TDP 0,7 ..10-SE	100	5400	2500	95	40
TDP 0,7 ..11-SE	110	4900	3000	115	36
TDP 0,7 ..12-SE	120	4500	3600	138	33
TDP 0,7 ..13-SE	130	4150	4200	161	31
TDP 0,7 ..14-SE	140	3850	4800	187	29
TDP 0,7 ..15-SE	150	3600	5600	215	27

Special voltages are feasible (extra costs)

Anschrift: Siemensstraße 7 35394 Giessen
Telefon (0641) 7969-0 Telex 482907 Teletex 6419027 = huebn Telefax (0641) 73845
Geschäftsführer: Wolfgang Riedl HRB 126 AG Gießen
Banken: Dresdner Bank AG Gießen 895404500 BLZ 51380040 S.W.I.F.T.-Adresse:
Sparkasse Gießen 200551450 BLZ 51350025 S.W.I.F.T.-Adresse: HELA DE FF
Volksbank Gießen 12505 BLZ 51390000
Commerzbank Gießen 2159945 BLZ 51340013
Deutsche Bank Gießen 0107300 BLZ 51370008
Postgirokonto Frankfurt/Main 147483-BLZ 500 100 60

Dimension Drawings

JOHANNES HÜBNER GIESSEN

TDP 0,7/8

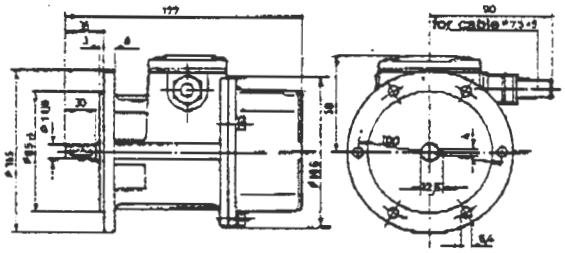

B 5 construction – HM 79 M 50953

TDP 0,7/6

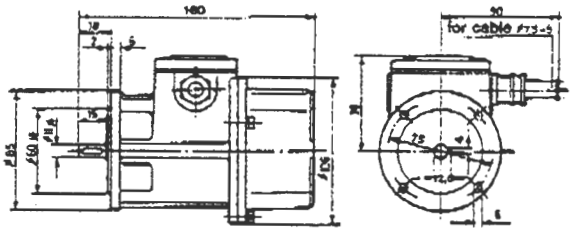

B 5 construction – HM 79 M 50939

TDP 0,7

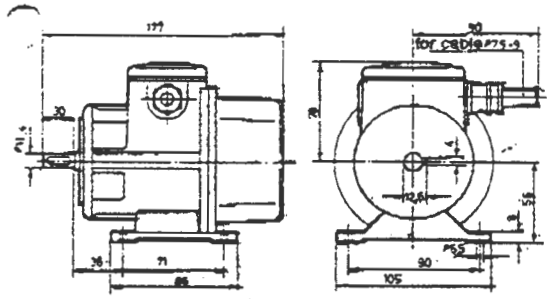

B 3 construction – HM 79 M 51240

TDP 0,7/6

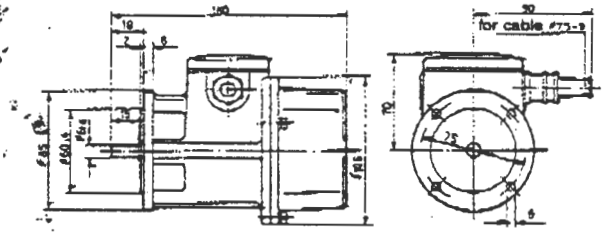

B 5 construction – HM 79 M 50938

TDP 0,7 with attached encoder type Litton 70

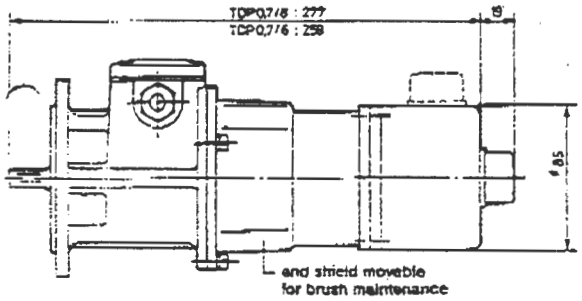

HM 31 M 51635

TDP 0,7/8 with speed-increasing gear Type ..16

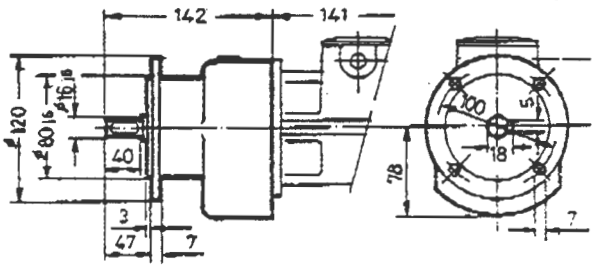

B 5 construction – HM 81 M 51872

TDP 0,7 with 2 shaft extensions

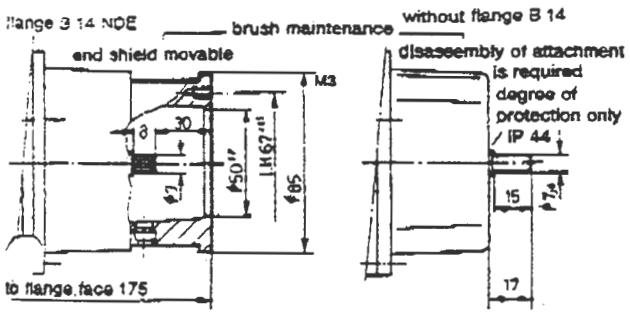

HM 82 M 51985 **HM 83 M 52109**

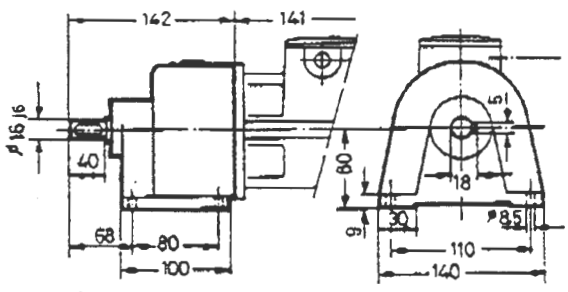

B 3 construction – HM 81 M 51873
modifications reserved!